Exploring and Modulating Platelet Adhesion and Platelet-Cell Interactions in Health and Disease

by

Alison Leigh Banka

A dissertation submitted in partial fulfillment
of the requirements for the degree of
Doctor of Philosophy
(Chemical Engineering)
in the University of Michigan
2022

Doctoral Committee:

Professor Omolola Eniola-Adefeso, Chair
Associate Professor Michael Holinstat
Clinical Research Scholar Yogendra Kanthi, National Institutes of Health
Assistant Professor Jouha Min
Associate Professor Sunitha Nagrath

Alison Leigh Banka

albanka@umich.edu

ORCID iD: 0000-0003-3731-4647

Dedication

To my biggest supporters and cheerleaders: Mom, Dad, Megan, Adrienne, and John

Acknowledgements

If it takes a village to raise a child, I'd also argue that it takes a village to write a dissertation (sorry to everyone with kids out there who are offended by that statement) and I have a lot of people to thank for helping and supporting me throughout the graduate school process.

First, thank you to my advisor, Professor Omolola Eniola-Adefeso, for welcoming me into her laboratory in 2015 and helping me to mature into a well-rounded, independent thinker and researcher. I especially appreciate the opportunities you have given me to follow my own research paths (for better or for worse) and for your support throughout the years. The help you gave me as I navigated the academic job market was invaluable this past year and I appreciated having somebody in my corner for advice. I look forward to seeing how the lab continues to evolve and produce science in the coming years.

Thank you also to the rest of my thesis defense committee: Professor Sunitha Nagrath, Professor Jouha Min, Professor Michael Holinstat, and Dr. Yogendra Kanthi. I appreciate all of your insights on my work and your infectious enthusiasm for science and research. In particular, I want to thank Dr. Kanthi for giving me an opportunity to work in his laboratory for several years. While it was not always a straightforward path, I gained extensive experience and confidence in the biomedical sciences while working with you and believe it played a major role in me developing into the scientist that I am now.

I also want to thank and acknowledge the other members of the Eniola lab, past and present, who made my graduate school experience what it was. As mentioned just about every Valentine's Day, you are all the people I spend the most time with on a daily basis and I wouldn't have it any

other way. Thank you to Professor Cathy Fromen and Dr. Margaret Fish for taking the time to train me extensively when I first started in the lab and for your guidance. Thank you also to Dr. Billy Kelley, Dr. Hanieh Safari, and Genesis Lopez for your friendship and support over the years. To Dr. Mario Gutierrez, thank you for being the best and most erratic officemate a person could ask for and for covering all of our office surfaces with entertaining, vaguely science-related photos and memes. Thank you to Dr. Korie Grayson for jumping into the lab during Covid times and being a great mentor, support system, and role model for all of us. Thank you also to Violet Sheffey, Jonathan Lee, Emma Brannon, Logan Piegols, Valentina Guevara, Rue Felder, Daniel Kupor, Saja Al-Saloum, Seun Akanbi, and Effy Chu. I have enjoyed working with each and every one of you as you started in the lab; you have been great friends and coworkers and I look forward to seeing what you all accomplish next.

Thank you to all of our collaborators who made this work possible. In particular, thank you to Professor Mike Holinstat and Dr. Raymond Adili, as well as other members of the Holinstat lab, for your guidance, support, and for allowing me to occupy your microscope room for many hours at a time. Thank you also to Dr. Sharon Singh and Dr. Mark Shamoun for working with us on the sickle cell disease project. Quite frankly, we could not have even thought about starting such clinical work without you.

Thank you in particular to Dr. Susan Montgomery; you pushed me as an undergraduate to do my best and you continue to be a kind mentor as I finish graduate school. I do not think I would be where I am now if not for your help and belief in me through this whole process.

Thank you to all of my graduate school/Ann Arbor-based friends for going on this rollercoaster ride with me. Graduate school has been no joke, but you have all made it bearable with help, support, commiseration, tears, and a shared love of Michigan football. Thank you also

to all my non-graduate school friends who are kind enough to remember to not ask how my research is going or when I am finally going to graduate (that time is here! It is now safe to ask!).

Finally, thank you to my biggest supporters; you have all been my cheerleaders when I was not able to do that myself (which was pretty much always). Mom and Dad, thank you for your love, support, and occasionally some perspective, as well as for lending an ear when I needed. Megan, thank you for proofreading this entire thesis in approximately 36 hours (putting you in a very small and exclusive group of people who will read it in its entirety) and, along with A, listening to my rants, occasionally sending me care packages in the mail, sending dog and baby photos to lighten my days, and doing all that you both could to support me from afar. You both have been great to me. Thank you to John for putting up with my neuroses for 4+ years now and for providing me with kind words, warm meals, entertainment, and the remote whenever I request it. You have all been better at believing in me than I am, and I could not have done this without you.

Table of Contents

List of Figures

List of Abbreviations

ACD	Acid Citrate Dextrose
ADAMTS-13	A Disintegrin and Metalloproteinase with a Thrombospondin type 1 motif, member 13
ADP	Adenosine Diphosphate
AF555	Alexa Fluor 555
ALI	Acute Lung Injury
APC	Allophycocyanin
APC/Cy7	Allophycocyanin-Cyanine 5
AR	Aspect Ratio
BSA	Bovine Serum Albumin
CO	Carbon Monoxide
CORM	Carbon Monoxide Releasing Molecules
COVID-19	Coronavirus Disease 2019
CT	Chronic Transfusion
Cy5	Cyanine 5
Cy5.5	Cyanine 5.5
DAPI	6-Diamidino-2-Phenylindole
DMSO	Dimethylsulfoxide
ECM	Extracellular Matrix
EDC	N-(3-Dimethxylaminopropyl)-N'-EthylcarboimmideHydrochloride
EI_{max}	Maximum Elongation Index
FDA	Food and Drug Administration
FITC	Fluorescein Isothiocyanate
GFP	Green Fluorescent Protein
GP	Glycoprotein
HbA	Hemoglobin A
HbS	Hemoglobin S
Hct	Hematocrit
HPLC	High Performance Liquid Chromatography

HU	Hydroxyurea
HUVEC	Human Umbilical Vein Endothelial Cells
IACUC	Institutional Animal Care and Use Committee
ICAM-1	Intracellular Adhesion Molecule 1
ICAM-2	Intracellular Adhesion Molecule 2
iCORM	Inactivated Carbon Monoxide Releasing Molecule
iECM	Infusible Extracellular Matrix
IgG	Immunoglobulin
IL-1β	Interleukin-1β
IP	Intraperitoneal
IRB-MED	University of Michigan Internal Review Board
IV	Intravenous
K2-EDTA	Tri-Potassium Ethylenediaminetetraacetic Acid
LFA-1	Lymphocyte Functional-Associated Antigen 1
LPS	Lipopolysaccharide
Mac-1	Macrophage-1 Antigen
MES	2-(N-morpholino)ethanesulfonic acid
MESF	Molecules of Equivalent Soluble Fluorochrome
MFI	Median Fluorescent Intensity
MI	Myocardial Infarction
NETs	Neutrophil Extracellular Traps
ns	Not Significant
PBS	Phosphate Buffered Saline
PE	phycoerythrin
PEG	Polyethylene Glycol
PET	Positron Emission Tomography
PLGA	Poly-Lactic-Co-Glycolic
PolyA	Poly Aspirin
PPFC	Parallel Plate Flow Chamber
PRP	Platelet-rich Plasma
PS	Polystyrene
PSGL-1	P-selectin Glycoprotein Ligand-1
PVA	Polyvinyl Alcohol
RBC	Red Blood Cell
RO	Retro-orbital
SCA	Sickle Cell Anemia

SCD	Sickle Cell Disease
SEM	Standard Error of the Mean/Scanning Electron Microscopy
sLe^A	Sialyl-Lewis A
sLe^X	Sialyl-Lewis X
T	Targeted
TBHP	tert-Butyl Hydroperoxide
TF	Tissue Factor
TNF-α	Tumor Necrosis Factor α
TRITC	Tetramethylrhodamine
UT	Untreated (Patients)/Untargeted (Particles)
VCAM-1	Vascular Cell Adhesion Protein-1
VOC	Vaso-Occlusive Crisis
vWF	von Willebrand factor
WBC	White Blood Cell

Abstract

Platelets play a major role *in vivo* in preventing bleeding, hemostasis, and contributing to uncontrolled clotting, thrombosis. Platelets are impacted in health and disease by the other cells they encounter in blood flow, including red blood cells (RBCs), white blood cells (WBCs), and the endothelial cell monolayer lining blood vessel walls. Despite this importance, the effect other cell types have on platelets in disease has yet to be fully explored, in part due to a lack of proper models to study human platelet behavior. In this thesis, we develop new, tunable *in vitro* methods to study platelet behavior that can be altered depending on disease conditions.

We examined platelet adhesion to a confluent endothelial cell monolayer cultured on crosslinked extracellular matrix proteins, which were exposed via manual damage. We attached the damaged endothelial cells to a parallel plate flow chamber and monitored human platelet behavior and adhesion over a wide variety of blood flow conditions. This model was validated using a known anti-platelet compound and we identified two additional novel compounds that significantly reduced platelet adhesion when administered either to blood or to the endothelial cells themselves.

Many diseases, including acute lung injury, venous and arterial thrombosis, and sepsis, fall under the umbrella of 'thromboinflammation,' when blood clots occur in combination with an overzealous immune cell response. A hallmark of these diseases is the presence of leukocyte-platelet aggregates at the site of inflammation. To capture this phenomenon, we included inflammation of endothelial cells in our flow model to facilitate the adhesion of leukocyte-platelet aggregates. We then utilized model polymeric drug carriers to reduce platelet adhesion to the

inflamed endothelium by interfering with platelet-bound leukocytes. Specifically, platelet adhesion in this model decreased by approximately two-fold after 2 μm polystyrene particles were introduced into the system. We verified that this impact of particles is translatable *in vivo* using a mouse model of systemic inflammation; 2 μm particles significantly reduced platelet adhesion to the mouse mesentery by up to 62% in comparison to non-particle controls. These findings represent a potential new particle-based therapeutic to reduce platelet accumulation in thromboinflammatory diseases by diverting platelet-leukocyte aggregates away from areas of inflammation.

Patients with sickle cell disease (SCD) have RBCs that are more stiff than non-SCD controls; we explored the impact that these stiff RBCs have on platelet behavior in blood flow *in vitro* using SCD patient whole blood samples and a model system where healthy RBCs are artificially stiffened to mimic SCD. The magnitude of SCD platelet adhesion varied greatly depending on patient treatment regimen, though untreated patients had the highest platelet adhesion in comparison to non-SCD controls. Our artificial system allowed us to examine the impact of stiff RBCs on platelet adhesion in a controlled environment, providing knowledge that can help inform how to provide chronic transfusions of RBCs to SCD patients to best reduce excessive platelet adhesion and clotting. We also determined that carbon monoxide releasing molecules (CORMs) reduce excessive platelet adhesion for a subset of patients, a promising new potential therapeutic for SCD. Overall, this work represents new methods to study platelet behavior under different disease conditions as well as novel potential therapeutics to modulate platelet adhesion in thromboinflammation and SCD.

Chapter 1 Introduction

1.1 Publication Information

The text in this chapter is partly from the publication listed below as well as from several manuscripts in preparation to be submitted in the upcoming weeks. This chapter provides both an overview of blood flow as well as the essential components of blood flow with a focus on platelet adhesion and behavior. An overview of methods to study platelet adhesion both *in vivo* and *in vitro* will be provided, plus several key diseases where platelets play a major role. These diseases include thrombosis, inflammation, and sickle cell disease. Finally, this chapter will conclude with a discussion of how particulate and/or targeted drug carriers are utilized to impact and modulate leukocyte and platelet behavior.

Alison Banka and Omolola Eniola-Adefeso. "Method article: an *in vitro* blood flow model to advance the study of platelet adhesion utilizing a damaged endothelium." *Platelets*, in press.

Alison Banka, Valentina Guevara, Reheman Adili, Michael Holinstat, and Omolola Eniola-Adefeso. "Polymeric Drug Carriers Modulate Platelet Adhesion in Thromboinflammation." In preparation.

1.2 Whole Blood Characteristics

1.2.1 Whole blood physiology

Blood is a complex, non-Newtonian fluid comprised of red blood cells (RBCs), white blood cells (WBCs), and platelets suspended in plasma. In blood flow, RBCs form a core in the middle of the vessel, while WBCs and platelets move toward the vascular wall ('margination') to an area known

as the red blood cell free layer[1–3]. The high concentration of WBCs and platelets near the endothelium, the monolayer of cells that line blood vessels, allows them to easily adhere to the vascular wall in situations of immune challenge or injury[2,4,5]. The formation of the RBC core and subsequent margination of WBCs and platelets from the core toward the wall is due to a combination of several different forces: a 'lift force' experienced by the RBCs due to their deformability[6], which results in lateral motion of the RBCs towards the core and of the WBCs and platelets towards the wall[7–9]; hydrodynamic interactions between RBCs and platelets[10]; and heterogenous collisions between the deformable RBCs and relatively stiff WBCs or platelets[11]. A schematic demonstrating the segregation of blood cell types to different areas of the blood vessel, highlighting margination of platelets and WBCs, is shown in Figure 1.1.

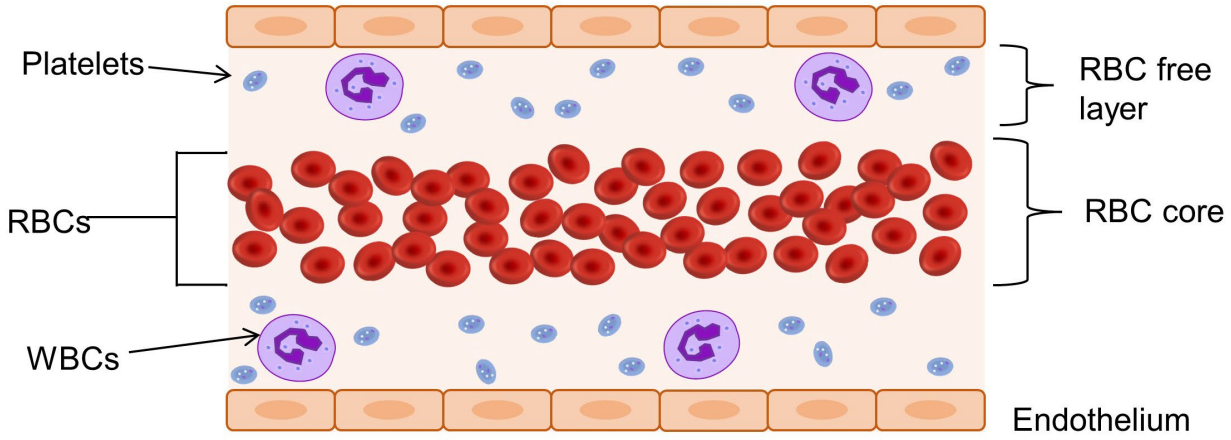

Figure 1.1: A schematic detailing the key components in blood flow.

1.2.2 Platelet behavior and adhesion

Platelets are anucleated cell fragments produced from bone marrow megakaryocytes[12]. The typical platelet count in humans ranges from 150-400*10^9/L[13]. Platelets must maintain a balancing act *in vivo* due to their contributions to both health and disease. A low platelet count or underperforming

platelets can lead to a disruption in hemostasis and elevated bleeding risk[14], whereas an excess of platelets or platelets that are overactive can contribute to thrombosis[15], cardiovascular events[15,16], and inflammation[17] in various diseases; hemostasis refers to the body's physiological response to vascular injury to avoid bleeding, while thrombosis refers to uncontrolled clotting. Due to this delicate balancing act, knowing the key steps in platelet aggregation and adhesion is essential to understand platelet behavior.

Under healthy conditions, platelets contact but do not adhere to the intact endothelial cell monolayer[2]. Upon vascular injury, the underlying extracellular matrix (ECM) proteins upon which endothelial cells grow are exposed[18]; key ECM proteins include but are not limited to collagen, vWF, and fibronectin[19]. These are some of the key proteins that platelets bind to, however, platelets may also adhere to other proteins, including laminin, fibrin, vitronectin, and thrombospondin[18]. The adhesion of platelets to the site of vascular injury is a key first step in both hemostasis and thrombosis and involves multiple points of binding between glycoproteins (GP) on platelets and the damaged vasculature. These points of binding include subendothelial von Willebrand factor (vWF), an adhesion glycoprotein whose source may be the endothelium, plasma, or platelets themselves, primarily via GP1bα and $\alpha_{2b}\beta_3$[20], and underlying collagen through GPVI[21] and integrin α2β1[22]. Specifically, upon vascular inflammation or damage, platelets begin to roll along immobilized vWF bound to the subendothelial surface[23] before firmly adhering to collagen via the aforementioned GPVI[21] and integrin α2β1[22]. After firm adhesion, platelets activate and release their granules, which include such cargo as vWF and other adhesive proteins, and form firm aggregates[23].

vWF plays a key role in platelet adhesion by allowing platelets to slowly roll across the damaged endothelial cell surface prior to firm adhesion to collagen or other ECM proteins. vWF

has several sources; the endothelium itself releases Weibel-Palade bodies containing not only ultra-long vWF multimers, but also P-selectin, after activation or stimulus[24]. These ultra-long vWF multimers can tether shorter, soluble vWF in plasma and, under normal conditions, are cleaved by the enzyme ADAMTS-13, an enzyme present in plasma[24,25]. The importance of vWF and ADAMTS-13 activity in causing and preventing thrombosis, respectively, is highlighted by the fact that ultra-long vWF multimer levels or a deficiency in ADAMTS-13 activity in plasma are associated with thrombotic diseases, including sickle cell disease[26], ischemic stroke[27], and thrombotic thrombocytopenic purpura[28].

1.3 Methods to Study Platelet Behavior

1.3.1 In vivo models

Due to the complexity surrounding platelet adhesion and the development of thrombosis, many researchers utilize small and large animal models of thrombosis to study platelet adhesion, aggregation, and clot formation. Small animal models of thrombosis include the use of rodents, such as rat and mice, and rabbits[29–34]. Benefits of using these models include their relatively low cost, small size, ease of availability, and reduced ethical concerns in comparison to large animal models[29]. In particular, genetically modified mice have been utilized in a large variety of thrombosis models to identify the specific contributions of different genes and proteins on platelet behavior and thrombus development[30]. Different models of thrombosis using mice specifically include laser-induced thrombosis, ferric chloride-induced arterial thrombosis, collagen/epinephrine-induced thrombosis via intravenous injection, and oxygen radical-induced (photochemical) injury[30,35]. Additionally, though wild-type mice are not prone to atherosclerotic plaque development and subsequent arterial thrombosis, genetically modified mice, i.e., mice deficient in apolipoprotein E, can be utilized for their ability to develop plaques which can then be

ruptured using an artificial method[30]. In addition to the murine thrombosis models discussed, mouse models of deep vein thrombosis have also been developed. Such models include the electrolytic inferior vena cava model[31,32], where a small amount of current is applied to wire inserted into the inferior vena cava, causing endothelial damage and thrombus initiation, as well as the 'stenosis' and 'stasis' models of deep vein thrombosis[33,34]. In the 'stasis' model, the inferior vena cava is fully ligated and all side branches cauterized to fully prevent blood flow[33], while in the 'stenosis' model, the inferior vena cava is only partially ligated, allowing some blood flow to continue[33,34]. Additionally, in many of these small animal models of thrombosis, platelet behavior can be monitored in real time using intravital microscopy[30,36].

Despite the benefits of using small animal models for studying thrombosis and platelet behavior, there exist many concerns with applying knowledge gained from small models to human behavior. In particular, there exist many species-related differences between small animals and humans on the cellular level and beyond. For example, there are many species-related differences between mice and human platelets. Mouse platelets are smaller than human platelets, have a shorter lifespan, and normal blood platelet concentrations for mice are several times higher than typical blood platelet concentrations in humans[37]. Further, mouse platelets lack a protease-activated receptor (PAR-1) that plays a major role in thrombin-mediated platelet activation[38]; Vorapaxar is a recently developed anti-platelet pharmaceutical that binds to the PAR-1 receptor on human platelets to inhibit platelet activation and downstream aggregation[39]. Use of a mouse model alone would not be able to predict the anti-platelet impact of Vorapaxar during preclinical development. With regards to RBCs, mouse RBCs are smaller, have shorter lifespans, and lower oxygen affinity in comparison to human RBCs[40]. Additionally, there are many key differences between mouse and human WBCs, including differences in circulating WBC populations. In mice, lymphocytes

represent the largest group of circulating WBC (~75-90%) while in humans, neutrophils make up the largest percentage of circulating WBC (~50-70%)[41]. Beyond simple differences in circulating WBC populations, there are countless other differences between mouse and human WBCs both in innate and adaptive immune cells[41].

Other than cell-specific differences between mice and humans, small animal models do not represent macrovascular thrombosis in humans well due to the differences in vessel sizes[29,42]. Also, most small animal models are performed in healthy animals with thrombus formation occurring due to researcher manipulation of the animals[29,30,42], which can make these results even less likely to be applicable to naturally occurring thrombotic disease in humans.

As an alternative to small models that do not represent human thrombus development, other researchers utilize large animal models to study platelet behavior and thrombosis. Large animal models include the use of pigs, dogs, and non-human primates[29]. Benefits of using these models include the greater numbers of similarities physiologically between large animals and humans, making them more ideal species with which to study macrovascular thrombosis[29,43]. Further, the flow hemodynamics, vasculature, vessel size, and vascular cells specifically of non-human primates mimics that of humans well[43]. Additionally, phylogenetic similarities and hematologic homology between non-human primates and primates allow primates specifically to be used for studies involving drug pharmacokinetics, antithrombotic testing, coagulation, platelet function, and fibrinolysis[43].

While use of large animal models is common to study platelet behavior and thrombus development, there are drawbacks as these models are expensive, require specific technical skills and equipment, and often results and conclusions gained from use of *in vivo* models do not direct translate to findings in humans due to species-related differences[44,45]. Further, the 'Three Rs' of

animal use ethics involves the Replacement, Reduction, and Refinement of animals: 'replacement' refers to methods that avoid animal use; 'reduction' refers to strategies utilizing fewer animals to obtain data, and 'refinement' refers to modifying animal protocols to minimize animal discomfort during use[46]. Together, all of these concerns with using animal models of hemostasis and thrombosis highlight the need for non-animal-based models to study platelet behavior.

1.3.2 In vitro models

Though *in vivo* models provide much information about platelet behavior in a physiological blood flow environment, there still remain species-related differences between animals and humans. Further, the 3 Rs of ethical animal research highlight that alternative methods should be explored, especially those that can utilize human blood cells to better understand human-specific blood cell behavior. To that end, many researchers utilize *in vitro* blood flow models to study platelet adhesion and aggregation. These models typically include the use of human whole blood or blood components, including isolated, washed platelets, which are perfused over a surface that facilitates platelet adhesion at a specific shear rate, which in turn can often be controlled by varying the volumetric flow rate of the blood or blood components. Further, platelet behavior in these models can often be viewed in real time using microscopy, an added benefit of these *in vitro* models.

One common type of surface used to facilitate platelet adhesion is either a single protein, often an ECM protein, or a combination of more than one. An extremely common protein to utilize is collagen, as it is a known ECM protein that firmly binds platelet in blood flow[47]. Indeed, countless *in vitro* flow methods utilize collagen as the sole ECM protein to study platelet adhesion[48–53], though many other papers utilize other proteins of interest, including tissue factor[47], vWF[51,54], or fibrinogen[51], or , alternately, use a mixture of several key proteins[47,55]. Use of these types of *in vitro* flow systems allows tight control over the exact binding proteins of interest to

study platelet behavior. However, systems utilizing protein-based platelet adhesion neglect the role that the endothelium plays in platelet behavior.

To address that issue, many researchers also utilize endothelialized fluidic models[56,57] to study platelet adhesion and behavior. Endothelialized models allow for activation of the endothelial monolayer, which can result in the secretion of ultra-long vWF multimers[24,25] and P-selectin[23]. Both of these molecules can bind platelets in blood flow. Further, endothelialized models allow for the secretion of ADAMTS-13 to cleave ultra-long vWF multimers and facilitate clot resolution[25]. Such models can be utilized to screen for potential anti-platelet therapeutics[56], but can vary greatly based on the blood flow shear rate, anticoagulant used, source of endothelial cells, and endothelial cell agonist[56,57]. New endothelialized fluidic models with increased complexity have been developed that attempt to create a compliant, hydrogel-based 3D environment[58]. Others explored the production of a 3D co-culture of endothelial cells and pericytes[59]. However, these models have yet to be used to explore platelet adhesion and behavior. Additionally, one potential issue with using endothelialized models is that they typically lack exposure of platelets to underlying ECM proteins, a key first step in platelet adhesion and aggregation[18,23].

1.4 Examples of Diseases Involving Platelets and Current Treatment Methods

1.4.1 Thromboinflammation

In 2013, Engelmann and Massberg coined the term 'thromboinflammation,' which refers to uncontrolled blood clot development that occurs alongside an excessive immune cell response, which can be a driver of thrombosis[60]. Practically, blood clots often form in the presence of underlying inflammation, and inflammation can occur or be worsened due to the development of blood clots. Many different diseases and conditions all fall under the umbrella of

'thromboinflammation,' which covers a wide range of disorders. For instance, both arterial and venous thrombosis are impacted by inflammation with immune cells with platelets playing key roles in each[61–65]. Other thromboinflammatory diseases where platelets can play a damaging role include but are not limited to ischemic stroke[61,65,66], atherosclerosis[64,67–69], acute lung injury[70,71], sepsis[68,72], sickle cell disease (SCD)[61,73,74], and Covid-19[75].

Platelets can adhere to an area of vascular damage by binding to vWF or the underlying ECM, as described above. However, in conditions of endothelial inflammation, platelets can also adhere to P-selectin via GP1bα on platelets and to ICAM-1 or αvβ3 via fibrinogen bridging to GPIIb/IIIa[68,76]. After platelet activation, there is a cascade of downstream events that occur that contribute to inflammation in the area. Platelets release their α and dense granules, secreting adhesion ligands and receptors, including P-selectin, GPIIb/IIIa, and GP1bα, signaling molecules, including CD40L, CXCL4, and CXCL8, and inflammatory molecules, including histamine and ADP[65,68,77,78]. The expression of these additional cell adhesion receptors and ligands allow platelets to capture or more firmly bind other cells, including other platelets, leukocytes, and the endothelium itself. Further, activation of the GPIIb/IIIa receptor helps stabilize the platelet aggregate by crosslinking either vWF or fibrinogen between receptors[68,69,77]. Many of the signaling molecules platelets release upon activation, including the aforementioned chemokines and cytokines, attract other cells to the area. Finally, platelet receptors bind ADP released from dense granules[68,77]. Overall, platelet adhesion and activation in a clot or area of inflammation contributes to local inflammatory cascade and recruits other immune cells to the area.

Platelets are not the only contributors to thromboinflammation; underling endothelial inflammation also recruits immune cells and, additionally, WBCs such as monocytes and neutrophils play a large role in thromboinflammatory diseases. In particular, platelets and WBC

often form aggregates at an area of inflammation. Circulating platelet-WBC aggregates can bind together or, alternatively, a bound platelet or bound WBC can bind the other from blood flow[61,79]. WBC can bind to an inflamed endothelium through several ligand-receptor pairs, including selectins on the endothelium via PSGL-1 on WBC, vWF or ICAM-1 via Mac-1, ICAM-1 or VCAM-1 on the endothelium via LFA-1 on the WBC surface[61,79]. Alternatively, WBC can bind directly to adherent platelets with the initial binding facilitated through P-selectin on activated platelets and PSGL-1 on WBC[71,77]. Firm adhesion between a platelet and WBC is facilitated through platelet GP1bα and WBC Mac-1, platelet GPIIb/IIIa and WBC Mac-1 via a fibrinogen bridge, and platelet ICAM-2 with WBC LFA-1[71,77].

Similar to platelets, leukocytes after initial activation, which can be triggered by PSGL-1/P-selectin binding, contribute to the local inflammatory cascade. Specifically, after activation, neutrophils upregulate adhesion molecule expression, such as Mac-1 and LFA-1, while shedding L-selectin; produce and release reactive oxygen species and granular enzymes; and release neutrophil extracellular traps (NETs)[61,64,71,79]. Monocytes also upregulate adhesion molecules and release granular enzymes and NETs, though in limited quantities in comparison to neutrophils[64,77,79]. However, monocytes contribute to thrombosis by increasing tissue factor (TF) activity, which helps generate thrombin[79]. Monocytes also release TF^+ microparticles and shift to a more pro-inflammatory phenotype[72,77,79].

The traditional treatment methods for thromboinflammatory diseases vary greatly by the specific condition or disease. For example, venous thrombosis is often treated with anti-coagulants to halt the contributions of the coagulation cascade or thrombolytics to disturb established clots[80]. Arterial thrombosis is often treated with anti-platelet compounds and/or aspirin[81]. Acute inflammatory diseases like acute lung injury or sepsis focus on control of the initial infection and

palliative or supportive care, which can include steroids or non-steroidal anti-inflammatory drugs[82–84]. Current treatment methods for SCD will be discussed in greater detail in the next section. There are often downsides to these current treatment methods, including sensitivity to anti-coagulants in venous thrombosis[85], bleeding risk due to anti-platelet compounds[86], or the suppression of the entire immune system[83] due to steroids that can leave a patient vulnerable to a secondary infection.

Due to the damaging presence of platelet-leukocyte aggregates in thromboinflammation, previous work attempted to target the initial PSGL-1/P-selectin interaction directly. Initial animal work showed promise that an anti-PSGL-1 antibody could improve outcomes in pig angioplasty[87], and mouse arterial injury[88]. However, anti-PSGL-1 therapeutics in humans were unsuccessful and did not improve end points in myocardial infarction[89,90], which effectively halted their use in human trials. Alternatively, a P-selectin antagonist helped reduce myocardial damage of patients after myocardial infarction at high dosages[91], but later did not improve patient outcomes after coronary artery bypass graft surgery[92] and since then has mostly been discontinued. A different study of venous thrombosis in baboons utilized an anti-P-selectin aptamer; this aptamer showed improved recanalization of veins in comparison to anti-vWF aptamers and heparin alone[93]. However, no clinical trials or follow-up studies have utilized this aptamer. Overall, there is great interest in obstructing platelet-leukocyte aggregate formation or adhesion in thromboinflammation to interfere with their contributions to the inflammatory cascade in many diseases and conditions.

1.4.2 Sickle cell disease (SCD)

Sickle cell disease (SCD) is comprised of a group of genetic diseases that occur due to mutations in the β-subunit of hemoglobin, causing polymerization of the β-globin subunits under conditions of deoxygenation[94]. This polymerization leads to stiffening of the red blood cells

(RBCs) as well as occasional irreversible sickling to form the trademark sickled RBC shape known in SCD. Patients with SCD face many acute and chronic complications, including acute chest syndrome, chronic pain, organ failure, and stroke, that are due to vaso-occlusive crises (VOC) and general immune system activation[94,95].

Even in industrialized countries, SCD patients with the most severe phenotype (sickle cell anemia) have a life expectancy that is shortened by 20 to 30 years in comparison to healthy individuals[96] in part due to their increased risk of many thrombotic events, including acute chest syndrome[97], pulmonary embolism and deep vein thrombosis[98–100], ischemic and transient strokes[101–103], and myocardial infarction[104,105]. To date, the most successful and widely prescribed treatment for SCD is hydroxyurea, which increases fetal hemoglobin and reduces white blood cell counts, ultimately leading to decreased painful crises and transfusions required by patients[106,107]. However, hydroxyurea has not been shown to improve patient outcomes for certain complications of SCD, including gallbladder disease and splenic sequestration in children[108], and priapism, stroke, and leg ulcer in adults[109]. Further, there remain significant barriers for patient compliance and treatment with hydroxyurea[109].

Two potential curative therapies currently being researched in clinical trials for SCD are gene therapy[110] and CRISPR/Cas9 gene editing[111]; though promising, these two treatments are in early stages of trials in humans and are complex therapeutics inaccessible to most patients worldwide with SCD. RBC transfusion is one common, easily accessible therapy for SCD, which focuses on decreasing the percentage of stiffened or sickled RBCs in circulation, typically to less than 30% of total RBCs, in order to reduce the risk of VOC[112]. Unfortunately, repeated RBC transfusions can lead to alloimmunization, and/or iron overload and subsequent organ damage in patients[113]. Furthermore, a complete mechanistic justification for the dilution of rigid RBCs to exactly 30%

during transfusion is lacking. Thus, improved knowledge of the disease and improved therapies are still needed.

In particular, there are gaps in knowledge regarding how different cell types other than irreversibly sickled RBCs, including the endothelium, WBCs, and platelets, all contribute to VOC in SCD patients that lead to many of their devastating complications. Platelets in SCD are known to reflect the pro-inflammatory, pro-coagulant state of the patient. For instance, seminal research in SCD showed that platelets express high levels of cell adhesion molecules[114,115], secrete high levels of soluble factors including platelet factor 4[116], β-thromboglobulin[116], IL-1β[17], and CD40-L[17], and are more likely to form RBC-platelet aggregates[114] and shed microparticles[115] than healthy controls. Activated and resting SCD platelets display higher adhesion to fibrinogen[117,118]. Despite this wealth of information about SCD platelets on a molecular level, less research has focused on the interactions between platelets and other cells, particularly other cells in blood flow.

1.5 Use of Targeted and/or Particulate Drug Carriers

1.5.1 Targeting drug carriers to platelets

Platelet activity must maintain balancing act *in vivo*, as a lack of platelets can lead to bleeding risk and overactive platelets can help lead to thrombosis or inflammation in various diseases. With that in mind, many previous studies examined methods to target therapeutics directly to platelets either for purposes of clot[119] or cancer[70] imaging, thrombolysis[120,121], or the formation and stabilization of platelet-based clots[122–127]. Past work on designing imaging agents targeted to platelets include a single-chain antibody that binds to the active conformation of GPIIb/IIIa (CD41/61) decorated with several different imaging agents, such as fluorescent Cy7, microbubbles suitable for ultrasound imaging, and 64Cu for PET imaging all for the imaging of tumor cells[70]. Other groups

radiolabelled fucidan, a sialyl Lewis X (sLe^X) mimetic, for use as an imaging agent in arterial thrombosis and myocardial ischemia-reperfusion *in vivo*[119].

Other works designed therapeutics specifically to help lyse established clots and prevent unregulated thrombosis. One example targets degradable, polymer-based capsules to GP11b/IIIa on platelet surfaces and delivers urokinase plasminogen activator locally to reduce clot size in acute thrombosis[120]. Other utilized liposomes targeted to activated platelets that release streptokinase at the site of thrombosis[121].

Work utilizing platelet mimics or targeted therapies to assist with clotting include capsules fabricated using polymers (dextran, poly-l-lysine, and poly-l-glutamic acid) and fibrinogen that can bind platelets and release Factor VIII at the site of a clot to assist with clotting for patients with bleeding disorders[122]. Other extensive work explored designing platelet mimics to assist in clotting[123]. These mimics are flexible and decorated with several binding peptides to collagen, vWF, and GPIIb/IIIa on platelets so the capsules can both bind to areas of injury and recruit platelets to the site[123,125]. Building upon these synthetic platelets, additional work examined loading these vesicles with tranexamic acid to stabilize clots locally[126]. Utilizing the synthetic platelet constructs, named 'SynthoPlate,' researchers determined that their artificial system could reduce blood loss after traumatic vessel injury in pigs[127]. Other novel work developed highly deformable microgel particles targeted to insoluble fibrin that, upon binding, mimic the contractile behavior of platelets and decrease bleeding time *in vivo*[124]. Overall, extensive prior work examined targeting platelets specifically for purposes of imaging, clot lysis, or clot strengthening.

1.5.2 Targeting drug carriers to circulating leukocytes

Given the role that circulating leukocytes, including neutrophils and monocytes, play in diseases such as atherosclerosis[128,129], acute respiratory distress syndrome/acute lung injury[130,131], thrombosis[129,130,132], and sickle cell disease[61,130], recent work examined targeting leukocytes in the blood stream directly via intravenously administered therapeutics. Specifically, recent publications utilize particles and the phagocytic ability of neutrophils and monocytes to either send therapeutic cargo to an area of interest[133] or to divert leukocytes away from an area of excess inflammation[134–138]. One relatively simple, elegant example involves utilizing polystyrene particles *in vitro* to reduce the adhesion of leukocytes to an inflamed endothelial monolayer, an impact that was magnified when particles were directed targeted to the endothelium[139]. In a different example, researchers examined the ability of neutrophils to traffic labelled liposomes decorated with an L-selectin-specific ligand to tumor-bearing mice *in vivo*[133].

Neutrophils are known to play a damaging role in many inflammatory diseases[74,78,128,130,140]. Many recent works leverage the phagocytic properties of neutrophils to 'distract' neutrophils. For example, researchers utilized dexamethasone-loaded liposomes targeted to neutrophils via sialic acid and demonstrated that the liposomes were trafficked to areas of arthritic inflammation in rats[134]. Rats receiving targeted liposomes demonstrated less inflammation, joint injury, and inflammatory cell infiltration than control rats or those received non-targeted liposomes[134]. Acute lung injury (ALI) is another inflammatory disease where neutrophils play a known, damaging role[130,131], leading many researchers to develop methods to divert neutrophils from the lung in ALI. Some researchers loaded a natural therapeutic, bergenin, into serum albumin nanoparticles and administered them to rats with LPS-induced ALI[135]. Higher nanoparticle dosages led to reduced cell infiltration into the lungs by both neutrophils and other

leukocytes, reduced inflammatory cytokines, and reduced lung damage as measured by histopathological lung tissue scores[135]. Other researchers utilized polystyrene nano- or microparticles in an LPS-induced ALI model in mice[136]. By administering mice an IV injection of particles one hour after LPS installation, the authors were able to divert neutrophils from the lung and reroute them to the liver, reducing the percent of neutrophils in the lung fluid[136]. Further researchers utilized a salicylic acid-based particle platform to reduce neutrophils and inflammation in the lung in both LPS- and bacterial injection-induced ALI models in mice[137], leveraging the anti-inflammatory properties of aspirin in a localized method.

Other researchers utilize PLGA nanoparticles to divert monocytes and neutrophils away from the area of damage in spinal cord injury, successfully reducing the number of immune cells accumulated and extent of scarring[141]. Similarly, other researchers demonstrated that polymeric microparticles could be phagocytosed by monocytes *in vivo* and improved outcomes in a variety of inflammatory diseases, including myocardial infarction, encephalomyelitis, colitis, peritonitis, and encephalitis[138]. Overall, there is great recent interest in leveraging the phagocytic abilities of both circulating neutrophils and monocytes to redirect immune cells away from areas of excessive inflammation to improve outcomes.

1.5.3 Targeting drug carriers to the vascular endothelium

Just as intravenously targeted therapeutics are an excellent way to deliver cargo directly to circulating platelets or leukocytes, similarly targeted therapeutics administered into the blood stream can be delivered directly to the vascular endothelial cells. Specifically, targeted carriers can be locally delivered to an area of inflammation or injury where the endothelium is upregulating cellular adhesion molecules, including selectins and cellular adhesion molecules[142]. Indeed, extensive prior research examined how vascular targeted drug carriers can be designed and

optimized for intravenous administration *in vivo*. In an *in vitro* blood flow model utilizing human cells, past work determined that micron-sized particles, not nano-sized particles, bound to an inflamed vascular wall best when functionalized with a sialyl Lewis A (sLe^A) targeting ligand that binds to E-selectin on the activated endothelial cell surface[143,144]. Binding of vascular targeted polymeric drug carriers can be further optimized by including two separate targeting ligands[145], such as sLe^A and ICAM-1, to better mimic the adhesion of leukocytes to an inflamed endothelium.

Modifying targeting mechanisms is not the only way to optimize a vascular targeted drug carrier for adhesion. Altering shape can also enhance particle adhesion; rod-shaped particles specifically are better able to bind to an inflamed endothelium than spherical particles[144,146,147]. Further, dense particles made of silica or titania exhibit improved adhesion to an inflamed endothelium in comparison to neutrally buoyant polymeric particles, despite having the same size[148]. Finally, deformable hydrogel microparticles outperform rigid hydrogel particles, specifically at low shear rate[149]; these hydrogel particles can be loaded with nanoparticle in a two-step method of particle adhesion and release of cargo that can be internalized by endothelial cells or enter tissue through leaky vasculature[150].

1.6 Dissertation Outline

Overall, there is an unmet need for *in vitro* blood flow models to study platelet adhesion and platelet-cell dynamics. The work described in this dissertation is focused first on the development of new *in vitro* models to study platelet adhesion. Second, we will focus on tuning that *in vitro* model to reflect conditions of thromboinflammation and will explore how particulate drug carriers can be used to impact platelet adhesion. Third, we will tune the model further to explore the behavior of platelets in sickle cell disease both using sickle cell blood and an artificial system of rigidifying healthy RBCs. We will use this model to screen novel therapeutics for sickle cell

disease. Finally, we will use the *in vitro* model to explore how a novel, extracellular matrix-based therapeutic to treat vascular damage behaves in human blood flow.

Chapter 1 provides background and motivation for the work presented in this dissertation, including an overview of major components in blood with a focus on platelets, methods to study platelets, key diseases that can impact platelet function and behavior, and the use of targeted and/or particulate drug carriers to modulate leukocyte and platelet behavior.

Chapter 2 describes materials and methods utilized in the experimental work throughout this entire dissertation.

In Chapter 3, we develop an *in vitro* human blood flow method for examining platelet adhesion to a 'damaged endothelium.' We discuss how different variables, including anticoagulant, shear rates, and activation level of platelets, impact platelet adhesion. Further, we explore how inflaming the endothelium impacts both platelet and leukocyte adhesion.

In Chapter 4, we utilize the inflamed, damaged endothelium *in vitro* blood flow model to elucidate how model polymeric particles can impact both leukocyte and platelet adhesion in a model of thromboinflammation. Specifically, we explore particles of varied size, shape, and targeting. We then explore how our *in vitro* findings that polymeric particles can modulate platelet-leukocyte aggregation adhesion can translate *in vivo* utilizing a murine mouse of systemic inflammation.

In Chapter 5, we explore the impact of stiffened RBCs on platelet behavior in two separate ways. First, we examine whole blood platelet adhesion from a sickle cell disease patient cohort and observed how essential variables, including treatment method, impacted platelet behavior. We then use a method to study stiffened RBC-platelet interactions using healthy donor blood that can be used to study these interactions in a more controlled environment. Finally, we use both sickle

cell patient blood samples and our idealized model to screen a novel, carbon monoxide-based therapy for its anti-platelet benefits.

In Chapter 6, we utilize the damaged endothelium *in vitro* blood flow model to explore the interactions between a novel extracellular matrix-based therapy and human blood and endothelial cells. The work in this chapter helps to bridge present work utilizing the therapy *in vivo* to its potential future uses in humans.

In Chapter 7, we conclude the dissertation and discuss potential future directions for this work.

Chapter 2 Materials and Methods

2.1 Introduction

The experimental protocols and materials described here were used to generate the data found in Chapters 3 through 6 and are in sufficient detail for the reproduction of the results described. Methods described here include preparing human blood for a variety of in vitro blood flow experiments ranging from whole blood flow to blood flow under conditions of inflammation to blood flow mimicking stiffened RBCs as seen in different disease states. Further, this chapter include a mouse model of systemic inflammation where blood cells and particles can be tracked in real time. The materials and their sources are listed within the specific subsection where that material was used.

2.2 Human and Animal Study Approvals

2.2.1 Non-SCD Human Study Approvals

Informed, written consent was obtained by all healthy blood donors according to a protocol approved by the University of Michigan Internal Review Board (IRB-MED; ID #HUM00013973). Phlebotomy was then performed with fresh human blood being obtained via venipuncture. Briefly, after researchers obtained consent from the subjects, research staff then attached a sterile butterfly needle to a syringe filled with warmed anticoagulant. Research staff then tied a tourniquet around the arm of the subject, cleaned the skin over the vein using a sterile alcohol pad, inserted a sterile butterfly needle into the vein, and slowly drew the desired amount of blood into the anticoagulant-containing syringe. After the draw was complete, research staff removed the needle, placed a clean

gauze over the incision, and remained with the subject until a clot fully formed. The clot was covered with a bandage or additional clean gauze. The anticoagulants used were either acid citrate dextrose (ACD), 3.2% sodium citrate, or heparin. For ACD and heparin, 7 mL anticoagulant were used for a total of 50 mL whole blood. For sodium citrate, 1 mL anticoagulant was used for a total of 10 mL whole blood. ACD is comprised of 111 mM dextrose (anhydrous), 100 mM sodium citrate tribasic dihydrate, and 71 mM citric acid monohydrate. If not stated otherwise, ACD was used as anticoagulant.

Umbilical cords (Mott Children's Hospital, Ann Arbor) were acquired under an IRB-MED approved human transfer protocol, which is exempt from informed consent (exempt ID #HUM00026898).

2.2.2 SCD Human Study Approvals

Both SCD donors and their legal guardians gave written, informed consent before blood collection. Blood draw protocols were again approved by the University of Michigan Internal Review Board (IRB-MED; ID #HUM00134561) and fresh blood was obtained on a day of the patient's routine clinical care via venipuncture (Mott Children's Hospital, Ann Arbor). Typically, 20 mL were drawn per day into standard Vacutainer Yellow ACD tubes. If blood draws were repeated, no more than 10 mL/kg was drawn from a single patient over a three month period of time by IRB guidelines.

2.2.3 Animal Study Approvals

All animal studies were conducted in accordance with the National Institute of Health guidelines for the care and use of laboratory animals and approved by the University of Michigan Institutional Animal Care and Use Committee (IACUC; approved animal protocol #PRO00010572). C57BL/6

mice were purchased from Jackson Laboratories and maintained in pathogen-free facilities at the University of Michigan.

2.3 Preparation and Functionalization of Particles

2.3.1 Production of Rod-shaped Polystyrene Microparticles

We produced rod-shaped particles of varying aspect ratios using a modified polymer stretching method[146]. Carboxylated polystyrene 2 μm diameter particles (Polysciences) were suspended in 7% w/v polyvinyl alcohol (PVA; Sigma Aldrich) and dried into a film. We then cut the film into strips and stretched them uniaxially at 200°C. We dissolved the stretched film in deionized water and washed the stretched particles in 70% isopropanol and deionized water to remove residual PVA. We imaged the particles using scanning electron microscopy (University of Michigan EMAL) and analyzed the images using ImageJ to calculate the aspect ratio (length of major axis: length of minor axis) of each particle type.

2.3.2 Production of PolyAspirin (PolyA) Particles

We produced particles from a polymer comprised of salicylic acid monomeric units (PolyAspirin, or 'PolyA;' produced by collaborators) using a single emulsion solvent evaporation technique, as described previously[137]. Briefly, we dissolved PolyA polymer in dichloromethane (Sigma Aldrich) and separately, mixed PVA solution on a stand mixer and added the polymer solution slowly to the PVA solution. Some of the PolyA polymer was conjugated to the fluorescent molecule cy5.5 (Lumiprobe) so the resultant particles would be fluorescently dyed for easy imaging via microscope. We allowed the solution to mix to evaporate the solvent, then washed and dried the particles. We imaged the particles using scanning electron microscopy (University of Michigan EMAL).

2.3.3 Production of PEGylated Polystyrene Particles

To PEGylate 2 μm particles, we conjugated fluorescent, carboxylated PS particles (Polysciences) with aminated, methoxy-terminated polyethylene glycol (PEG, 5k molecular weight; Sigma Aldrich) via carboimmide chemistry[151]. Briefly, we suspended 10 mg 2 μm PS particles in 500 μL 60 mg/mL PEG in 50 mM 2-(N-morpholino)ethanesulfonic acid buffer (MES; Sigma Aldrich) and allowed the mixture to rotate at room temperature for 15 minutes. After, we added 500 μL 120 mg/mL N-(3-dimethxylaminopropyl)-N'-ethylcarboimmide hydrochloride (EDC, Sigma Aldrich) to the particles and allowed them to rotate at room temperature overnight. We quenched the reaction with glycine (Sigma Aldrich) and washed the particles thoroughly with phosphate buffered saline (PBS. To quantify the PEG site density on the surface of the particles, we followed a similar protocol using rhodamine-labeled, amine terminated PEG (Nanocs) and utilized a microplate reader and rhodamine-PEG standard curve to calculate the PEG density[151,152].

2.3.4 Functionalization of Particles with Targeting Ligands

We conjugated carboxylated polystyrene particles (200 nm, 500 nm, 2 μm, or 4.5 μm; Polysciences) with NeutrAvidin (Thermo Fisher Scientific) through carboiimide chemistry[143]. For untargeted *in vitro* flow experiments, we then conjugated the avidin-functionalized particles with biotin rat IgG2b (Biolegend) to prevent non-specific binding to the inflamed endothelium. To quantify IgG2 site density, particles were stained with anti-rat IgG2b-phycoerythrin (PE, Biolegend) or biotin-PE (Invitrogen). We analyzed the stained particles and standard beads with known fluorescence (MESF beads, Bangs Laboratories) using flow cytometry using an Attune NxT Acoustic Focusing Cytometer. We used the MESF beads to create a calibration curve linking fluorescent intensity (median fluorescent intensity, 'MFI') and the number of fluorescent molecules on the particle. We held IgG2 site densities constant at 1,000 sites/μm^2. For targeted

experiments, we conjugated avidin-functionalized particles with biotinylated sialyl Lewis A (sLe^A), which were then stained with anti-CLA-PE to quantify the site density. We held sLe^A site densities constant at 1,000 sites/μm^2 for the 'low' site density targeting experiments and 13,500 sites/μm^2 for the 'high' site density targeting experiments.

For *in vivo* intravital experiments, we conjugated avidin-conjugated 2 μm PS particles with both anti-E-selectin (R&D Systems) and anti-ICAM-1 (Biolegend) for targeted experiments or anti-IgG2b isotype controls for untargeted experiments. The site density for dual targeted particles was 50,000 sites/μm^2 total with 30,000 anti-E-selectin sites/μm^2 and 20,000 anti-ICAM-1 sites/μm^2. The site density for untargeted particles was held constant at 30,000 anti-IgG2b sites/μm^2; site density quantified as described above. For untargeted 500 nm PS particles, the site density was kept at 30,000 anti-IgG2b sites/μm^2 to match the 2 μm experiments

We also conjugated polyA particles for *in vivo* experiments with avidin using carboimmide chemistry for two hours the night before use. To prevent particle degradation, we centrifuged particles and removed all liquid before storing the particles at -20°C. The following day, we conjugated the particles with anti-IgG2b and calculated their site density, as described above, and used the conjugated particles the same day for *in vivo* experiments.

2.4 Human Blood Characterization

2.4.1 SCD Patient Ektacytometry and Complete Blood Count

Phlebotomists drew SCD patient blood into K2-EDTA Vacutainer tubes, which were shipped directly at 4°C to the Erythrocyte Diagnostics Laboratory of the Cancer and Blood Diseases Institute at the Cincinnati Children's Hospital. The following day, lab personnel diluted SCD blood samples in polyvinylpyrrolidone and measured red blood cell (RBC) deformation using a LoRRca Maxsis Ektocytometer (Mechantronics Instruments BV). Cell deformation is represented using the

maximum elongation index, as described in previous work[153]. Lab personnel at the hematology lab at Michigan Medicine analyzed separate K2-EDTA-anticoagulated SCD patient samples for complete blood counts using a Sysmex 9100 XN automated machine. Lab personnel also evaluated the hemoglobin genotypes of each patient using a Bio-Rad Variant II cation exchange high performance liquid chromatography (HPLC) system.

2.4.2 SCD and Healthy Donor Platelet Activation Analysis

We analyzed ACD-anticoagulated SCD and healthy donor whole blood samples for levels of platelet activation. Briefly, we stained 100 µL of donor whole blood with anti-CD41/61 PE (Biolegend) and anti-CD62P APC (Biolegend) for ten minutes at 37°C. After staining, we fixed each sample for five minutes at 37°C using an equal volume of 4% paraformaldehyde (Thermo Fisher Scientific) and washed each sample three times with phosphate buffered saline (PBS) containing calcium and magnesium. We analyzed each sample using flow cytometry within 20 hours using an Attune NxT Acoustic Focusing Cytometer. Specifically, we gated single cells and then identified the platelet population via forward and side scatter. We then used the platelet-specific stain, CD41/61 PE, to confirm the platelet population before quantifying the percentage of the platelets that expressed CD62P APC as a marker of relative platelet activation levels.

For some experiments, we mixed platelet rich plasma (PRP) with artificially rigidified RBCs, described in more detail below, and allowed the RBCs to settle in static for ~2 hours. For some samples, we activated the PRP/RBC mixture with 20 µM adenosine diphosphate (ADP; MP Biomedicals) at the time of mixture. After, we gently pipetted 100 µL PRP from the mixture and stained the platelets with anti-CD41/61 PE and anti-CD62P for analysis using flow cytometry, as described in the paragraph above. We evaluated the P-selectin expression of each condition relative to the 0% RBC rigidified condition for each donor.

2.4.3 Healthy Donor Leukocyte Activation Analysis

We drew whole blood into ACD-anticoagulant. To separate out white blood cell (WBC)-containing PRP from RBCs, we added 1.4 mL dextran to 10 mL anticoagulated whole blood and mixed it well to coat the RBCs, which then settled for two hours at 37°C. We mixed the WBC-containing PRP with artificially rigidified RBCs, described in more detail below, and allowed the RBCs to settle in static for ~2 hours. After settling, we pipetted 100 µL WBC-containing PRP from the mixture and stained the leukocytes with anti-CD45 FITC, anti-CD11b Brilliant Violet 421, anti-CD11a APC, and anti-CD62l APC/Cy7 (all from Biolegend) on ice for 20 minutes. After staining, we added an equal volume of 4% paraformaldehyde to fix the cells for 15 minutes at room temperature and washed the WBCs three times with PBS. We analyzed the leukocytes for activation level and change in cell adhesion molecule expression change using an Attune NxT Acoustic Focusing Cytometer. Specifically, we gated single cells, then $CD45^+$ cells, and then identified the monocyte and neutrophil populations via forward and side scatter. We evaluated the median fluorescent intensity (MFI) of the monocyte and neutrophil populations separately, examining CD11b, CD11a, and CD62L expression levels as fold change over the 0% rigidified sample for each donor.

2.5 *In vitro* Microscopy Flow Assays

2.5.1 Preparation of Endothelial Cell Monolayer

We acquired umbilical cords (Mott Children's Hospital, Ann Arbor) under an IRB-MED approved human transfer protocol. We obtained human umbilical vein endothelial cells (HUVEC) using a collagenase perfusion technique[154] and pooled three or more umbilical cords per batch. Briefly, we rinsed umbilical cord veins with PBS buffer containing 1% glucose and incubated them with

collagenase. After a 20 minute incubation, we rinsed umbilical veins with media and the resultant cells were centrifuged at 500g to pellet. We cultured HUVEC in T75 flasks until confluent at 37°C and 5% CO_2 using M199 media supplemented with fetal bovine serum (10%), bovine calf serum (10%), penicillin/streptomycin (1%), fungizome (1%), glutamine (1%), HEPES (1%), and heparin (1%) and endothelial cell growth supplement. We utilized HUVEC between passages one and six for these experiments.

We prepared glass coverslips (Warner Instruments) by crosslinking 1% gelatin (Sigma Aldrich) with 0.5% glutaraldehyde (Fisher Scientific), which was quenched with 0.1M glycine (Sigma Aldrich) and washed with PBS (Thermo Fisher)[155]. We cultured isolated HUVEC at 37°C and 5% CO_2 until confluent, then trypsinized the HUVEC and seeded them onto the glutaraldehyde-crosslinked gelatin coverslips at least 36 hours before use.

2.5.2 Parallel Plate Flow Chamber (PPFC) Set-up

We treated the HUVEC with inflammatory stimuli depending on the specific experiment. Then, we attached the coverslip to a parallel plate flow chamber (PPFC; Glycotech) fitted with a silicone gasket (2 cm x 0.25 cm x 127 μm in height) via vacuum pump and attached the outlet to a syringe pump (KD Scientific). The blood or blood components were perfused over the damaged HUVEC perpendicular to the scalpel scores for 5 minutes at a fixed wall shear rate described by Equation 1:

$$\gamma_w = \frac{6Q}{h^2 w} \qquad (1)$$

Where Q is the volumetric flow rate (mL/s), h is the channel height (0.0127 cm), and w is the channel width (0.25 cm). We monitored the HUVEC and blood components throughout the course of the experiments utilizing an upright fluorescent microscope (Nikon Eclipse Ti) and used a digital camera (Andor) to take photos of the HUVEC and/or adherent cell types after rinsing the chamber according to the specific experiment.

2.5.3 Anti-vWF Staining and Analysis

In experiments testing different agonists to induce von Willebrand factor (vWF) secretion in Chapter 3, we activated HUVEC on coverslips with calcium ionophore (10 μM; Fisher Scientific) for 10 minutes, or histamine (100 μM; Acros Organics) for 2 minutes with or without mechanical injury with a scalpel before being attached to a PPFC. To visualize vWF multimer strands, we flowed 5 μg/mL anti-vWF-FITC (Novus Biologicals) over the endothelium for 5 minutes and rinsed the coverslips with flow buffer for 5 minutes. We took 10 fluorescent images of vWF multimers around the scalpel scores and used ImageJ to calculate the median fluorescent intensity (MFI) and surface coverage of vWF on the HUVEC.

2.5.4 Platelet Adhesion Assays

To examine platelet adhesion in the absence of underlying endothelial inflammation, we obtained human whole blood via venipuncture and drawn into acid citrate dextrose (ACD), 3.2% sodium citrate, or heparin. If the anticoagulant used is not directly stated, we utilized ACD for anticoagulation. For some experiments, we adjusted the hematocrit of the anticoagulated blood to 40% using packed RBCs or extra plasma obtained from the same donor to normalize for the known impact of hematocrit on platelet accumulation *in vivo* and *in vitro*[54,156].

To isolate platelets, we obtained platelet-rich plasma (PRP) through whole blood centrifugation at 200g for 20 minutes. We added an additional 10% ACD and 1 μL apyrase (New England Biolabs) per 2.5 mL PRP to prevent platelet activation during a 10 minute, 1000g centrifugation. We resuspended isolated platelets in a 'flow buffer' solution of phosphate buffered saline containing calcium and magnesium ions (PBS $^{+/+}$; pH 7.4; Thermo Fisher) with 1% BSA (Sigma Aldrich). We obtained packed RBCs through a centrifugation of whole blood at 2250g for 10 minutes and washed with PBS. We combined isolated platelets with washed RBCs at a 40% hematocrit for experiments utilizing isolated platelets with RBCs in flow buffer.

One hour prior to blood flow experiments, we stained isolated platelets or platelets in whole blood with 5 μL/mL anti-CD41/61 PE (Biolegend) and where stated, activated the platelets with 20 μM ADP (MP Biomedicals) for one hour to induce platelet activation and aggregation similar to prior publications[157–160].

Where stated in Chapter 3, we treated whole blood with 50 μM Bimosiamose (MedChemExpress) or with 10 μM ticagrelor (Cayman Chemical Company) in other experiments for one hour prior to use in flow experiments. In other experiments, we pretreated HUVEC with 1 or 50 μM Cimetidine (Alfa Aesar) five hours prior to use in flow experiments.

We mildly agonized a HUVEC monolayer with 100 μM histamine for two minutes. After two minutes, we used a scalpel to scratch the coverslip with parallel lines to induce an acute vascular injury and expose the underlying extracellular matrix (ECM) proteins. We then attached the damaged HUVEC coverslip to the PPFC and perfused it with blood or blood components as described above. After five minutes of laminar flow, we took 10 digital fluorescent images of the damaged HUVEC monolayer and utilized ImageJ to calculate the surface coverage by platelets. The 'damaged endothelium' images were taken around the scalpel score. Using ImageJ, we

subtracted the background fluorescence for each image and set a threshold for the image. ImageJ then automatically calculated the percentage of the image covered with platelets.

2.5.5 Platelet Adhesion to Functionalized Glass Coverslips

For experiments where we examined platelet adhesion to patterned proteins instead of a HUVEC monolayer in Chapter 3, we cleaned glass coverslips (Warner Instruments) with Piranha solution (3:1 concentrated sulfuric acid: 30% hydrogen peroxide; Fisher Scientific) and silanated the covesrlips with 2% 3-(trimethoxylsilym)propyl methacrylate (MPS; Sigma Aldrich) by volume in 95% ethanol for 30 minutes. We coated the cleaned coverslips with 1 mg/mL collagen (Corning) or gelatin (Sigma Aldrich) for 2 hours at room temperature, rinsed the coverslips with PBS, then attached the coverslips to the PFFC and perfused them with blood and analyzed the surface for platelet adhesion as described above.

2.5.6 Platelet-Leukocyte Adhesion Assays

For experiments where we examined both leukocyte and platelet adhesion to an inflamed HUVEC monolayer in Chapter 3 and 4, we activated HUVEC with 1 ng/mL IL-1β (Fitzgerald) in complete media for four hours prior to use in flow experiments. Immediately before blood flow, we also activated the HUVEC with 100 μM histamine for two minutes and scored the HUVEC surface with a scalpel to maintain consistency with previous flow experiments. We stained platelets with anti-CD41/61 PE and activated the platelets with 20 μM ADP where stated, as described above. We attached the inflamed, damaged HUVEC monolayer to the PPFC and perfused stained, activated whole blood over the surface at $1000s^{-1}$ [143]. After five minutes of laminar flow and two minutes of rinsing with flow buffer, we imaged adherent platelets using fluorescent microscopy

and adherent leukocytes using brightfield images. We quantified platelet adhesion as described above and manually counted firmly adherent leukocytes using ImageJ's Cell Counter function.

For experiments examining the impact of particulate drug carriers on platelet and leukocyte adhesion in Chapter 4, we added particles immediately to blood prior to blood flow and mixed the particles gently using a micropipetter. We utilized ACD-anticoagulated blood to inhibit phagocytosis of the particles by WBCs.

2.5.7 SCD Blood Flow Assays

For experiments examining the behavior of SCD blood in flow in Chapter 5, phlebotomists drew SCD patient blood into ACD-anticoagulated vacutainers (BD Biosciences); we picked patient samples up directly from the hospital or had them delivered by hospital personnel shortly after blood draw. We stained SCD patient blood samples using 5 μL/mL blood anti-CD41/61 PE (Biolegend) for 30 minutes prior to blood flow and perfused the blood over a histamine-activated, scalpel-scored HUVEC monolayer at 100, 500, or 1000s^{-1}. We treated some SCD patient samples with 20 μM CORM-A1 (Sigma Aldrich) or CORM-401 (Sigma Aldrich) for 30 minutes prior to blood flow. Upon receipt, we resuspended CORM-A1 in deionized water and CORM-401 in dimethylsulfoxide (DMSO; Fisher Scientific) and froze individual aliquots of each for single-time use. For some SCD patients, we also treated their blood with an 'inactivated' form of CORMs, where CO has been released and only the CORM scaffold remains. To produce inactivated CORM-A1 or CORM-401 (iCORM-A1 or iCORM-401), we allowed CORMs to remain at room temperature overnight and perfused argon through the aliquot. After five minutes of laminar blood flow and two minutes of rinsing the surface with flow buffer, we took 10 images near the scalpel score and analyzed the images for platelet adhesion using ImageJ as described above.

2.5.8 Artificially Rigidified RBC Flow Assays

For experiments utilizing artificially rigidified RBCs in Chapter 5, we acquired venous blood via venipuncture into ACD anticoagulant and stored the blood at 37°C. We then acquired platelet-rich plasma (PRP) via whole blood centrifugation at 200g for fifteen minutes and stored at 37°C until use. One hour prior to blood flow assays, we stained the PRP with 5 μL/mL anti-CD41/61 PE (Biolegend) and unless otherwise stated, activated the PRP with 20 μM ADP (Acros Organics).

We isolated red blood cells (RBCs) via centrifugation at 2250g for ten minutes and washed them twice with PBS to remove contaminating buffy coat cells. We artificially rigidified select fractions of the isolated RBCs using a 2% hematocrit solution of *tert*-butyl hydroperoxide (TBHP) for thirty minutes as described previously[153,161,162]. We used 1.0 mM TBHP to produce 'highly rigid' RBCs, 0.75 mM TBHP to produce 'moderately rigid' RBCs, and 0.5 mM TBHP to produce the 'least rigid' RBCs.

After rigidification, we washed the RBCs once with PBS. PRP, healthy RBCs, and artificially rigidified RBCs were reconstituted to a specific hematocrit (40% unless otherwise stated) and volume fraction of RBCs that are rigidified (ranging from 0% in a healthy, non-rigid sample to 100% for a completely rigid sample) immediately before blood flow.

For experiments with varied (20, 40, 60%) hematocrit, we obtained plasma from the blood sample after removal of PRP through a centrifugation at 2250g for eight minutes. In the 60% hematocrit sample, we combined 0.8 mL PRP (40% v/v) with 1.2 mL RBCs (60% v/v) with no added plasma. In the 40% hematocrit sample, we combined 0.8 mL PRP with 0.8 mL RBCs (40% v/v) with an additional 0.4 mL plasma (20% v/v). In the 20% hematocrit sample, we combined 0.8 mL PRP with 0.4 mL RBCs (20% v/v) with an additional 0.8 mL plasma (40% v/v). In this way, we fixed the number of platelets for each donor with varying hematocrit. For experiments utilizing

whole blood flow, we added 1.4 mL dextran to 10 mL anticoagulated whole blood and mixed it well to coat the RBCs, which then settled for two hours at 37°C. We stained and activated the WBC-containing PRP and mixed them with rigidified RBCs as described above.

We flowed a mixture of PRP and healthy and rigid RBCs over a histamine-activated and scalpel-scored HUVEC monolayer at 500, 1000, or 1500s^{-1} for five minutes of laminar flow. We utilized WBC-containing PRP and RBCs at 1000s^{-1}. For pulsatile flow experiments, we programmed a syringe pump to induce pulsatile flow[143]. In short, the pump was programmed to loop fourteen seconds of forward flow, followed by seven seconds of reverse flow at a shear rate of 1000s^{-1} for a total of fifteen minutes of flow. The choice of this flow pattern and length of time ensured the same volume of blood passes through the channel as during a five minute laminar flow experiment. After each experiment, we rinsed the PPFC for two minutes with flow buffer, took 10 fluorescent images of bound platelets to the scalpel score, and analyzed the platelet surface coverage using ImageJ.

For some flow experiments, we mixed PRP and a combination of healthy and rigid RBCs together along with 50 μM CORM-A1, CORM-401, iCORM-A1, or iCORM-401 for 30 minutes prior to platelet stain and activation for one hour prior to blood flow to the 'damaged endothelium.'

2.5.9 Anti-vWF and anti-P-selectin Staining with Artificially Stiffened RBCs

We isolated plasma from ACD-anticoagulated whole blood and artificially stiffened a fraction of the RBCs. We flowed the mixture over an undamaged HUVEC monolayer for five minutes of laminar flow using a PPFC. After two minutes of rinsing with flow buffer to remove excess blood components from the surface, we stained the HUVEC surface with anti-vWF-FITC (Novus Biologicals; 1 μg/mL) and anti-P-selectin PE (Biolegend; 1 μg/mL). After a five minute rinse with flow buffer, we took 10 fluorescent images using the FITC (anti-vWF) and TRITC (anti-P-

selectin) channels. We then utilized ImageJ to calculate the surface coverage of vWF and P-selectin in comparison to a 0% rigid RBC sample for each independent donor.

2.5.10 Infusible Extracellular Matrix (iECM) Perfusion over HUVEC

In Chapter 6 experiments examining the interactions between an infusible extracellular matrix (iECM) and human endothelial and blood cells, we utilized three different methods of HUVEC damage and inflammation. For experiments mimicking acute vascular injury, we manually 'damaged' HUVEC via parallel scalpel scores to expose the underlying ECM. For experiments mimicking severe inflammation, we activated HUVEC for 24 hours with 100 ng/mL tumor necrosis factor α (TNF- α) in cell media to increase vascular permeability[163]. For experiments mimicking vascular damage with moderate inflammation, we first activated HUVEC for 4 hours with 10 ng/mL TNF- α and then manually damaged the HUVEC using scalpel score to expose the ECM. We also drew venous blood into ACD anticoagulant and isolated plasma and washed RBCs, as described in above sections.

For experiments examining iECM adhesion to damaged or inflamed HUVEC, we mixed thawed aliquots of iECM (produced by the Christman laboratory at UCSD) and resuspended them to a concentration of 10 mg/mL in sterile water. We resuspended Alexa Fluor 555 NHS Ester (Succinimidyl Ester) ('AF555;' ThermoFisher Scientific) to 10 mg/mL in DMSO and mixed together iECM with AF555 at a ratio of 100:1 (v/v) for one hour at room temperature to fluorescently label the iECM. After, we further diluted iECM-AF555 in sterile PBS and added iECM-AF555 at a final concentration of 1 mg/mL to a mixture of isolated human plasma and RBCs at 40% hematocrit. For non-iECM control experiments, we added the equivalent volume of sterile PBS to a plasma/RBC mixture at 40% hematocrit instead. We then flowed the iECM-AF555, plasma, and RBC mixture over an inflamed or damaged HUVEC monolayer using a PPFC

at $100s^{-1}$ or $1000s^{-1}$ for 5 minutes of laminar flow. Afterward, we thoroughly rinsed the PPFC with flow buffer and utilized an inverted microscope and digital camera to take 10 images of the endothelium and 10 fluorescent images of iECM-AF555 utilizing a TRITC filter. For experimental conditions involving a 'damaged' endothelium, we took images along the scalpel score.

2.5.11 Infusible Extracellular Matrix (iECM) Impact on Platelet Adhesion to HUVEC

In Chapter 6 experiments examining the impact of iECM on platelet adhesion, we utilized just the 'damaged endothelium' model without TNF stimulation. We drew venous blood into ACD anticoagulant without further manipulation. We stained platelets in whole blood 1 hour prior to flow using anti-CD41/61 FITC (Biolegend). We added iECM-AF555 (or PBS for non-IECM controls) to whole blood at a final concentration of 1 mg/mL immediately before flowing over a damaged HUVEC monolayer at 100 or $1000s^{-1}$. After 5 minutes of laminar blood flow and rinsing, a digital camera was utilized to take 10 images of the endothelium, iECM-AF555 (TRITC filter), and adherent platelets (FITC filter).

2.6 Intravital Microscopy

We briefly anesthetized female C57BL/6 mice (aged 3-4 weeks, ~20 g) using isofluorane and gave mice a retro-orbital (RO) injection of anti-Ly6G Brilliant Violet 421 (Biolegend), anti-GP1b DyLight 649 (Emfret Analytics), and a 10 mg/kg 2 µm polystyrene particle dosage ($\sim 4.5*10^7$ particles) for mice receiving a 'preventative' particle treatment. We conjugated particles with anti-E-selectin and anti-ICAM-1 ('targeted') or anti-IgG2b ('untargeted') as described above. The mice then received an intraperitoneal (IP) injection of 5 mg/kg lipopolysaccharide (LPS from *E. coli* O111:B4; Sigma Aldrich) in 100 µL PBS to induce systemic inflammation[164,165]. We administered an 'intervention' particles treatment to anesthetized mice 2 hours after LPS IP injection of 10

mg/kg 2 μm polystyrene via RO injection. 3 hours after IP LPS injection, mice were anesthetized with a mixture of ketamine and xylazine and mesentery visualized as described previously[149,166]. Briefly, after anesthetization, we made a midline incision, and exteriorized the mesentery. Mice were placed on a custom-made microscopic stage with exposed mesentery on a glass coverslip. Mesentery vessels were visualized using a 25x oil objective on an inverted fluorescence microscope (Zeiss Axio Observer Z1Marianas) using Slidebook 6 software. We imaged mesenteric blood vessels veins of approximately 150 μm every 100 ms using both brightfield and fluorescent microscopy using DAPI, GFP, and Cy5 fluorescent channels to image $Ly6G^+$ neutrophils, polystyrene particles, and $GP1b^+$ platelets, respectively. Each vessel was imaged for 15 seconds. 2-4 independent vessels were imaged per mouse.

For some experiments, we varied the type of particles. We administered 'prevention' anti-IgG2b conjugated PolyA particles to one experiment group of mice (also at 10 mg/kg; ~$5.18*10^7$ particles/mouse); for these mice, we instead stained platelets with anti-GP1b Alexa Fluor 488 so polyA-Cy5.5 particles could be imaged using the Cy5 fluorescent channel. For other experiments, we utilized 'prevention' untargeted 500 nm PS particles (10 mg/kg; ~$2.9*10^9$ particles), which could be visualized using the GFP microscope filter like the 2 μm PS particles. In separate experiments, we injected mice with a 'prevention' of PEGylated 2 μm PS particles (10 mg/kg; ~$4.5*10^7$ particles), which also could be visualized with the GFP microscopy filter.

For some experimental groups, we depleted neutrophils from mouse circulation prior to intravital microscopy. First, we measured a baseline complete blood count for each mouse using saphenous vein blood draws collected into EDTA-coated tubes and measured using a Hemavet Analyzer (Drew Scientific). We then administered an IP injection of 500 μg anti-Ly6G depletion antibody (Biolegend). One day later, we measured the complete blood count for each mouse again

and utilized mice whose neutrophil counts were depleted to the minimum normal range or below. Depletion mice also receive an additional 200 μg anti-Ly6G, administered at the same time as labeling antibodies via RO injection. A subset of these mice also received a 'prevention' treatment of 2 μm untargeted PS particles, as described in above paragraphs. We confirmed that neutrophil depletion was maintained by again measuring the complete blood count of mice with blood samples obtained via cardiac puncture after euthanasia.

We blinded file names and performed image analysis using ImageJ and Slidebook 6. We recorded the number of adherent particles, neutrophils, and platelets, which were considered firmly adherent if they did not move over the course of the 15 second video. We counted non-adherent neutrophils passing through the frame. We also counted the number of platelets associated with neutrophils; platelets and neutrophils were considered associated if the platelet and neutrophil maintained contact for the entire 15 second video. The size of the vessel was calculated using ImageJ and the number of adherent particles and cells was scaled per mm^2 of the vessel.

2.7 Statistics and Data Analysis

For all studies, no outliers were excluded, and all data points were included in analysis. In general, data are represented with standard error of the mean (SEM). Specific statistical analysis utilized for each experiment is described within each figure caption and unless stated were analyzed using GraphPad Prism. Asterisks or pound signs indicate p values of * < 0.05, ** < 0.01, *** < 0.001, and **** < 0.0001. A lack of asterisks or pound signs indicate a lack of significance (ns).

For *in vitro* PPFC flow experiments involving HUVEC, each data point represented is the average of 10 fluorescent or brightfield images from each individual experiment. For example, 10 non-fluorescent images of bound leukocytes and 10 fluorescent images of bound platelets were taken for each independent donor for experiments described in Chapter 4. Unless otherwise stated,

$n \geq 3$ independent donors were utilized for experiments involving platelet adhesion (Chapter 3 and Chapter 5) and $n = 5$ used for experiments evaluating the impact of particles on platelet and leukocyte adhesion (Chapter 4). For *in vitro* flow experiments utilizing SCD blood, $n = 1$ for each donor unless otherwise stated. For *in vivo* experiments visualizing mouse mesentery vessels, 2-4 independent vessels were imaged per mouse with $n = 5$ mice for each experimental group, unless otherwise stated.

Chapter 3 Developing an *In Vitro* Blood Flow Model to Advance the Study of Platelet Adhesion Utilizing a Damaged Endothelium

3.1 Publication Information

Much of the work written in this chapter is published as "An *in vitro* blood flow model to advance the study of platelet adhesion utilizing a damaged endothelium" in *Platelets* with author list **Alison Banka** and Omolola Eniola-Adefeso. Modifications of the published work have been made to adapt the content to this chapter.

3.2 Abstract/summary

Platelets play a key physiological role in preventing bleeding after a blood vessel injury (hemostasis) but can also contribute to inflammation and uncontrolled clotting (thrombosis). Methods to study platelet behavior include *in vivo* animal models, which may be costly and not representative of platelet behavior in humans, or *in vitro* blood flow models. These *in vitro* models typically either utilize only an intact endothelium or a single extracellular matrix protein, both of which neglect key binding motifs for platelets. In this work, we develop an improved *in vitro* blood flow model that incorporates both an inflamed endothelium and underlying extracellular matrix proteins for platelet adhesion. Further, the 'damaged endothelium' model can be altered to include binding of leukocyte-platelet aggregates, a hallmark of inflammatory diseases. We show that this model is both tunable and supports platelet adhesion utilizing a variety of blood flow shear rates, anticoagulants, and extracellular matrix proteins of interest. To verify this model, we highlight that ticagrelor, a known anti-platelet compound, significantly decreases platelet adhesion to the

damaged endothelium. Further, we demonstrate that two other potential therapeutics, a pan-selectin inhibitor and histamine receptor antagonist, also significantly decrease platelet adhesion. Overall, the work describes a new *in vitro* blood flow model that can be utilized to study platelet adhesion under a variety of physiological conditions.

3.3 Background and Introduction

Platelets must maintain a balancing act *in vivo* due to their contributions to both health and disease. The adhesion of platelets to the site of vascular injury is a key early step in both hemostasis and thrombosis and involves multiple points of binding between glycoproteins (GP) on platelets and the damaged vasculature. A low platelet count or underperforming platelets can disrupt hemostasis, leading to bleeding risk[14]. In contrast, excess or overactive platelets can contribute to thrombosis[15], cardiovascular events[15,16], and inflammation[17] in various diseases; overall, there is great interest in understanding the contributions of different receptors and signaling molecules that tip the balance from hemostasis to thrombosis.

Researchers often use thrombosis animal models, especially murine models, to study thrombosis in humans. However, major differences between mouse and human physiology and the development of disease can make translating findings from animal models to humans difficult or inaccurate[42]. Therefore, many researchers utilize *in vitro* flow assays with human platelets or whole blood, including the use of microfluidic devices[55] that may require custom design and fabrication, to study platelet adhesion and behavior contributing to hemostasis and thrombosis. These *in vitro* assays typically fall under one of two categories: platelets under flow conditions adhere to either patterned extracellular matrix (ECM) proteins[55] or an inflamed, intact endothelium that supports platelet adhesion[56,57]. Utilizing ECM proteins or other factors alone allows for tight control of platelet adhesion to one or more specific binding motifs but neglects the essential role

the damaged endothelium plays in regulating thrombosis and hemostasis[167]. Similarly, an intact endothelium alone does not include adhesion of platelets to the subendothelial matrix, a key first step in platelet aggregation and adhesion upon vascular injury[18].

A damaged or activated endothelium contributes to the coagulation cascade through upregulation of tissue factor[168] and suppression of thrombomodulin expression[169], among others. When the endothelium is activated, it releases Weibel-Palade bodies containing ultra-long vWF multimers and P-selectin[24]. The ultra-long vWF multimers can tether soluble vWF present in plasma and directly bind platelets from flowing blood. The link between high or dysregulated vWF levels and thrombotic diseases has been well established using data from both clinical trials and animal models[170]. Consequently, inclusion of an endothelium that can produce vWF-containing Weibel-Palade bodies and tether vWF is essential for studying platelet behavior in thrombosis and hemostasis. In addition to vWF multimers, Weibel-Palade bodies also contain P-selectin. Upon release, P-selectin can directly bind both platelets and leukocytes and recruit them to the growing thrombus[61]. Prolonged endothelial inflammation leads to expression of other cellular adhesion molecules, e.g. ICAM-1 and E-selectin, to further recruit circulating leukocytes to the thrombus[142]. Adherent leukocytes bound to the endothelium can then bind to platelets via cell-cell interactions[61], demonstrating yet another way that the endothelium impacts platelet behavior.

Beyond clot formation, the endothelium continues to play a role in clot resolution by secreting ADAMTS-13, an enzyme in plasma that cleaves ultra-long vWF multimers into smaller, less thrombogenic fractions. Reduced ADAMTS-13 activity is associated with increased risk of thrombotic events, including ischemic stroke and cardiovascular disease[171,172]. Thus, recombinant ADAMTS-13 is being explored as a therapeutic in thrombotic diseases[173]. All of these facts

highlight the importance of including the endothelium in an *in vitro* model designed to study thrombus resolution.

Indeed, endothelialized microfluidic models for studying platelet behavior have gained recent attention in the literature[56,57]. For example, researchers recently developed a novel, biologically patterned 3D hydrogel that supports endothelial cell growth[58] and other research established a 3D endothelial cell-pericyte co-culture microfluidic 'blood vessel' *in vitro*[59]. While these new models represent steps towards producing more physiological, 3D blood vessels *in vitro*, they have not yet been utilized to study platelet behavior. Moreover, a commonality between previous endothelialized microfluidic models is the reliance on a completely confluent endothelial cell monolayer, i.e., an absence of a vascular injury, which does not allow for a critical first step in platelet aggregation – platelet adhesion to the underlying extracellular matrix (ECM)[18].

One recent work attempts to include the ECM by examining platelet adhesion to a deliberately non-confluent endothelium[174]. Unfortunately, this approach is likely to yield a wide variation in ECM spacing between endothelial cells, i.e., where platelet adhesion occurs. Such lack of tight control over the ECM spacing likely limits the consistency of platelet adhesion observed across experiments. Further, in this work the endothelial cells utilized were not stimulated, which omits the endothelium's role in platelet adhesion through the release of vWF and expression of cell adhesion molecules. Cell adhesion molecules can include P-selectin[61], plus E-selectin and ICAM-1 if inflammation is sustained over longer time periods[142]. All of these cell adhesion molecules have the ability to bind passing leukocytes from blood flow, which can further recruit platelets to the area of inflammation[61,79]. With that, *in vitro* models to study platelet adhesion should be tunable and have the ability to examine platelet-leukocyte interactions due to the

importance of those interactions in many thromboinflammatory diseases, including sickle cell disease[175] and COVID-19[176].

Overall, there is an unmet need for an improved and tightly controlled *in vitro* model that incorporates all components of a damaged vasculature *in vivo*. Here, we describe a 'damaged endothelium model' that combines a functional inflamed endothelium with a pronounced and consistent exposed ECM, i.e., injury area. This model is straightforward, highly tunable, and allows for platelet adhesion in whole blood, both to the underlying ECM and the adjacent injured endothelium, which creates an opportunity to elucidate the complex dynamics of platelet functions in human health and disease. Further, we demonstrate that this model successfully screens potential anti-inflammatory and anti-thrombotic molecules that target either platelets or the endothelium.

3.4 Results

3.4.1 Development and characterization of the 'damaged endothelium' model for platelet adhesion

The first essential step in developing an *in vitro* model to study human platelet adhesion and behavior under flow conditions is to determine a reliable agonist for the section of von Willebrand factor (vWF) multimers from endothelial cells. vWF plays an essential role in both platelet rolling and adhesion to inflamed endothelial cells[18], which is an important first step in platelet aggregation at the point of vascular injury. Two commonly used chemical agonists to induce vWF secretion include histamine and calcium ionophore[177]. To test these two compounds, we activated a HUVEC monolayer with 100 μM histamine for 2 minutes or 10 μM calcium ionophore for 10 minutes in complete media with or without mechanical injury using a scalpel to expose the underlying extracellular matrix (ECM) proteins. Then we attached the HUVEC to a

parallel plate flow chamber, stained with anti-vWF-FITC for 5 minutes, thoroughly rinsed the chamber to remove excess antibody, and then imaged the HUVEC using a fluorescent microscope. We stained the HUVEC within the chamber in flow to prevent cleavage of vWF strings by the enzyme ADAMTS-13 that is secreted by HUVEC[24,25]. Using ImageJ software, we calculated the median fluorescence intensity (MFI) and area coverage of vWF; the change in MFI and area coverage were calculated as fold change over unstimulated HUVEC from the same day and batch of cells to negate any differences between cell passages or batches. The fold change in vWF MFI and area coverage as well as representative images are shown in Figure 3.1. Figure 3.1A demonstrates that all agonists or combinations of agonists lead to an increase in vWF secretion in comparison to unstimulated controls. However, the largest increases in vWF secretion came from a combination of chemical and mechanical stimulus (either histamine and scalpel score or calcium ionophore and scalpel score). Further, Figure 3.1B shows that histamine either alone or in combination with scalpel score led to a consistent, large increase in area coverage by vWF. The representative images shown in Figure 3.1C highlight this increase in vWF secretion, particularly

around the scalpel score. Due to its clear increase in vWF release from HUVEC, a combination of histamine and mechanical injury via scalpel score was chosen for future experiments.

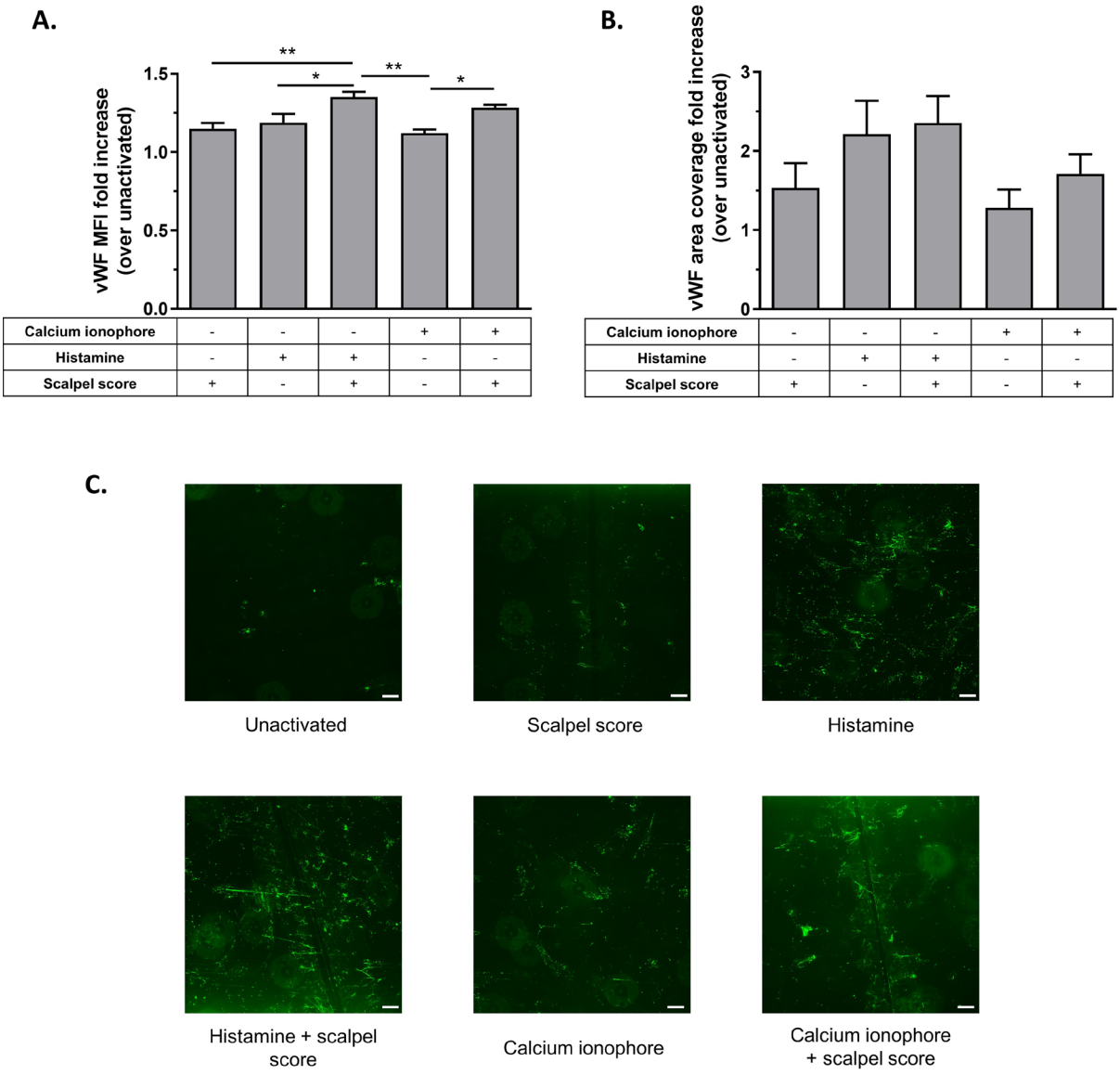

Figure 3.1: Maximizing vWF secretion from HUVEC.

(A) Change in median fluorescent intensity (MFI) of von Willebrand factor secreted by cultured HUVEC in comparison to unstimulated controls, (B) Change in area coverage of von Willebrand factor secreted by cultured HUVEC in comparison to unstimulated controls, (C) Representative images of vWF (green) on endothelial cells activated with different stimulants, scale bar 100 µm. Statistical analyses were performed using one-way ANOVA with Tukey's multiple comparisons test, where (*) indicates $p<0.05$, and (**) indicates $p<0.01$.

A schematic of this model is shown in Figure 3.2A. First, confluent HUVEC are stimulated with histamine. Then, the confluent HUVEC are subject to mechanical injury via scalpel score. Next, the inflamed, damaged HUVEC are attached a parallel plate flow chamber via vacuum. Blood or blood components can then be perfused over the HUVEC using a syringe pump while monitored in real time using microscopy. Figure 3.2B demonstrates that the 'damaged endothelium' model facilitates the adhesion of ADP-activated human platelets (red) to both tethered vWF multimers (long strings, green) and to the underlying ECM proteins (immediately around the scalpel score). Manual damage via scalpel scores resulted in a 'gap' in the confluent HUVEC monolayer of approximately 157 ± 3 μm; a representative brightfield image of the damaged HUVEC, with an endothelial cell-free gap visible, and overlaid with a fluorescent image showing adherent, fluorescently-labelled platelets shown in Figure 3.2C.

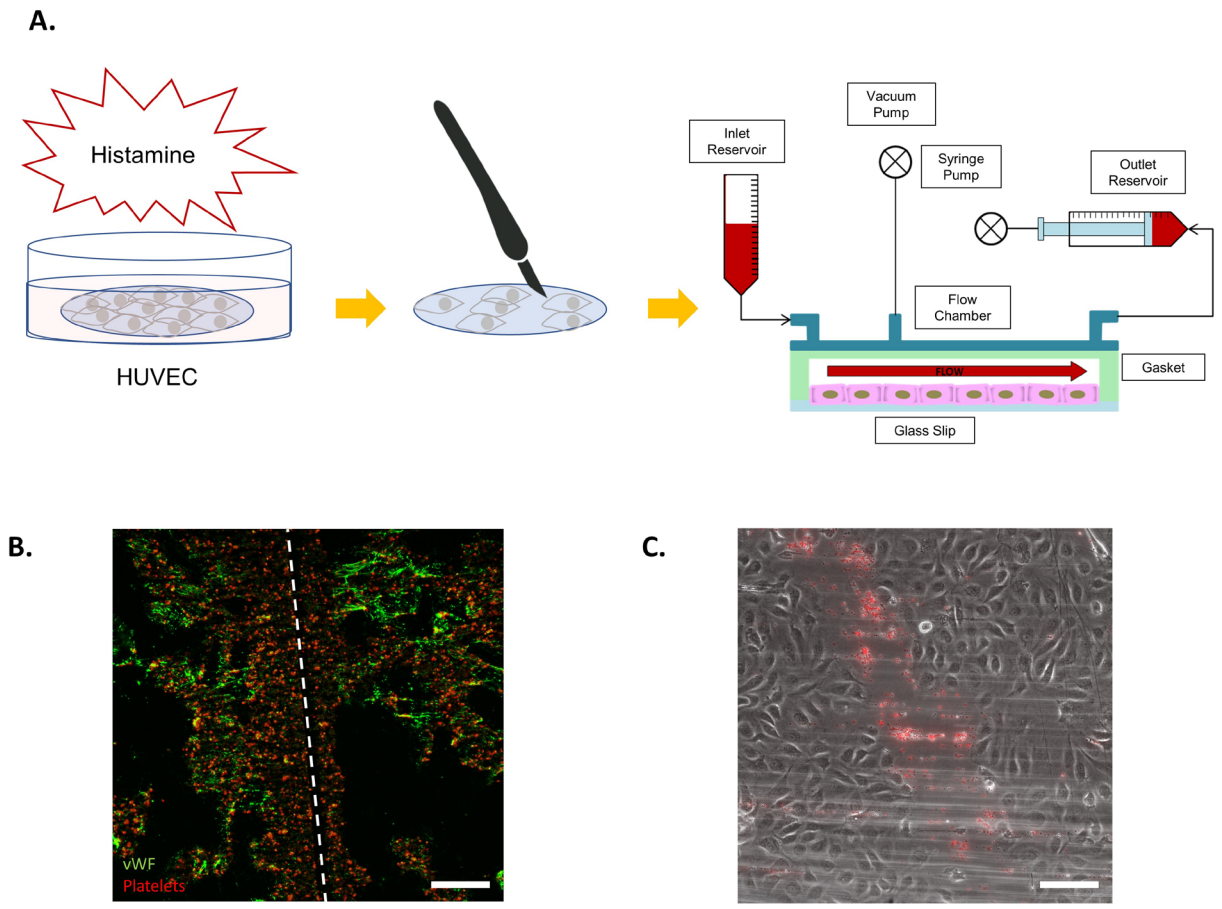

Figure 3.2: Development of in vitro flow model utilizing an endothelium.

(A) Schematic detailing the major steps to create the damaged endothelium model for flow experiments, (B) Representative fluorescence image of endothelium activated with histamine and physically disrupted with scalpel (scalpel mark shown in white), allowing for adhesion of platelets. Green represents von Willebrand factor multimers and red represents adherent platelets, and (C) Platelet adhesion of activated, anti-CD41/61 PE-stained platelets (red) overlaid on top of a HUVEC monolayer activated with histamine and manually damaged with scalpel (average width of scalpel score: 157 µm) using ACD-anticoagulated blood, scale bar 200 µm.

Previous works examining whole blood platelet adhesion in fluidic devices observed differing platelet adhesion behavior across varying shear rates. These discrepancies may be due to studies utilizing different flow channels, microfluidic surface coatings for platelet adhesion, and anticoagulants. As such, we examined the impact of shear on platelet adhesion after establishing the damaged endothelium flow model. Blood flow is represented here using shear rates as opposed

to volumetric flow rates due to the latter's known, direct impact on convective transport of soluble factors as well as cell-surface interactions[178]. We chose a range of shear rates representative of blood flow in different vessels *in vivo*. Specifically, we utilized $100s^{-1}$ (representing blood flow in veins), $500s^{-1}$ (representing large arteries), and $1000s^{-1}$ (representing arterioles and capillaries)[56]. Activation of platelets in whole blood with 20 μM ADP led to significant increased platelet adhesion at $100s^{-1}$ (Figure 3.3A) in comparison to flow experiments utilizing resting platelets. This increase in adhesion highlights the known ability of ADP to stimulate platelets, an important step in platelet adhesion at shear rates $<1000s^{-1}$ [179]. Further, activated platelet adhesion at low shear rates ($100s^{-1}$) was higher than that at higher shear rates ($1000s^{-1}$). This observation aligns with other works that observed maximal platelet adhesion at low shear rates in whole blood, an impact the authors hypothesized was due to the lag time in plasma protein adsorption onto the microfluidic surface at high shear rates[48].

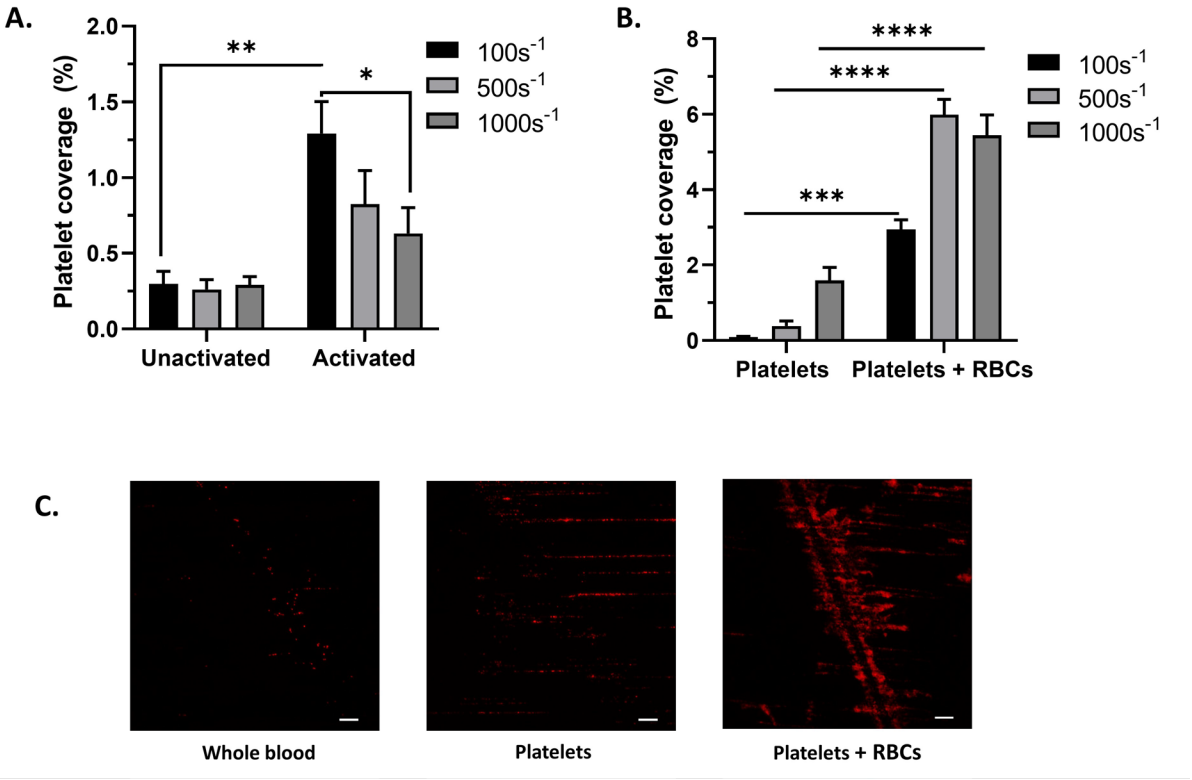

Figure 3.3: Platelet adhesion to damaged endothelium under different flow conditions.

(A) Platelet coverage (as % of total surface area of photo) after 5 minutes of laminar flow in whole blood at a 40% hematocrit and at either 100, 500, or 1000s^{-1} on histamine-stimulated and mechanically disrupted HUVEC. Platelets were either quiet or activated with 20 µM ADP, (B). Platelet coverage (%) on damaged endothelium of activated platelets after 5 minutes of laminar flow. Platelets were anticoagulated with ACD at varying shear rates either isolated in flow buffer, or in flow buffer with RBCs at 40% hematocrit, (C) Representative image of adherent, activated platelets (red) on damaged endothelium after 5 minutes of laminar flow at 1000s^{-1} in whole blood at 40% hematocrit, isolated platelets in flow buffer, or isolated platelets and RBCs at 40% hematocrit in flow buffer. Statistical analyses were performed using two-way ANOVA with Tukey's multiple comparisons test, where (*) indicates $p<0.05$, (**) indicates $p<0.01$, (***) indicates $p<0.001$, and (****) indicates $p<0.0001$. Scale bar 100 µm.

To further explore the binding mechanism and the role of different components of blood in this model, we examined activated platelet adhesion in buffer alone or buffer containing human RBCs at 40% hematocrit. Platelet adhesion in buffer flow was greatest at high shear rates (1000s^{-1}; Figure 3.3B). In the absence of plasma, high shear allows for ultra-long vWF multimers released from activated endothelial cells to elongate and expose adhesion sites without cleavage by plasma ADAMTS-13, which enhances platelet binding[20,180]. Previous works determined that HUVEC in

flow do not release sufficient quantities of ADAMTS-13 to cleave ultra-long vWF multimers tethered to their surface without the presence of healthy plasma or purified ADAMTS-13[24,25,180]. Therefore, the high level of platelet adhesion in buffer at high shear rates suggests that vWF plays an important role in this model. As expected, the addition of RBCs to platelets in buffer increased platelet flow adhesion at all shear rates (Figure 3.3B), highlighting the importance of RBCs to facilitate margination of platelets towards the vascular wall and to increase binding to the damaged endothelium[1]. Representative images of activated platelet adhesion at $1000s^{-1}$ in whole blood, isolated in buffer, and isolated in buffer with the addition of RBCs are shown in Figure 3.3C. For all conditions, platelet adhesion predominates at and around the scalpel score and adjacent endothelium area, i.e., the injury region, including adhesion to long vWF strings attached to the endothelium at high shear rates, especially in the absence of plasma.

Thus far, all flow experiments were conducted using acid citrate dextrose (ACD)-anticoagulated blood. However, there are other anticoagulants that are commonly used to study platelet behavior, including sodium citrate and heparin. To ensure platelet adhesion is supported across a variety of anticoagulants, we examined activated platelet adhesion at $1000s^{-1}$ of platelets in blood anticoagulated with ACD, heparin, and sodium citrate (Figure 3.4A). We find that the highest platelet adhesion occurred when sodium citrate (3.2%) is used as the anticoagulant, leading to a significant increase in platelet coverage compared to ACD-anticoagulated blood. Adherent platelets are primarily localized to the area near the scalpel score for all anticoagulant types, as illustrated in an overlay image of heparinized, fluorescently-labelled platelets and damaged endothelium in Figure 3.4B. This finding confirms that our model is tunable; users may choose any number of common anticoagulants in examining platelet adhesion using the 'damaged endothelium' model.

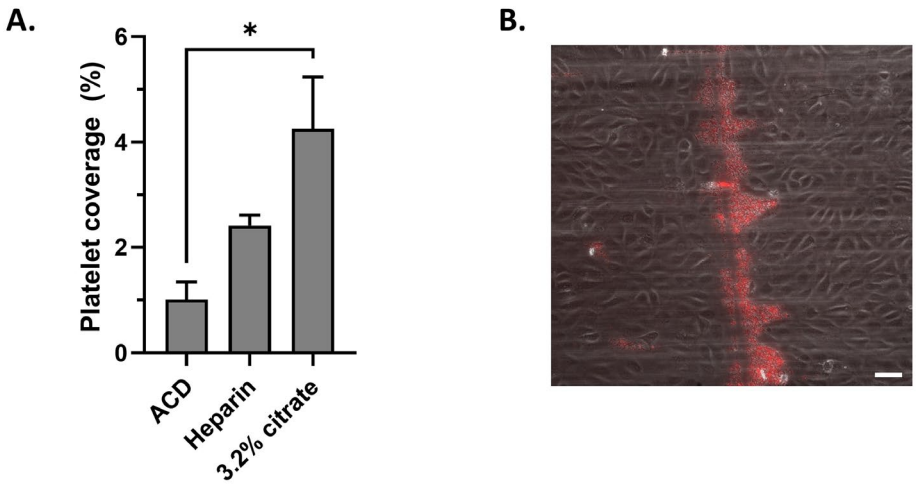

Figure 3.4: Impact of anticoagulant on platelet adhesion.

(A) Activated platelet coverage (%) on damaged endothelium of whole blood at $1000s^{-1}$ anticoagulated in ACD, heparin, or sodium citrate, (B) Platelet adhesion in heparinized blood of activated, anti-CD41/61 PE-stained platelets (red) overlaid on top of a HUVEC monolayer stimulated with histamine and manually damaged with scalpel. Statistical analyses were performed using one-way ANOVA, where (*) indicates $p<0.05$. Scale bar 100 µm.

3.4.2 Comparison of damaged endothelium model to typical protein controls

A common method of examining platelet behavior in flow involves platelet adhesion to patterned ECM proteins, especially collagen. To determine how platelet adhesion using our 'damaged endothelium' model compared to the standard, we examined platelet adhesion in whole blood flow to the damaged endothelium and to collagen alone at 1 mg/mL[48–50]. We included another control of platelet adhesion to gelatin alone at the same concentration as collagen because crosslinked gelatin is used in our damaged endothelium model. Figure 3.5A shows that when platelets in blood are activated, they adhere with the same frequency to the damaged HUVEC model as to collagen alone; there was no difference between magnitude of platelet adhesion to the damaged HUVEC model and to collagen at any of the shear rates examined. Qualitatively, platelet adhesion to collagen was distributed randomly in small aggregates on the collagen surface. Conversely, platelet adhesion to the damaged endothelium was concentrated mostly on the

exposed ECM between endothelial cells for all shear rates examined and to long vWF strands bound to the endothelium for higher shear rates examined. Adhesion to collagen alone follows the same general trend of higher adhesion under low shear rate conditions ($100s^{-1}$) than to higher shear conditions (500, $1000s^{-1}$). Platelet adhesion to gelatin followed similar trends but adhesion at $100s^{-1}$ was significantly lower than platelet adhesion to collagen at the same shear rate, suggesting that gelatin alone at 1 mg/mL does not facilitate platelet adhesion as well as collagen. Conversely, when platelets were resting, there was no significant differences between adhesion to the damaged HUVEC, collagen, or gelatin at any of the shear rates tested (Figure 3.5B).

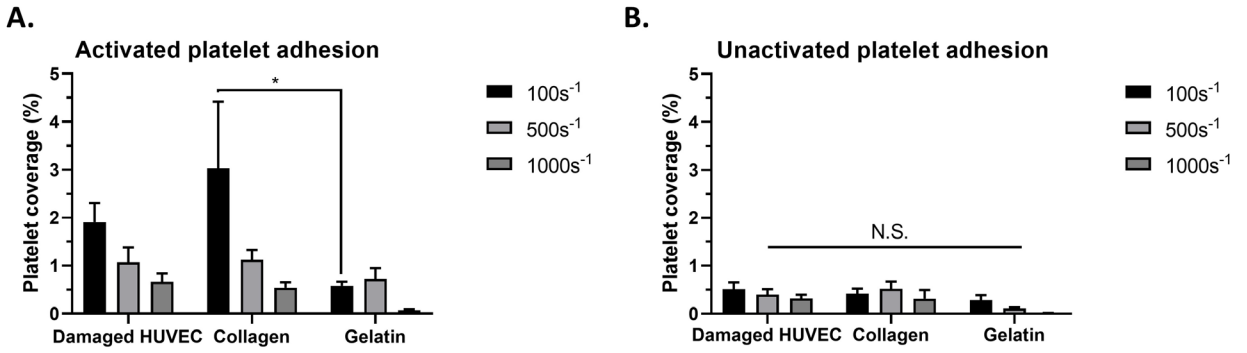

Figure 3.5: Platelet adhesion on damaged endothelium in comparison to ECM protein controls.

(A) Platelet coverage (as % of total surface area of photo) on damaged endothelium, collagen (1 mg/mL), or gelatin (1 mg/mL) of activated platelets in whole blood at 40% hematocrit after 5 minutes of laminar flow, and (B) Platelet coverage (as % of total surface area of photo) on damaged endothelium, collagen (1 mg/mL), or gelatin (1 mg/mL) of resting platelets in whole blood at 40% hematocrit after 5 minutes of laminar flow. Statistical analyses were performed using two-way ANOVA with Tukey's multiple comparisons test, where (*) indicates $p<0.05$.

One benefit of functionalizing glass coverslips for HUVEC culture by crosslinking gelatin with glutaraldehyde is that this is also tunable; glutaraldehyde crosslinks proteins by reacting with their free primary amines[181], so proteins of interest other than gelatin can be utilized for HUVEC culture with this method. To directly compare the impact of changing the crosslinking protein of interest, we examined platelet adhesion to damaged HUVEC cultured on either glutaraldehyde-crosslinked gelatin or collagen. In both conditions, we lowered the concentration of protein (gelatin

or collagen) to 0.5 mg/mL as crosslinking higher concentrations of collagen led to a gel-like substance on the surface of glass that could not be fully washed off. Figure 3.6 shows that there is no significant difference between either resting or activated platelet adhesion to damaged HUVEC cultured on either gelatin or collagen. Further, this work confirms that this method is tunable based on the specific protein of interest the user would like to use for HUVEC cell culture.

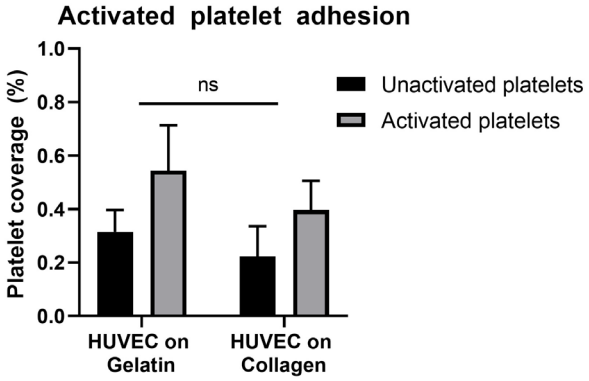

Figure 3.6: Platelet adhesion on damaged endothelium while varying crosslinking protein and concentration.

Platelet coverage on damaged endothelium cultured on glutaraldehyde-crosslinked gelatin (0.5 mg/mL) or collagen (0.5 mg/mL) of activated platelets in whole blood at 40% hematocrit after 5 minutes of laminar flow. Statistical analyses were performed using two-way ANOVA with Tukey's multiple comparisons test, where lack of * indicates lack of significance.

3.4.3 Validation of 'damaged endothelium' model using a known platelet inhibitor

To ensure that our model is sensitive enough to be used to screen potential anti-platelet or anti-inflammatory therapeutics, we validated our model using a common platelet inhibitor, ticagrelor. Ticgrelor is a $P2Y_{12}$ receptor binding antagonist that leads to a reduction in platelet aggregation and adhesion[86,182]. We examined the impact of pretreating whole blood, anticoagulated with either ACD or heparin, with 10 μM ticagrelor one hour prior to blood flow. In both ACD-anticoagulated (Figure 3.7A) and heparin-anticoagulated (Figure 3.7B) whole blood, ticagrelor led to a significant decrease in the binding of activated platelets to the damaged

endothelium (p = 0.0033 for ACD and p = 0.0101 for heparin). In ACD-anticoagulated blood, platelet adhesion dropped to 61% of untreated controls while in heparinized blood, platelet adhesion was reduced to 66% of untreated controls. Further, the magnitude of decrease in platelet adhesion is not statistically different between ACD and heparin (p = 0.719). This set of experiments confirms that: 1. The damaged endothelium model is sensitive enough to detect changes in platelet adhesion due to pharmaceuticals with anti-platelet properties, and 2. That several anticoagulants can all be used in the model to screen anti-platelet compounds.

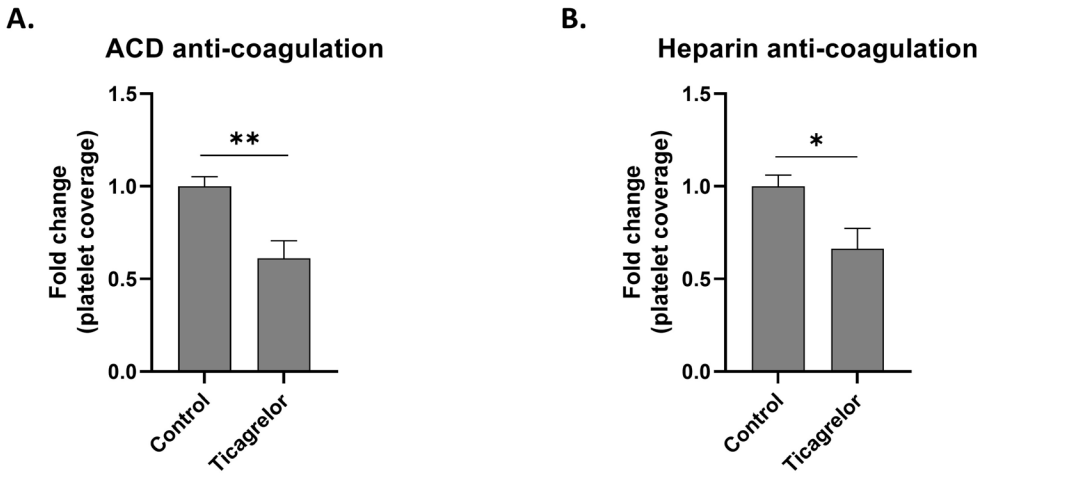

Figure 3.7: Impact of ticagrelor on platelet adhesion.

Platelet adhesion (% of total surface area) of activated platelets after 1 hour treatment with 10 μM ticagrelor using (A) ACD or, (B) heparin-anticoagulated whole blood. Blood was perfused for 5 minutes of laminar flow at 40% hematocrit and $1000s^{-1}$ over an activated, damaged HUVEC monolayer. Statistical analysis was performed using a Student's unpaired t-test, where (*) indicates $p<0.05$ and (**) indicates $p<0.01$.

3.4.4 Screening of two potential new anti-platelet compounds using the damaged endothelium model

One benefit of utilizing the damaged endothelium model is the inclusion of multiple binding motifs for platelets, both the damaged endothelium itself and the underlying extracellular matrix proteins. These multiple binding motifs make this model ideal to screen potential drug

compounds for impact on platelet adhesion using human whole blood in flow. One compound of interest is Bimosiamose, a siayl Lewis^x mimetic and pan-selectin inhibitor[183]. Despite the ability of this antagonistic compound to target E-selectin, P-selectin, and L-selectin, Bimosiamose has primarily been studied for its ability to inhibit leukocyte binding and recruitment *in vitro*[183], *in vivo*[184,185], and in clinical trials[186,187].

To determine if Bimosiamose's ability to inhibit selectins could impact platelet adhesion in the damaged endothelium model, we pretreated whole blood with 50 μM Bimosiamose for 1 hour prior to flow experiments. Like all previous experiments thus far, we stimulated the endothelium with histamine with mechanical injury via scalpel, which does not facilitate the adhesion of leukocytes in blood flow; these conditions allow us to examine the impact of Bimosiamose on platelet adhesion alone. We treated blood with ADP to induce platelet activation at the same time as Bimosiamose. The Bimosiamose treatment led to a 40% reduction in activated platelet adhesion to the damaged endothelium model relative to its untreated counterparts (Figure

3.8A; p = 0.0006). In comparison, Bimosiamose treatment did not impact platelet adhesion in whole blood to the collagen-only substrate (Figure 3.8A; p = 0.6394).

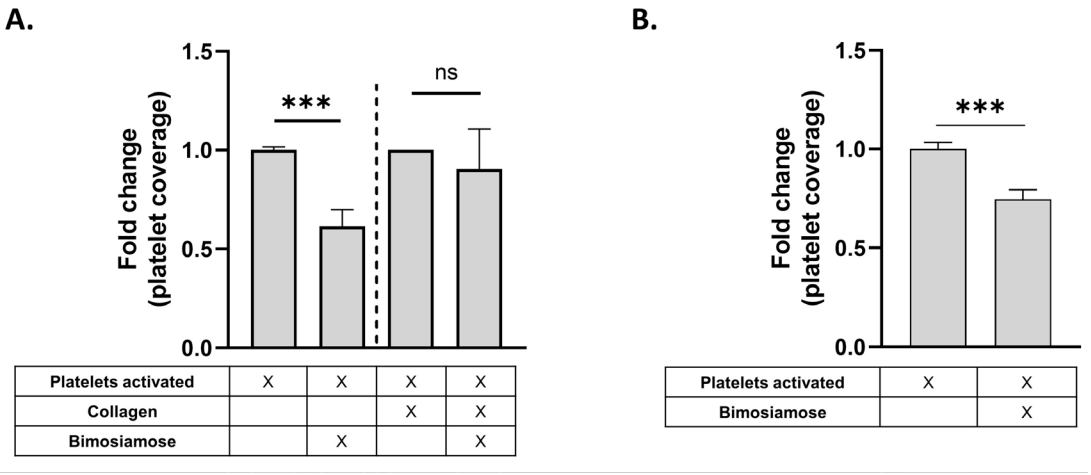

Figure 3.8: Pan-selectin inhibitor decreases platelet adhesion to HUVEC.

(A) Activated platelet adhesion fold change of (A) ACD-anticoagulated, or (B) heparin-anticoagulated whole blood on damaged HUVEC at 40% hematocrit at 1000 s^{-1} for 5 minutes with the addition of 50 μM Bimosiamose to whole blood 1 hour before flow experiments. Statistical analyses were performed using Student's unpaired t-test where (***) indicates p<0.001.

To once again confirm that the anticoagulant used in this model is tunable, we repeated this experiment using heparinized blood, omitting collagen-only controls as we already determined that collagen alone does not have the ability to capture the platelet inhibition effect of Bimosiamose. In heparinized blood, Bimosiamose significantly decreased activated platelet adhesion to the damaged endothelium to a similar degree as ACD-anticoagulated blood (Figure 3.8B; p = 0.0005). Specifically, Bimosiamose-treated heparinized blood led to a 25% decrease in platelet adhesion in comparison to untreated controls.

The inclusion of the endothelium in this model also allows for the testing of compounds that have a direct therapeutic impact on the endothelium instead of on platelets themselves. One

potential candidate to screen for impact on platelet adhesion is Cimetidine, a relatively inexpensive, FDA-approved, and accessible histamine receptor antagonist marketed under the brand name 'Tagamet' to treat heartburn and peptic ulcers. More recently, Cimetidine has gained interest for its ability to inhibit the expression of selectins by endothelial cells. In particular, Cimetidine was found to decrease neutrophil adhesion to endothelial cells activated by high concentrations of glucose, decreasing the expression of cellular adhesion molecules P-selectin and ICAM-1 on the surface of HUVEC[188]. Further, Cimetidine has been repurposed in combination with other oncological therapeutics and pharmaceuticals in a variety of clinical trials for different cancers to capitalize on several qualities of Cimetidine, including its ability to inhibit cancer cell adhesion to endothelial cells[189].

To take advantage of Cimetidine's ability to decrease cellular adhesion molecule expression as well as its histamine receptor antagonism, we treated HUVEC with low (1 μM) or high (50 μM) concentrations of Cimetidine 5 hours prior to use in blood flow experiments. Similar to all previous experiments, we treated the endothelium only with histamine and mechanical injury to determine if Cimetidine has an effect on platelet adhesion in the absence of adherent leukocytes. Due to treating the endothelium itself with Cimetidine instead of whole blood, there was no corresponding collagen-only control for this experiment. Treatment with either low or high concentrations of Cimetidine significantly decreased activated platelet adhesion to approximately 67% of untreated HUVEC (Figure 3.9; $p = 0.0279$ and $p = 0.0349$ for low and high concentrations of Cimetidine, respectively), demonstrating that even a low dosage of the compound was enough to significantly decrease platelet adhesion in this model. This decrease in platelet adhesion occurred even in the absence of leukocyte adhesion, highlighting Cimetidine's effectiveness at modulating platelet adhesion behavior. Further, this experiment demonstrates that this damaged

endothelium model can be used to screen potential therapeutics for impact on platelet adhesion, even if the target of the therapeutic is the endothelium instead of platelets themselves.

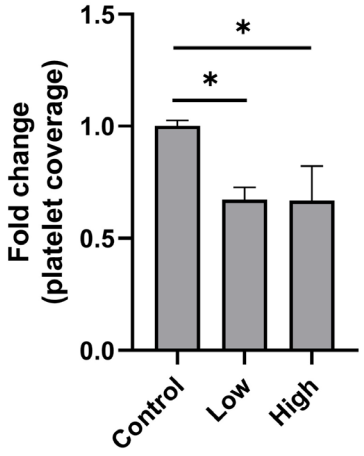

Figure 3.9: Histamine receptor antagonist decreases platelet adhesion to HUVEC.

Activated platelet adhesion fold change of ACD-anticoagulated whole blood on damaged HUVEC at 40% hematocrit at 1000 s^{-1} for 5 minutes with the addition of 1 μM (low) or 50 μM (high) Cimetidine to HUVEC 5 hours prior to blood flow experiments. Statistical analyses were performed using Student's unpaired t-test where (*) indicates $p < 0.05$.

3.4.5 Addition of endothelial cell inflammation increases leukocyte, platelet adhesion

So far, we inflamed HUVEC over a short period in this model to induce the secretion of their Weibel-Palade bodies containing vWF multimers and P-selectin. However, often platelet adhesion, aggregation, and thrombus formation occur in blood vessels with underlying inflammation, which recruits circulating leukocytes to the area of inflammation[142]. These leukocytes may then bind platelets from flowing blood, adding them to the growing thrombus and area of inflammation[61]. To determine if we could induce the formation of platelet-leukocyte aggregates bound to inflamed endothelial cells *in vitro*, we examined both platelet and leukocyte adhesion to a HUVEC monolayer while activating platelets and the HUVEC using an inflammatory cytokine (IL-1β). We additionally included a collagen-only control, which is

representative of commonly used protein-only substrates used in flow experiments. Figure 3.10A shows the impact of platelet and HUVEC activation on platelet adhesion at $1000s^{-1}$; activation of HUVEC leads to a modest, non-significant increase in platelet adhesion and, separately, activation of platelets leads to a non-significant increase in platelet adhesion. However, activation of both platelets and HUVEC leads to the largest, significant increase in overall platelet adhesion to the endothelium. Further, if we examine instead the behavior of leukocytes, we see that only activation of the HUVEC leads to leukocyte adhesion (Figure 3.10B). No leukocyte adhesion is seen either on the unactivated HUVEC or collagen, regardless of platelet activation. Representative images of these different activation schemes are shown in Figure 3.10C, which can further explain these adhesion trends. When HUVEC are activated but platelets unactivated, we still see a few platelets binding to the intact area of the endothelium, corresponding to the few platelets bound to adherent leukocytes. However, when both HUVEC and platelets are activated, we see a large amount of platelet adhesion to the intact HUVEC monolayer, corresponding to platelet-leukocyte aggregates bound to the monolayer. Practically, this makes sense as activation of platelets leads to P-selectin expression on their surface, which is required to initiate binding via PSGL-1 on the surface of leukocytes[61]. The addition of HUVEC inflammation transitions the 'damaged endothelium' model from simply a model to examine platelet adhesion to one that can be used to study

'thromboinflammation' and the interplay between leukocytes, platelets, and the endothelium.

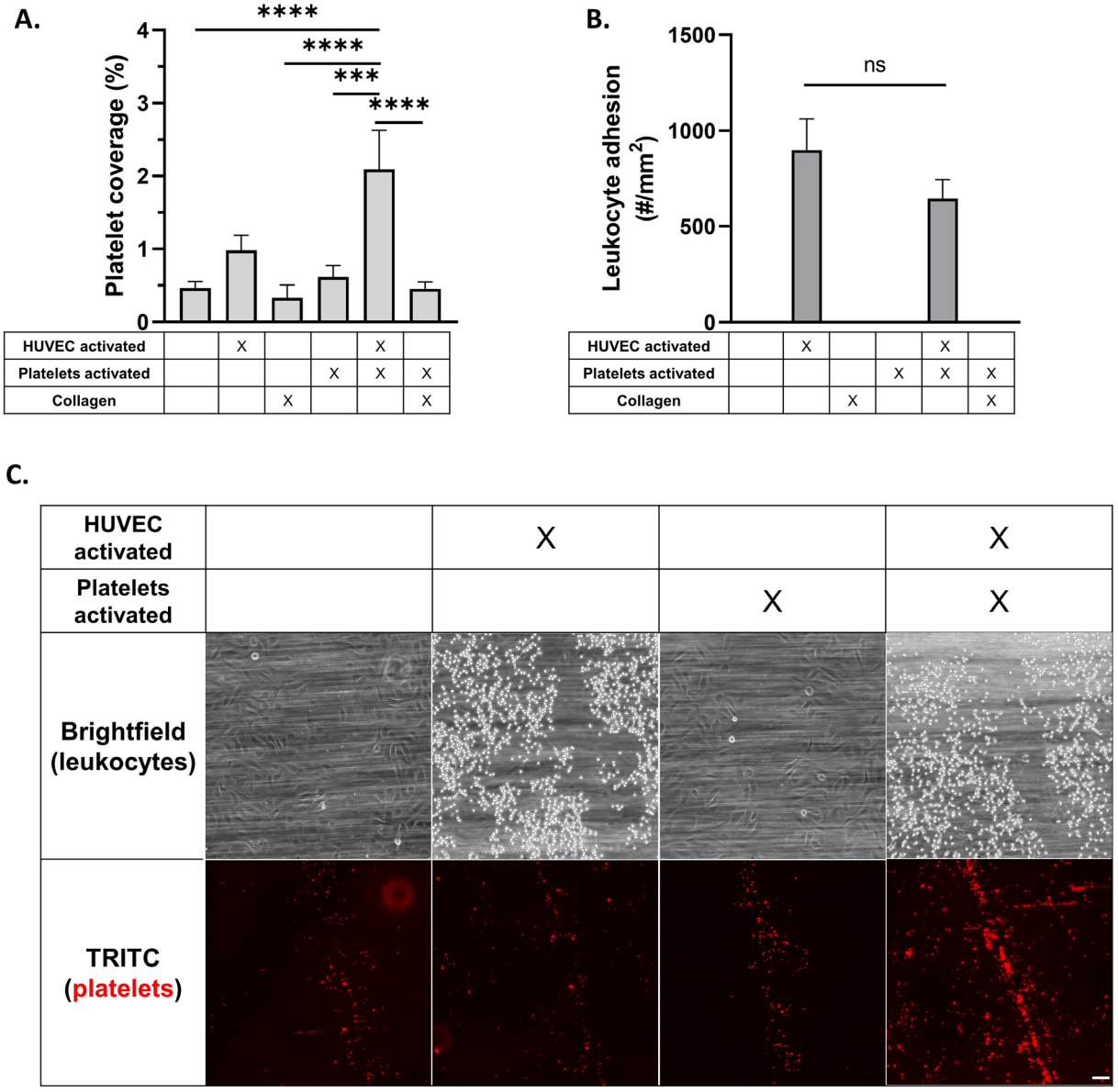

Figure 3.10: Activation of HUVEC with IL-1β increases leukocyte and platelet adhesion to damaged endothelium.

(A) Platelet adhesion (%) on damaged HUVEC or collagen alone of whole blood at 40% hematocrit at 1000 s^{-1} for 5 minutes, (B) Leukocyte adhesion on damaged HUVEC or collagen of whole blood at 40% hematocrit at 1000 s^{-1} for 5 minutes, (C) Representative images of adherent leukocytes (via brightfield microscopy) and platelets (red, via fluorescent microscopy), scale bar 100 µm. Statistical analyses were performed using were performed using one-way ANOVA with Tukey's multiple comparisons test where (***) indicates $p<0.001$, and (****) indicates $p<0.0001$.

3.4.6 Screening of two potential new anti-platelet compounds using the damaged endothelium model of thromboinflammation

We previously demonstrated that both new, potential anti-platelet compounds Bimosiamose and Cimetidine significantly decreased platelet adhesion to a damaged endothelium. However, both compounds may have the ability to interfere with leukocyte adhesion, as well. Specifically, Bimosiamose is a selectin inhibitor and is known to reduce leukocyte adhesion in many models[183–187]. To determine if Bimosiamose's anti-leukocyte properties can be successfully screened with our model, we pretreated whole blood with 50 μM of Bimosiamose once again before examining platelet and leukocyte adhesion to an inflamed, damaged endothelium. Figure 3.11A and B show that this Bimosiamose pretreatment leads to a significant decrease to 68% ($p = 0.0026$) and 56% ($p < 0.0001$) of platelet and leukocyte adhesion in comparison to untreated controls, respectively.

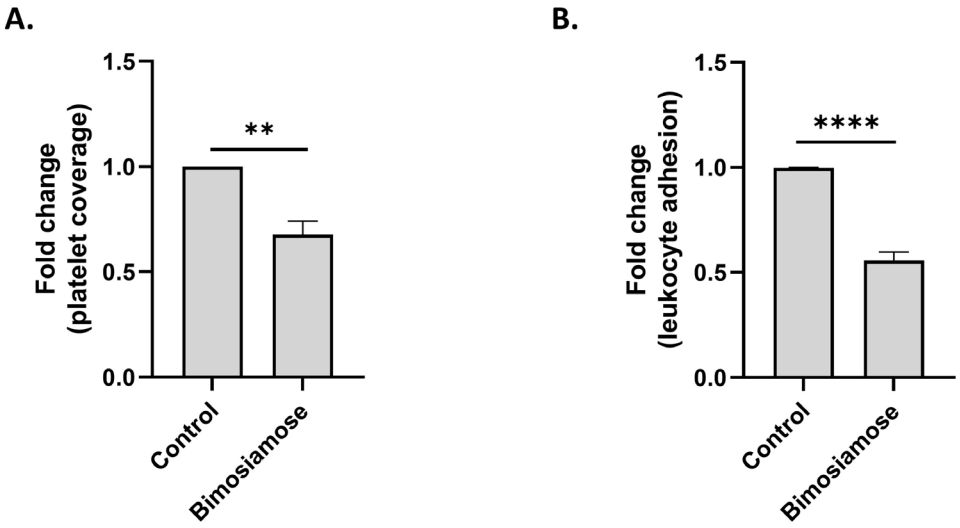

Figure 3.11: Pan-selectin inhibitor decreases platelet and leukocyte adhesion to IL-1β activated HUVEC.

(A) ACD-anticoagulated activated platelet adhesion fold change, and (B) ACD-anticoagulated leukocyte adhesion fold change on IL-1β-activated, damaged HUVEC of whole blood at 40% hematocrit at 1000 s^{-1} for 5 minutes with the addition of 50 μM Bimosiamose to whole blood 1 hour before flow experiments Statistical analyses were performed using Student's unpaired t-test where (**) indicates $p<0.01$, and (****) indicates $p<0.0001$.

Cimetidine is known to reduce neutrophil adhesion to activated HUVEC by reducing the expression of cellular adhesion molecules[188,190]. Similarly, we examined the impact of a 5 hour pretreatment of HUVEC with Cimetidine, 1 hour before HUVEC activation with IL-1β[190]. Both platelet (Figure 3.12A; p = 0.0116 and 0.0014 for low and high concentrations, respectively) and leukocyte (Figure 3.12B; p = 0.0002 and 0.0001 for low and high concentrations, respectively) adhesion was significantly reduced when HUVEC were treated with Cimetidine.

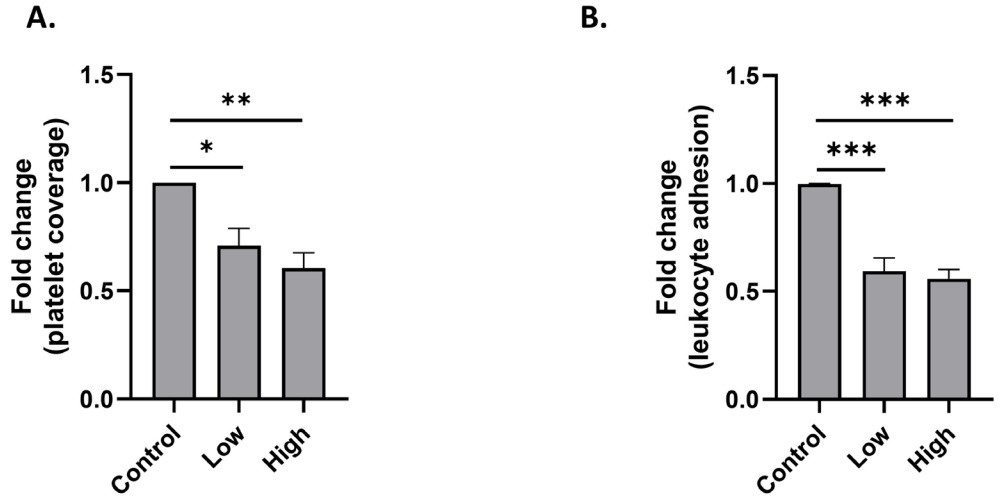

Figure 3.12: Platelet and leukocyte adhesion to activated HUVEC decreases with Cimetidine pretreatment of HUVEC.

(A) Activated platelet adhesion fold change, or (B) Leukocyte adhesion fold change on IL-1β-activated, damaged HUVEC of whole blood at 40% hematocrit at $1000s^{-1}$ for 5 minutes with the addition of 1 μM (low) or 50 μM (high) Cimetidine to HUVEC 5 hours prior to blood flow experiments. Statistical analyses were performed using one-way ANOVA with Dunnett's multiple comparisons test where (*) indicates $p < 0.05$, (**) indicates $p<0.01$, and (***) indicates $p<0.001$.

3.5 Discussion

The study of human platelets is essential to understanding both hemostasis and thrombosis. Further, the use of *in vitro* models allows researchers to 1. Adhere to the ethics of humane animal research by replacing and reducing the number of animals needed for biomedical science work, and 2. Utilize human blood as opposed to blood collected from other species that may not be

directly translatable to human health and disease. However, most *in vitro* models either neglect the role of the endothelium or lack an exposed ECM, both of which are essential for studying platelet behavior and understanding platelet dynamics *in vivo*. The minimal work trying to incorporate both endothelial cells and exposed ECM proteins tend to lack fine control over the location and amount of space between endothelial cells[174].

Here, we developed a tightly controlled, tunable method for examining platelet adhesion both to a damaged endothelial cell monolayer and to its underlying ECM proteins after acute vascular damage without requiring the design and production of custom microfluidic devices. This model supports platelet adhesion across anticoagulants and shear rates, with vWF secretion and tethering by the endothelium an essential aspect of platelet adhesion at high shear rates. Further, this model can be tuned based on if the user wants to include leukocyte-platelet aggregates in a 'thromboinflammatory' study of platelet adhesion; the study of platelet-leukocyte aggregation *in vitro* is of great use to many researchers, yet most methods utilized occur in static using flow cytometry or *in vivo* animal models[191]. This model allows researchers to view platelet-leukocyte-endothelium interactions in a much more physiological environment.

We used two different chemical stimuli in this model—histamine and IL-1β. Histamine stimulates endothelial cells quickly and induces the fusion of Weibel-Palade bodies with the endothelial cell membrane where its cargo, including vWF and P-selectin, are released[192]. Stimulation of the histamine H1 receptor on the endothelial cell surface leads to additional downstream changes in the endothelium, including cell contraction, synthesis of prostacyclin and platelet-activating factor, and nitric oxide release[193]. IL-1β activates NF-κB, a transcription factor that plays a major role in mediating inflammation, in endothelial cells via the 'canonical' pathway[192]. A major downstream impact of IL-1β activation of endothelial cells is the expression

of cellular adhesion molecules on the surface, including ICAM-1, VCAM-1, and E-selectin[192], and the expression of IL-8[194]. However, IL-1β also leads to gene-level changes in endothelial cells related to apoptosis, chemotaxis, the immune response, angiogenesis, and hemopoiesis, among others; these gene-level changes lead to the expression of signaling molecules, including chemokines and cytokines, and increased vascular permeability[194]. Overall, both these stimuli have downstream impacts on endothelial cells that vary greatly from each other.

To confirm that our 'damaged endothelium' model is suitable to identify potential anti-platelet therapeutics, we verified our model utilizing a known anti-platelet compound, ticagrelor. Ticagrelor is an FDA approved, reversible, non-competitive $P2Y_{12}$-receptor antagonist[195]. Because ticagrelor's anti-platelet effects are well studied *in vivo*[86,168] and *in vitro*[182], confirmation that ticagrelor reduces platelet adhesion in our flow model was essential before utilizing this model to identify more novel, unstudied anti-platelet therapeutics.

In the absence of leukocyte adhesion (i.e., when HUVEC are not activated with IL-1β) we attribute Bimosiamose's effectiveness in decreasing platelet adhesion on the damaged endothelium to the increased platelet binding motifs present that are not present on the collagen substrate. Specifically, we hypothesize that Bimosiamose in whole blood blocked the GPIb-IX-V receptor complex on platelets that binds to P-selectin on the endothelium[18]. The lack of P-selectin on collagen alone renders this blocking impact inconsequential. Further, excess Bimosiamose in blood may also have blocked P-selectin on the endothelial cell surface once blood flow through the chamber began. The capability of Bimosiamose to block leukocyte adhesion via blocking of selectins has been well established[183–187]. However, we demonstrated that Bimosiamose further has the ability to directly modulate platelet behavior in the complete absence of leukocyte adhesion.

Cimetidine pretreated of non-IL-1β activated HUVEC also yielded a significant decrease in platelet adhesion. We hypothesize that this anti-platelet impact has one primary cause--Cimetidine has the ability to decrease the cellular adhesion molecule expression of inflamed endothelial cells[190], including P-selectin[188]. Decreasing P-selectin expression of acutely activated HUVEC could interfere with the binding of the GPIb-IX-V receptor complex on platelets to P-selectin on the endothelial cell surface. Less likely, excess Cimetidine in cell media could have come in direct contact with platelets in blood, inhibiting their activation directly[196].

In the model that includes endothelial activation using IL-1β, the mechanism of action for Bimosiamose's impact on leukocyte adhesion is straightforward; inhibiting both L-selectin on leukocytes and E-selectin on the HUVEC itself can both reduce leukocyte adhesion. However, Bimosiamose's anti-platelet activity in this model is likely due to several mechanisms, both blocking the GPIb-IX-V receptor complex on platelets that binds to P-selectin on the endothelium (as demonstrated with a non-IL-1β inflamed endothelium) and also due to interfering with leukocyte-platelet aggregates on the endothelial cell surface.

Again, the mechanism of action for reduced leukocyte adhesion is clear due to Cimetidine's ability to inhibit cellular adhesion molecule production and expression[188,190]. Cimetidine's impact on platelet adhesion is likely a combination of its histamine receptor antagonism, which directly impacts platelets similarly to the non-IL-1β inflamed HUVEC treatments in Section 3.4.4, and through reducing platelet-bound leukocytes on the endothelium.

A limitation of this work is that only one specific type of protein was utilized for HUVEC culture (gelatin). However, since glutaraldehyde crosslinks proteins by reacting with their free primary amines[181], proteins of interest other than gelatin can be utilized for HUVEC culture with this method. Future work utilizing this adaptive model can explore how tuning the crosslinked

protein or proteins can alter platelet behavior, in addition to elucidating the behavior of endothelial cells isolated from different vascular beds with shear rates corresponding to those vessels (i.e. studying saphenous vein endothelial cells at ~100s^{-1} in contrast to coronary artery endothelial cells at ~400s^{-1},[56]).

3.6 Conclusions

Overall, this work demonstrates a new method of exploring platelet-blood cell and platelet-endothelium interactions *in vitro* using human whole blood and includes both an inflamed endothelium and underlying extracellular matrix in a controlled manner and does not require the custom design or production of microfluidic devices. This method is extremely tunable; users can easily control the shear rate, anticoagulant, and extracellular matrix proteins for endothelial cell culture. The ability of this model to screen anti-platelet compounds was verified using a known anti-platelet and, further, two additional potential anti-platelet compounds were screened utilizing the method as well. Overall, the screening of these compounds demonstrates the ability of this damaged endothelium model as an initial screening method of potential anti-thrombotic or anti-platelet compounds that can impact either platelets or the endothelium itself and represents a novel method to study future platelet-cell and platelet-drug interactions.

Chapter 4 Polymeric Drug Carriers Modulate Platelet Adhesion in Thromboinflammation

4.1 Publication Information

This data is not yet published, though much of the work written in this chapter will be submitted to the journal *Nature Communications* as "Polymeric Drug Carriers Modulate Platelet Adhesion in Thromboinflammation" with author list **Alison Banka**, Valentina Guevara, Reheman Adili, Michael Holinstat, and Omolola Eniola-Adefeso. Modifications of the published work have been made to adapt the content to this chapter.

4.2 Abstract/Summary

Platelet-leukocyte aggregates are a hallmark of inflammatory diseases and can contribute to excessive thromboinflammation in an area of vascular damage or underlying inflammation. While particulate drug carriers have previously been shown to divert leukocytes away from areas of inflammation *in vitro* and *in vivo*, the impact of particles on platelet accumulation under thromboinflammatory conditions has yet to be fully explored. Here, we investigated the effect of model polymeric particles on platelet and leukocyte adhesion. *In vitro*, micron-sized polystyrene particles significantly decreased both platelet and leukocyte adhesion to an inflamed endothelium, an effect which was enhanced at low particle concentration by the addition of sLe^A targeting. This diversion of platelet-leukocyte aggregates was confirmed *in vivo* using a mouse model of systemic inflammation; an intraperitoneal injection of lipopolysaccharide led to a neutrophil-dependent accumulation of platelets in the mouse mesentery, which significantly decreased with IV-injection of untargeted and targeted polystyrene particles. Specifically, 2 μm polystyrene particles injected at the time of LPS installation led to a 57% reduction in platelets bound to the mouse mesentery, which increased to a 64% reduction when particles made from salicylic acid monomers were utilized. Overall, this work demonstrates that polymeric particles can have a downstream impact

on platelet accumulation to areas of inflammation both *in vitro* and *in vivo* and presents a new potential treatment method to reduce platelet and leukocyte accumulation in thromboinflammation.

4.3 Background and Introduction

In blood flow, platelets occupy the red blood cell free layer[3] near the endothelium, or the monolayer of cells lining the vessel wall. The position of platelets near the vascular wall puts them in position to bind to the endothelial cells and underlying extracellular matrix proteins that become exposed when the monolayer is injured or compromised, highlighting the importance of platelets in maintaining hemostasis to prevent excessive blood loss and permanent damage.

The contribution of platelets to the development of vascular thrombi, including ischemic stroke[27], atherosclerosis[65], deep vein thrombosis[197,198], and myocardial infarction[199,200], has been well-established. However, more recent research has illustrated the role of other cells, including the endothelium and members of the innate immune system, in inflammatory thrombus development. Far from being an inert surface, under healthy conditions the endothelium secretes coagulation inhibitors, including tissue factor pathway inhibitor[201] and ectonucleotidases, such as CD39[202], that prevent clotting, and that are suppressed under diseased conditions. Further, the endothelium releases Weibel-Palade bodies containing von Willebrand factor (vWF) multimers and P-selectin to the surface upon stimulation with agonists including thrombin, TNF-α, and trauma[203]. vWF multimers bind platelets through GP1bα[20] and P-selectin binds platelets plus circulating leukocytes, including neutrophils and monocytes, all via PSGL-1[204,205]. Sustained inflammation of the endothelium results in the production and expression of additional cellular adhesion molecules E-selectin, ICAM-1, and VCAM-1 to better recruit leukocytes to the area of injury[142].

Both monocytes and neutrophils contribute to thrombus development upon adhering to an area of inflammation. Monocytes are the single largest source of tissue factor (TF) in the blood vessel and upon recruitment and activation drive TF-induced thrombin generation[206]. Further, activated monocytes release TF-positive microparticles into the circulation that can carry pro-coagulant signals and contribute to thrombosis in other areas of the body[207]. Neutrophils assist in thrombus development in several ways, including the generation of neutrophil extracellular traps (NETs), which can trap platelets, red cells, and vWF in an area of inflammation[208], and the release of granular enzymes, including cathepsin G and elastase, that promote the activation of the coagulation system[79].

Additionally, neutrophils and other leukocytes can form aggregates with platelets under conditions of thrombosis or inflammation via binding between PSGL-1 on leukocytes and P-selectin on activated platelets. Circulating neutrophil-platelet aggregates are found in a variety of inflammatory diseases, including sickle cell disease[175], deep vein thrombosis[209], and acute coronary syndrome[210]. More recently, circulating platelet-neutrophil and platelet-monocyte aggregates were found to be significantly higher in patients with moderate and severe COVID-19 in comparison to non-COVID controls[75,176,211], contributing to the hallmark thromboinflammatory phenotype of COVID patients. These neutrophil-platelet aggregates can be recruited to an inflamed or damaged endothelium either through interactions between the neutrophil and the endothelium at lower shear rates, or binding of platelets to vWF or exposed ECM at higher shear rate[61]. Due to this synergistic increase in recruitment of neutrophil-platelet aggregates in different diseases, many therapeutics have been developed and tested to limit neutrophil-platelet interactions. For example, PSGL-1 antagonists were tested in clinical trials in addition to thrombolytic therapies during acute myocardial infarction, but were not found to improve end points[89,90]. Later clinical trials examined

the use of an anti-P-selectin antagonist, which did not lead to improved patient outcomes after coronary artery bypass surgery[92]. Other alternatives examined in animal models include aspirin-based therapeutics in murine acute lung injury models; though these lessened injury and disease burden[212,213], the known bleeding risk associated with aspirin use may outweigh its potential benefits.

Given the importance of platelets and leukocytes in thromboinflammation, many efforts have been made to develop targeted, injectable therapeutics to modulate platelet and leukocyte behavior. Platelet-targeted therapeutics include artificial platelet-like constructs to assist in clotting in situations of trauma or thrombocytopenia, such as fibrinogen-targeted liposomes loaded with tranexamic acid to stabilize clots[126], liposomes functionalized with collagen, fibrinogen, and vWF binding motifs[127], and fibrin-binding, ultra-low crosslinked microgels with the ability to contract upon incorporation into a clot[124]. Other targeted therapeutics aim to target clots directly for local delivery of thrombolytics, including Annexin V-targeted micelles loaded with lumbrokinase[214].

Alternatively, extensive research has also explored targeting drug carriers to a damaged or inflamed endothelium[145,215] as well as targeting particulate drug carriers to leukocytes, including polymeric particles designed to reduce the number of infiltrating immune cells in a model of spinal cord injury[141]. Recent, novel work examined the impact of model particulate drug carriers on leukocyte adhesion to an inflamed endothelium in blood flow. Non-targeted polystyrene nano- and microparticles decreased leukocyte adhesion to an activated endothelium and particles conjugated with siayl Lewis^{A} (sLe^{A}) ligands to bind to E-selectin further decreased leukocyte adhesion[139]. This work suggests that simple polymeric drug carriers can be utilized to reduce leukocyte recruitment to areas of inflammation and excessive innate immune cell recruitment. Additionally,

in a murine model, particulate drug carriers decreased neutrophil recruitment to the lungs in a model of acute lung injury[136], where neutrophils and neutrophil-platelet aggregates are known to play a damaging role. Despite the promise of model particulate drug carriers in reducing leukocyte adhesion and recruitment in models of inflammation, the ability of such drug carriers to modulate platelet adhesion in thrombo-inflammation has yet to be studied.

In this chapter, we detail the ability of model particulate drug carriers to modulate platelet adhesion under thrombo-inflammatory conditions in blood flow *in vitro* and *in vivo*. Utilizing an *in vitro* flow model that facilitates platelet-leukocyte aggregate adhesion to an inflamed endothelium as described in Chapter 3, we demonstrate that model polymeric particulate drug carriers significantly decrease platelet adhesion to an inflamed endothelium through interfering with platelet-leukocyte adhesion. Further, we used intravital microscopy to demonstrate that our results are translatable *in vivo*; particulate drug carriers were also able to divert platelets from an inflamed mesentery in mice.

4.4 Results

4.4.1 Micron-sized particles decrease platelet adhesion to an inflamed endothelium by interfering with bound platelet-leukocyte aggregates

Under conditions of inflammation, platelets can be recruited to an area of thrombus formation in a variety of ways. In particular, circulating platelet-leukocyte aggregates may bind to an inflamed, intact endothelium[61]. To mimic conditions of thromboinflammation, we utilized a damaged and inflamed endothelium in our *in vitro* flow experiments utilizing a four-hour activation with IL-1β. As mentioned previously, this facilitates the adhesion of platelet-leukocyte aggregates to the endothelium (Figure 3.10). First, we examined the impact of 2 μm PS particles conjugated with anti-IgG2b; these particles were chosen initially as prior work demonstrated that micron-sized

particles are more likely to come into contact with the vascular wall than nano-size particles[143]. Further, the particles were conjugated with avidin and an antibody to prevent non-specific binding to the activated endothelium.

Addition of untargeted, 2 μm model PS particles to whole blood immediately before flowing human whole blood over the damaged, activated endothelium led to a concentration-dependent decrease of platelet adhesion as measured by the surface coverage of fluorescently labeled platelets (Figure 4.1A). While low concentrations of untargeted particles (10^6/mL) did not alter platelet adhesion, particle concentrations at or above $5*10^6$/mL significantly decreased platelet adhesion. Specifically, at $5*10^6$ particles/mL, the fold change in platelet adhesion in comparison to non-particle controls was 79% ($p = 0.034$), which decreased to 62% ($p < 0.0001$) and 53% ($p < 0.0001$) at 10^7 and $5*10^7$ particles/mL, respectively. Representative images of fluorescently stained, adherent platelets and unstained, adherent leukocytes without addition of particles and with the addition of 10^7 particles/mL are shown in Figure 4.1B. When examining the corresponding change in leukocyte adhesion (Figure 4.1A), leukocyte adhesion also decreased with increasing particle concentration. However, specifically at high particle concentrations, fold change in leukocyte adhesion exceeded that of platelet adhesion; for instance, at $5*10^7$ particles/mL leukocyte adhesion decreased to 30% in comparison to non-particle controls ($p < 0.0001$).

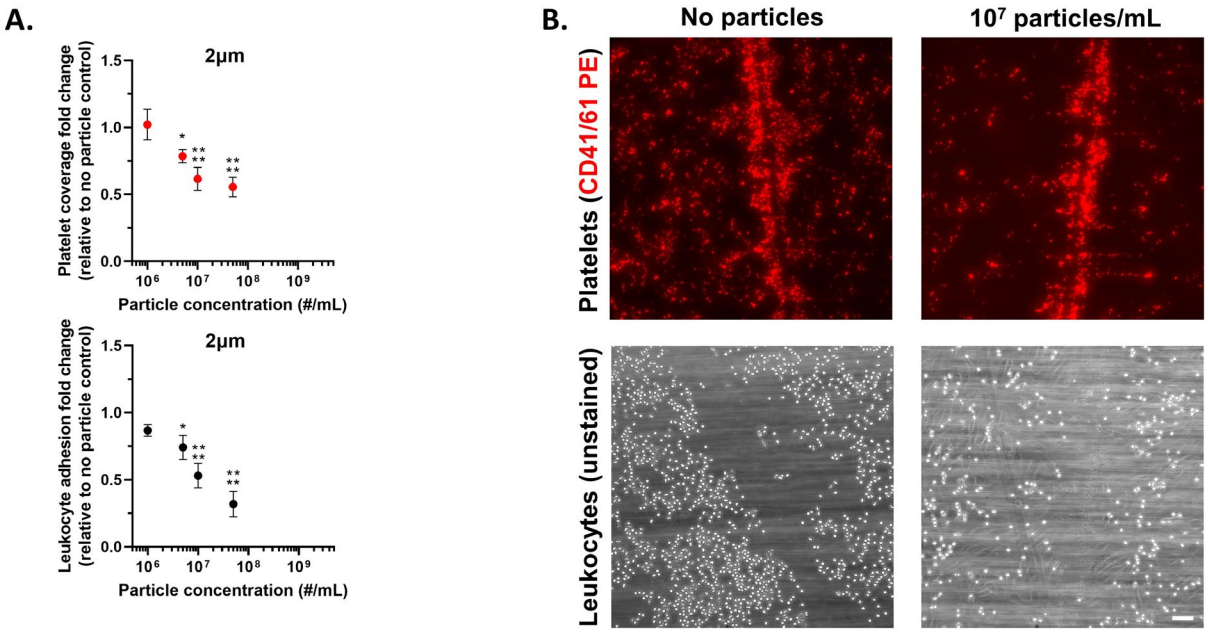

Figure 4.1: Micron-sized particles decrease platelet-leukocyte aggregate adhesion to an inflamed endothelium.

(A) Impact of 2 μm IgG-conjugated model polystyrene particles on platelet adhesion (red) and leukocyte adhesion (black) to an inflamed, damaged endothelium in whole blood flow in comparison to non-particle controls, (B) Representative images of adherent platelets (red) and leukocytes (unstained) to inflamed, damaged HUVEC monolayer in the absence (left) or presence (right) of 2 μm IgG-conjugated polystyrene particles. Statistical analyses were performed using two-way ANOVA with Tukey's multiple comparisons test. (*) indicates $p<0.05$, and (****) indicates $p<0.0001$ in comparison to no particle controls. Lack of symbols indicates no statistical significance. Error bars represent standard error, scale bar 100 μm.

We hypothesized that the mechanism of action causing decreased platelet adhesion using high, concentrations of untargeted PS particles was due to particles interfering with leukocytes, bound to platelets, adhering to the endothelium. To interrogate this hypothesis, we removed leukocytes from whole blood and reconstituted blood containing platelet-rich plasma and red blood cells. We then repeated flow experiments examining platelet adhesion to an inflamed, damaged endothelium in the presence of untargeted 2 μm PS particles. In contrast to the decrease in platelet adhesion seen in Figure 4.1A with leukocytes present, no change in platelet adhesion occurred when leukocytes were removed from the system (Figure 4.2), even at high particle concentrations ($5*10^7$/mL). This finding demonstrated that the presence of leukocytes is essential to see an impact

of untargeted particles on platelet adhesion. However, this result did not clarify if leukocytes must be adherent to the endothelium for there to be an impact of particles on platelet adhesion or if the simply the presence of leukocytes in the system is enough for an impact to be seen.

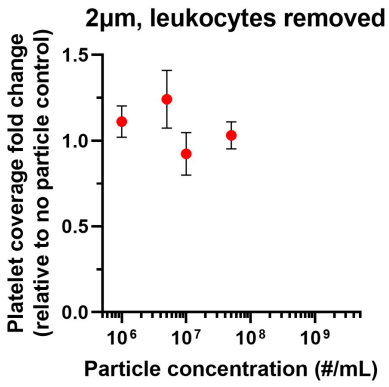

Figure 4.2: Removal of leukocytes neutralizes anti-platelet impact of 2 µm particles.

Impact of 2 µm IgG-conjugated polystyrene particles on platelet adhesion to inflamed, damaged endothelium with leukocytes removed from blood. Statistical analyses were performed using two-way ANOVA with Tukey's multiple comparisons test. Lack of symbols indicates no statistical significance. Error bars represent standard error.

To further confirm our hypothesis, we prevented leukocyte adhesion in whole blood to endothelium by blocking E-selectin on the surface of IL-1β-activated HUVEC[216]. Use of anti-E-selectin blocking antibodies led to a decrease in platelet adhesion to 38% of non-blocked controls (Figure 4.3A, $p = 0.0015$). In contrast, a IgG1 antibody control did not impact platelet adhesion ($p = 0.9224$). More drastically, leukocyte adhesion in E-selectin blocking experiments decreased to <1% in comparison to non-blocking controls ($p < 0.0001$) and did not decrease due to a non-blocking IgG1 control (Figure 4.3B, $p = 0.2243$).

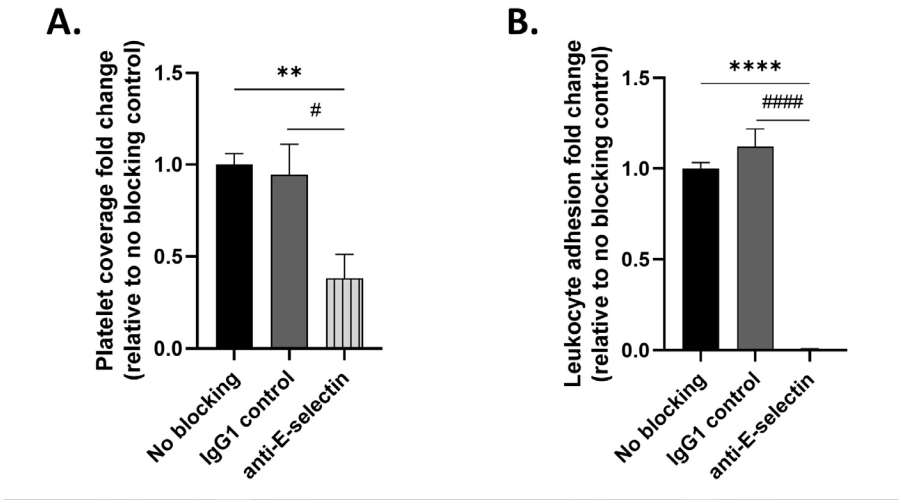

Figure 4.3: Blocking E-selectin on HUVEC surface leads to reduction in platelet adhesion and complete reduction of leukocyte adhesion.

Change in platelet (A) or leukocyte (B) adhesion to activated endothelium after blocking E-selectin on surface of HUVEC. Statistical analyses were performed using one-way ANOVA (D) with Tukey's multiple comparisons test. (**) indicates $p<0.01$ and (****) indicates $p<0.0001$ in comparison to no blocking controls and (#) and (####) in comparison to IgG1 controls. Lack of symbols indicates no statistical significance. Error bars represent standard error.

4.4.2 Polystyrene particles do not impact resting platelet adhesion in a non-inflammatory endothelial cell model

To further confirm that adherent leukocytes are required for PS particles to reduce platelet adhesion, we examined the impact of carboxylated PS particles on resting platelet adhesion to a non-IL-1β-activated endothelium. Particles were spiked into whole blood immediately before perfusion at a range of concentrations. Figure 4.4 shows the impact of 200 nm (Figure 4.4A), 2 µm (Figure 4.4B), and 2 µm sLe^A targeted (Figure 4.4C) on resting platelet adhesion. sLe^A is a small carbohydrate that binds to E-selectin[217] and can be used as a targeting ligand facilitating particle adhesion to an inflamed endothelium expressing E-selectin[139,145]. Even at high particle concentrations, there was no significant change to platelet adhesion for any of the particle types tested.

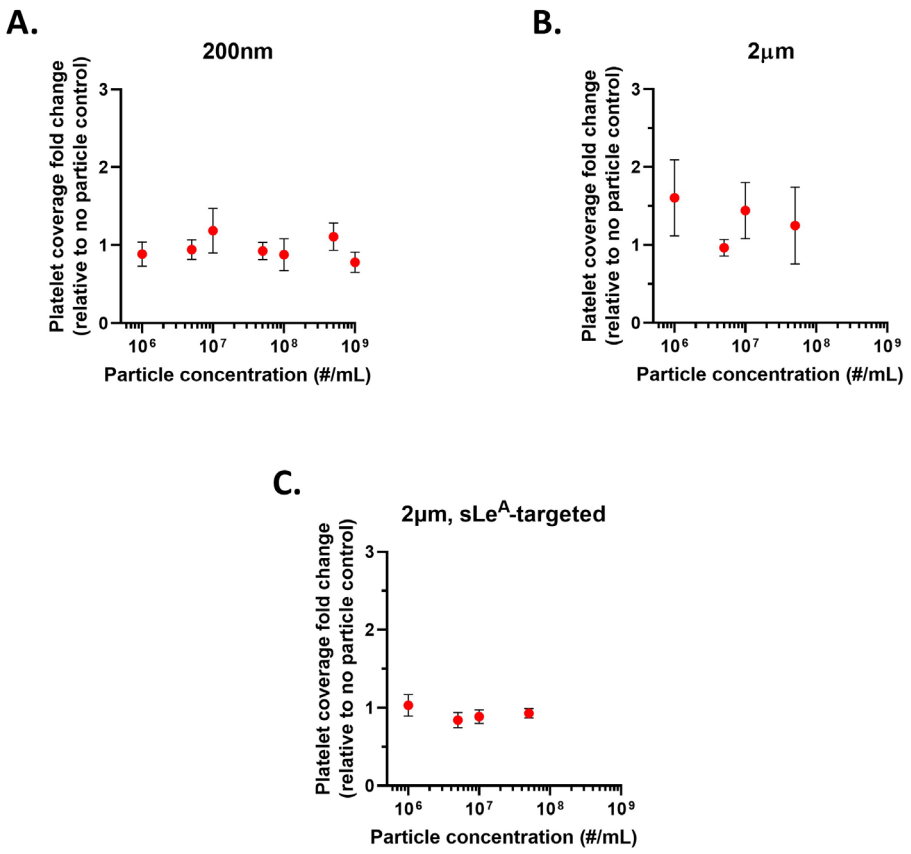

Figure 4.4: Polystyrene particles do not impact resting platelet adhesion to a damaged, unactivated endothelium.

Change in platelet adhesion in whole blood after 5 minutes of laminar flow at $1000s^{-1}$ to a damaged, inflamed endothelium with the addition of (A) unconjugated 200 nm polystyrene, (B) unconjugated 2 µm polystyrene, or (C) or sialyl Lewis-A conjugated 2 µm polystyrene particles. Statistical analyses were performed using two-way ANOVA with Tukey's multiple comparisons test. Lack of symbols indicates no statistical significance. Error bars represent standard error.

4.4.3 Polystyrene particles do not impact activated platelet adhesion to a non-inflammatory endothelial cell model

Figure 4.4 demonstrated that carboxylated and targeted PS particles do not impact the adhesion of resting platelets. However, elevated platelet activation often occurs in diseases[65,75,114]. To determine if particles impact the adhesion of activated platelets, we examined the impact of the same types of particulate drug carriers (200 nm and 2 µm carboxylated, 2 µm sLe^A-targeted) on

activated platelet adhesion to a damaged endothelial cell monolayer. Platelets were activated for one hour prior to blood flow using adenosine diphosphate (ADP). Similar to the results for unactivated platelets (Figure 4.4), there was no change in platelet adhesion for carboxylated 200 nm particles (Figure 4.5A), carboxylated 2 µm particles (Figure 4.5B), or sLe^A-targeted 2 µm particles (Figure 4.5C), regardless of particle concentration.

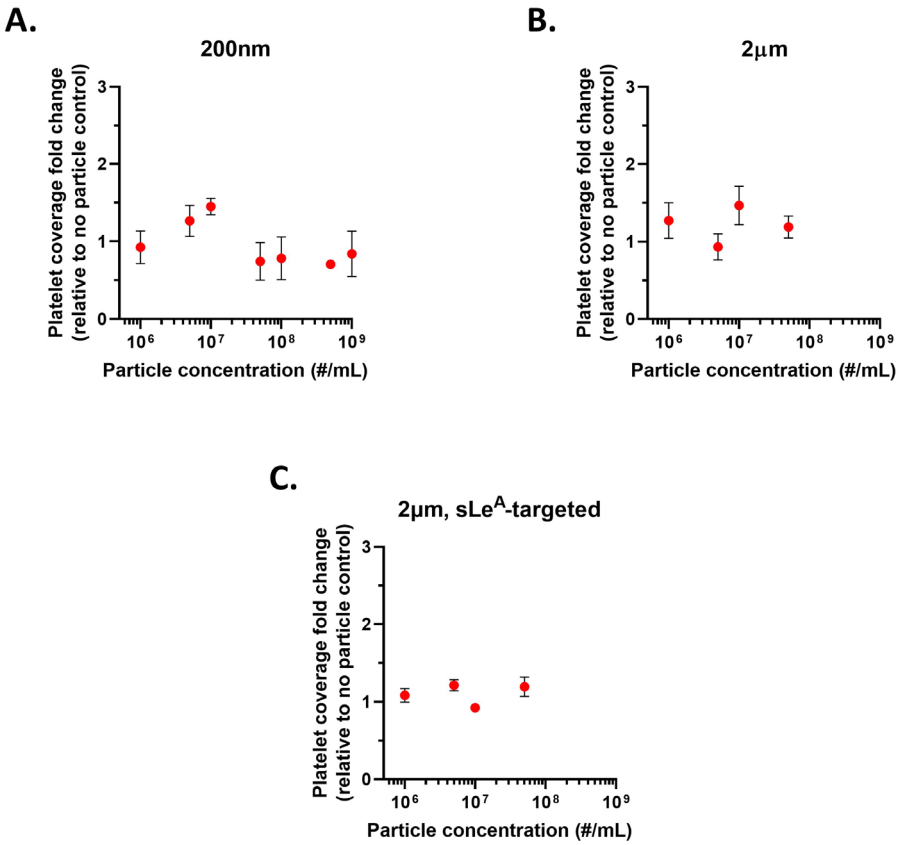

Figure 4.5: Polystyrene particles do not impact activated platelet adhesion to a damaged, unactivated endothelium.

Change in adhesion of platelets activated with 20µm ADP in whole blood after 5 minutes of laminar flow at $1000s^{-1}$ to a damaged, inflamed endothelium with the addition of (A) unconjugated 200 nm polystyrene, (B) unconjugated 2 µm polystyrene, or (C) sialyl Lewis-A conjugated 2 µm polystyrene particles. Statistical analyses were performed using two-way ANOVA with Tukey's multiple comparisons test. Lack of symbols indicates no statistical significance. Error bars represent standard error.

Together with the results shown in Figure 4.2, 4.3, and Figure 4.4, these results demonstrate that leukocyte adherence to an activated endothelium is essential for micron-sized particles to have a

downstream impact on platelet adhesion. Specifically, these results confirm our hypothesis that particles decreased platelet adhesion to inflamed HUVEC by removing platelet-bound leukocytes from the endothelial cell surface.

4.4.4 High leukocyte adhesion leads to high platelet adhesion and larger impact on platelet adhesion using 2 μm drug carriers

We previously demonstrated that untargeted, micron-sized particles can decrease activated platelet adhesion to an inflamed endothelium by interfering with platelet-leukocyte aggregates bound to the surface. The next natural query, then, is if magnitude of leukocyte adhesion directly impacts first, the magnitude of platelet adhesion and second, the impact of particulate drug carriers on platelet adhesion. To explore the first question, we compiled a scatterplot of leukocyte adhesion versus platelet adhesion of a wide variety of donors and experimental days. The results of this compilation are shown in Figure 4.6A. A basic linear regression on this data led to a statistically non-zero slope ($p < 0.0001$); in short, there is a correlation between leukocyte adhesion and platelet adhesion with higher leukocyte adhesion leading to higher platelet adhesion. This correlation aligns well with E-selectin blocking data shown in Figure 4.3A that demonstrated blocking leukocytes from adhering to an inflamed endothelium significantly decreased platelet adhesion. To explore whether the magnitude of leukocyte adhesion for a particular donor alters the impact of particles on that donor's platelet adhesion, we compiled another scatterplot (Figure 4.6B) of leukocyte adhesion in a donor's non-particle control trials versus that donor's platelet adhesion fold change after adding untargeted 2 μm PS particles at $1*10^7$ particles/mL. Interestingly, donors with higher leukocyte adhesion (prior to the addition of particles) did see a larger knockdown of platelet adhesion with the addition of particles. Donors with very low amounts of leukocyte adhesion generally saw a muted impact of particles on platelet adhesion. A simple linear regression

led to a statistically non-zero slope (p = 0.0028), suggesting that there is a correlation between donor leukocyte adhesion and the impact particles have on platelet adhesion.

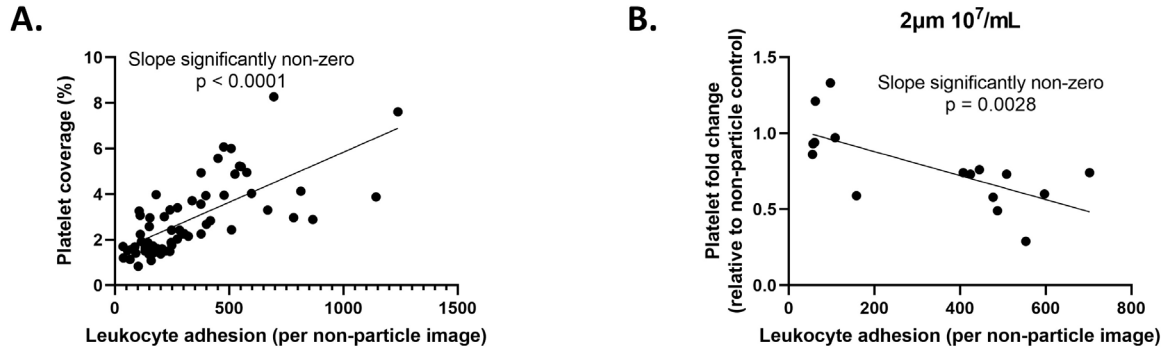

Figure 4.6: Higher leukocyte adhesion leads to higher activated platelet adhesion to an inflamed endothelial cell monolayer.

Scatterplots demonstrating relationship between (A) raw leukocyte adhesion versus platelet adhesion for non-particle control experiments, and (B) leukocyte adhesion for non-particle control experiments versus the platelet adhesion fold change for the same donor after addition of untargeted, 2 μm PS particles at 10^7 particles/mL. Analyses were performed using a simple linear regression.

4.4.5 Micron-sized particles outperform nano-sized particles at impacting leukocyte and platelet adhesion to an inflamed endothelium

After establishing that 2 μm untargeted particulate drug carriers significantly decrease platelet adhesion to an inflamed endothelium by removing leukocyte-platelet aggregates bound to the vascular wall, we further wanted to explore the design space of particulate drug carriers and how particle size impacts platelet and leukocyte adhesion. To that end, we examined the impact of a range of untargeted PS particles (200 nm, 500 nm, and 4.5 μm) on platelet and leukocyte adhesion at a variety of particle concentrations. Like the 2 μm untargeted particles, 4.5 μm untargeted particles were effective at decreasing both platelet (red) and leukocyte (black) adhesion at or above particle concentrations of 10^7. Specifically, at $5*10^7$ particles/mL platelet adhesion decreased to 47% (Figure 4.7A, $p < 0.0001$) and leukocyte adhesion decreased to 24% (Figure 4.7A, $p < 0.0001$) of non-particle controls.

Conversely, decreasing particle size led to a muted impact on platelet and leukocyte adhesion. For instance, untargeted 500 nm particles only significantly impacted platelet and leukocyte adhesion at the highest particle concentration tested, $5*10^8$/mL. At this high concentration, platelet adhesion decreased to 65% (Figure 4.7B, $p = 0.0013$) and leukocyte adhesion decreased to 35% (Figure 4.7B, $p < 0.0001$) of non-particle controls. Even more strikingly, 200 nm particles did not significantly impact platelet or leukocyte adhesion, even at the highest concentration examined. At 10^9 particles/mL, platelet adhesion stayed constant at 104% of non-particle controls (Figure 4.7C, $p = 0.9964$) and leukocyte adhesion was not significantly impacted (Figure 4.7C, $p = 0.2151$).

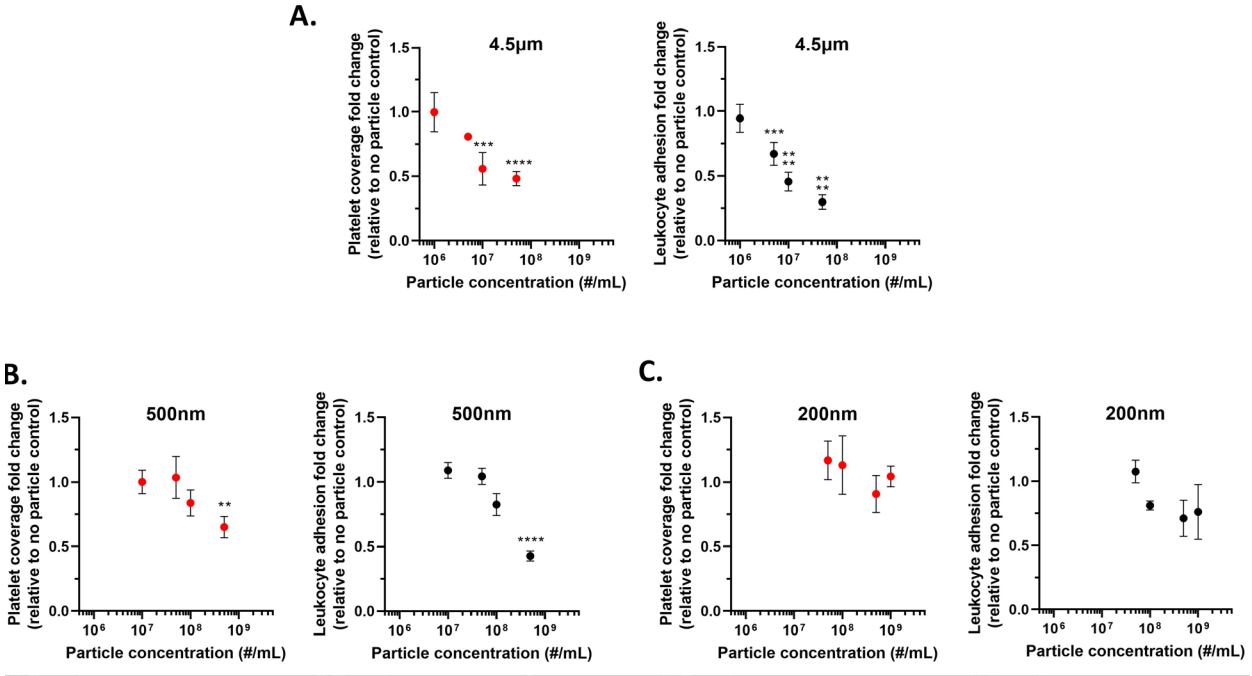

Figure 4.7: Micron-sized particles outperform nano-sized particles in modulating platelet and leukocyte adhesion to an inflamed endothelium.

Change in platelet (red) and leukocyte (black) adhesion to a damaged, inflamed endothelium with the addition of untargeted (A) 4.5 µm, (B) 500 nm, or (C) 200 nm IgG-conjugated polystyrene particles. Statistical analyses were performed using two-way ANOVA with Tukey's multiple comparisons test. (*) indicates $p<0.05$, (**) indicates $p<0.01$, (***) indicates $p<0.001$, and (****) indicates $p<0.0001$ in comparison to no particle controls. Lack of symbols indicates no statistical significance. Error bars represent standard error.

4.4.6 Addition of high levels of targeting improves particle impact at low concentrations

Figures 4.1 and 4.7 demonstrated that untargeted, micron-sized particles significantly decrease platelet and leukocyte adhesion to an inflamed, damaged endothelium at high concentrations (approximately 10^7 particles/mL and higher). We wanted to further explore the particle design space to determine if we could improve the efficacy of micron-sized particles, especially at low concentrations where they are underperforming in reducing platelet and leukocyte adhesion. To this end, we conjugated sLe^A targeting ligands to the surface of 2 μm particles. We utilized two different sLe^A site densities, 1,000 sites/um^2 ('low') and 13,500 sites/um^2 ('high') to interrogate not only the importance of targeting, but the importance of amount of targeting on particle ability to impact platelet and leukocyte adhesion.

At 10^6 particles/mL, particles with 'high' levels of targeting significantly decreased platelet adhesion to an inflamed endothelium compared to both no particle controls (Figure 4.8A, $p = 0.0186$) and untargeted particles ($p = 0.024$). Highly targeted 2 μm particles decreased platelet adhesion to 68% of non-particle controls. Conversely, particles with 'low' levels of targeting did not significantly impact platelet adhesion compared to either non-particle controls or untargeted particles. The impact of targeted particles on leukocyte adhesion followed a similar trend; highly targeted particles decreased leukocyte adhesion to 41% of non-particle controls (Figure 4.8B), a significant change in comparison to non-particle controls ($p = 0.0002$), untargeted particles ($p = 0.0076$), and also to particles with low levels of sLe^A ($p = 0.0289$).

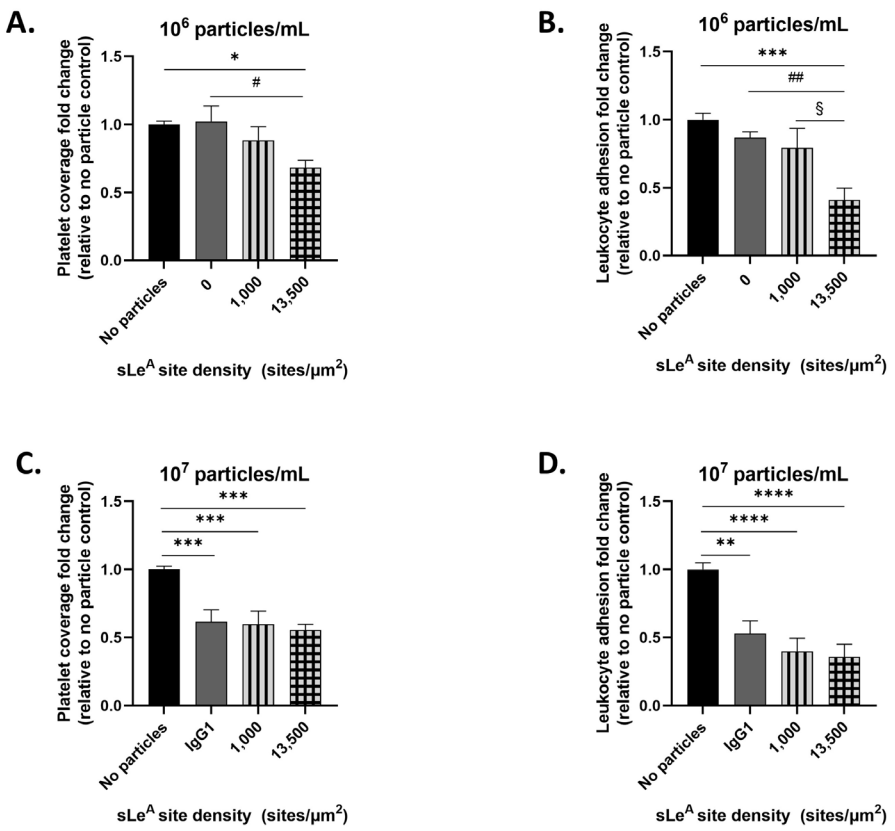

Figure 4.8: Targeted particles outperform non-targeted particles at low particle concentration.

Impact of sLe^A-conjugated particles at 10^6 particles/mL on (A) platelet adhesion, or (B) leukocyte adhesion. Impact of sLe^A-conjugated particles at 10^7 particles/mL on (C) platelet adhesion, or (D) leukocyte adhesion. Statistical analyses were performed using a one-way ANOVA with Tukey's multiple comparisons. (*) indicates $p<0.05$, (**) indicates $p<0.01$, (***) indicates $p<0.001$, and (****) indicates $p<0.0001$ in comparison to no particle controls. (##) indicates $p<0.01$ in comparison to untargeted (IgG conjugated) particles and § indicates $p<0.05$ in comparison to 'low' sLe^A targeted particles. Lack of symbols indicates no statistical significance. Error bars represent standard error.

We wanted to know if this improvement in ability of targeted particles to reduce platelet and leukocyte adhesion was consistent at higher particle concentrations. To this end, we also examined the impact of 'low' and 'high' targeted 10^7/mL particles on platelet and leukocyte adhesion. At 10^7 particles/mL, particles with either amount of targeting (high or low) were both able to significantly decrease platelet adhesion (Figure 4.8C; $p = 0.0006$ and $p = 0.0002$ for high and low particles, respectively, compared to no particle controls). However, at this particle concentration, addition of targeting did not improve the ability of particles to decrease platelet

adhesion. Untargeted particles were also able to significantly decrease platelet adhesion ($p = 0.001$) and there was no difference between the platelet adhesion decrease due to the different particle types; untargeted particles decreased platelet adhesion to 62% of non-particle controls, while targeted particles decreased adhesion to 60% and 55% (low targeting and high targeting, respectively). Similarly, all particle types were able to significantly decrease leukocyte adhesion at 10^7 particles/mL, though targeted particles slightly outperformed untargeted particles (Figure 4.8D). Untargeted particles decreased leukocyte adhesion to 53% of non-particle controls and low and high targeted particles decreased leukocyte adhesion to 40% and 36% of non-particle controls, respectively; greater amounts of targeting at 10^7 particles/mL led to a greater reduction in leukocyte adhesion.

4.4.7 Rod-shaped particles outperform spherical particles at decreasing leukocyte adhesion, but not platelet adhesion, at low concentrations

Targeting, as shown in Figure 4.8, improves the ability of 2 μm particles at low concentrations (10^6/mL) to decrease both platelet and leukocyte adhesion to an inflamed, damaged endothelium. However, targeting is not the only method used to increase the interaction between micron-sized polymeric particles and the vascular wall. Instead, previous groups demonstrated that altering the shape of spherical particles can improve their utility as vascular-targeted drug carriers. Specifically, targeted rod-shaped particles experiments adhere better to inflamed HUVEC in blood flow *in vitro* in comparison to spherical particles due to their increased surface area to volume ratio and large contact area between particle and endothelial cell monolayer[146]. To determine if rod-shaped particles could outperform spherical particles at decreasing platelet and leukocyte adhesion, we fabricated polystyrene rods at two aspect ratios (AR2 and AR8) from 2 μm spherical particles. At 10^6 particles/mL, both AR2 and AR8 particles led to a slight but non-significant

decrease in platelet adhesion in comparison to non-particle controls ($p = 0.2416$ and 0.2625, respectively; Figure 4.9A). Conversely, rod-shaped particles led to a significant decrease in leukocyte adhesion ($p = 0.0062$ for AR2 rods and $p = 0.0003$ for AR8 rods in comparison to non-particle controls; Figure 4.9B) and decreased leukocyte adhesion to 70% (AR2) and 59% (AR8) of non-particle controls. Spherical particles at the same concentration did not decrease leukocyte adhesion.

Because AR8 showed more promise than AR2 rods at reducing leukocyte adhesion at low concentrations, we selected AR8 rods only to examine their impact on platelet and leukocyte adhesion at a higher concentration. At 10^7 particles/mL, AR8 rods significantly decreased platelet adhesion (Figure 4.9C, $p = 0.0002$), but spherical particles performed just as well ($p = 0.0002$); both particle types reduced platelet adhesion to 62% of non-particle controls. Impact of AR8 rods on leukocyte adhesion followed a similar trend; AR8 rods and spherical particles both reduced leukocyte adhesion (Figure 4.9D, $p = 0.0002$ and $p < 0.0001$, respectively) to 57% (AR8 rods) and 53% (spheres) of non-particle controls.

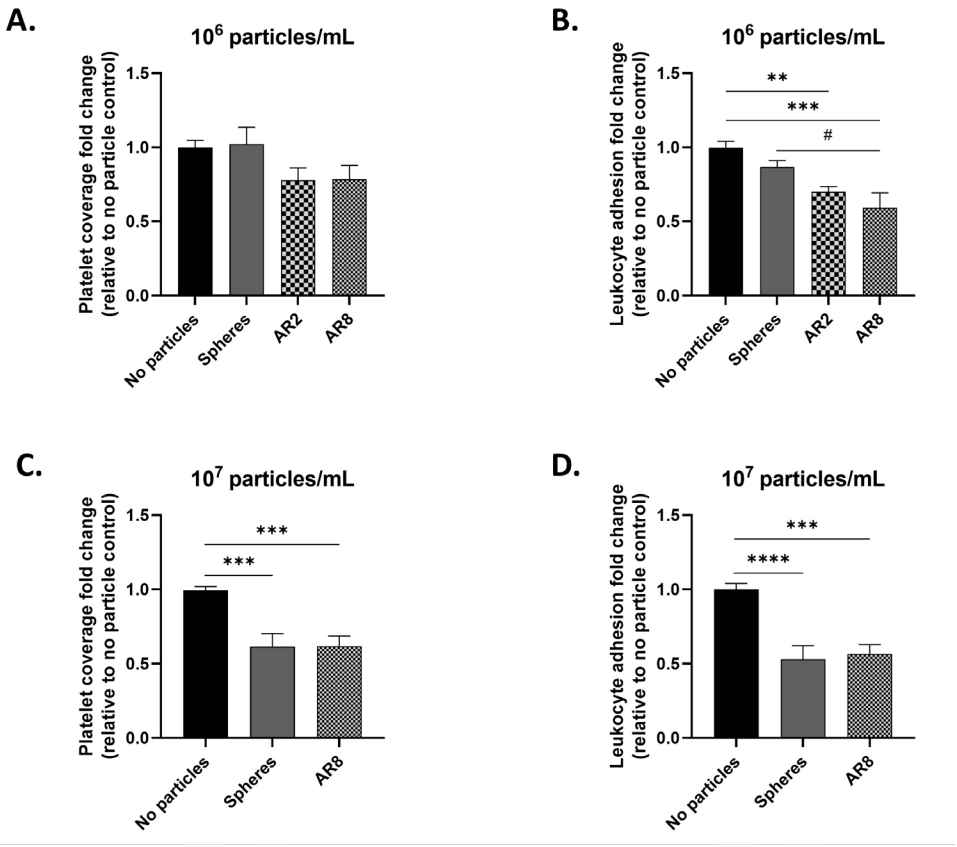

Figure 4.9: Rod-shaped particle outperform spherical particles in decreasing leukocyte, but not platelet, adhesion.

Impact of untargeted, rod-shaped particles at 10^6 particles/mL on (A) platelet adhesion, or (B) leukocyte adhesion. Impact of AR8 rod-shaped particles at 10^7 particles/mL on (C) platelet adhesion, or (D) leukocyte adhesion. Statistical analyses were performed using a one-way ANOVA with Tukey's multiple comparisons. (**) indicates $p<0.01$, (***) indicates $p<0.001$, and (****) indicates $p<0.0001$ in comparison to no particle controls and (#) indicates $p<0.05$ in comparison to spherical particles. Lack of symbols indicates no statistical significance. Error bars represent standard error.

4.4.8 Polymeric particles decrease neutrophil-mediated platelet adhesion to mesentery in a mouse model of systemic inflammation

To determine if particles could reduce leukocyte-mediated platelet adhesion in a more physiologically relevant environment, we utilized a murine model of inflammation. Specifically, we induced endotoxemia via an intraperitoneal (IP) injection of bacterial lipopolysaccharide (LPS), which leads to neutrophil-dependent platelet adhesion in the mesenteric vessels[164,165]. A

timeline and schematic for this procedure are shown in Figure 4.10A; mice were anesthetized and given a retro-orbital injection of neutrophil and platelet labeling antibodies along with an IP injection of 5 mg/kg LPS.

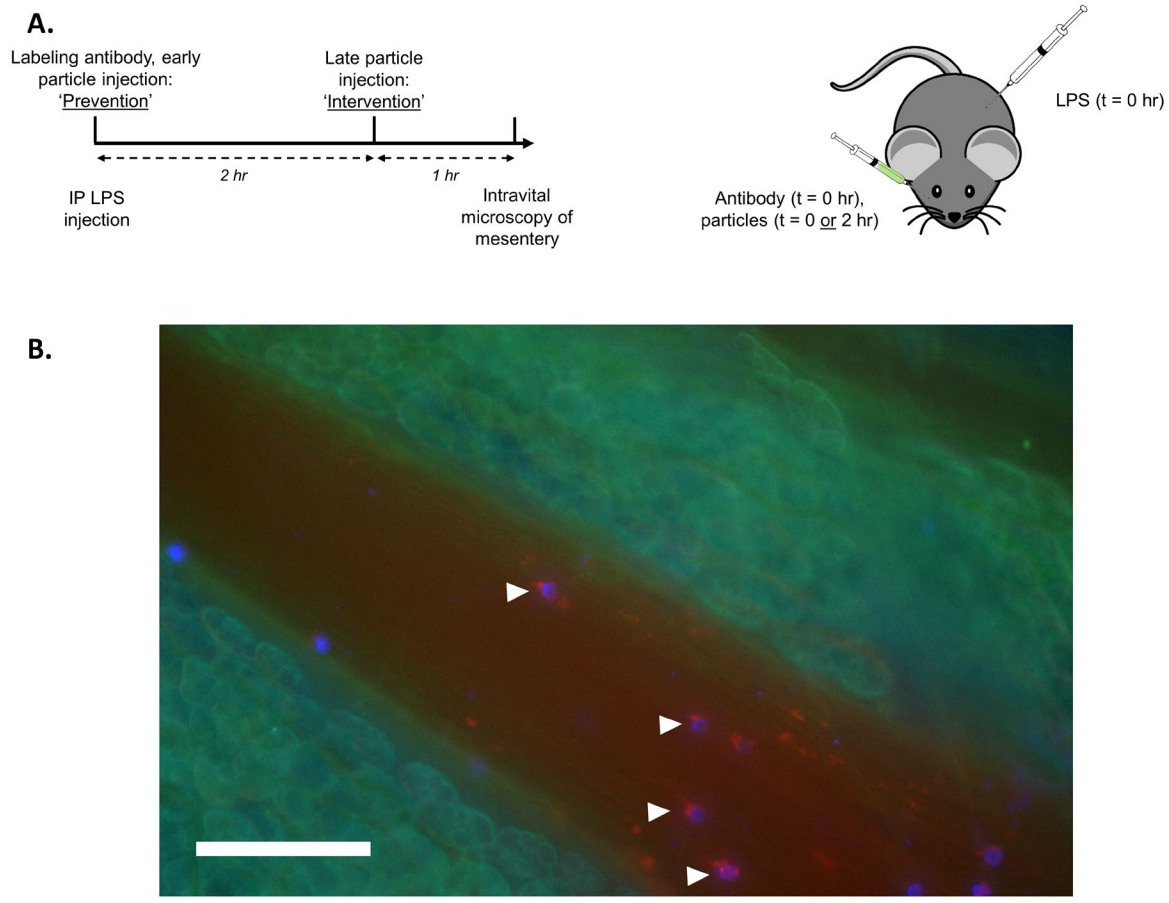

Figure 4.10: Intraperitoneal lipopolysaccharide induces platelet-neutrophil adhesion in mouse mesentery.

(A) Timeline, dosing scheme, and experimental schematic of intravital microscopy of inflamed mouse mesentery. Mice receive an IP injection of LPS and a RO injection of labeling antibodies at t = 0 and for particle groups, a RO injection of particles at t = 0 ('prevention') or t = 2 hours ('intervention'). Mice were imaged at t = 3 hours. (B) Representative merged image of a mouse mesenteric blood vessel after 3-hour IP LPS injection with channels fluorescent Brilliant Violet 421 Ly6G+ neutrophils (blue), FITC polystyrene particles (green), anti-GP1b DyLight 649 platelets (red), scale bar 100 μm. White arrows highlight platelet-neutrophil aggregates.

Mice receiving particle therapeutics fell into two groups: the 'prevention' group received 10 mg/kg polystyrene particles at the time of LPS administration while the 'intervention' group received 10 mg/kg polystyrene particles two hours after LPS administration. Particles were either

conjugated with anti-E-selectin and anti-ICAM1 antibodies ('T,' targeted) or isotype controls ('UT,' untargeted). Mice were anesthetized three hours after being given LPS and their mesentery examined for adherent neutrophils, platelets, and particles. A representative image of platelets and leukocytes bound to an LPS-inflamed mesentery are shown in Figure 4.10B with arrows specifically highlighting platelet-neutrophil aggregates bound to the endothelium. Representative images of all treatment groups are shown in Figure 4.11.

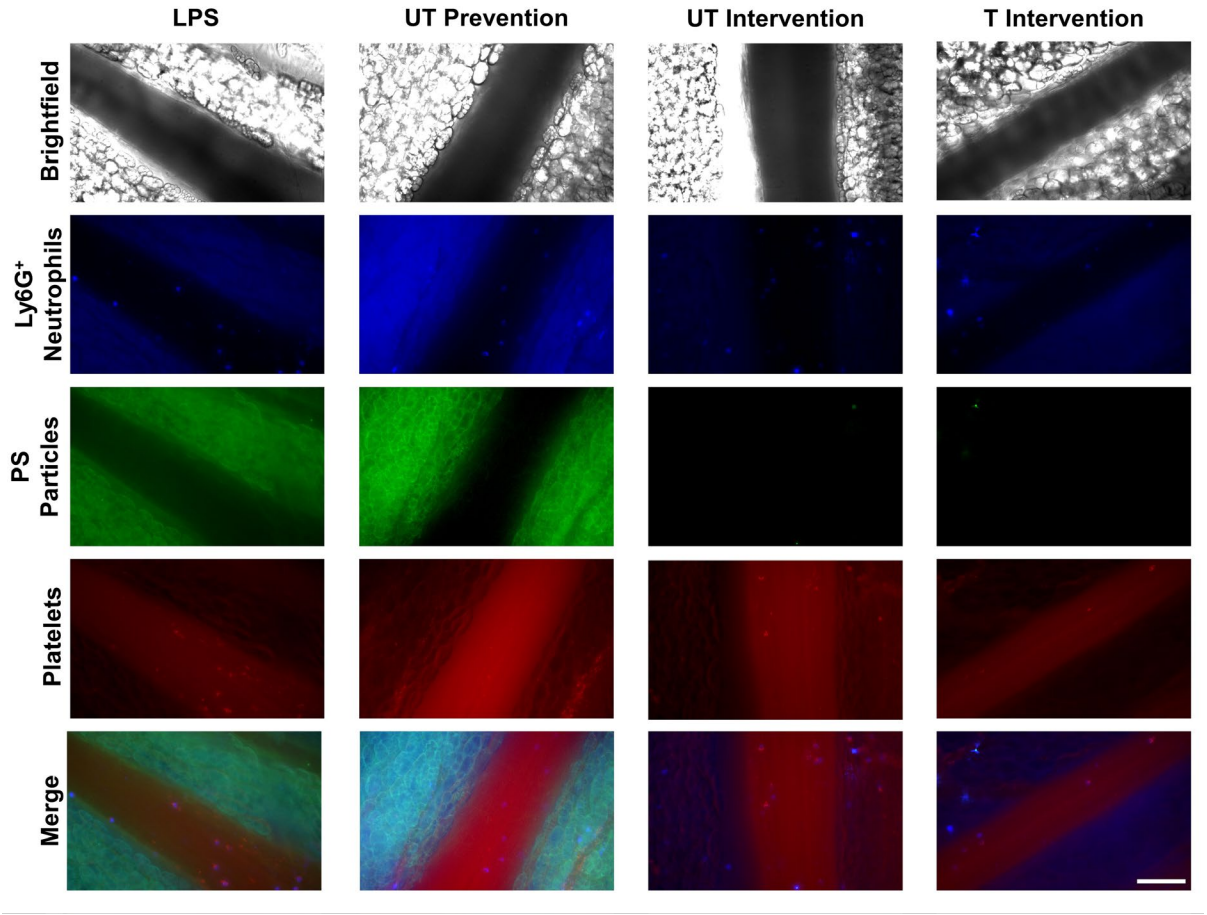

Figure 4.11: Particles reduce LPS-induced platelet-neutrophil adhesion in mouse mesentery.

Representative images of brightfield microscopy blood vessels and fluorescent Brilliant Violet 421 Ly6G+ neutrophils (blue), FITC polystyrene particles (green), anti-GP1b DyLight 649 platelets (red) within mouse mesenteric blood vessel, scale bar 100 µm.

The firm adhesion of neutrophils, platelets, and particles was quantified for each experimental group, as well as the number of non-adherent neutrophils either rolling along the endothelial cell surface or in the blood free stream. All quantified adhesion values were scaled to the surface area of the vessel, which varied from animal to animal. The injection of particles significantly decreased platelet adhesion to the mesentery for the UT prevention and T intervention groups (Figure 4.12A); the number of adherent platelets decreased by 57% (untargeted prevention; $p = 0.0053$), and 60% (targeted intervention; $p = 0.0035$) due to particle treatments. To determine if this decrease in platelet adhesion was tied to neutrophil adhesion, we also examined the number of $Ly6G^+$ neutrophils adherent in the mesentery. Again, two particle treatments decreased adherent neutrophils bound to the mesentery wall (Figure 4.12B). The number of adherent neutrophils decreased from a maximum of $313/mm^2$ for LPS-only mice by 54% (untargeted prevention; $p = 0.0133$), and 62% (targeted intervention; $p = 0.0046$). We then examined what percentage of platelets were associated with neutrophils at the vascular wall to ascertain whether platelets were binding directly to neutrophils or if a decrease in neutrophils in the mesentery indirectly impacted platelet adhesion to the mesentery wall. For all experimental groups, 84% or more of the platelets bound to the wall were directly bound to a neutrophil; this percentage did not change with particle treatment (Figure 4.12C).

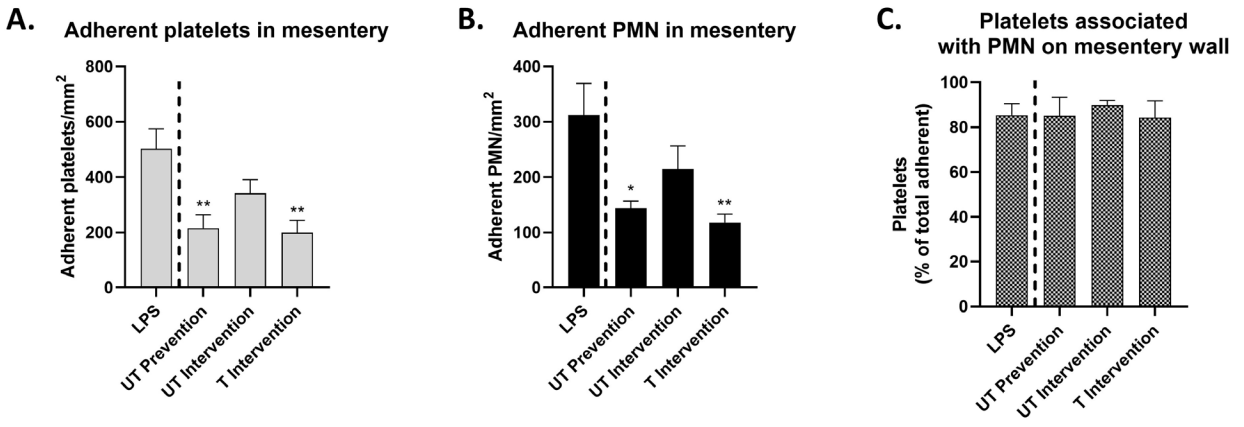

Figure 4.12: Particles reduce platelet accumulation in inflamed mouse mesentery by diverting neutrophils.

Quantified results of (A) platelet adhesion, and (B) neutrophil (PMN) adhesion in mouse mesentery 3 hours after IP injection of LPS, scaled by the surface area of the blood vessel. (C) The percent of total platelets adherent to mesentery that are associated with a bound PMN. Experimental groups consist of N=5 mice per group with 2-4 independent vessels imaged per mouse. Statistical analyses were performed using a one-way ANOVA with Tukey's multiple comparisons. (*) indicates $p<0.05$ and (**) indicates $p<0.01$ in comparison to LPS-only controls. Lack of symbols indicates no statistical significance. Error bars represent standard error.

We wanted to determine if introduction of particles changed the phenotype of neutrophils in the mesentery from firmly adherent to rolling or in the blood stream. To do so, we quantified the number of firmly adherent and non-adherent neutrophils that passed through the frame over the course of each video. The percentage of neutrophils that are firmly adherent is shown in Figure 4.13A; no particle group led to a significant difference in the percentage of firmly adherent neutrophils in comparison to the LPS-only control. However, the targeted intervention group did lead to a nearly significant decrease in the percentage of firmly adherent neutrophils ($p = 0.061$). We further quantified the number of adherent platelets per adherent neutrophil; for all experimental groups, on average each firmly bound neutrophil was associated with >1 adherent platelet (Figure 4.13B). Because each bound neutrophil was associated with at least one bound platelet and ≥84% of all adherent platelets are bound directly to neutrophils, even a modest decrease in adherent

neutrophils due to particle treatment had a large downstream impact on platelet adhesion, diverting platelets away from an area of inflammation.

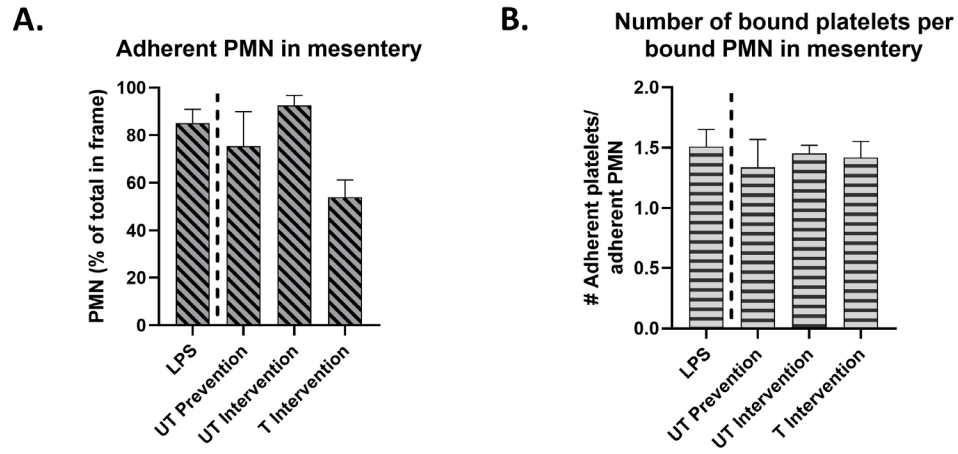

Figure 4.13: Particles do not impact neutrophil phenotype or the number of platelets bound to each neutrophil.

Quantified results of (A) The percent of all PMN (adherent, rolling, and in blood flow) that are firmly adherent to the mesentery. (B) The average number of platelets adherent to each adherent neutrophil in the mesentery. Experimental groups consist of N=5 mice per group with 2-4 independent vessels imaged per mouse. Statistical analyses were performed using a one-way ANOVA with Tukey's multiple comparisons. Lack of symbols indicates no statistical significance. Error bars represent standard error.

One major difference between the different particles tested is the inclusion of targeting ligands for the targeted intervention group. The number of adherent particles in each experimental group is quantified in Figure 4.14A. For all particle groups there was minimal particle adhesion to the mesentery wall and no particle adhesion seen for the prevention treatment group. Inclusion of anti-E-selectin and anti-ICAM-1 targeting did not significantly impact the adhesion of particles and in fact, untargeted intervention particles bound more to the vessel than intervention targeted particles. Interestingly, any particles bound firmly to the imaged blood vessels were associated with firmly adherent neutrophils and not directly bound to the endothelium. One such example is shown in Figure 4.14B; in this image, an untargeted particle from the intervention treatment group is associated with a neutrophil bound to the mesentery.

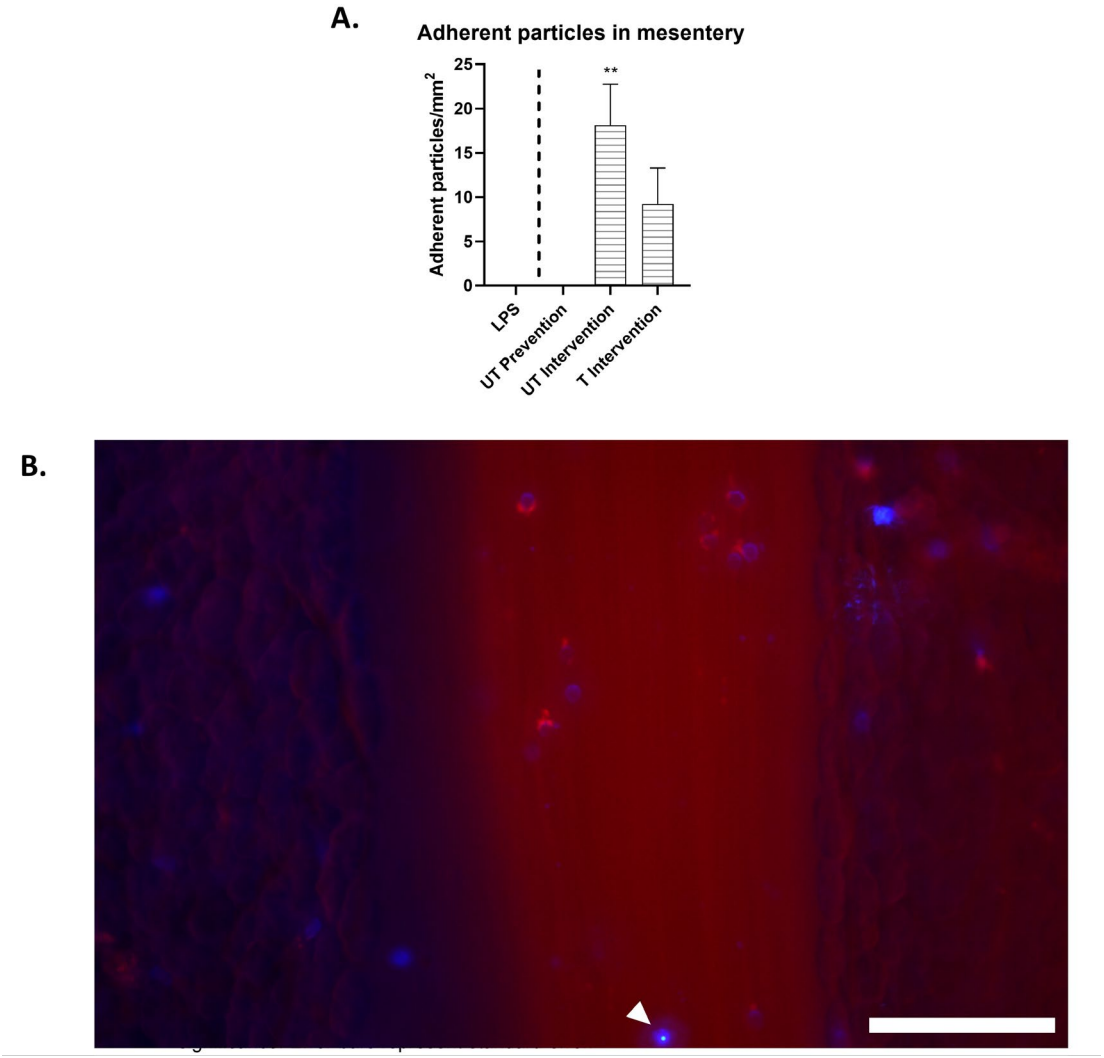

Figure 4.14: Particles bound to vascular wall are associated with neutrophils.

(A) Quantified results of particle adhesion in mouse mesentery 3 hours after IP injection of LPS, scaled by the surface area of the blood vessel. (B) Representative merged image of a mouse mesenteric blood vessel after 3-hour IP LPS injection with channels fluorescent Brilliant Violet 421 Ly6G+ neutrophils (blue), FITC polystyrene particles (green), anti-GP1b DyLight 649 platelets (red), scale bar 100 μm. White arrows highlight particle associated with bound neutrophil. Statistical analyses were performed using a one-way ANOVA with Tukey's multiple comparisons. (**) indicates $p<0.01$ in comparison to LPS-only controls. Lack of symbols indicates no statistical significance. Error bars represent standard error.

To further explore the design space of particles *in vivo*, we examined the impact of untargeted, 500 nm PS particles given as a 'prevention' treatment to mice, similarly as the untargeted, 2 μm PS particles. Unlike their micron-sized counterparts, nano-sized particles did not

significantly impact platelet (Figure 4.15A) or neutrophil (Figure 4.15B) adhesion to the mesentery.

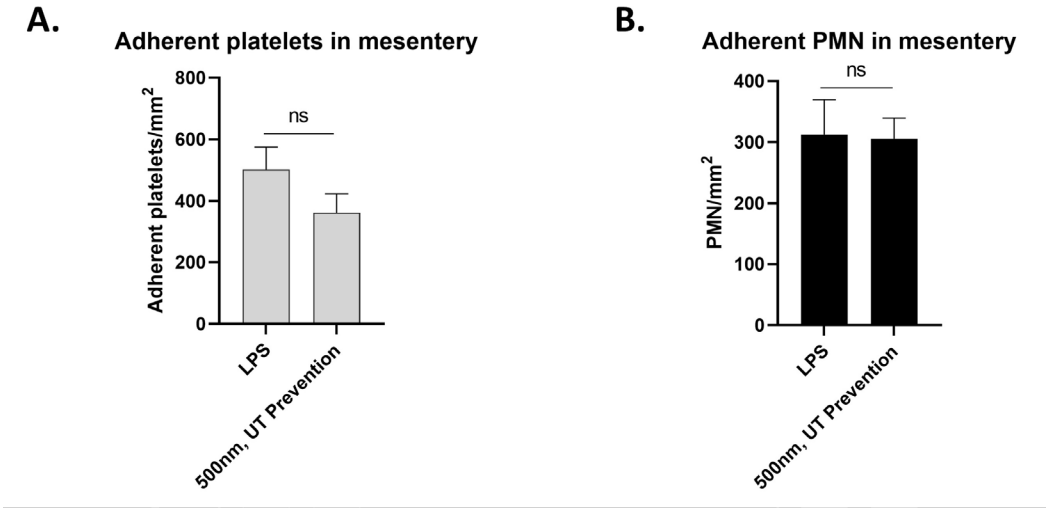

Figure 4.15: Nano-sized particles do not reduce leukocyte or platelet adhesion to mouse mesentery.

Quantified results of (A) platelet adhesion, and (B) neutrophil (PMN) adhesion in mouse mesentery 3 hours after IP injection of LPS, scaled by the surface area of the blood vessel. Experimental groups consist of N=5 mice per group with 2-4 independent vessels imaged per mouse. Statistical analyses were performed using an unpaired Student's t-test. Lack of symbols indicates no statistical significance. Error bars represent standard error.

To determine if particle phagocytosis by neutrophils is responsible for diverting neutrophils away from the inflamed mesentery, we conjugated polyethylene glycol (PEG) onto the surface of 2 μm PS particles to reduce phagocytosis by the mouse neutrophils and increase circulation time[151,218]. We administered PEG-PS particles as a 'prevention' treatment to mice; though PEG-PS particles did reduce platelet adhesion (Figure 4.16A), the particles did not significantly reduce neutrophil adhesion (Figure 4.16B) to the mouse mesentery. Upcoming work will confirm the presence of PEG on the surface of PS particles as well as reduced phagocytosis of PEG-PS particles in comparison to PS particles by mouse phagocytes.

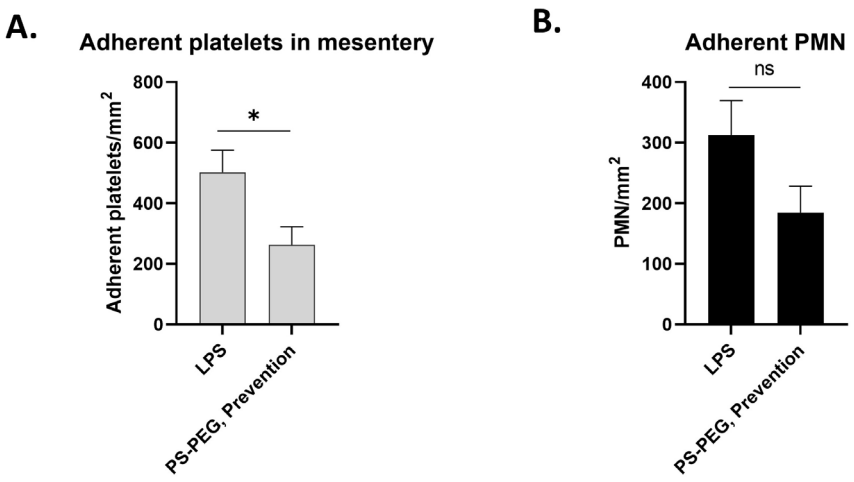

Figure 4.16: PEGylated, micron-sized particles reduce platelet adhesion to mouse mesentery.

Quantified results of (A) platelet adhesion, and (B) neutrophil (PMN) adhesion in mouse mesentery 3 hours after IP injection of LPS, scaled by the surface area of the blood vessel. Experimental groups consist of N=4-5 mice per group with 2-4 independent vessels imaged per mouse. Statistical analyses were performed using an unpaired Student's t-test. (*) indicates $p<0.05$ in comparison to LPS-only controls. Lack of symbols indicates no statistical significance. Error bars represent standard error.

4.4.9 Salicylic acid-based microparticles reduce platelet and leukocyte adhesion to the mesentery

PS-based microparticles thus far successfully reduced both platelet and leukocyte adhesion to an inflamed mouse mesentery. However, PS is not biodegradable and contains no active therapeutic compounds. Recently, a salicylic acid-based polymer was utilized to make micron-sized particles; in a mouse model of acute lung injury, these poly-aspirin (or PolyA) particles significantly reduced neutrophil infiltration into the lung and reduced inflammation, outperforming both PS and poly-lactic-co-glycolic (PLGA) particles[137]. To determine if these PolyA particles can reduce cell adhesion in our mouse model of systemic inflammation, we dosed mice with an 'intervention' of PolyA particles. Results from these experiments are shown in Figure 4.17. PolyA particles led to a significant decrease in platelets to the mesentery (Figure 4.17A), though not a significant

decrease of neutrophils (Figure 4.17B). This result differs from PS particles, where all particle types that significantly decreased platelet adhesion also decreased leukocyte adhesion (Figure 4.12). For PolyA particle-treated mice, there is no significant decrease of the percentage of platelets that are bound to neutrophils (Figure 4.17C). Strikingly, mice treated with PolyA particles had a significant reduction in the percentage of neutrophils that are firmly adherent as opposed to rolling or in free stream (Figure 4.17D) and a significant reduction in the number of platelets bound per adherent neutrophil (Figure 4.17E). Both of these results are unique to PolyA particles only and suggests that PolyA particles have an addition therapeutic effect that alters the phenotype of neutrophils. Large, representative images of the mouse mesentery after an UT intervention of PS particles is shown in Figure 4.18A and after an UT intervention of PolyA particles is shown in Figure 4.18B to highlight the difference in number of platelets decorating each adherent neutrophil between PS-treated (1.45 adherent platelets/adherent neutrophil; Figure 4.13B) and PolyA-treated (0.75 adherent platelets/adherent neutrophil; Figure 4.17E) mice.

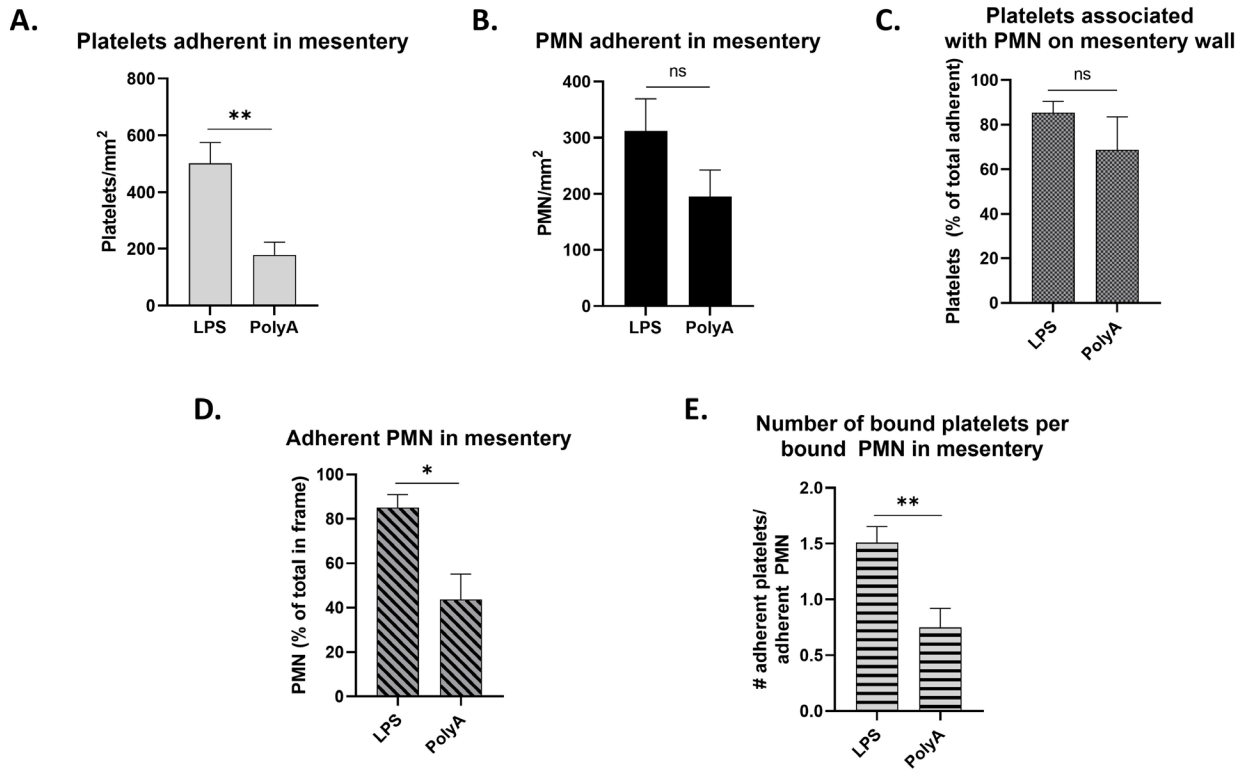

Figure 4.17: Salicylic acid-based particles reduce platelet and leukocyte adhesion to mouse mesentery.

Quantified results of (A) platelet adhesion, and (B) neutrophil (PMN) adhesion in mouse mesentery 3 hours after IP injection of LPS, scaled by the surface area of the blood vessel (C) The percent of total platelets adherent to mesentery that are associated with a bound PMN., (D) The percent of all PMN (adherent, rolling, and in blood flow) that are firmly adherent to the mesentery, and (E) The average number of platelets adherent to each adherent neutrophil in the mesentery. Experimental groups consist of N=5 mice per group with 2-4 independent vessels imaged per mouse. Statistical analyses were performed using an unpaired Student's t-test where (*) indicates $p<0.05$ and (**) indicates $p<0.01$ in comparison to LPS-only controls. Lack of symbols indicates no statistical significance. Error bars represent standard error.

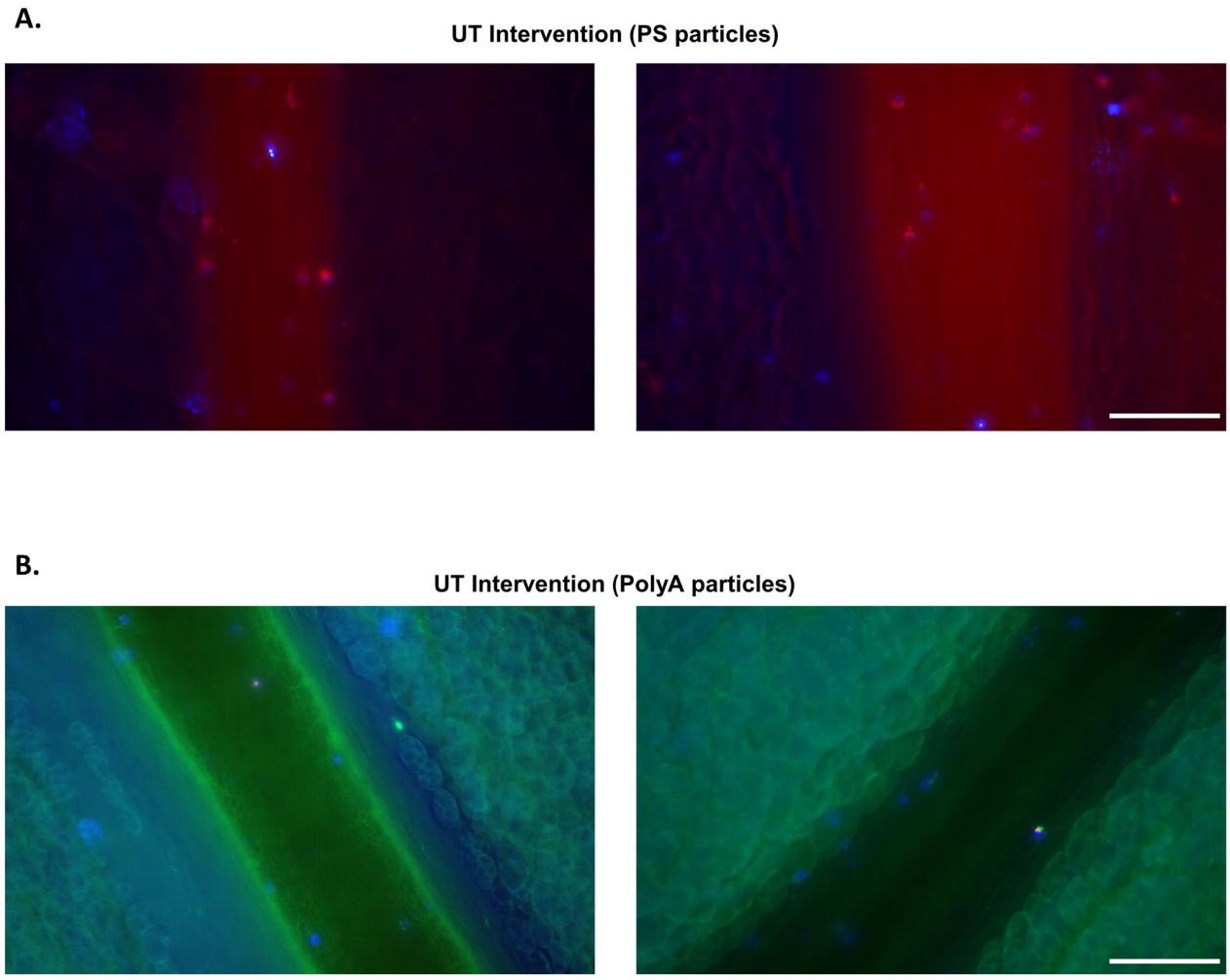

Figure 4.18: Neutrophils from mice treated with PolyA particles are adherent to fewer platelets than those treated with PS particles.

(A) Representative merged images of mouse mesenteric blood vessels after 3-hour IP LPS injection and receiving an 'intervention' treatment of untargeted PS particles with channels fluorescent Brilliant Violet 421 Ly6G+ neutrophils (blue), FITC PS particles (green), anti-GP1b DyLight 649 platelets (red). (B) Representative merged images of mouse mesenteric blood vessels after 3-hour IP LPS injection and receiving an 'intervention' treatment of untargeted PolyA particles with channels fluorescent Brilliant Violet 421 Ly6G+ neutrophils (blue), anti-GP1b Dylight 488 platelets (green), Cy5.5 PolyA particles (red), scale bar 100 μm.

4.4.10 Depletion of neutrophils in mice reduces platelet adhesion to mesentery and negates impact of micron-sized particles on platelet adhesion

Thus far, our data suggested that most platelet adhesion to the mesentery is neutrophil-dependent and that injection of particles reroutes neutrophils from the inflamed mesentery in mice, potentially via phagocytosis. To support this theory, we depleted neutrophils from mice using an anti-Ly6G depletion antibody[219]; we administered 500 μg of anti-Ly6G to mice one day prior to intravital imaging via intraperitoneal injection and an additional 200 μg of anti-Ly6G via retro-orbital injection to mice at the same time as LPS installation. A subset of these mice also received untargeted, 2 μm PS particles given as 'prevention' therapies to determine if particles impact platelet adhesion in the absence of neutrophils. We confirmed the reduction of neutrophil counts using a complete blood count before administering anti-Ly6G intraperitoneally, the following day before LPS installation, and at the time of euthanasia.

The impact of neutrophil depletion with or without untargeted 2 μm PS on platelet adhesion to the mouse mesentery after LPS installation is shown in Figure 4.19. Both depleting neutrophils and depleting neutrophils with addition of 'prevention' UT PS particles led to a statistically significant decrease in platelet accumulation in the mesentery in comparison to non-depleted LPS controls ($p = 0.0003$ and $p = 0.0009$, respectively). There was no difference between depleted mice receiving PS particles with those that did not ($p = 0.9993$), which confirms previous work that platelet adhesion in the mesentery after an IP installation of LPS is neutrophil dependent[164]. These findings also confirm our hypothesis that particles impact neutrophils specifically and that any downstream reduction in platelet adhesion to the inflamed mesentery is due to particle-neutrophil interactions. Overall, the decrease in platelet adhesion in the mesentery with particle treatment is due directly to particles removing or rerouting neutrophils from the mesenteric wall.

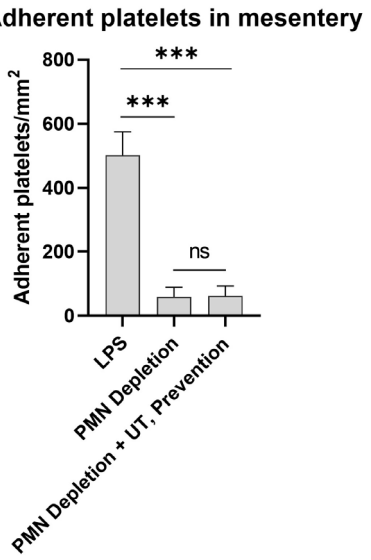

Figure 4.19: Neutrophil depletion reduces platelet adhesion and impact of particles on platelet adhesion to mouse mesentery.

Quantified results of platelet adhesion in mouse mesentery 3 hours after IP injection of LPS, scaled by the surface area of the blood vessel. Experimental groups consist of N=3-5 mice per group with 2-4 independent vessels imaged per mouse. Statistical analyses were performed using a one-way ANOVA with Tukey's multiple comparisons. (***) indicates $p<0.001$ in comparison to non-depleted, LPS controls. Error bars represent standard error.

4.5 Discussion

Overall, we demonstrated in this chapter that particulate drug carriers can be used to decrease excess platelet adhesion to an area of thromoinflammation by decreasing the number of platelet-leukocyte aggregates bound to an inflamed endothelium (Figure 4.1). We confirmed that the mechanism of this decrease in platelet adhesion is in fact due to the decrease in adherent leukocytes through several experiments. First, we confirmed that both untargeted and targeted polystyrene (PS) particles (200 nm and 2 μm) do not impact either resting (Figure 4.4) or activated (Figure 4.5) platelet adhesion to a damaged endothelial monolayer in the absence of endothelial inflammation. After noting that untargeted 2 μm PS particles decrease both platelet and leukocyte adhesion to an IL-1β inflamed HUVEC monolayer (Figure 4.1), we then neutralized that particle

impact by completely removing the leukocytes (Figure 4.2). Once leukocytes were removed from whole blood, we saw no impact of untargeted PS particles on platelet adhesion, even at high particle concentration (up to $5*10^7$/mL). Finally, we prevented binding of leukocytes to the inflamed HUVEC monolayer by blocking the HUVEC surface with anti-E-selectin blocking antibodies (Figure 4.3). In this set of experiments, leukocytes were not removed from whole blood, but rather their interactions with the endothelium were eliminated. By blocking E-selectin on the endothelial cell surface, we saw a significant decrease in platelet adhesion and a complete knock-down of leukocyte adhesion (Figure 4.3). Overall, these experiments confirm our hypothesis that micron-sized particles decrease platelet adhesion to an IL-1β inflamed HUVEC monolayer by interfering with firm adhesion of platelet-leukocyte aggregates to the endothelium. In addition, the experiments utilizing a non-activated endothelium (Figure 4.4 and 4.5) demonstrate that at these particle sizes and concentrations, PS particles neither contribute to clotting nor inhibit the ability of platelets to bind. Both of these aspects are essential in designing particulate drug carrier therapeutics as increased clotting risk or clotting reduction could both be potentially dangerous side effects when translating particle therapeutics to use in humans.

After confirming our mechanism of action, we further examined the particulate drug carrier design space to determine how changing properties of particles, including size, shape, and inclusion of targeting, impacts their ability to modulate platelet adhesion in thromboinflammation. Micron-sized PS particles (2 μm, 4.5 μm) had similar, significant impacts on both platelet and leukocyte adhesion (Figure 4.1 and 4.7A), particularly at particles concentrations at or above 10^7/mL. Conversely, nano-sized PS particles (200 nm, 500 nm) had muted impacts on platelet adhesion (Figure 4.7B and C). While nano-sized particulate drug carriers are often utilized due to their long circulation times *in vivo*[220] and to take advantage of the enhanced permeability and

retention effect[221], extensive previous work demonstrates that nano-sized drug carriers struggle to marginate towards the vascular wall in blood flow[143,144]. In fact, previous work also showed that nano-sized particles with or without active targeting have a muted ability to interfere with leukocyte adhesion to an inflamed HUVEC monolayer than micron-sized particles[139]. Our results align with this previous research and demonstrates that micron-sized particles outperform nano-sized particles at decreasing platelet adhesion in thromboinflammation.

Thus far, all particles were untargeted and did not bind to the activated HUVEC monolayer. In an *in vivo* scenario, there may be a benefit to sending particles directly to an area of acute inflammation to decrease platelet-leukocyte aggregate adhesion in that location specifically. To examine if targeted particles have increased efficacy in decreasing platelet adhesion, particularly at low concentrations where micron-sized particles are underperforming, we conjugated sLe^A onto the surface of 2 μm PS particles. At low particle concentrations (10^6/mL), addition of high levels of targeting led to a significant decrease in both platelet and leukocyte adhesion in comparison to no particle controls and untargeted particles (Figure 4.8A and B). However, at high particle concentrations (10^7/mL), addition of targeting did not increase the ability of particles to decrease platelet or leukocyte adhesion (Figure 4.8C and D). These data suggest that there is a specific particle concentration threshold where the addition of targeting does not improve particle efficacy because particles have already saturated the system. However, in an *in vivo* setting, the ability to send particles specifically to an area of inflammation may be beneficial as to not give such a systemic, excessive particle dosage. For instance, platelet-leukocyte aggregates bind in the lungs during acute lung injury and contribute to excessive, localized inflammation there[213]. In such a model of acute lung injury, an injection of targeted particles could bind specifically to the lung and

prevent platelet-leukocyte aggregate adhesion there without particles flooding the body systemically.

Beyond size, altering the shape of spherical particles is one method to increase their interactions with the vascular wall[146]. We produced AR2 and AR8 rod-shaped PS particles from 2 μm spherical particles. At low particle concentrations (10^6/mL), untargeted AR2 rods decreased leukocyte adhesion in comparison to no particle controls and untargeted AR8 rods decreased leukocyte adhesion in comparison to no particle controls and untargeted spheres (Figure 4.9B). However, this impact on leukocyte adhesion did not directly translate to a decrease in platelet adhesion as well; there was no significant impact on platelet adhesion using either type of rod (Figure 4.9A).

For all these *in vitro* flow experiments, we added particles to whole blood immediately before blood flow and used ACD as an anticoagulant, which chelates calcium and prevents or severely slows calcium-mediated processes. One such calcium-mediated process is phagocytosis, or the uptake of particles by phagocytic cells. We believe then that minimal or no phagocytosis of particles occurs prior to the blood flow experiment. As such, our hypothesis is that particles are impacting the adhesion of platelet-leukocyte aggregates by near-wall collisions removing or interfering with leukocytes bound to the endothelium. Further, sLe^A-targeted particles can directly bind to the IL-1β-inflamed HUVEC and directly compete with leukocytes for binding sites. Previous work demonstrated that phagocytosis of particles made of different material (PS and PLGA) changed the expression of key surface molecules of neutrophils[139]. Because initial aggregation of leukocytes and platelets depends on PSGL-1 expression on the leukocyte surface[205], future work could examine how phagocytosis of particles impacts PSGL-1 expression and downstream binding to activated platelets. In addition, upcoming work will examine the impact of

biodegradable micron-sized particles (PLGA) on platelet and leukocyte adhesion *in vitro* as PS itself is not biodegradable or could be translatable to human therapies.

To determine if the impact of particles on platelet and leukocyte adhesion seen *in vitro* translates to a more physiological *in vivo* environment, we examined the impact of injected particles on platelet and neutrophil adhesion to mouse mesenteric blood vessels in a model of systemic inflammation using intravital microscopy. Intraperitoneal injection of LPS led to the adhesion of platelet-neutrophil aggregates to the mouse mesentery (Figure 4.10B), which confirms previous reports[164,165]. The addition of micron-sized PS particles significantly decreased both platelet and leukocyte adhesion when administered at the same time as LPS (Figure 4.12A and B), though the same particles led to a non-significant decrease in both cell times when administered two hours after LPS. Similar to *in vitro* results, decreasing particle size to 500 nm did not significantly reduce either platelet or leukocyte adhesion (Figure 4.15A and B) when administered at the same dosage as the micron-sized particles. Upcoming work will examine if particles made of a biodegradable polymer, PLGA, also successfully divert platelets and neutrophils from the mouse mesentery to ensure this therapeutic can be translated to human use.

Addition of targeting to E-selectin and ICAM-1 led to a significant decrease in platelet and leukocyte adhesion when administered two hours after LPS (Figure 4.12A and B), though upon closer inspection the dual-targeted particles are not necessarily adhering to the inflamed mesentery (Figure 4.14B). Instead, any particles 'bound' to the mesentery are instead co-localized with adherent neutrophils, perhaps after particle phagocytosis. We hypothesize that, due to systemic inflammation caused by an IP injection of LPS, particles may be adhering to other areas of inflammation in the body. In particular, this model of systemic inflammation is known to induce inflammation and recruit neutrophils to the brain[222], liver[223,224], lungs[223–225], as well as the

peritoneum[225]. With that knowledge, targeted particles may be migrating to and adhering to other inflamed organs, including the lungs, accounting for the low number of adherent particles specifically in the mesentery. Further, based on our dosing scheme, mouse phagocytes, including neutrophils, have between one and three hours from time of particle injection to phagocytose particles, removing them from circulation. It is likely that targeted particles are both being cleared from circulation but also may be adherent in other vessels.

Though PS particles successfully rerouted neutrophils and platelets from the inflamed mesentery in mice, the particles themselves contained no therapeutic compounds other than the actual particle itself. To test if a particle containing additional anti-inflammatory therapeutics had an additional impact on platelet and neutrophil recruitment *in vivo*, we utilized untargeted particles produced from a salicylate-based polymer ('PolyA') which previous researchers demonstrated could reduce WBC trafficking to the lungs in a mouse model of acute lung injury beyond PS or PLGA particles[137]. Figure 4.17 shows that PolyA particles significantly reduced platelet adhesion to the mouse mesentery without impacting firm neutrophil adhesion. Interestingly, our data suggests that PolyA particles, though not PS particles, alter the neutrophil phenotype; the percentage of all neutrophils in the mesentery that are firmly adherent was significantly reduced after PolyA treatment in comparison to LPS controls (Figure 4.17D). Conversely, no PS particle treatment impacted the percent of adherent neutrophils (Figure 4.13A). Further, PolyA particle treatment reduced the average number of platelets adherent to each neutrophil in the mesentery in comparison to LPS-only controls (Figure 4.17E), which again was not a result seen after any PS treatment (Figure 4.13B). Future work will further explore the mechanism of action that causes PolyA to have an added therapeutic benefit in systemic inflammation.

Previous *in vitro* data observed that human neutrophils that phagocytosed PolyA particles shed less L-selectin and PSGL-1 in response to LPS in comparison to untreated neutrophils and those phagocytosing PLGA particles[137]. We hypothesize that the salicylic acid-based polymer backbone of PolyA contributes additional anti-inflammatory impacts on the blood cells it encounters, explaining the phenotypic change in neutrophils from mice receiving PolyA treatments. Further work will explore if these PolyA particles are primarily impacting neutrophils or if the presence of PolyA in the bloodstream is contributing anti-thrombotic or anti-inflammatory effects on circulating platelets. The use of polymeric particles, especially those containing anti-inflammatory compounds like PolyA, could be a new potential therapeutic for reducing platelet and leukocyte accumulation in areas of inflammation in thromboinflammatory diseases. Specifically, such a particulate drug could be an alternative to systemically administered anti-platelet or steroidal compounds that suppress clotting or the immune system broadly and can lead to negative downstream effects.

To interrogate our hypothesis that mouse phagocytes are engulfing and clearing particles from circulation, we injected PEGylated PS particles into mice at the time of LPS challenge. Unlike their non-PEGylated counterparts, PS-PEG particles did not significantly decrease adherent neutrophils in the mesentery (Figure 4.16B), though they did reduce platelet adhesion (Figure 4.16A). Future work will confirm the PEG conformation on the particle surface to ensure it is dense enough to prevent phagocytosis by mouse phagocytes.

We depleted neutrophils from mice to confirm that platelet adhesion to the mouse mesentery after LPS IP injection is neutrophil-dependent. We administered a total of 700 µg anti-Ly6G to mice over the course of 24 hours prior to intravital microscopy; mice were used for intravital microscopy if their neutrophil counts were consistently decreasing and if the complete

blood count at the time of euthanasia yielded neutrophils that were either lower than the typical range or right on the border. Because neutrophil counts and percentages of total circulating leukocytes in mice increase after LPS IP installation[226–228], we were not able to completely knock out all neutrophils in circulation even by increasing depletion antibody dosages further than what we reported in this chapter. Depleting neutrophils led to a significant decrease in platelet adhesion to an inflamed mesentery (Figure 4.19) and addition of untargeted PS particles did not further alter platelet adhesion in depleted mice. Because we used an anti-Ly6G depletion antibody, we were not able to stain for neutrophils using a fluorescent anti-Ly6G antibody. However, we could see some rolling and adherent leukocytes via brightfield microscopy in the inflamed mesentery. Without further staining and confirmation, we cannot definitively conclude if these are neutrophils or other leukocytes. However, Figure 4.19 clearly shows that minimal platelet adhesion occurs after neutrophil depletion, even if some adherent leukocytes remain in the mesentery. Upcoming work will confirm how circulating neutrophil counts change after LPS installation in non-depleted mice.

4.6 Conclusions

The work presented here is a thorough, first demonstration that model polymeric particles can divert platelets away from an area of inflammation by reducing platelet-leukocyte aggregates bound to an inflamed endothelial cell monolayer. Overall, this work presents a comprehensive exploration of how changing variables within the design space of polymeric particle therapeutics impacts not only leukocyte adhesion but also downstream platelet adhesion. In particular, increasing particle size from nano- to micro-sized and adding a targeting ligand (sLe^A) to the particle surface both improved particle efficacy while elongating spheres into rods did not lead to a significant improvement in reducing platelet adhesion to an activated endothelium *in vitro*.

Further, we confirmed that the mechanism leading to a decrease in platelet adhesion due to particles is specifically due to particles interfering with platelet-bound leukocytes on the inflamed endothelium; this is encouraging from a translational point of view because polymeric particles at this size neither contribute to clotting nor prevent it, important considerations when designing particle therapeutics for human use. After demonstrating that micron-sized PS particles successfully decrease leukocytes and platelets to an activated endothelium, we explored if these same particles could divert platelet-leukocyte aggregates away from an area of inflammation *in vivo* in a mouse model of systemic inflammation. Micron-sized particles significantly reduced both platelet and leukocyte adhesion to the inflamed mouse mesentery, though nano-sized particles did not. Use of poly-aspirin (PolyA) particles further reduced platelet adhesion with an added therapeutic benefit. After depleting neutrophils from circulation, mice had severely reduced platelet adhesion to the mesentery with no additional decrease with the addition of particles. Overall, the work presented here demonstrates that polymeric particles can reduce platelet adhesion to areas of thromboinflammation and represents initial steps towards develop particle-based therapeutics to reduce excessive platelet accumulation in inflammation.

Chapter 5 Impact of Stiffened RBCs on Platelet Adhesion and Modulation with Carbon Monoxide

5.1 Publication Information

This data is not yet published, though much of the work written in this chapter will be submitted as a hematology methods paper in the coming weeks.

5.2 Abstract/Summary

Patients with sickle cell disease (SCD) are at increased risk for different thrombotic diseases, including pain crises, stroke, and cardiovascular disease. Previous research has established that RBCs that are more stiff than usual, like in SCD, lead to a disrupted RBC core and disturbed margination of platelets and WBC. Limited research, however, has examined the interplay between RBC stiffness, fraction of RBCs stiffened, and platelet adhesion and behavior. Here, we investigated the impact of stiff RBCs on platelet adhesion in blood flow using both SCD patient whole blood and a model system where RBCs are artificially rigidified and recombined with blood components. Magnitude of platelet adhesion depended on SCD patient treatment; in particular, untreated SCD patients had the largest increase in platelet adhesion in comparison to non-SCD controls. In the artificial system, platelet adhesion depended on RBC stiffness, fraction of RBCs rigidified, shear rate, and hematocrit. We also examined the impact of carbon monoxide releasing molecules (CORMs) on platelet adhesion. Patients on hydroxyurea treatment and those untreated were more likely to have a significant decrease in platelet adhesion with CORM pretreatment than patients receiving chronic transfusions of RBCs. Overall, this work examined the interplay

between stiffened RBCs and platelet adhesion as well as how CO therapeutics can decrease platelet adhesion in SCD.

5.3 Background and Information

SCD is a genetic disease where the β-subunit of hemoglobin is mutated; this mutation causes the β-globin subunits to polymerize and stiffen during deoxygenation[94]. SCD patients experience a wide range of complications, including chronic pain, organ failure, and acute chest syndrome, that are all linked to vaso-occlusive crises (VOC) which cause blockages in blood vessels[94,95]. Even in industrialized countries, SCD patients with sickle cell anemia (SCA), considered the most severe phenotype, have a reduction in life expectancy of 20-30 years[96] in comparison to non-SCD patients in part due to complications due to VOC and immune cell activation. Though exact mortality is difficult to quantify, in Africa, where SCD is prevalent[94], it is estimated that the mortality rate is between 50-90% in the first few years of life for children born with SCA[229]. Overall, there is a great need to better understand the cell-cell dynamics leading to VOC so improved treatments can be developed.

While sickle-shaped RBCs remain a hallmark of SCD, these irreversibly sickled RBCs are prone to lysis and represent only a small fraction of total RBCs present in a patient at any given time[230]. Instead, the bulk of circulating RBCs in SCD patients are either healthy (non-rigid) hemoglobin A (HbA) RBCs or diseased (rigid) hemoglobin S (HbS) RBCs that maintain their normal, discoid shape. However, there is a limited understanding of how these regular-shaped but stiff RBCs impact other types of cells in blood flow. In flow, RBCs form a core in the middle of the vessel, while WBCs and platelets migrate toward the vascular wall to an area known as the red blood cell free layer[1–3]. Given that the ability of RBCs to deform is critical to the physiological distribution of cells in blood[11,231], the increased stiffness of the RBCs in SCD disrupts the

separation of blood cells where rigid RBCs can expand into the cell free layer and adhere to the endothelium, contributing to occlusions[232,233].

Despite the contributions of both RBCs and platelets to occlusions in SCD, most research has focused on cells on a molecular level and not on the biophysical interactions between rigid RBCs and platelets. The impact of rigid RBCs on other cell types in blood flow has not been fully explored. Previous *in vitro* work showed that the inclusion of artificially rigidified RBCs in whole blood decreased the adhesion of WBCs to an inflamed endothelium[162]. One experimental work showed that increasing RBC rigidity increased platelet binding to umbilical vein arteries *in vitro*[234]. While this study provided insight into the impact RBCs have on platelet adhesion *in vitro*, platelet binding was examined with 100% of RBCs in the system having their stiffness altered. In SCD, the percentage of stiff RBCs varies depending on the individual patient, the severity of their disease[235], and the current treatment method, and ranges from as low as <5% after RBC exchange[236] to >90% for untreated patients[237].

Computational models of blood flow exist and have demonstrated that RBC deformability contributes to platelet margination (localization) to the vascular wall[7,231,238]. However, margination may not directly translate to adhesion. Thus, to entirely understand the effect that RBC rigidity plays on platelet adhesion, a full range of RBC rigidities and fractions needs to be explored in adhesion assays in whole blood flow. Further, the severity of SCD complications vary greatly from patient to patient, yet there currently is no way to easily screen and determine which patients will experience severe complications and need interventions. A method that can be utilized to predict VOC or complications for SCD patients is thus essential, as is a method that can be used to screen potential therapeutics for SCD as no easily accessible treatments for SCD have been developed since hydroxyurea. While gene therapy[110] and CRISPR/Cas9[111] gene editing are currently being

researched as potential cures for SCD, the fact remains that these are relatively early in human trials and will be inaccessible for most SCD patients throughout the globe.

One potential therapeutic for SCD is carbon monoxide (CO); while this may seem counterintuitive, CO is an endogenous biogas that has potential anti-inflammatory benefits[239]. In fact, the use of CO to reduce RBC sickling in SCD was identified as early as 1963[240]; additionally, epidemiological reports regarding air pollution noted that, in London, low CO levels in the air were correlated with an increase in hospital admission for SCD-related pain[241]. CO has several hypothesized potential benefits for treatment of SCD, including its anti-polymerization of HbS, hydration of sickled RBCs, anti-oxidative properties, and anti-inflammatory properties, among others[242]. Preliminary work in mice demonstrated that inhaled CO reduced leukocytosis[243] and oral CO reduced leukocytosis, increased hematocrit, and decreased microvascular clots[244]. Further, PEGylated human hemoglobin saturated with CO decreased hypoxia/reperfusion vascular stasis and heme-induced acute lung injury in mice[245], and separately were demonstrated to be safe in humans in a Phase I clinical trial[246]. Extensive work utilized carbon monoxide releasing molecules (CORMs)[247–250] as a potential delivery method other than inhaled CO, which requires careful control in a hospital setting to avoid deadly side effects. Despite this potential of CO for SCD treatment both theoretically and using mouse models, ultimately minimal work has examined the impact of CO on SCD patients directly.

In this chapter, we explore how stiffened RBCs impact platelet adhesion *in vitro* using both SCD patient blood samples as well as a system where healthy RBCs are artificially rigidified. Using the 'damaged endothelium' *in vitro* flow model described in Chapter 3, we demonstrate that SCD patients often have increased platelet adhesion in comparison to non-SCD controls, but also that there is great variability between individuals and treatment groups. Further, we show that

carbon monoxide releasing molecules (CORMs) can decrease platelet adhesion for certain SCD patients; in particular, CORM treatment shows great promise to reduce excessive platelet adhesion for SCD patients on hydroxyurea treatment or patients that are currently untreated.

5.4 Results

5.4.1 SCD patient platelets are more likely to adhere to 'damaged endothelium' than non-SCD controls for certain cohorts and in specific flow conditions

Though previous researchers determined that SCD patient platelets are more activated than non-SCD controls[114,115], less research has explored the dynamics of SCD blood cells in whole blood. Specifically, we examined the magnitude of resting platelet adhesion from SCD patients in whole blood to the 'damaged endothelium' model described in Chapter 3. Platelet adhesion for SCD patients at a low shear rate ($100s^{-1}$) is shown in Figure 5.1; non-SCD patient data is shown using unfilled circles and SCD patients are displayed by treatment group. Patients receiving chronic transfusions of RBCs are displayed with filled black circles (Figures 5.1A and B); patients on hydroxyurea are represented using red, upwards facing triangles (Figures 5.1A and C); patients not receiving treatment are represented using blue, downwards facing triangles (Figures 5.1A and D); and patients whose treatment regiments are unknown are represented with purple diamonds.

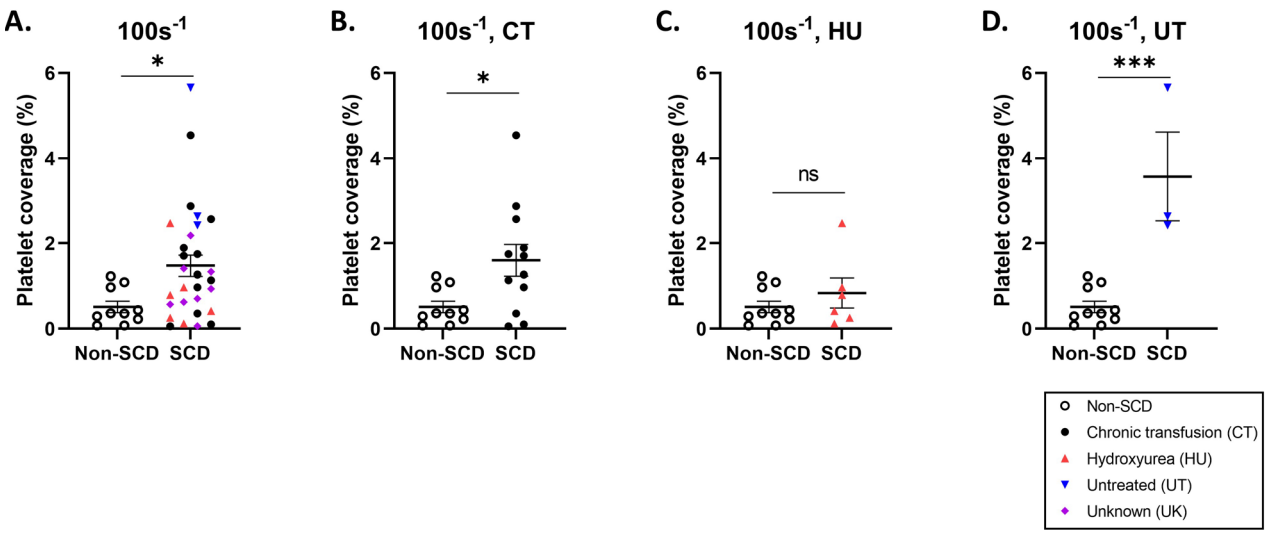

Figure 5.1: SCD platelets are more likely to bind than non-SCD platelets at low shear rates.

Platelet coverage (as % of total surface area of photo) after 5 minutes of laminar flow in whole blood of either non-SCD controls (open circles) or (A) all SCD patients, (B) SCD patients being treated with chronic transfusion (CT) of RBCs (filled black circles), (C) SCD patients being treated with hydroxyurea (HU; red upwards triangles), or (D) SCD patients not currently being treated (UT; blue downwards triangles) at $100s^{-1}$ on histamine-stimulated and mechanically disrupted HUVEC. Patients whose treatment status is unknown ('UK') are represented with purple diamonds. Statistical analyses were performed using a Student's unpaired t-test, where (*) indicates $p<0.05$ and (***) indicates $p<0.001$.

When all SCD patients are grouped together, there is a statistically significant increase in platelet adhesion of SCD patients in comparison to non-SCD controls (Figure 5.1A; $p = 0.042$). However, this result does not hold when each SCD treatment group is viewed separately. Patients receiving chronic transfusions of RBCs (CT; Figure 5.1B) have increased platelet adhesion in comparison to non-SCD controls ($p = 0.0189$). However, patients receiving hydroxyurea (HU; Figure 5.1C) do not have increased platelet adhesion in comparison to non-SCD controls ($p = 0.3225$). Even more strikingly, the small number of patients that are currently untreated (UT; Figure 5.1D) have the largest increase in platelet adhesion compared to non-SCD controls ($p =$

0.0002). At $100s^{-1}$, the groups driving the increased level of platelet adhesion shown in Figure 5.1A are thus untreated patients and those receiving chronic transfusions.

Similarly, we examined platelet adhesion of these same donors at 500 (Figure 5.2) and $1000s^{-1}$ (Figure 5.3). Collectively, SCD patients do not have a significant increase in platelet adhesion at $500s^{-1}$ (Figure 5.2A; $p = 0.5433$). Once again, these results vary by individual treatment group. At $500s^{-1}$, neither patients receiving chronic transfusion (Figure 5.2B) nor hydroxyurea (Figure 5.2C) have elevated platelet adhesion in comparison to non-SCD controls. Conversely, untreated patients alone have a significant increase in platelet adhesion when compared to non-SCD controls ($p = 0.013$). Platelet adhesion data at $1000s^{-1}$ yielded similar results; as a whole, SCD patients did not have elevated platelet adhesion in comparison to non-SCD controls (Figure 5.3A; $p = 0.3493$). Neither chronic transfusion patients (Figure 5.3B) nor hydroxyurea-treated patients (Figure 5.3C) had elevated platelet adhesion in comparison to controls. However, untreated SCD patients again had a significant increase in platelet adhesion at $1000s^{-1}$ in comparison to non-SCD controls (Figure 5.3D; $p = 0.0018$).

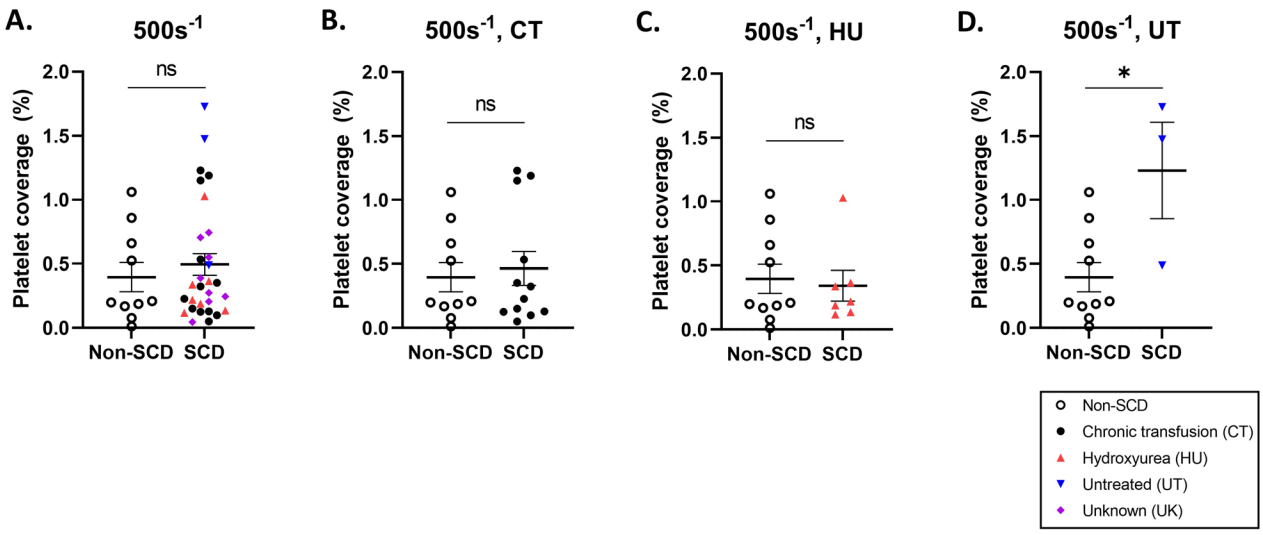

Figure 5.2: Some SCD patient treatment groups' platelets are more likely to bind than non-SCD platelets at medium shear rates.

Platelet coverage (as % of total surface area of photo) after 5 minutes of laminar flow in whole blood of either non-SCD controls (open circles) or (A) all SCD patients, (B) SCD patients being treated with chronic transfusion (CT) of RBCs (filled black circles), (C) SCD patients being treated with hydroxyurea (HU; red upwards triangles), or (D) SCD patients not currently being treated (UT; blue downwards triangles) at $500s^{-1}$ on histamine-stimulated and mechanically disrupted HUVEC. Patients whose treatment status is unknown ('UK') are represented with purple diamonds. Statistical analyses were performed using a Student's unpaired t-test, where (*) indicates $p<0.05$.

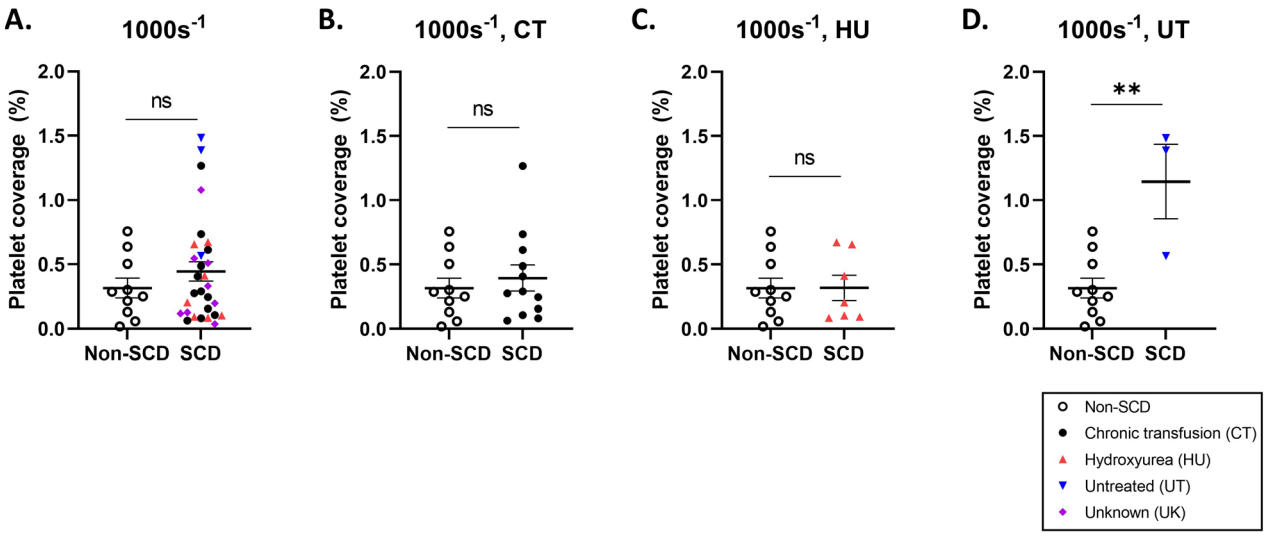

Figure 5.3: Some SCD patient treatment groups' platelets are more likely to bind than non-SCD platelets at high shear rates.

Platelet coverage (as % of total surface area of photo) after 5 minutes of laminar flow in whole blood of either non-SCD controls (open circles) or (A) all SCD patients, (B) SCD patients being treated with chronic transfusion (CT) of RBCs (filled black circles), (C) SCD patients being treated with hydroxyurea (HU; red upwards triangles), or (D) SCD patients not currently being treated (UT; blue downwards triangles) at $1000s^{-1}$ on histamine-stimulated and mechanically disrupted HUVEC. Patients whose treatment status is unknown ('UK') are represented with purple diamonds. Statistical analyses were performed using a Student's unpaired t-test, (**) indicates $p<0.01$.

Because SCD patients' circulating platelets are known to have elevated levels of activation, we also measured SCD patient platelet activation level in comparison to non-SCD patients through staining for P-selectin and analyzing using flow cytometry. As a group, SCD patients have elevated levels of P-selectin in comparison to non-SCD controls (Figure 5.4A; $p = 0.042$). Broken out by treatment group, SCD patients receiving chronic transfusions had elevated levels of P-selectin (Figure 5.4B; $p = 0.0124$), as did patients receiving hydroxyurea (Figure 5.4C; $p = 0.0389$). However, untreated SCD patients did not have elevated levels of P-selectin in comparison to non-

SCD controls (Figure 5.4D; p = 0.1078). While only three independent, untreated SCD patients were used in this study, P-selectin expression for two patients was measured on two separate days, leading to five total points graphed in Figure 5.4D.

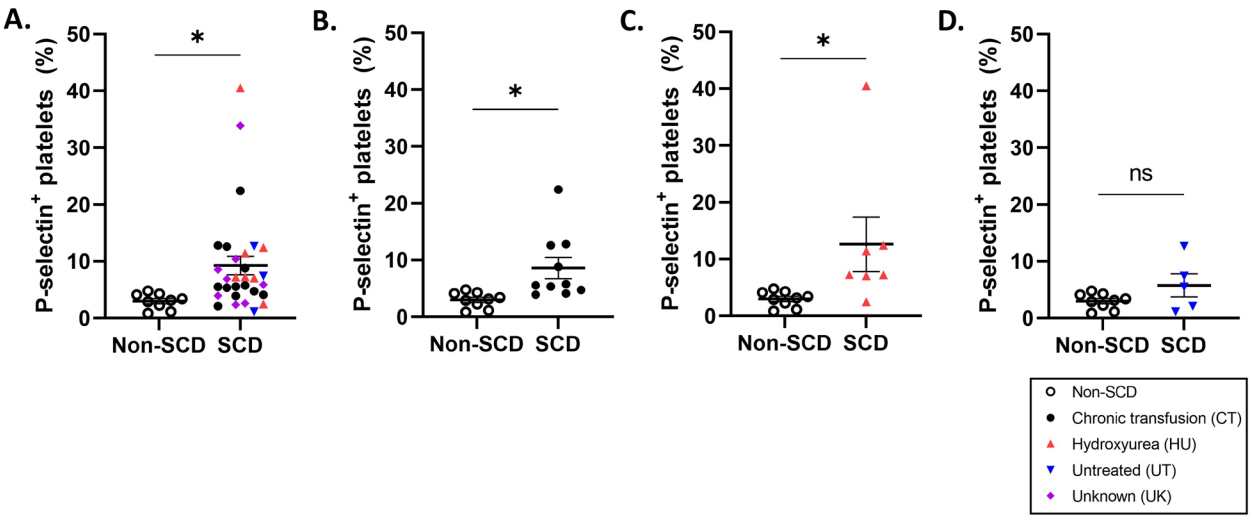

Figure 5.4: SCD patient platelets are more activated than non-SCD control platelets.

Percent of resting platelets expressing P-selectin as analyzed by flow cytometry of non-SCD controls (open circles), SCD patients receiving chronic transfusions (CT; blacked filled circles), SCD patients receiving hydroxyurea (HU; red upwards triangles), SCD patients currently untreated (UT; blue downwards triangles), and SCD patients whose treatment status is unknown (UK; purple diamond). Statistical analyses were performed using a Student's unpaired t-test, where (*) indicates $p<0.05$.

5.4.2 Many variables in SCD blood lead to magnitude of SCD platelet adhesion in vitro

Despite untreated patients having overall high levels of platelet adhesion at all shear rates tested *in vitro* (Figures 5.1, 5.2, and 5.3), untreated SCD patients did not necessarily have extremely high levels of platelet activation (Figure 5.4), in comparison to non-SCD controls. With that, we explored what other variables could impact levels of SCD patient platelet adhesion in blood flow *in vitro*. Figure 5.5 highlights linear regressions between SCD platelet coverage at $100s^{-1}$ and different blood variables, including hematocrit (Hct; Figure 5.5A and B), platelet count (in K platelets/µL; Figure 5.5C and D), percent HbS (%S; Figure 5.5E and F), and platelet activation

level as measured by P-selectin positivity (P-selectin^{+} platelets; Figure 5.5 G and H). Figures 5.5A, C, E, and G demonstrates a linear regression for all patients, regardless of treatment group and Figures 5.5B, D, F, and H demonstrates a linear regression by each treatment group (chronic transfusion, hydroxyurea, or untreated). Significantly non-zero slopes are denoted within the graphs.

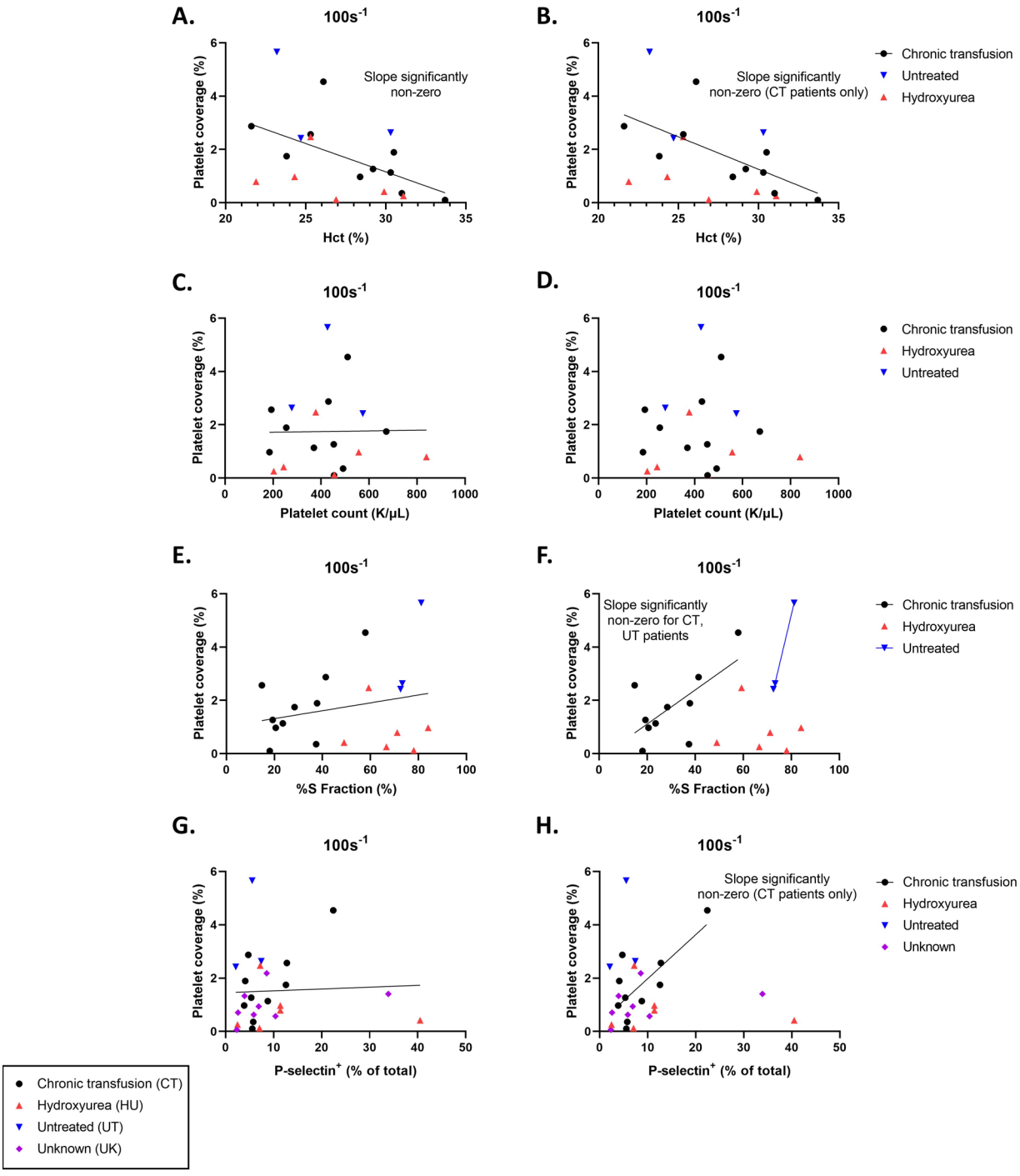

Figure 5.5: Linear regressions of SCD patient blood variables and platelet adhesion at $100s^{-1}$.

Platelet adhesion (% of surface) of platelets in whole blood to a damaged HUVEC monolayer at $100s^{-1}$ (y-axis) versus patient (A, B), hematocrit, (C, D) platelet count, (E, F) S fraction of hemoglobin, or (G, H) Percent of resting platelets expressing P-selectin. Statistical analyses were performed by simple linear regression and were performed using all patient data (A, C, E, G) or by treatment group (B, D, F, H). Linear regressions with significantly non-zero slopes are denoted in writing within the graph.

When all SCD patients are grouped together, the only variable that led to a significantly non-zero slope was hematocrit with higher hematocrit being associated with lower platelet coverage (Figure 5.5A; $p = 0.0298$). When separated into treatment groups, only chronic transfusion had a significantly non-zero slope with respect to hematocrit (Figure 5.5B; $p = 0.0286$). HbS percentage was correlated with platelet adhesion for both chronic transfusion and untreated groups (Figure 5.5F; $p = 0.0391$ and 0.0104, respectively). P-selectin expression was correlated with platelet adhesion for the chronic transfusion SCD group only (Figure 5.5H; $p = 0.0153$). The scatterplots shown in Figure 5.5 allow us to calculate linear regressions between platelet coverage and different measurable variables but also allow us to qualitatively examine how different characteristics change by treatment group. For instance, there does not visually appear to be clear differences in platelet count by treatment group (Figure 5.5D). However, the impact of chronic transfusion and hydroxyurea on %S fraction is clear by examining Figure 5.5F; patients receiving chronic transfusions tend to have lower %S than either hydroxyurea or untreated patients with untreated patients having among the highest %S of all the patients examined.

We similarly plotted platelet coverage of SCD patients at $1000s^{-1}$ with different variables in Figure 5.6 to determine if there were any major differences between the two shear rates. Figure 5.6 highlights linear regressions between SCD platelet coverage at $1000s^{-1}$ and different blood variables: hematocrit (Figure 5.6A and B); platelet count (Figure 5.6C and D); %S (Figure 5.6E and F); and P-selectin expression (Figure 5.6 G and H). Similarly to Figure 5.5, Figure 5.6A, C, E, and G represent linear regressions for all SCD patients as one group while Figure 5.6B, D, F, and H represents linear regressions for SCD patients separated out into three treatment groups. As one group, no variables examined were significantly correlated with SCD platelet adhesion at $1000s^{-1}$. However, when separated into treatment groups, P-selectin expression of chronic

transfusion SCD patients was correlated with platelet coverage. Like Figure 5.5, Figure 5.6 can be used to qualitatively examine differences between the three treatment groups. For example, Figure 5.6F demonstrates the clear differences between each group and %S.

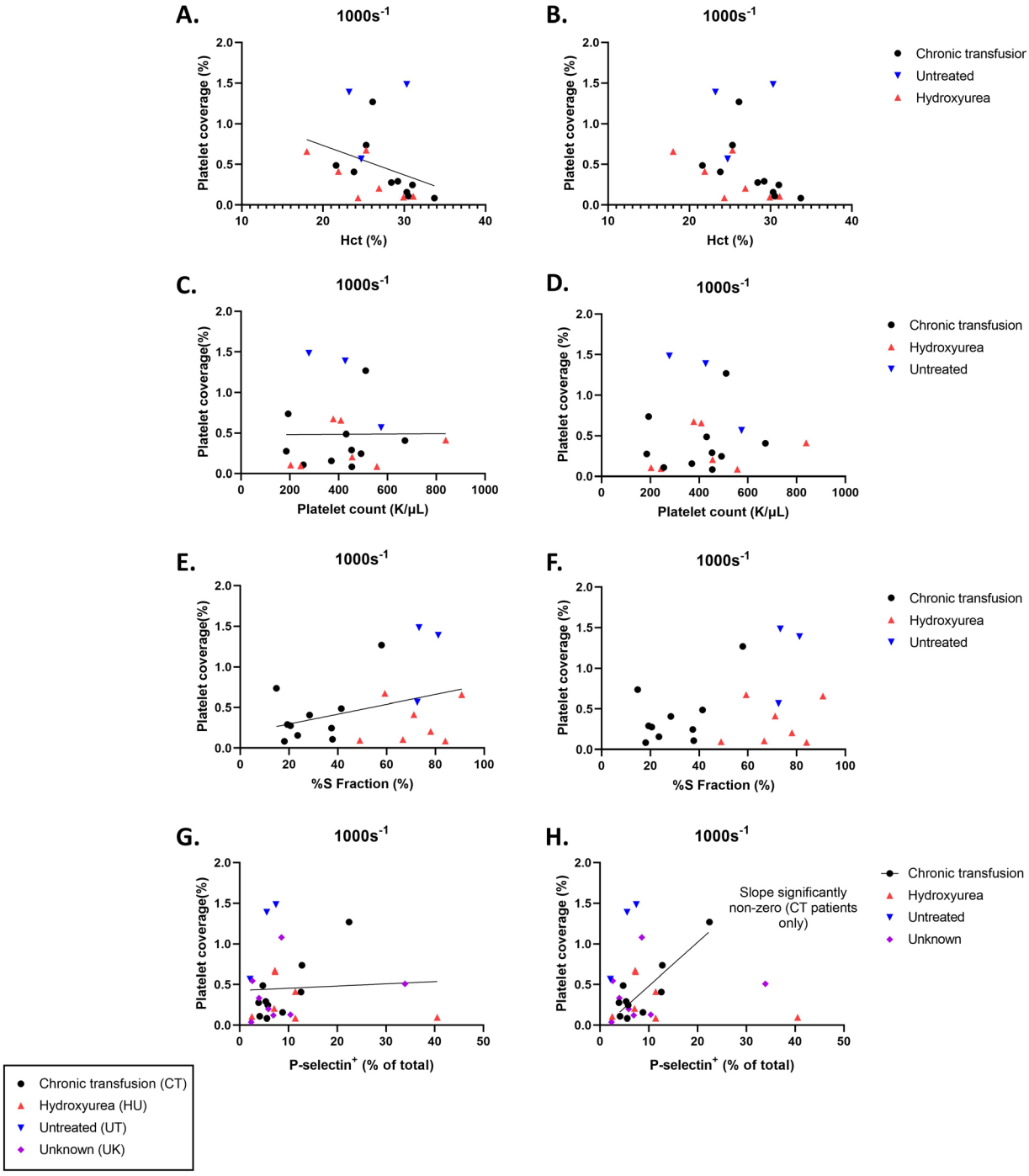

Figure 5.6: Linear regressions of SCD patient blood variables and platelet adhesion at 1000s^{-1}.

Platelet adhesion (% of surface) of platelets in whole blood to a damaged HUVEC monolayer at 1000s^{-1} (y-axis) versus patient (A, B), hematocrit, (C, D) platelet count, (E, F) S fraction of hemoglobin, or (G, H) Percent of resting platelets expressing P-selectin. Statistical analyses were performed by simple linear regression and were performed using all patient data (A, C, E, G) or by treatment group (B, D, F, H). Linear regressions with significantly non-zero slopes are denoted in writing within the graph.

Our research group previously examined the stiffness of RBCs from a subset of our SCD cohort using ektacytometry[153]. Though this represented a fraction of the total number of SCD patients in our study, we explored whether RBC deformability, represented by the elongation index of a patient's RBCs, was correlated with that patient's platelet adhesion in our flow model. A scatterplot of the maximum elongation index (EI_{max}) and platelet adhesion at 100s and $1000s^{-1}$ can be seen in Figure 5.7. Neither set of data yielded a significantly non-zero slope.

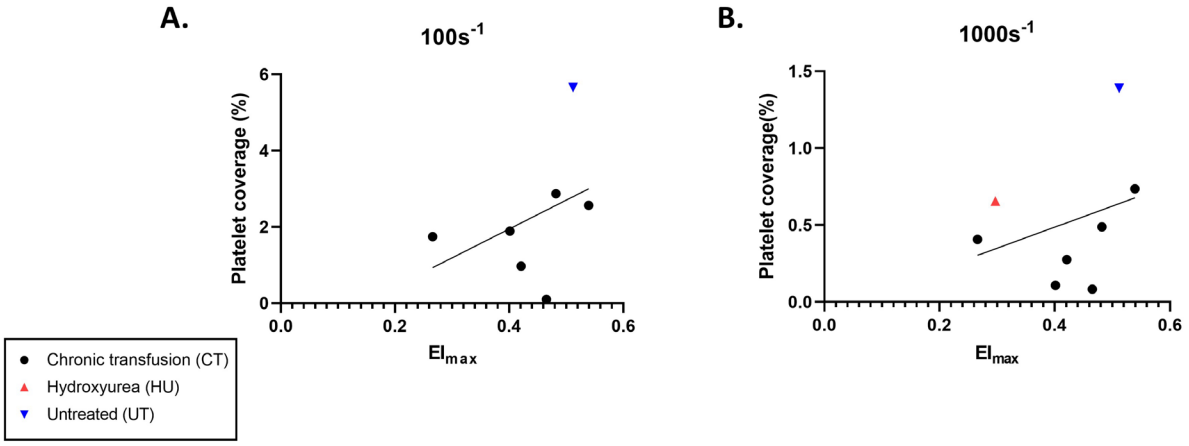

Figure 5.7: Linear regressions of SCD RBC EImax and platelet adhesion at 100 and $1000s^{-1}$.

Platelet adhesion (% of surface; y-axis) of platelets in whole blood to a damaged HUVEC monolayer at $100s^{-1}$ (A) or $1000s^{-1}$ (B) versus patient RBC maximum elongation index (EImax) as measured by ektacytometry. Statistical analyses were performed by simple linear regression and were performed using all patient data. Linear regressions with significantly non-zero slopes are denoted in writing within the graph with a lack of writing indicating a lack of significance.

5.4.3 Artificial rigid RBC method can be used to explore interplay between RBC stiffness and platelet adhesion

While use of SCD patient samples is incredibly valuable to better understand and develop improved therapeutics for SCD, there are many difficulties when directly interfacing with patients. First, not all researchers are physicians or work directly with patients, limiting researcher-patient interactions. Second, even researchers who can directly interface with SCD patients should be

mindful of the vulnerability of this patient population. Third, even amongst a SCD patient cohort, there are many complexities within the group. For instance, in our SCD patient cohort, unknown factors include if patients are in crisis or stable conditions, if patients can comply with treatment methods successfully, and so forth. All of these variables combined can make it difficult to elucidate exact results from such a heterogenous group. It is then essential to develop an alternative method to understand the interactions between stiffened RBCs and other blood cells that does not require directly interfacing with patients.

Previous work utilized a method to artificially rigidify healthy donor RBCs to study the impact of stiffened RBCs on leukocyte and vascular-targeted drug carrier behavior in blood flow *in vitro*[161,162]. Moreover, this method can be used to match specific characteristics of individual SCD patients, allowing the method to be personalized to best understand the cell-cell dynamics of each donor[153]. We utilized this method to artificially rigidify healthy RBCs and to recombine them with platelet-rich plasma before flowing the mixture over the 'damaged endothelium' *in vitro* model used previously with SCD patient whole blood. WBCs were excluded from these initial experiments to determine the impact of rigid RBCs on platelets without the additional complication of WBC adhesion. Figure 5.8A shows the impact of artificially stiffened RBCs on platelet adhesion over a wide range of RBC fractions rigidified and stiffnesses. For all rigidities, increasing the fraction of RBCs stiffened leads to an increase in platelet adhesion, reaching a maximum at 70-100% rigidified depending on the magnitude of stiffness. Figure 5.8A also demonstrates how the interplay between magnitude of rigidity and RBC fraction rigidified can lead to a similar platelet adhesion outcome. For example, the platelet fold change of the 'least rigid' RBCs when 70% of the RBCs have been rigidified is approximately 2.3. With moderately rigid RBCs, when 50% of the RBCs are rigidifed, the platelet fold change similarly is 2.2. With the most rigid RBCs, only

20% of them need to be stiffened to yield a platelet fold change of 2.2. This example highlights how a small fraction of extremely stiff RBCs can have a similar downstream effect on elevated platelet adhesion as a larger fraction of less stiff RBCs. Figure 5.8B shows representative images over a range of RBC fractions rigidified for the 'highly rigid' samples with fluorescently labelled platelets shown in red.

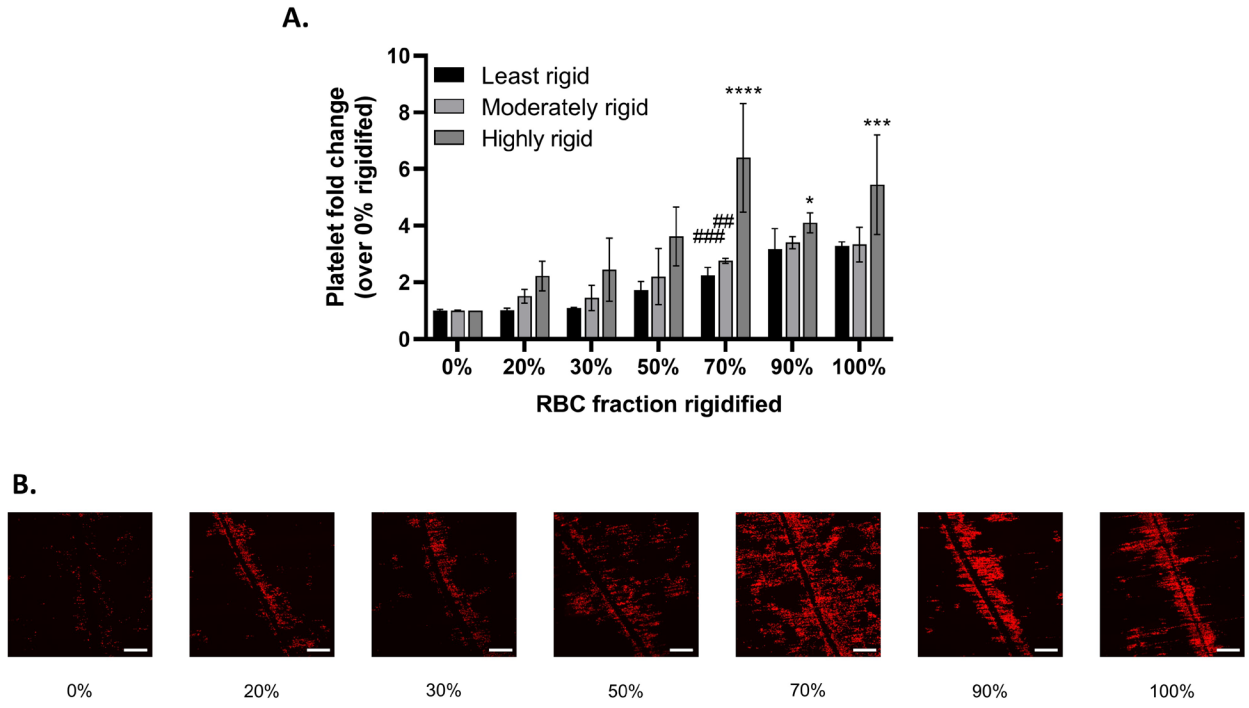

Figure 5.8: Effect of RBC rigidity on platelet adhesion.

(A) Fold change in activated platelet adhesion (% of surface) of platelets in plasma at 40% hematocrit and $1000s^{-1}$ containing RBCs artificially rigidified using 0.5 ('least rigid'), 0.75 ('moderately rigid'), or 1.0 ('highly rigid') mM TBHP in comparison to healthy (non-rigidified) blood, and (B) Representative fluorescence images of platelets (red) bound to endothelium after 5 minutes of laminar flow in the presence of 0-100% volume fraction highly rigidified RBCs, scale bar 200 µm. Statistical analyses were performed using two-way ANOVA with Tukey's multiple comparisons test where (*) indicate $p < 0.05$, (***) indicates $p<0.001$, and (****) indicates $p<0.0001$ in comparison to 0% rigidifed and (##) indicates $p<0.01$, and (###) indicates $p<0.001$ in comparison to 'highly rigid' fold change at that RBC fraction rigidified.

5.4.4 High shear rate and hematocrit lead to large increases in platelet adhesion

We also explored how a range of shear rates, representing both arteries and arterioles[251], impact platelet adhesion in the presence of highly rigid RBCs. For all shear rates tested (500, 1000, and 1500s^{-1}), platelet adhesion increased with increasing rigid RBC fraction and reached a maximum between 70% and 100% (Figure 5.9). However, the presence of highly rigid RBCs had a larger impact on platelet adhesion for high shear rates (1000 and 1500s^{-1}) than for the lowest shear rate (500s^{-1}). Specifically, at 500s^{-1}, platelet adhesion increased with increasing RBC fraction rigidified, but never significantly in comparison to the healthy, unstiffened control. Conversely, platelet adhesion behavior was similar at 1000 and 1500s^{-1}, leading to significant increases in platelet fold change at 50, 70, 90, and 100% rigidified for 1500s^{-1} and 70, 90, and 100% for 1000s^{-1}.

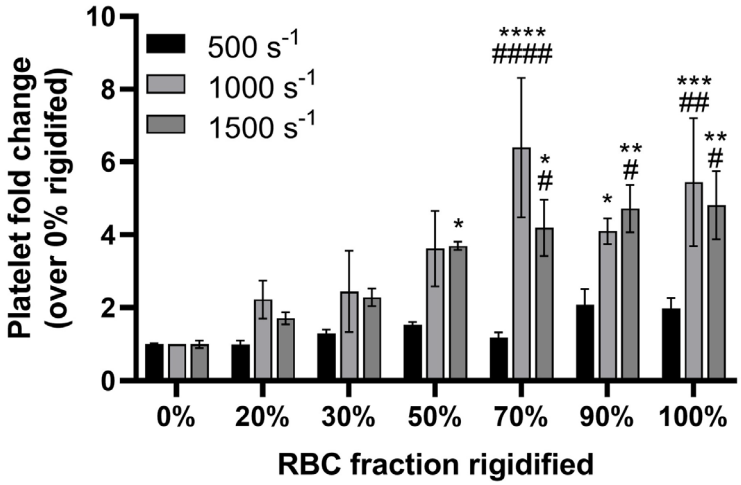

Figure 5.9: Impact of shear rate in platelet adhesion in the presence of rigid RBCs.

Fold change in activated platelet adhesion (% of surface) of platelets in plasma at 40% hematocrit and 500, 1000, or 1500s^{-1} containing RBCs artificially rigidified using 1.0 ('highly rigid') mM TBHP in comparison to healthy (non-rigidified) blood Statistical analyses were performed using two-way ANOVA with Tukey's multiple comparisons test where (*) indicates $p < 0.05$, (**) indicates $p<0.01$, (***) indicates $p<0.001$, and (****) indicates $p<0.0001$ in comparison to 0% rigidifed and (#) indicates $p < 0.05$, (##) indicates $p<0.01$, (###) indicates $p<0.001$, and (####) indicates $p<0.0001$ in comparison to 500s^{-1} fold change at that RBC fraction rigidified.

Raised hematocrit, i.e., volume fraction of RBCs, in whole blood is known to contribute to thrombosis and platelet adhesion using other models[156]. We wanted to explore the impact of an elevated hematocrit on activated platelet adhesion in this model in the presence of rigid RBCs. We investigated this variable by holding the number of platelets present in the system constant for each donor while altering the hematocrit to separate the variables of hematocrit and platelet concentration in our experiments. Figure 5.10A shows platelet fold change data where the platelet adhesion at each RBC fraction rigidified is normalized by the healthy (0% rigidified) platelet adhesion for that donor and specific hematocrit. Unsurprisingly, the higher hematocrit samples (40 and 60%) yielded a larger increase in platelet binding than the low hematocrit (20%) samples (Figure 5.10A) at high RBC fractions rigidified. For example, when 100% of the RBCs were highly rigid, the increase in platelet adhesion relative to a healthy, non-rigid control at each hematocrit was four-fold at a 60% hematocrit ($p = 0.0009$), five-fold at a 40% hematocrit ($p < 0.0001$), but only about two-fold at a 20% hematocrit (not significant). At 20% hematocrit, the platelet fold change increased only to ~2.4 at its maximum when 90-100% of RBCs were stiffened, which was not statistically significant in comparison to non-rigidified controls ($p = 0.5081$ and 0.5257, respectively). The general trend that increasing the rigid RBC fractions increased platelet adhesion held for all hematocrits tested but was greatly muted for the low hematocrit samples. Again, all hematocrits tested had a maximum fold change in platelet adhesion at 90-100% RBCs rigidified.

Figure 5.10B further demonstrates the interplay between hematocrit, RBC fraction rigidified, and platelet adhesion; here, data is plotted as the platelet adhesion fold change over the ‘healthy’ (0% rigidified) platelet adhesion at 20% hematocrit for each donor.

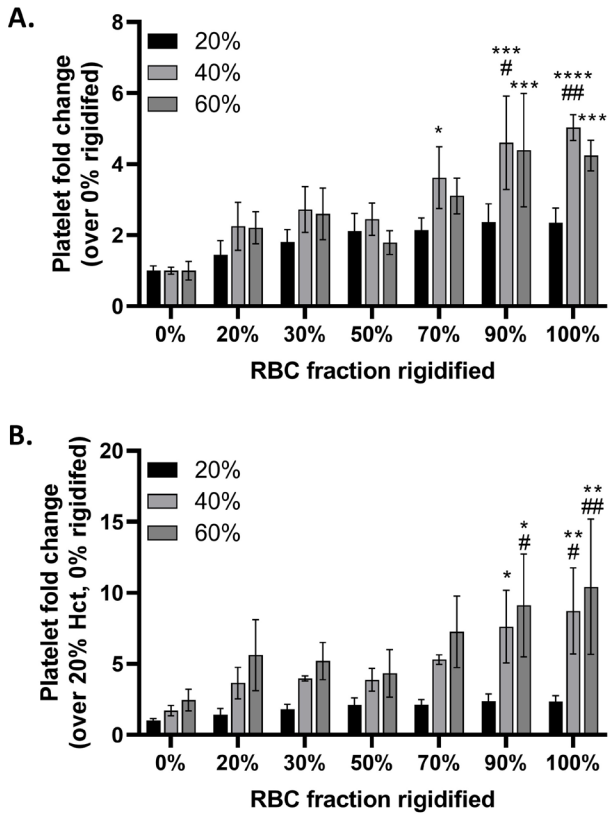

Figure 5.10: High hematocrit leads to largest increase in platelet adhesion at high percent rigidity.

(A) Fold change in activated platelet adhesion (% of surface) of platelets in plasma at 20, 40, or 60% hematocrit and 1000s^{-1} containing RBCs artificially rigidified using 1.0 ('highly rigid') mM TBHP in comparison to healthy (non-rigidified) blood at that specific hematocrit. (B) Fold change in activated platelet adhesion (% of surface) of platelets in plasma at 20, 40, or 60% hematocrit and 1000s^{-1} containing RBCs artificially rigidified using 1.0 ('highly rigid') mM TBHP in comparison to healthy (non-rigidified) blood at 20% hematocrit. Platelet number was fixed for all donors with change in hematocrit. Statistical analyses were performed using two-way ANOVA with Tukey's multiple comparisons test where (*) indicates $p < 0.05$, (***) indicates $p<0.001$, and (****) indicates $p<0.0001$ in comparison to 0% rigidifed and (#) indicates $p < 0.05$, and (##) indicates $p<0.01$ in comparison to 20% hematocrit fold change at that RBC fraction rigidified.

5.4.5 Platelet adhesion trends are maintained in whole blood, using resting platelets, and utilizing pulsatile flow patterns

Thus far, we utilized laminar blood flow and only a combination of RBCs and activated platelets in plasma to precisely elucidate the impact of rigid RBCs on platelets in the absence of other complicating variables. Here, we explored how the platelet adhesion response to highly rigid RBCs

changes with leukocytes (WBCs) in whole blood flow conditions. Inclusion of WBCs yielded similar platelet adhesion trends (Figure 5.11A) as observed for the platelet/RBC only mixture (Figure 5.8), though platelet adhesion increased at a lower magnitude with inclusion of WBCs. In the PRP/RBC mixtures both with (Figure 5.11A) and without (Figure 5.8) the inclusion of WBCs, adhesion of activated platelets reached a maximum when 70% of the RBCs were artificially rigidified. In general, adding rigid RBCs into whole blood increased platelet adhesion similarly to the platelet adhesion in the presence of RBCs only. While the platelet adhesion trends were similar for the platelet/RBC mixtures with or without WBC, the increase in platelet adhesion was more muted with the inclusion of WBCs in reconstituted whole blood (a 4-fold increase with 70% of the RBCs rigidified in whole blood compared to a 6.4-fold increase in the RBC-platelet only flow).

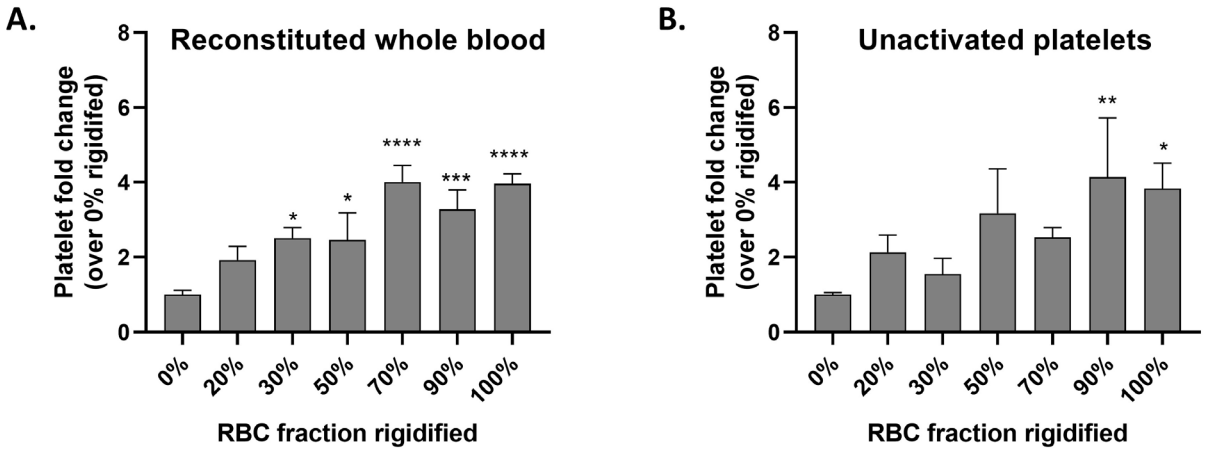

Figure 5.11: Impact of rigidified RBCs on platelet adhesion is maintained in whole blood and with resting platelets.

(A) Fold change in activated platelet adhesion (% of surface) of reconstituted whole blood at 40% hematocrit and 1000s^{-1} containing RBCs artificially rigidified with 1.0 ('highly rigid') mM TBHP in comparison to healthy (non-rigidified) blood, and (B) Fold change in resting platelet adhesion (% of surface) of platelets in plasma at 40% hematocrit and 1000s^{-1} containing RBCs artificially rigidified with 1.0 ('highly rigid') mM TBHP in comparison to healthy (non-rigidified) blood. Statistical analyses were performed using one-way ANOVA with Dunnett's multiple comparisons test where (*) indicate $p < 0.05$, (**) indicates $p<0.01$, (***) indicates $p<0.001$, and (****) indicates $p<0.0001$ in comparison to 0% rigidifed.

In all previous experiments, we activated the platelets with a mild agonist, ADP, to mimic the activated phenotype of platelets reported in SCD patients[114,115]. We wanted to explore the impact highly rigid RBCs have on resting platelets in flow to determine if rigid RBCs cause an increase in platelet adhesion even under quiescent conditions. We discovered that there is still an increase in the platelet adhesion fold change when the platelets are unactivated (Figure 5.11B), but it is to a lesser extent than when the platelets are activated with ADP (Figure 5.8). There was a greater range of resting platelet adhesion between individual donors, suggesting that stiffened RBCs may have a muted impact on individual donors with low levels of platelet activation; the data in Figure 5.11B is representative of 10 independent donors while previous data utilized only 3 donors.

To determine if the platelet adhesion trends seen in the presence of highly rigid RBCs in laminar flow are maintained through different blood flow patterns, we examined platelet adhesion using a pulsatile flow pattern and compared it directly to the laminar flow pattern. Both utilized the same total volume of blood with the key difference being the back-and-forth nature of the pulsatile flow pattern. Results of the laminar and pulsatile flow comparison are shown in Figure 5.12. The general platelet adhesion patterns were maintained regardless of flow pattern; in both experiments, platelet adhesion fold change reached a maximum when 70% of the RBCs were artificially stiffened. One key difference is that the impact of rigid RBCs on platelet adhesion was somewhat muted in pulsatile flow when the RBC fraction rigidified was at or below 50%.

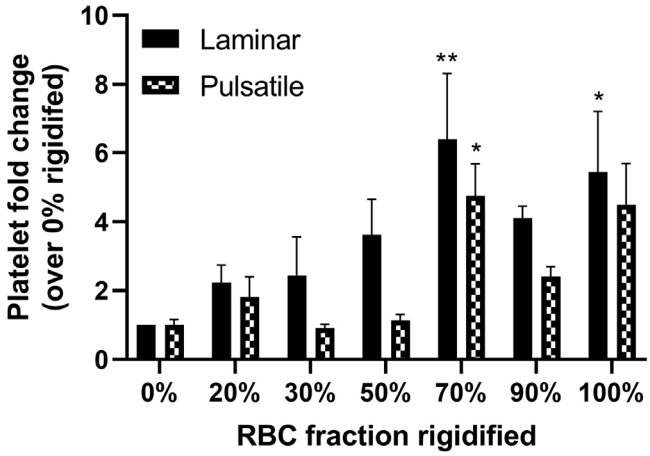

Figure 5.12: Impact of rigidified RBCs on platelet adhesion is maintained in pulsatile flow patterns.

Fold change in activated platelet adhesion (% of surface) of platelets in plasma at 40% hematocrit and 1000s^{-1} containing RBCs artificially rigidified with 1.0 ('highly rigid') mM TBHP in comparison to healthy (non-rigidified) blood either in laminar flow or pulsatile flow. Statistical analyses were performed using two-way ANOVA with Tukey's multiple comparisons test where (*) indicates $p < 0.05$, and (**) indicates $p<0.01$ in comparison to 0% rigidifed. Lack of # indicates lack of significance between platelet fold change of laminar and pulsatile flow conditions.

5.4.6 Stiffened RBCs contribute to platelet and leukocyte activation but not HUVEC activation

Thus far, we explored the impact of stiffened RBCs on platelet adhesion using both SCD patient whole blood and an artificial system where RBCs can be separated, rigidified, and reintroduced to platelets or other blood components. However, a major question that remains is if there is a dominating mechanism of action that causes increased platelet adhesion in the presence of stiff RBCs. Prior computational and experimental work demonstrated that margination of platelets towards the vascular wall actually decreases in the presence of stiff RBCs[252] and that platelet adhesion increases despite that decrease in margination. Because we know margination is not contributing to increased platelet adhesion, three key potential mechanisms are: 1) stiffened RBCs activate platelets, making near-wall platelets more likely to bind; 2) stiffened RBCs contact and activate endothelial cells, making near-wall platelets more likely to bind to the increased cellular

adhesion molecules and vWF on the endothelium; 3) or near-wall collisions between stiff RBCs and platelets lead to an increase in platelet binding. We sought to begin preliminary experiments to elucidate this mechanism of action. First, we artificially stiffened RBCs and mixed them together with platelet-rich plasma with or without ADP agonist, then allowed the RBCs to settle in static. We then collected platelets and examined them for a marker of inflammation, P-selectin, using flow cytometry. When no ADP is present, addition of rigid RBCs does not increase P-selectin expression on platelets (Figure 5.13A). However, when ADP is present, rigid RBCs lead to an increase in platelet activation level at the highest RBC fraction rigidified (Figure 5.13B), suggesting that stiffened RBCs contribute to platelet activation when platelets are already primed with a different agonist.

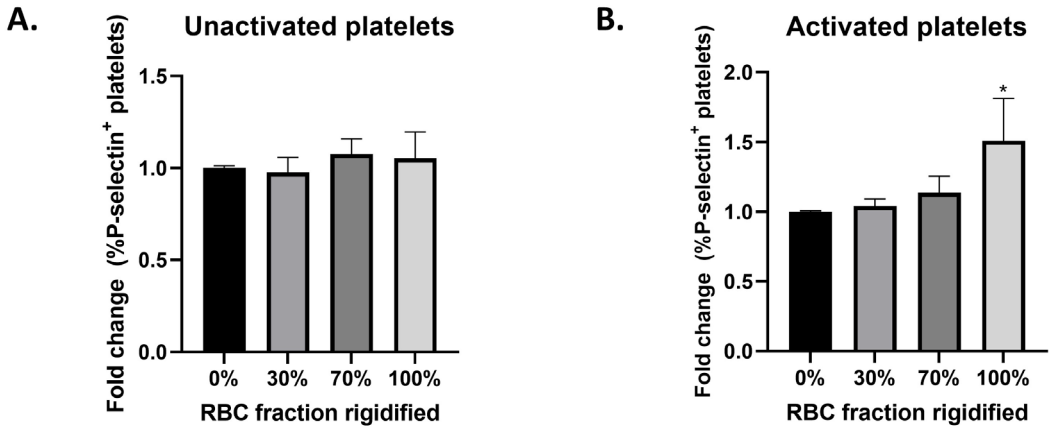

Figure 5.13: Rigid RBCs contribute to platelet activation levels in static conditions.

Fold change in percentage of CD41/61$^+$ platelets positive for P-selectin in comparison to 0% healthy (non-rigid) conditions as analyzed by flow cytometry for (A) resting platelets, or (B) platelets activated by 20 μm ADP. RBCs were 'highly rigidified,' or treated with 1.0 mM TBHP. Statistical analyses were performed using one-way ANOVA with Dunnett's multiple comparisons test where (*) indicates $p < 0.05$ in comparison to 0% rigidifed.

Because prior work demonstrated that artificially stiffened RBCs lead to decreased leukocyte adhesion to an inflamed endothelium in comparison to non-rigidified controls[162], we wanted to determine if rigidified RBCs activate leukocytes in static conditions, similar to the

platelet data shown in Figure 5.13. Similar to the experiments involved platelets, we combined leukocyte-containing platelet-rich plasma with artificially rigidified and healthy RBCs and allowed the RBCs to settle in static. We then collected the leukocytes and examined them for several cell surface markers. Specifically, monocytes mixed with stiffened RBCs had significantly increased CD11a expression (Figure 5.14A) and non-significant changes in CD62L (Figure 5.14B) and CD11b (Figure 5.14C) expression. Neutrophils mixed with stiffened RBCs had changes to expression of different cell surface markers in comparison to non-rigidified samples. Specifically, neutrophils exposed to RBCs that were 30% and 70% stiffened by volume had significant increases in CD11b and CD11b expression (Figure 5.14D and F, respectively), while stiffened RBCs led to a non-significant decrease in CD62L expression (Figure 5.14E). This data may represent one mechanism where rigid RBCs impact leukocyte cell adhesion molecule expression in SCD patients.

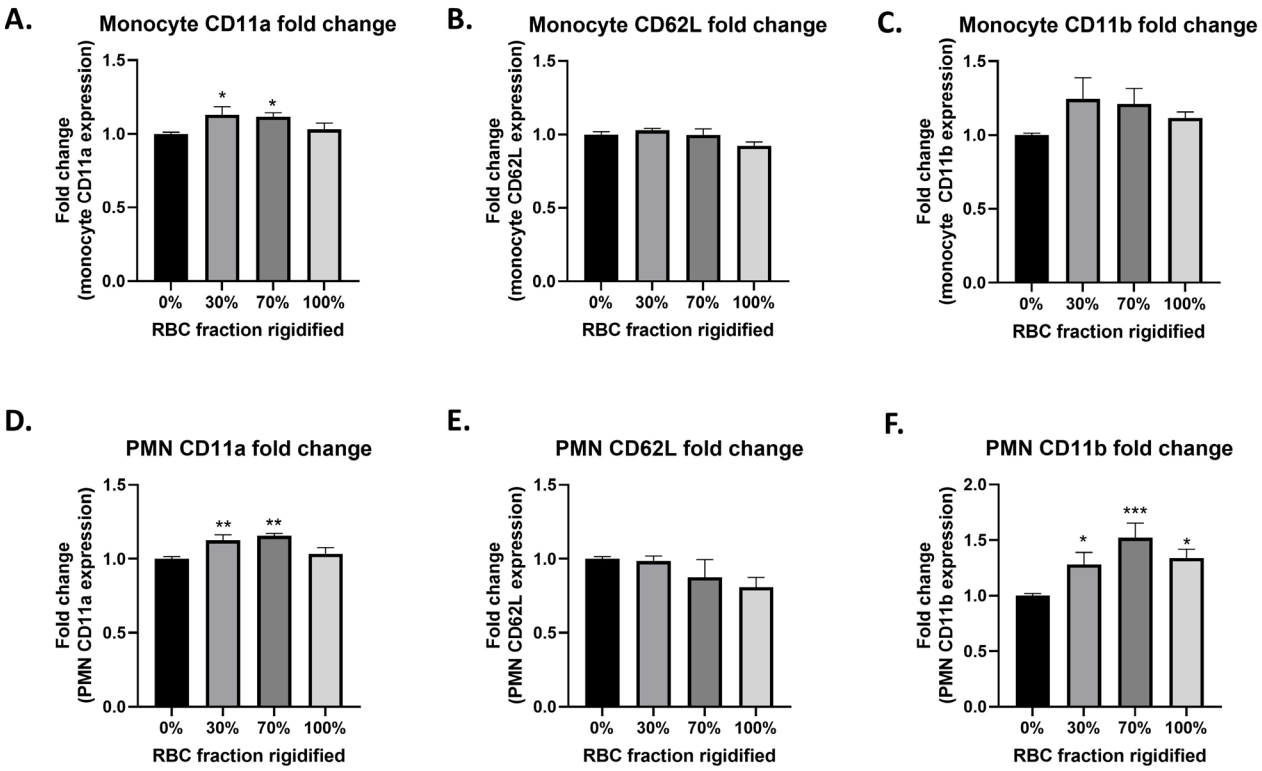

Figure 5.14: Rigid RBCs activate leukocytes in static conditions.

Fold change in median fluorescent intensity of monocyte expression of (A) CD11a, (B) CD62l, (C) CD11b, or neutrophil (PMN) expression of (D) CD11b, (E) CD62L, or (F) CD11b markers in comparison to 0% healthy (non-rigid) conditions as analyzed by flow. RBCs were 'highly rigidified,' or treated with 1.0 mM TBHP. Statistical analyses were performed using one-way ANOVA with Dunnett's multiple comparisons test where (*) indicates $p < 0.05$, (**) indicates $p<0.01$, and (***) indicates $p<0.001$ in comparison to 0% rigidifed.

To determine if rigid RBCs activate HUVEC over the short time course of our flow experiments, we artificially stiffened RBCs, mixed them with plasma, and flowed the mixture over confluent HUVEC. Immediately afterwards, we stained HUVEC in flow using antibodies to identify vWF and P-selectin on the surface. After 5 minutes of laminar flow, we saw no increase in vWF or P-selectin expression by HUVEC (Figure 5.15).

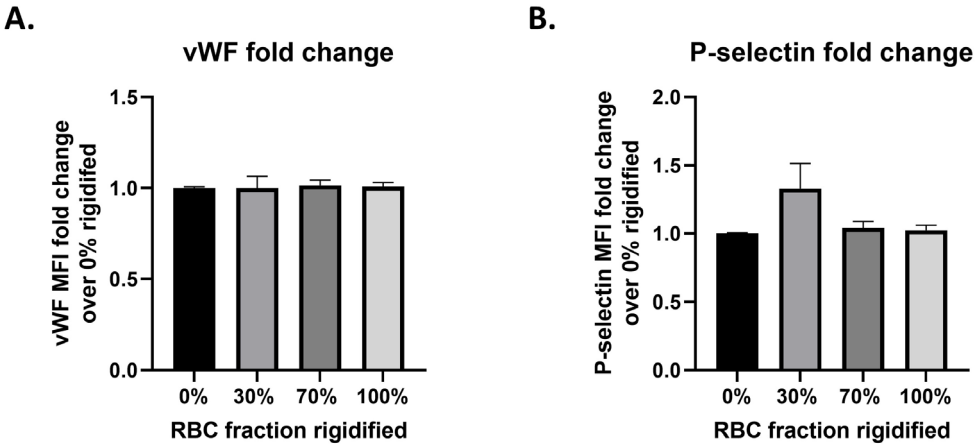

Figure 5.15: Rigid RBCs do not activate HUVEC in shear conditions.

Fold change in HUVEC (A) vWF expression, or (B) P-selectin expression after 5 minutes of plasma and RBC laminar flow in comparison to 0% healthy (non-rigid) conditions as analyzed by fluorescent microscopy. RBCs were 'highly rigidified,' or treated with 1.0 mM TBHP. Statistical analyses were performed using one-way ANOVA with Dunnett's multiple comparisons test where lack of * indicates lack of significance.

5.4.7 Carbon monoxide releasing molecules (CORMs) reduce platelet adhesion in vitro for some SCD patients

While understanding the dynamics between stiffened RBCs and platelets is important to understanding SCD, even more important is to use that information to develop and test new potential therapeutics and to understand for which patients those treatments may be useful. With that, we examine the impact of CORMs on SCD platelet adhesion as CO is highly touted as a potential therapeutic in SCD[242]. To determine if CORMs could decrease platelet adhesion of SCD patients, we pretreated SCD whole blood with 20 μM CORM-A1 or CORM-401 for 30 minutes prior to an *in vitro* blood flow experiment. The impact of CORMs on SCD platelet adhesion at $100s^{-1}$ is shown in Figure 5.16. As before, patients receiving chronic transfusions of RBCs are represented with filled black circles (Figure 5.16B); patients on hydroxyurea are represented with red, upwards facing triangles (Figures 5.16C); patients not receiving treated are represented using

blue, downwards facing triangles (Figures 5.16D); and patients whose treatment regiments are unknown are represented as purple diamonds. Figure 5.16A demonstrates that, for SCD patients as a whole, pretreatment with CORM-A1 leads to a non-significant decrease in platelet adhesion ($p = 0.3513$) while pretreatment with CORM-401 leads to a significant decrease in platelet adhesion ($p = 0.0034$). Separating SCD patients by treatment group, patients receiving chronic transfusions of RBCs were not significantly impacted by CORM pretreatment (Figure 5.16B), though treatment with CORM-401 was nearly significant ($p = 0.0562$). Patients treated with hydroxyurea were also not significantly impacted by CORM pretreatment (Figure 5.16C). However, untreated patients had a significant reduction in platelet adhesion with pretreatment of CORM-401 specifically (Figure 5.16D; $p = 0.0401$).

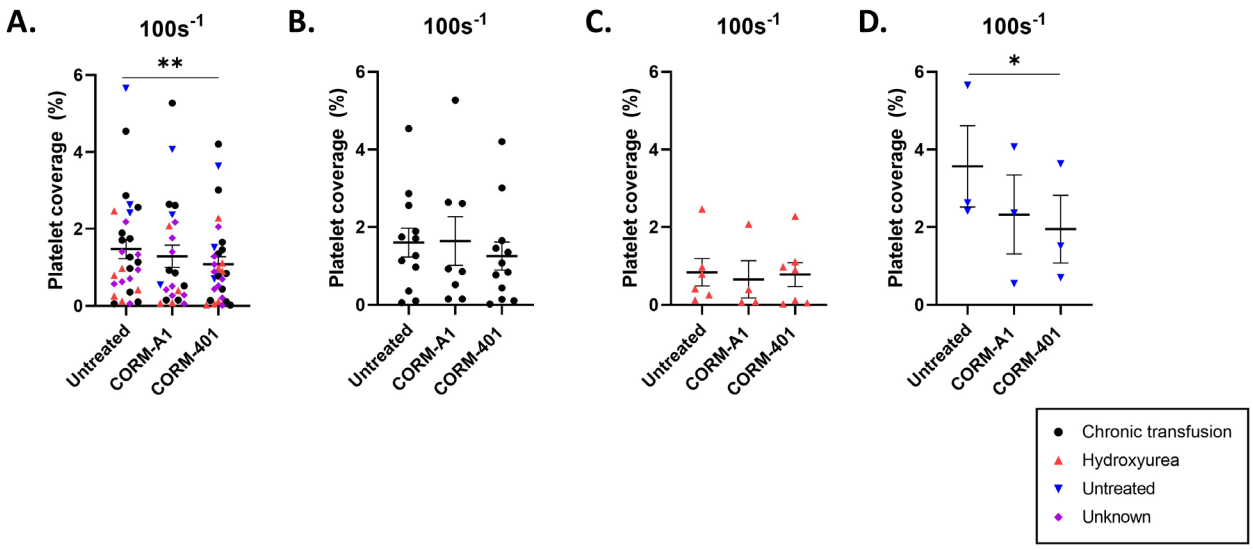

Figure 5.16: Carbon monoxide releasing molecules (CORMs) decrease SCD platelet adhesion for some treatment groups at low shear.

Platelet coverage (as % of total surface area of photo) after 5 minutes of laminar flow in whole blood of either non-SCD controls (open circles) or (A) all SCD patients, (B) SCD patients being treated with chronic transfusion (CT) of RBCs (filled black circles), (C) SCD patients being treated with hydroxyurea (HU; red upwards triangles), or (D) SCD patients not currently being treated (UT; blue downwards triangles) at $100s^{-1}$ on histamine-stimulated and mechanically disrupted HUVEC after 30 minute pretreatment with 20 µm CORM-A1 or CORM-401. Patients whose treatment status is unknown ('UK') are represented with purple diamonds. Statistical analyses were performed using a Student's unpaired t-test, where (*) indicates $p<0.05$.

We also examined the impact of CORMs on SCD platelet adhesion at $1000s^{-1}$. Taken as one group, pretreatment with CORM-A1 led to a non-significant decrease ($p = 0.2031$), and pretreatment with CORM-401 led to a significant decrease ($p = 0.0139$), in platelet adhesion (Figure 5.17A). When separated out into treatment groups, neither patients receiving chronic transfusions (Figure 5.17B), patients receiving hydroxyurea (Figure 5.17C), nor untreated patients (Figure 5.17D) were significantly impacted by CORM pretreatment.

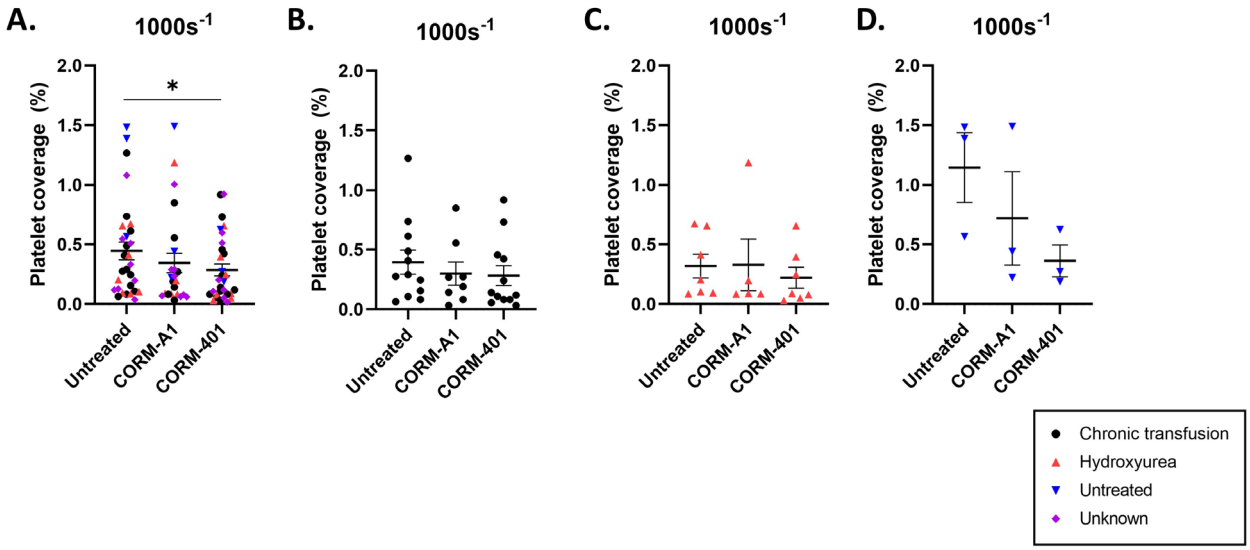

Figure 5.17: Carbon monoxide releasing molecules (CORMs) decrease SCD platelet adhesion for some treatment groups at high shear.

Platelet coverage (as % of total surface area of photo) after 5 minutes of laminar flow in whole blood of either non-SCD controls (open circles) or (A) all SCD patients, (B) SCD patients being treated with chronic transfusion (CT) of RBCs (filled black circles), (C) SCD patients being treated with hydroxyurea (HU; red upwards triangles), or (D) SCD patients not currently being treated (UT; blue downwards triangles) at $1000s^{-1}$ on histamine-stimulated and mechanically disrupted HUVEC after 30 minute pretreatment with 20 µm CORM-A1 or CORM-401. Patients whose treatment status is unknown ('UK') are represented with purple diamonds. Statistical analyses were performed using a Student's unpaired t-test, where (*) indicates $p<0.05$.

Our previous analysis looked at SCD patients as an entire group or within the same treatment group. We also examined each individual patient and whether CORMs led to a decrease in platelet adhesion for them specifically. Whenever possible, four separate CORM experimental

trials were utilized for each SCD patient: $100s^{-1}$ with CORM-A1; $100s^{-1}$ with CORM-401; $1000s^{-1}$ with CORM-A1; and $1000s^{-1}$ with CORM-401. In some instances, we only had enough whole blood to run 2/4 of these trials instead of all four. To determine if CORM pretreatment impacted patient platelet adhesion, we utilized a one-way ANOVA to compare platelet adhesion of a patient both untreated and treated with CORMs. If 0/4 or 0/2 CORM trials yielded a significant decrease in platelet adhesion, that patient is described as '0%' because 0% of their trials yielded a decrease in adhesion. If 1/4 CORM trials were significant, that patient is described as '25%.' If 1/2 or 2/4 CORM trials were significant, that patient falls under the '50%' category and so on. A graphical representation of SCD patients and what percentage of CORM trials led to a significant decrease in platelet adhesion is shown in Figure 5.18. On top of each bar is a number representing the total number of SCD patients in each treatment group.

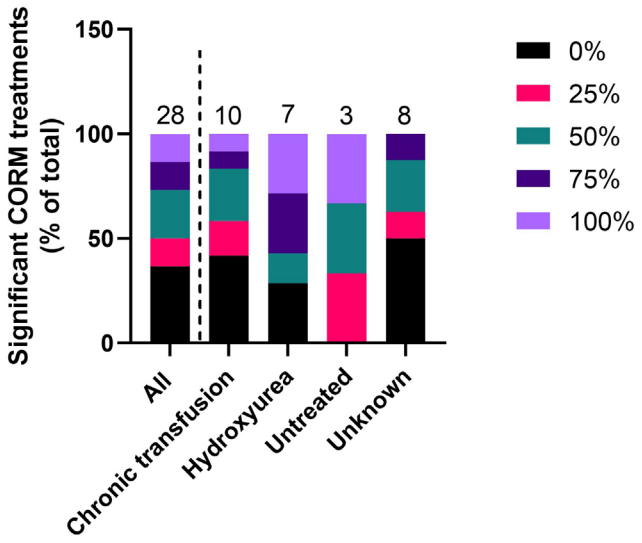

Figure 5.18: CORM pretreatments is most likely to lead to significant decrease in platelet adhesion for untreated or hydroxyurea-treated SCD patients.

Data represents the % of flow experiments (out of 2 or 4 total) for each individual SCD patient where CORMs led to a statistically significant decrease in platelet adhesion in comparison to non-CORM controls. Numbers on top of each bar represent the total number of individual SCD patients in each group.

Looking at all SCD patients as a whole, there is a distribution of patients for whom CORM treatments were not useful (0%), some for whom CORM treatments were somewhat useful (25, 50%), and some for whom CORM treatments were very useful (75, 100%) in decreasing platelet adhesion to a damaged endothelium. When examining treatment groups, both the hydroxyurea-treated group and the untreated group had a larger percentage of patients that responded to CORM treatment than the chronic RBC transfusion-treated patients. Finally, patients whose treatment method is unknown behave similarly to the 'all' category, with many patients not responding to CORM treatment.

5.4.8 Artificially stiffened RBCs can be used to examine impact of CORMs on platelet adhesion using non-SCD controls

Figure 5.18 demonstrates that SCD patients are a heterogenous population and that not all patients or treatment groups respond similarly to CORM treatments to decrease platelet adhesion. There is great benefit to having a more controlled method to explore the dominating mechanism of action of CORMs on platelet adhesion for SCD. To demonstrate that our artificial model can be utilized to explore novel SCD therapeutics, we examined the impact of CORM-A1 and CORM-401 on activated platelet adhesion in the presence of highly rigidified RBCs at $1000s^{-1}$. We artificially stiffened RBCs and mixed them with platelet-rich plasma before adding 50 μM CORM-A1 or CORM-401 to the mixture. After a 30 minute pretreatment, we activated the mixture with ADP to mimic our previous artificially stiffened RBC/platelet experiments and to represent the activated platelet phenotype of SCD[114,115]. The results from these experiments are shown in Figure 5.19. iCORM-A1 and iCORM-401 refer to the CORM molecule backbone after release of carbon monoxide and serves as a CORM vehicle control. CORM-A1 pretreatments lead to a decrease in platelet adhesion, which is significant at 70% RBCs rigidified (Figure 5.19A). CORM-401

pretreatment also leads to a decrease in platelet adhesion, which is significant at 100% RBCs rigidified (Figure 5.19B).

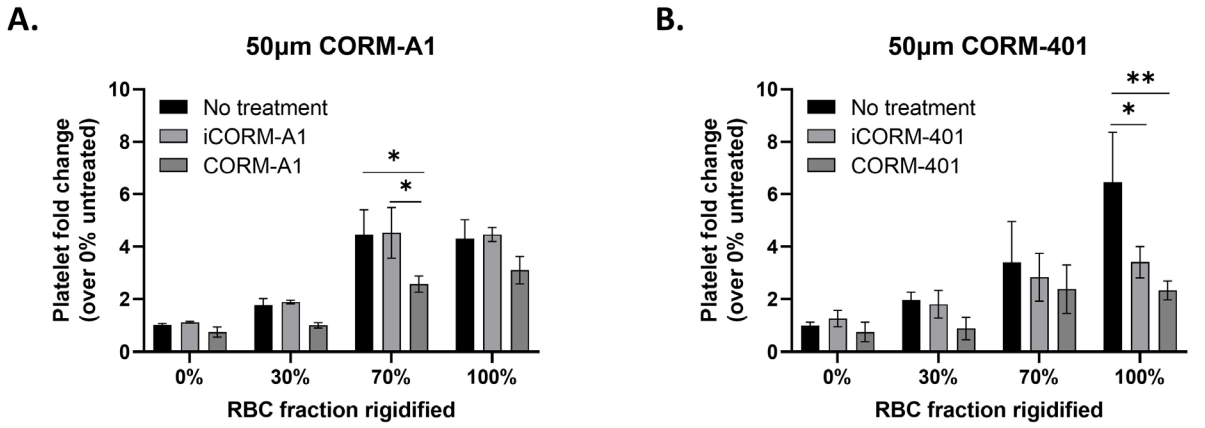

Figure 5.19: Artificial method of RBC rigidification can be used to screen therapeutics for SCD.

Fold change in activated platelet adhesion (% of surface) of platelets in plasma at 40% hematocrit and $1000s^{-1}$ containing RBCs artificially rigidified with 1.0 ('highly rigid') mM TBHP in comparison to healthy (non-rigidified) blood with a 30 minute pretreatment of (A) 50 µM CORM-A1 or (B) 50 µM CORM-401. iCORM-A1 or iCORM-401 refer to inactivated CORM treatments. Statistical analyses were performed using two-way ANOVA with Tukey's multiple comparisons test where (*) indicates $p < 0.05$, and (**) indicates $p<0.01$ in comparison to no treatment at that specific RBC fraction rigidifed.

5.5 Discussion

Overall, we demonstrated in this chapter that some SCD patients have elevated platelet adhesion to a damaged endothelium in comparison to non-SCD controls (Figures 5.1, 5.2, and 5.3). However, there was great heterogeneity between individual patients. When examined collectively, SCD patients had elevated platelet adhesion at $100s^{-1}$ in comparison to non-SCD controls (Figure 5.1A); however, collectively, SCD patients did not have elevated platelet adhesion at 500 or $1000s^{-1}$, despite SCD patients having increased risk of arterial thrombotic events like acute chest syndrome[97], ischemic stroke[101–103], and myocardial infarction[104,105]. There is a clear potential reason for this discrepancy; we have limited information about these SCD patients, including

whether they are in crisis or stable conditions. When stable, it is very possible that treatment of chronic transfusion or hydroxyurea helps decrease the excessive platelet reactivity and adhesion that SCD patients may experience in crisis. This hypothesis is supported by the untreated cohort having significantly elevated platelet adhesion in comparison to non-SCD controls at all shear rates examined (Figure 5.1D, 5.2D, and 5.3D). Interestingly, however, untreated SCD patients did not have elevated platelet activation as measured by P-selectin expression in comparison to non-SCD controls, unlike all other treatment groups (Figure 5.4). It is likely that the level of platelet adhesion to the damaged endothelium is thus not only dependent on platelet activation levels, but also other characteristics of blood as well.

We also explored these other measurable characteristics to determine if any of these variables are predictive of high platelet adhesion at low ($100s^{-1}$) or high ($1000s^{-1}$) shear rate. Much of the data was inconclusive with no clear linear correlation between the measure variable and platelet adhesion level (Figure 5.5 and 5.6). However, there were several exceptions. Taken as a whole, platelet adhesion at $100s^{-1}$ for all SCD patients was inversely correlated with hematocrit (Figure 5.5A), a trend that was maintained for chronic transfusion patients specifically (Figure 5.5B). This observation was interesting as it runs contrary to previous work demonstrating increased platelet adhesion with an increase in hematocrit[54,156]. However, this again is a heterogenous population of patients undergoing treatment methods. Figure 5.5B demonstrates a cluster of chronic transfusion and hydroxyurea patients at high hematocrit and relatively low platelet adhesion. Both treatment methods help increase RBC count, so the fact that patients receiving treatment have both high hematocrit and low platelet adhesion is entirely reasonable. At $100s^{-1}$, platelet count was not correlated with platelet adhesion for all SCD patients or by treatment group (Figure 5.5C and D). HbS fraction (%S) did correlate to platelet adhesion for both chronic

transfusion patients and untreated patients at $100s^{-1}$ (Figure 5.5F); Figure 5.5F also highlights the impact that chronic transfusion of HbA RBCs and hydroxyurea have on HbS fraction as untreated patients represent a cluster of high %S fraction and high platelet adhesion. Finally, at $100s^{-1}$ P-selectin expression is positively correlated with platelet coverage for chronic transfusion patients only. Platelet adhesion at $1000s^{-1}$ was less likely to be correlated with any of the measurable variables than platelet adhesion at $100s^{-1}$ (Figure 5.6), though again P-selectin expression was positively correlated with platelet adhesion for chronic transfusion patients only (Figure 5.6H). Because chronic transfusion patients represented the largest cohort of patients in this study, we cannot speculate whether this is a chronic transfusion-related correlation or if the total number of patients contributed to this linear regression.

While working with SCD patient blood samples directly gave us a lot of information on how platelets from different treatment groups behave and what variables impact platelet adhesion, the fact remains that this is a heterogenous population of patients undergoing different treatment methods. Further, we cannot know whether these patients are stable or in crisis, as well as other factors that could impact the severity of their condition. With that, it would be beneficial to create an artificial system of SCD that allows us tight control over each blood variable we want to explore. Such a system would also allow for researchers not directly working with SCD patients to study the disease. We utilized a method of artificially stiffening non-SCD RBCs that allowed us to tightly control the magnitude of RBC stiffness as well as the fraction of all RBCs that are artificially rigidified[153,161,162]. We examined how artificially stiffened RBCs impact platelet adhesion to a damaged endothelium and confirmed that platelet adhesion increases in the presence of stiff RBCs, which is similar to previous results[234]. We also determined that stiffer RBCs have a larger impact on platelet adhesion than less stiff RBCs (Figure 5.8A). However, even when we severely

artificially stiffened RBCs, they did not lead to a significant increase in platelet adhesion when only 30% of them were rigidified (Figure 5.8A).The maximum platelet adhesion of over six-fold in comparison to a healthy control occurred at 70%; this maximum is particularly interesting as it corresponds to the same maximum decrease in white blood cell adhesion to activated HUVEC in the presence of rigid RBCs previously reported[162]. Further, previous research determined that, in crisis, the percentage of rigid RBCs (%S) in SCD patients increases from ~30% under stable conditions to ~70%[235]. Our data, along with this clinical data, suggests that under controlled, stable conditions, stiffened RBCs may not lead to a significant increase in platelet adhesion but under crisis conditions, the increase in the stiff proportion of RBCs can contribute to excessive platelet adhesion. This finding represents one potential way for rigid RBC/platelet interactions to lead to VOC when a patient is in crisis.

In our own SCD patient cohort, %S (rigid RBC) fractions ranged from 14.8% to 90.8% (Figure 5.5 and 5.6) with chronic RBC transfusion patients generally having lower %S than hydroxyurea-treated or untreated patients. Our own artificial data ranges from 0% to 100% rigid (mimicking a wide range of %S); while our 100% rigidified RBC data is likely not physiological, any RBC rigid fraction less than 100% falls into our own measured %S range for SCD patients and our findings in that range are physiologically relevant. Comparing our artificial data in Figure 5.8A to SCD platelet coverage in comparison to %S in Figure 5.5 and 5.6, hydroxyurea-treated patients with high %S were not necessarily associated with high platelet adhesion and instead formed a cluster at high %S and relatively low platelet adhesion. Conversely, untreated patients formed their own cluster at high %S and relatively high platelet adhesion. Hydroxyurea treatment reduces patient WBC and platelet counts, which contribute to inflammation and VOC in SCD[107].

It is possible that in the absence of this platelet and WBC-mediated inflammation, highly stiffened RBCs have a muted impact on platelet adhesion.

After determining that inclusion of severely rigid RBCs impacts platelet adhesion to a damaged endothelium, we further explored variables including RBC rigidity, shear rate, hematocrit, and flow patterns. Inclusion of the highly rigid RBCs (those treated with 1.0 mM TBHP) in blood flow led to the largest increase in platelet adhesion to the endothelium in comparison to the moderately and slightly rigidified RBCs treated with 0.75 and 0.5 mM TBHP, respectively (Figure 5.8). Of note, the fraction of RBCs rigidified that produced the maximum fold change in platelet adhesion decreased with increasing RBC stiffness; the maximum platelet adhesion occurred when 100% of the RBCs were rigid for the slightly rigid treatment, when 90% of the RBCs were rigid for the moderately rigid treatment, and when 70% of the RBCs were rigid for the highly rigid treatment. This shift in maxima suggests that a smaller percentage of extremely stiff RBCs may have a similar impact on platelet adhesion as a larger percentage of less severely stiffened RBCs. These results are in line with previous work by Gutierrez *et al.* that showed the largest decrease in WBC binding to inflamed HUVEC was in the presence of the most highly rigidified, 1.0 mM TBHP-treated RBCs[162]. Previous research studying the stiffness of SCD patient RBCs established that patients experience a decrease in RBC deformability during painful crisis in comparison to RBC deformability at steady state[253,254]. Our results showing that the most rigid RBCs impact platelet adhesion to the largest degree fits with this clinical observation. What remains to be determined is if steady state RBC stiffness itself can predict risk of VOC events for SCD patients and is something that should be investigated further.

Interestingly, inclusion of rigid RBCs in a mixture of PRP and healthy RBCs at $1000s^{-1}$ increased platelet adhesion to the endothelium to a larger extent than either the lower shear rate,

$500s^{-1}$, or the higher shear rate tested, $1500s^{-1}$, for all volume fractions of rigid RBCs (Figure 5.9). This maximum effect at $1000s^{-1}$ may be due to a balance between opposing forces that all increase with increasing shear rate—total number of platelets in the system and tendency of platelets to form thrombi in high shear[53], versus removal of platelets bound to the endothelium due to shear force, and cleavage of long vWF strands by ADAMTS-13 in plasma at high shear rates[180]. Platelet adhesion increased with higher hematocrits (40 and 60% in comparison to 20%; Figure 5.10), specifically when high percentages of RBCs were stiffened (70-100%). This is unsurprising because there is a recognized connection between elevated hematocrit and cardiovascular disease and thrombosis[255], as an increase in hematocrit leads to a greater concentration of platelets near the vascular wall[54]. This phenomenon has been explored both experimentally and computationally[54,156]. Practically, this information can help inform how chronic transfusion impacts platelet adhesion for SCD patients. Figure 5.10 demonstrates that both a high hematocrit and high %S are required to see a significant increase in platelet adhesion. However, SCD patients typically do not have such elevated hematocrits due to RBC lysis[94]. In our SCD cohort, hematocrits for all patients ranged from 18 to 33.7% (Figure 5.5 and 5.6); no patients reached the 40% threshold our data suggests is needed to see increased platelet adhesion at high %S. This data suggests that chronic transfusions of RBCs for SCD patients do not place them into danger for excessive platelet adhesion. However, further work can confirm the impact of more muted increases in hematocrit (i.e., 20-35%) on platelet adhesion in the presence of stiffened RBCs in a more narrow and physiologically relevant range. Inclusion of WBCs in our model resulted in similar adhesion trends as the base case of RBCs in PRP, suggesting that the rigid and deformable RBCs have a direct impact on platelet adhesion (Figure 5.11A).

Resting platelet adhesion did not increase in the presence of highly rigid RBCs to the same extent as platelets activated with ADP with great variation between 10 separate donors (Figure 5.11A); specifically, there was no significant impact on resting platelet adhesion when 70% of the RBCs were stiffened, unlike when platelets were activated (Figure 5.8A). SCD patients have increased levels of platelet activation at baseline, which increases further during crisis[115,256]. Platelet activation levels are correlated to pulmonary hypertension in SCD patients, one of the features of which is thrombosis in situ[257]. Our results demonstrate a link between platelet activation and increased adhesion in the presence of rigid RBCs, which may provide a mechanism for action for SCD patients with highly activated platelets that experience increases in platelet-mediated VOC. This result in our artificial system supports our previous observation specifically about hydroxyurea-treated patients with high %S and low platelet adhesion (Figure 5.5 and 5.6); in the absence of inflammation that may be lessened due to hydroxyurea treatment, stiffened RBCs appear to have a muted impact on platelet adhesion. Further research should explore if platelet adhesion levels alone conclusively correspond to increased risk of VOC events, if they can be predictive of VOC outcomes in SCD patients, and if there is a link between patients with high levels of inflammation and high platelet adhesion *in vitro*.

We examined the impact of carbon monoxide releasing molecules (CORMs) on SCD platelet adhesion at low and high shear rates. Taken as a whole group, CORM-401 specifically significantly decreased platelet adhesion of SCD patients at 100 and $1000s^{-1}$ (Figure 5.16A and 5.17A). Taken as individual treatment groups, only untreated patients at $100s^{-1}$ as a group had significantly decreased platelet adhesion with CORM-401 (Figure 5.16D). However, as mentioned before, there can be downfalls in viewing an entire cohort of SCD patients as one group due to the inherent differences between each patient. Figure 5.18 thus demonstrates how CORMs impacted

platelet adhesion of SCD patients as a group but analyzed separately; raw platelet adhesion for each CORM trial was compared to untreated trials for that individual patient without addition of CORMs. Overall, and unsurprisingly, patients responded to CORM treatments differently. Examined as an entire group, CORM pretreatment led to no significant impact on platelet adhesion for 36% of patients and 13% of patients had a significant decrease in platelet adhesion for all trials with CORMs (Figure 5.18). Similarly, when examined in treatment groups, 42% of chronic transfusion patients and 50% of patients for whom treatment regimen was unknown saw no benefit with CORM treatment. Only 9% of chronic transfusion patients and 0% of 'unknown' patients saw a benefit of CORM treatment for all trials. However, patients who received hydroxyurea and those who were untreated responded very differently to CORM treatment. 29% of hydroxyurea patients and 0% of untreated patients saw no benefit with CORM treatment, while another 29% of hydroxyurea patients and 33% of untreated patients saw a benefit with CORM treatment for every experimental trial. This data highlights how different patients on different treatment regiments may benefit from CO treatment, potentially in addition to their current treatment method.

Previous work hypothesized that CO treatment could benefit SCD patients through several potential mechanisms[242]. The results shown in Figure 5.18 point towards one potential dominating mechanism of action for CORMs reducing platelet adhesion. Patients receiving chronic transfusion were less likely than other groups to see a reduction in platelet adhesion due to CORM treatment. These patients also have reduced HbS (%S) and increased HbA fractions (Figure 5.5 and 5.6), though still maintain an activated platelet phenotype (Figure 5.4). Thus, we hypothesize that CORMs are therapeutically acting upon stiffened HbS RBCs, potentially causing them to depolymerize, and are not simply preventing platelet activation and adhesion. This hypothesis helps explain why patients receiving hydroxyurea and patients that are untreated, who have high

HbS fractions (Figure 5.5 and 5.6), benefit more from CORM treatment than those receiving chronic transfusions. Future work utilizing SCD samples can explore whether CORM treatment impacts RBC stiffness as measured by ektacytometry and if CORM treatment also reduces the sickled fraction of RBCs using blood smears.

Figure 5.19 demonstrates that we can use an artificial system to explore the impacts of CORMs on platelet adhesion. Future work can utilize this model to further explore and confirm our hypothesized mechanism of action. For instance, future work can explore treating only artificially rigidified RBCs with CORMs instead of the entire rigid RBC/platelet mixture; comparing this data with data where only platelets are treated with CORMs and where the entire blood mixture is treated with CORMs can help confirm upon which blood cells the CORMs are primarily acting. These experiments can include the proper inactivated CORM ('iCORM') controls utilizing the CORM molecule skeleton after CO has been released to confirm that the skeleton molecule itself has no therapeutic effect.

5.6 Conclusions

Here, we demonstrate how stiff RBCs impact platelet adhesion to a damaged endothelial monolayer using both SCD patient whole blood samples and a model system where non-SCD RBCs are artificially rigidified. Within the SCD patient cohort, untreated patients had the largest increase in platelet adhesion over non-SCD controls, while patients receiving chronic transfusions or hydroxyurea were more variable and less likely to be significantly greater than controls. Most measurable characteristics of blood, including platelet count, did not correlate directly with magnitude of platelet adhesion for SCD patients. However, there were several exceptions: at $100s^{-1}$, hematocrit was inversely correlated with platelet adhesion for SCD patients as a group, which is likely due to patients receiving chronic transfusions of RBCs or hydroxyurea to treat SCD leading

to an increased hematocrit. Further, when examined in individual treatment groups, HbS fraction was positively correlated with platelet adhesion at $100s^{-1}$ for chronic transfusion and untreated groups. Using our artificial system allowed us to examine the impact of stiffened RBCs on platelet adhesion in a more controlled environment. We observed that high RBC stiffness, shear rate, and hematocrit all led to an increase in platelet adhesion. This work also presents an overview of how CO treatment may benefit SCD patients specifically in the area of VOC and clotting. To our knowledge, this is the first study examining the impact of CORMs on SCD patient platelet behavior in blood flow directly. We observed that only a subset of SCD patients received a 'benefit' from CORM treatment, defined as a significant reduction in platelet adhesion in comparison to that patient's untreated controls. Specifically, patients on hydroxyurea treatment or those untreated were more likely to see a significant benefit on platelet adhesion with CORM pretreatment than those receiving chronic transfusions of RBCs. This finding led us to hypothesize that the dominant mechanism of action of CORM pretreatment is by softening or depolymerizing stiffened RBCs, though more research is needed to confirm this hypothesis. Overall, the work presented here demonstrates an exploration of the blood variables that lead to increased platelet adhesion in SCD and how that adhesion may be modulated.

Chapter 6 Infusible Extracellular Matrix Hydrogel Interacts with Human Endothelial Cells and Platelets in Blood Flow

6.1 Publication Information

This data is not yet published. This chapter has been composed as part of a manuscript, which is under review at *Nature Medicine*. A preprint of the manuscript is currently available with the title "Healing Tissues from the Inside Out: Infusible Biomaterial for Targeting and Treating Inflammatory Tissues via Intravascular Administration."

6.2 Abstract/Summary

Heart failure following a heart attack impacts millions of adults per year in the United States alone, yet current treatments, including heart transplants, are costly, invasive, and out of reach for many patients. An upcoming treatment method is regenerative medicine, particularly the use of injectable extracellular matrix (ECM) scaffolds to facilitate cell growth, healthy remodeling, and tissue regeneration in areas of damage. In this chapter, we describe novel work examining the behavior of an infusible ECM (iECM) hydrogel. Specifically, we found that iECM bound to areas of damaged or inflammation on a HUVEC monolayer in human blood flow *in vitro*, both at low and high shear rates. Further, iECM helped facilitate platelet adhesion to a damaged HUVEC monolayer at low shear rates. Overall, our data demonstrates that iECM has the potential to be translatable for use in humans in treatment of heart failure or other diseases where endothelial dysfunction or damage occurs.

6.3 Background and Introduction

Ischemic heart disease occurs when adequate oxygen is not delivered to myocardium, which lead to myocardial infarction (MI, commonly known as a 'heart attack') and ultimately to heart failure. Approximately 6.2 million adults in the United States have heart failure[258] and globally, projections suggest that 13.4% of total deaths worldwide will be due to ischemic heart disease by 2030[259]. Treatments for heart failure are limited to whole heart transplants and left ventricular assist devices, both of which are expensive and greatly limit the quality of life of patients[260]. Heart failure occurs after MI due to a series of events in the body which all stem from the inability of the myocardium to properly regenerate after damage or injury. After an MI, the myocardium undergoes extensive remodeling of the extracellular matrix (ECM) due to enzymatic degradation of the ECM by matrix metalloproteinases and increased collagen deposition, leading to fibrosis[261–263]. This remodeling eventually leads to tissue necrosis and, ultimately, heart failure.

With current treatment methods for heart failure being invasive, expensive, and unfeasible for much of the globe, there has been extensive recent research on alternative treatment methods for heart failure. In particular, one area of research focus is on cardiac tissue engineering to either transplant myocardial cells into the area of infarct or otherwise facilitate the self-regeneration of the myocardium after an MI[264,265]. A promising candidate in the area of myocardial regenerative medicine is the use of biomaterial cell scaffolds, especially those made of extracellular matrix proteins, to encourage the growth and proliferation of cells. For example, previous research found that injecting decellularized cardiac extracellular matrix isolated from murine neonates into post-MI ischemic heart tissue in mice led to an improvement in cardiac function, reduction in fibrosis, and increase in angiogenesis[266]. Separately, other research identified a specific proteoglycan, agrin, as a component of the murine neonatal myocardial extracellular matrix; this group utilized a direct

injection of agrin into the ischemic mouse myocardium after MI, which led to improvements in cardiac function and retention in vessel wall thickness compared to MI control mice[267].

One recently developed ECM scaffold is a decellularized porcine myocardial ECM hydrogel[268]. Benefits of this type of scaffold include its ability to self-assemble into nanofibers, its relatively 'soft' modulus, and the fact that the scaffold is a collective of many different ECM proteins[260]. These qualities make myocardial ECM hydrogels attractive candidates for myocardium regenerative treatment after an infarction as they all help facilitate cell growth. This directly injectable ECM hydrogel has been tested for efficacy in several animal models, including peripheral arterial disease[269] and MI[270]; ECM hydrogel improved outcomes in both of these models. More remarkably, this ECM hydrogel has been tested for safety in Phase I clinical trials in humans[271]. Post-MI patients received a percutaneous transendocardial injection of ECM and were evaluated at 1, 3, and/or 6 months after treatment. The authors reported no serious adverse events and that patients had some improved outcomes at 3 or 6 months, including an increase in distance covered in the '6 minute walk' in comparison to baseline[271].

Despite the potential promise of this injectable ECM treatment, the direct, localized injection of a therapeutic into an area of damage (i.e., into myocardial tissue post-MI) comes with potential concerns and risks. Direct injection is invasive and could potentially contribute to damage in an already fragile organ. To combat these potential issues surrounding directly injected ECM hydrogels, the Christman laboratory at the University of California San Diego recently developed an infusible form of ECM hydrogel that can be delivered intravenously[272]. Further, these researchers examined the impact of the infusible ECM (iECM) in several preclinical animal models where a damaged or leaky vasculature occurs. During this work, researchers found that iECM localized to the damaged organs and specifically bound to areas of vascular damage, binding

to endothelial cells and gaps in the vasculature[272]. Conversely, in healthy animals, iECM did not bind indiscriminately to endothelial cells but was eliminated in urine and the kidneys[272]. iECM improved animal outcomes and promoting tissue repair in both a small and large animal acute MI model[272].

Here, we present *in vitro* research examining how this novel iECM interacts with human blood cells to help determine if this treatment method is translatable from animal to human. Specifically, we utilized our 'damaged endothelium' model with or without underlying endothelial cell inflammation to track if fluorescently tagged iECM bound to areas of vascular damage using human endothelial cells in human blood flow. We also examined the ability of iECM to facilitate platelet adhesion to areas of vascular damage to determine if iECM *in vivo* recruits platelets to assist in clotting.

6.4 Results

6.4.1 Infusible extracellular matrix (iECM) binds to human endothelial cells in blood flow

Past research examining the behavior of an infusible extracellular matrix (iECM) focused on *in vivo* animal models, but how iECM interacts with human cells is still unknown. To determine if iECM can bind to damaged or inflamed human vasculature in the same way that it does *in vivo*, we utilized and altered the damaged endothelium model described in Chapter 3. First, we isolated human red blood cells and plasma; we removed leukocytes and platelets from blood to examine if iECM can bind to endothelial cells in a simplified model system without the interference of other blood cells. Then, we cultured HUVEC for one week *in vitro* while refreshing their media every three days. The purpose of the extended culture time was to give HUVEC an opportunity to start producing large amounts of their own extracellular matrix proteins to better represent an *in vivo* environment where endothelial cells produce their own complex ECM. HUVEC were stimulated

one of three ways; HUVEC were either manually damaged with scalpel to represent an acute vascular injury, manually damaged with a four hour activation with 10 ng/mL TNF-α to represent an acute injury with underlying inflammation, or activated for 24 hours with 100 ng/mL TNF- α to represent severe inflammation leading vascular permeability and gaps between endothelial cells[163]. After stimulation, HUVEC were attached to a parallel-plate flow chamber and perfused with a mixture of RBCs, plasma, and either fluorescently tagged iECM at 1 mg/mL in phosphate buffered saline (PBS) or an equivalent volume of PBS without iECM as a vehicle control.

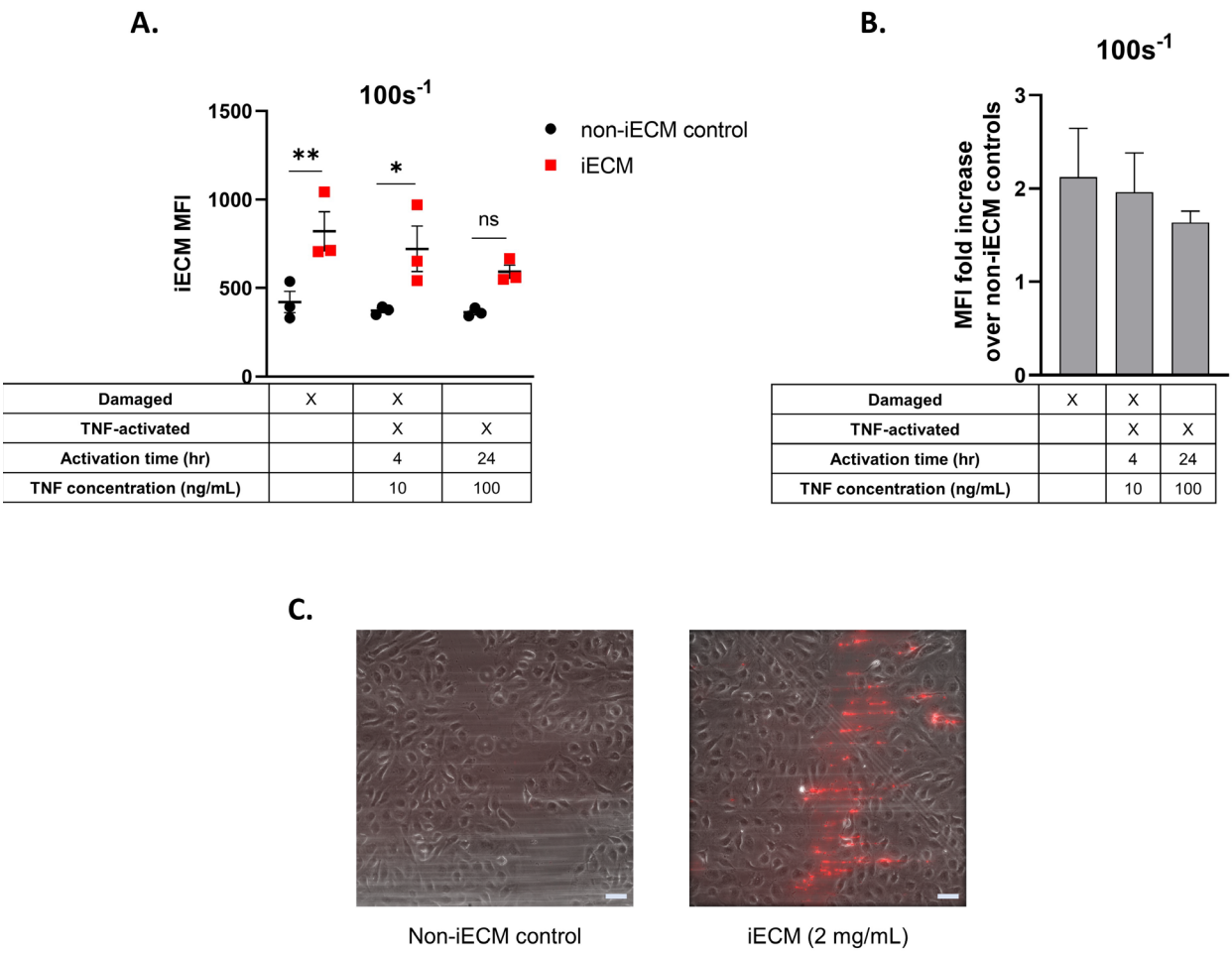

Damaged	X	X	
TNF-activated		X	X
Activation time (hr)		4	24
TNF concentration (ng/mL)		10	100

Damaged	X	X	
TNF-activated		X	X
Activation time (hr)		4	24
TNF concentration (ng/mL)		10	100

Figure 6.1: iECM binds to human endothelial cells in blood flow at low shear rate.

(A) iECM median fluorescent intensity (MFI) of a damaged and/or inflamed HUVEC monolayer with or without iECM (1 mg/mL) after 5 minutes of RBCs and plasma flow at $100s^{-1}$, (B) Change in median fluorescent intensity (MFI) of HUVEC after 5 minutes of $100s^{-1}$ isolated RBCs in plasma (40% hematocrit) with either 1 mg/mL iECM or buffer control. HUVEC were either damaged, damaged and inflamed, or highly inflamed, and (C) representative images of damaged HUVEC (brightfield microscopy) overlaid with TRITC fluorescent channel (red) either of non-iECM buffer controls (left) or iECM (2 mg/mL, right), scale bar 100µm. Statistical analyses were performed using two-way ANOVA with Tukey's multiple comparisons test (A) where (*) indicates $p<0.05$ and (**) indicates $p<0.01$.

At low shear rates representative of blood flow in human veins[56], fluorescently tagged iECM bound to HUVEC under 2/3 stimulatory conditions as represented by the increase in raw median fluorescent intensity (MFI) values in samples containing iECM ('iECM,' red squares) in comparison to non-iECM buffer controls (Figure 6.1A). Specifically, there is a significant increase in MFI for all conditions tested except for the 'highly inflamed,' non-damaged experiments. To

negate any potential donor-specific differences in MFI, we then calculated the change in MFI for each donor and experimental condition ('non-iECM control,' black circles; Figure 6.1B). Here, data is represented as the MFI of a specific donor's iECM trial divided by the MFI of that specific donor's non-iECM trial for each specific inflammatory condition. For all stimulatory conditions, the MFI increased by about two-fold for iECM conditions over non-iECM conditions. Qualitatively, iECM bound between endothelial cells in the gaps induced either by high concentrations of TNF-α or by a manual scalpel score (Figure 6.1C). It should be noted that the images shown in Figure 6.1C utilized a higher concentration of iECM (2 mg/mL) to better visualize the bound iECM but were not used in quantitative analysis. Conversely, non-iECM controls demonstrated no obvious fluorescence, even between endothelial cells (Figure 6.1C).

We also wanted to explore the impact of iECM at higher shear rates representative of faster-moving blood in different vessels of the human body. To that end, we examined the binding of iECM in a similar manner as described above but at $1000s^{-1}$, representative of arterioles or capillaries[56]. Similar to the results at $100s^{-1}$, fluorescently tagged iECM bound to damaged and inflamed HUVEC at all stimulatory conditions explored (Figure 6.2A), leading to a significant increase in MFI for all experimental conditions tested. The iECM MFI was roughly twice as high as the non-iECM MFI for all conditions tested (Figure 6.2B). A representative image demonstrating iECM binding between gaps in the endothelial cell monolayer at $1000s^{-1}$ is shown in Figure 6.2C. Figure 6.2C qualitatively demonstrates iECM binding in string-like patterns, parallel to the direction of blood flow. This pattern of adhesion could suggest that iECM is co-localizing with von Willebrand factor (vWF) multimers secreted by and tethered to inflamed HUVEC, but further research is needed to be conclusive.

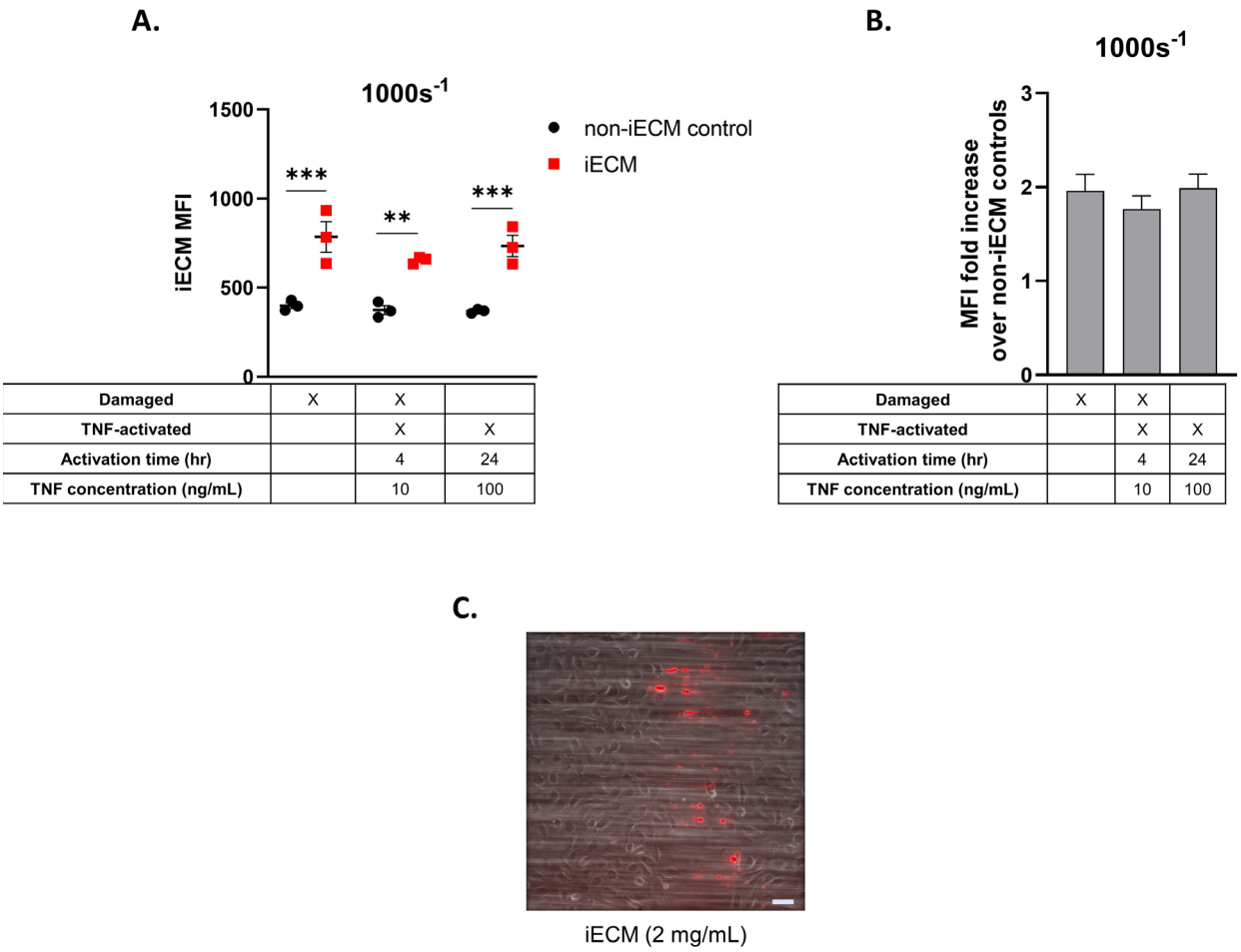

Figure 6.2: iECM binds to human endothelial cells in blood flow at high shear rate.

(A) iECM median fluorescent intensity (MFI) of a damaged and/or inflamed HUVEC monolayer with or without iECM (1 mg/mL) after 5 minutes of RBCs and plasma flow at $1000s^{-1}$, (B) Change in median fluorescent intensity (MFI) of HUVEC after 5 minutes of $1000s^{-1}$ isolated RBCs in plasma (40% hematocrit) with either 1 mg/mL iECM or buffer control. HUVEC were either damaged, damaged and inflamed, or highly inflamed, and (C) representative image of damaged HUVEC (brightfield microscopy) overlaid with TRITC fluorescent channel (red) of iECM (2 mg/mL), scale bar 100µm. Statistical analyses were performed using two-way ANOVA with Tukey's multiple comparisons test (A) where (**) indicates $p<0.01$ and (***) indicates $p<0.001$.

6.4.2 Infusible extracellular matrix (iECM) leads to an increase in human platelet adhesion to damaged HUVEC in vitro

Previously, we demonstrated that iECM binds to human endothelial cells in blood flow (Figures 6.1 and 6.2). The next objective was to determine if iECM can facilitate clotting (i.e., platelet

adhesion) as it would represent one way that iECM can treat acute injuries *in vivo*. We examined the impact of iECM on platelet adhesion to a damaged HUVEC monolayer *in vitro* both at low ($100s^{-1}$) and high ($1000s^{-1}$) by adding fluorescently labelled iECM into whole blood immediately before perfusing over HUVEC. Figure 6.3A shows platelet adhesion at 100 and $1000s^{-1}$ with iECM ('iECM,' red squares) or with buffer-only controls ('non-iECM control,' black circles). At $100s^{-1}$, all donors had an increase in platelet adhesion when iECM was added to blood, though the difference was not statistically significant. Conversely, at $1000s^{-1}$ addition of iECM did not impact magnitude of platelet adhesion for 4/5 donors, though for 1/5 donors addition of iECM did greatly increase platelet adhesion in comparison to non-iECM controls. To control for the inherent differences in platelet adhesion from donor to donor, we then calculated the platelet coverage fold change for each donor (Figure 6.3B); this was calculated by dividing the platelet adhesion of each donor with iECM at a set shear rate by that donor's platelet adhesion without iECM at the same shear rate. At $100s^{-1}$, the average platelet fold change was ~3 across 4 donors. At $1000s^{-1}$, the average platelet fold change was ~2 over 5 donors, though this average was heavily influenced by one donor whose platelet adhesion went up by >6-fold with the inclusion of iECM. Without that one donor, the average platelet fold change was ~1.3, or barely above baseline platelet adhesion without iECM.

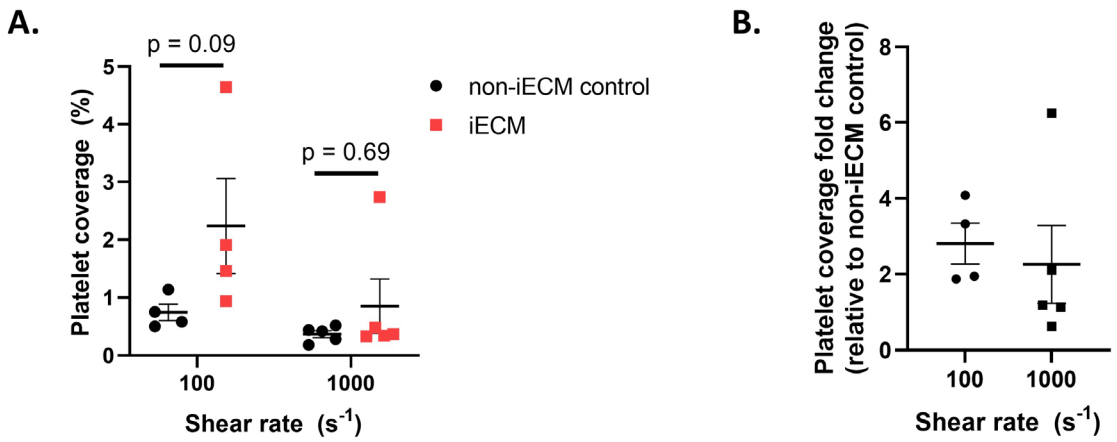

Figure 6.3: iECM increases resting platelet adhesion to a damaged endothelial cell monolayer.

(A) Platelet adhesion (% of surface) of platelets in whole blood to a damaged HUVEC monolayer at 100 or 1000s^{-1} with or without iECM (1 mg/mL), and (B) platelet adhesion fold change of iECM samples relative to each donor's non-iECM control at 100 or 1000s^{-1} of whole blood flow to a damaged HUVEC monolayer. Statistical analyses were performed using two-way ANOVA with Tukey's multiple comparisons test (A) or an unpaired student's t-test (B), where lack of * indicates lack of significance.

6.5 Discussion

In this chapter, we demonstrated that an infusible form of myocardial extracellular matrix: 1. Successfully binds to a damaged human endothelial cell monolayer both at low and high shear rates, and 2. Helps facilitate the adhesion of resting platelets to a damaged endothelial cell monolayer, particularly at low shear rates. This work represents the first time that the impact of iECM on human blood cells has been examined and suggests that iECM, which has been utilized in preclinical animal models[272], may be translatable to humans as well. Previous work demonstrated that fluorescently-tagged iECM localized specifically to areas of vascular damage and permeability in models of myocardial infarction, traumatic brain injury, and pulmonary arterial hypertension[272]. Specifically, iECM does not block the blood vessel lumen, but preferentially binds to gaps between endothelial cells. Utilizing our *in vitro* damaged endothelium model, we examined binding of iECM to a damaged and/or inflamed HUVEC monolayer in a mixture of human plasma

and RBCs. At both low (Figure 6.1) and high (Figure 6.2) shear rates, iECM successfully bound to a damaged HUVEC monolayer, specifically localizing to gaps between the endothelial cells. This data suggests that iECM behaves similarly *in vitro* in a human blood flow system as to *in vivo* preclinical animal models; iECM binds specifically to areas of vascular damage. Further, the ability of iECM to bind at both low and high shear rates suggests it may be therapeutically useful for diseases that impact different parts of the body accessible by blood vessels that experience different shear rates (i.e., veins at low shear rate and arterioles at high shear rate).

We used HUVEC in this work as they are a useful primary source of human-specific endothelial cells that overperform immortalized endothelial cell lines[273]. However, previous research highlighted that there are many key differences between primary endothelial cells isolated from different organs and vascular beds[274–276]. Specifically, analysis from DNA microarrays demonstrated that there are large differences between: endothelial cells isolated from large vessels and microvessels; endothelial cells isolated from arteries and veins; and endothelial cells isolated from different organs[275]. With that knowledge, endothelial cells isolated from umbilical veins (HUVEC) may not represent arterial vasculature and their interactions with iECM and represents one limitation in this initial work.

One of the models of inflammation and damaged that we used in this research involved manually scoring the endothelial cell surface to expose the underlying ECM proteins prior to blood and iECM flow both at low and high shear rates. Exposure of the underlying ECM is a hallmark of arterial thrombosis but not necessarily venous thrombosis; in venous thrombosis, several cell types, including platelets, RBCs, and WBCs, together with blood hypercoagulability and endothelial dysfunction and/or inflammation all contribute to clotting[277]. Considering the known link between TNF-α and venous thrombosis[278,279], our experiments utilizing highly inflamed but

not manually damaged HUVEC may be the most relevant for the study of iECM-endothelial cell interactions at low shear.

Images of damaged HUVEC overlaid with fluorescent iECM perfused at $1000s^{-1}$ (Figure 6.2C) show that iECM is forming red strings either attached to or between endothelial cells, parallel to blood flow. This string-like structure is reminiscent of long vWF strands bound to an inflamed endothelial cell monolayer (Figures 3.1 and 3.3). Future work could explore if iECM colocalizes with vWF multimers. If this colocalization takes place, an important study should examine if at high dosages iECM contributes to excessive, vWF-mediated platelet accumulation beyond useful therapeutic efficacy.

We inflamed endothelial cells in this work using TNF-α, which, similarly to IL-1β, is a strong activator of NF-κB in endothelial cells and plays a role in thromboinflammatory diseases[192]. Specifically, TNF-α activates NF-κB via the canonical pathway after binding to either TNF receptor on the endothelial cell surface[192,280]. Like IL-1β, TNF-α treatment of endothelial cells leads to the expression of cell adhesion molecules on the surface, such as E-selectin and ICAM-1[192]. Other target genes that are upregulated after TNF activation of endothelial cells include cytokines and chemokines, other transcription factors, regulators of apoptosis, and enzymes, among others[192,281]. TNF can also lead to the intracellular formation of reactive oxygen species[282] and even apoptotic cell death in endothelial cells[281].

One way in which iECM may therapeutically treat areas of vascular damage *in vivo* is by recruiting platelets to an area of vascular damage to 'patch' the vessel with a clot. To test this hypothesis, we examined the impact of iECM on platelet adhesion *in vitro* using human whole blood and platelet adhesion to the damaged endothelium model. At $100s^{-1}$, inclusion of iECM led to a consistent but non-significant increase in resting platelet adhesion (Figure 6.3A), or

approximately a 3-fold increase in platelet adhesion (Figure 6.3B). Conversely, at $1000s^{-1}$, inclusion of iECM did not lead to a consistent increase in resting platelet adhesion, with the exception of a single donor (Figure 6.3A). This data suggests that iECM may help facilitate platelet adhesion to an area of vascular damage, particularly at low shear rates, but these results are not conclusive and there might be variability across human donors that could be explored further. Interesting future work could examine what specific components of iECM, if any, facilitate platelet adhesion and if there is variability across donors that could impact the ability of iECM to be translatable to use in humans.

6.6 Conclusions

In this chapter, we report that a new, infusible extracellular matrix (iECM) hydrogel has the ability to bind to human endothelial cells, specifically in areas of damage and increased permeability, *in vitro* in human blood flow. Further, iECM may help facilitate platelet adhesion to a damaged endothelial monolayer, particularly at low shear rates representative of blood flow in large, slow-moving blood vessels like veins[56]. This work represents a key first step in determining the translatability of iECM from preclinical animal models to human studies. Future *in vitro* studies will help elucidate: 1. the mechanism of action of iECM adhesion, in particular determining how iECM binding assists with platelet accumulation to an area of injury, and 2. If altering iECM concentration impacts iECM adhesion and platelet binding and specifically, if iECM has a dose-dependent effect on these outcomes.

Chapter 7 Conclusions and Future Directions

7.1 Dissertation Conclusions and Summary

Despite the importance that platelets play in both health and disease, there remains much that is yet unknown about their function and in particular, how other cells (RBCs, WBCs, and the endothelium) modulate platelet behavior. Understanding the interplay between platelets and other cells using disease-specific *in vitro* models and exploring ways to tune platelet behavior motivated the bulk of this work. There are many different types of *in vitro* and *in vivo* models to study platelet adhesion, but most of them do not fully represent human platelet behavior *in vivo*. Thus, we established a tunable *in vitro* flow model using human endothelial and blood cells that examines platelet adhesion both to the underlying ECM and to endothelial cells themselves all without the need for custom-designed and produced microfluidic channels. We utilized and altered this model to identify novel anti-platelet therapeutics, explore platelet-leukocyte aggregate adhesion and the ability of particulate drug carriers to reduce excess platelet adhesion, examine platelet adhesion in the presence of stiffened RBCs in SCD, explore novel anti-platelet therapeutics for SCD, and examine the interactions between an infusible ECM hydrogel and human cells in blood flow. This work is particularly important as it highlights new therapeutics for diseases involving platelets where current treatments are lacking; such examples include increased bleeding risk due to current anti-platelet treatments for arterial thrombosis and risk of breakthrough infections after steroidal use for thromboinflammation diseases like sepsis and ALI.

In Chapter 3, I developed an *in vitro* blood flow model using human endothelial cells and human blood that allows for platelet adhesion to inflamed endothelial cells as well as the

underlying ECM, which can be tuned depending on protein of interest. Further, I validated this model using a known platelet inhibitor and explored two novel anti-platelet compounds. These results highlight that this model can be utilized as a first screening method for potential anti-thrombotic or anti-platelet compounds whose target can be either platelets themselves or the endothelium.

In Chapter 4, I utilized a version of the 'damaged endothelium' model with underlying inflammation to explore the adhesion of platelet-leukocyte aggregates to an activated endothelial cell monolayer. I showed that particulate drug carriers could significantly decrease platelet adhesion to the endothelium by interfering with bound platelet-leukocyte aggregates. Specifically, untargeted 2 μm PS particles decreased platelet adhesion to 53% of non-particle controls at high particle concentrations ($5*10^7$/mL). Conversely, nano-sized particles had a muted impact on decreasing platelet adhesion. I further confirmed this effect *in vivo* using a systemic model of inflammation in mice caused by an IP injection of LPS; this model leads to neutrophil-dependent platelet adhesion in the mouse mesentery that can be monitored in real time using intravital microscopy. *In vivo*, both untargeted and targeted micron-sized PS particles significantly decreased both platelet and neutrophil adhesion to the inflamed mesentery, an impact that was not seen with nano-sized particles. This work represents promising early data that particulate drug carriers can divert not only phagocytic leukocytes, but also platelets away from areas of inflammation *in vitro* and *in vivo* and suggests a new therapeutic opportunity for thromboinflammatory diseases.

In Chapter 5, I examined the impact of stiff RBCs on platelet adhesion using both SCD patient whole blood and a model system where healthy donor RBCs are artificially rigidified. Taken as a single group, SCD patients had increased platelet adhesion at $100s^{-1}$ but not at higher

shear rates in comparison to non-SCD controls. However, the magnitude of platelet adhesion varied greatly by donor and by treatment method. I also utilized the model system where RBCs are artificially rigidified to examine RBC impact on platelet adhesion in a more controlled environment; stiffened RBCs increased platelet adhesion to a damaged endothelium by up to a factor of six times more than in unstiffened samples. High RBC stiffness, fractions of RBCs rigidified, shear rates, and hematocrits were all associated with drastic increases in platelet adhesion. I also examined the impact of carbon monoxide releasing molecules (CORMs) on platelet adhesion; CORMs significantly reduced platelet adhesion for some but not all SCD patients with wide variability between individual patients and treatment groups. Overall, the results from this chapter represent a method to examine stiffened RBC/platelet interactions in blood flow, even for researchers not interfacing directly with SCD patients. This chapter also presents concrete data that CO can be utilized to reduce platelet adhesion for SCD patients.

In Chapter 6, I utilized several *in vitro* flow models to evaluate how an infusible ECM (iECM) interacts and binds to human endothelial cells in blood flow. I showed that at both low ($100s^{-1}$) and high ($1000s^{-1}$) shear rates, iECM binds between endothelial cells exposed to vascular damage and/or inflammation. Further, I showed that particularly at low shear rates, iECM may help facilitate platelet adhesion to areas of vascular damage. Overall, this chapter represents initial work that iECM is translatable for treatment in humans.

7.2 Future Directions

The work presented in this thesis represents exciting new methods to explore platelet behavior and new findings about platelet-leukocyte, platelet-RBC, and platelet-endothelium interactions. This data lays a foundation for many future studies, with some key potential areas of interest for future research listed below:

1. The impact of altering crosslinked proteins of interest in the 'damaged endothelium' model to produce a more thrombogenic surface. The data demonstrated in Chapter 3 uses primarily crosslinked gelatin for HUVEC culture. However, there is interest in incorporating other proteins or molecules of interest into the ECM, including tissue factor, to shift from a hemostatic surface to a more thrombogenic surface.
2. The behavior of human endothelial cells isolated from different vascular beds *in vitro*. Thus far, we explored platelet behavior using human endothelial cells isolated from umbilical cord veins. However, there is interest in exploring the differences in behavior of endothelial cells isolated from different parts of the vasculature (i.e., endothelial cells isolated from saphenous and umbilical cord veins in comparison to cells isolated from the coronary or carotid artery) and in particular, if we can tune the *in vitro* damaged endothelium model for each vascular bed by altering the key ECM proteins used for crosslinking and the shear rate of that bed.
3. The impact of particle phagocytosis on platelet-leukocyte firm adhesion via P-selectin and PSGL-1. The majority of the work in Chapter 4 examining the use of particulate drug carriers to modulate leukocyte and platelet adhesion occurred in an environment where phagocytosis is not likely to occur (i.e., in ACD-anticoagulated blood *in vitro*). However, past work noted that particle phagocytosis by blood neutrophils altered their surface expression of PSGL-1, which varied by particle material[139]. Allowing phagocytes, including neutrophils and monocytes, to uptake particles of different materials and then examining their interactions with platelets in a controlled environment could shed light on another mechanism for particles impacting leukocyte-platelet aggregate formation.

4. Use of biodegradable particles to reduce platelet-leukocyte adhesion in thromboinflammation. Most work in Chapter 4 utilized a model polymer, PS. However, PS is not suitable as a therapeutic for humans. Upcoming work will examine the impact of model, biodegradable particles (i.e., PLGA) both *in vitro* and *in vivo* to ensure the work presented in Chapter 4 is translatable.
5. Mechanism of action when using PolyA particles to divert platelets and leukocytes from area of inflammation. Preliminary work in Chapter 4 using particles made from a polymer comprised of salicylic acid monomers ('PolyA') demonstrated that *in vivo*, these particles could significantly reduce platelet adhesion to the inflamed mouse mesentery without a significant reduction in neutrophil adhesion. In fact, PolyA particles were the only particle type to significant reduce the percentage of adherent neutrophils associated with platelets on the mesentery wall and the average number of platelet bound to each adherent neutrophil in comparison to LPS-only controls. Future work can elucidate the precise impact that PolyA has on both platelets and neutrophils to determine this addition anti-inflammatory mechanism.
6. Particle and neutrophil trafficking in a systemic mouse model of inflammation. Chapter 4 demonstrated that particulate drug carriers can reduce platelet and neutrophil adhesion to the mouse mesentery without significant adhesion of targeted particles themselves. We hypothesize that in this systemic model, targeted particles are either already being removed from circulation via phagocytosis or are adhering to other areas of inflammation such as the lungs. Future work can examine how particles, both targeted and untargeted, are being removed from circulation, how neutrophils are exiting areas of inflammation, and where both particles and neutrophils ultimately localized to in the body.

7. Utilizing particulate drug carriers to reduce platelet accumulation in other disease models. Thromboinflammation occurs in many different diseases, with platelets often playing a damaging role. We demonstrated using a systemic model of inflammation that particles can reduce platelet adhesion by interfering with bound platelet-leukocyte aggregates. However, there are many other diseases where this type of therapeutic can be applied, such as in ALI where platelets accumulate in the lung. Future work can examine the impact of particles on platelet adhesion in such models and further, can determine if particles loaded with an extra therapeutic have an added benefit *in vivo*.
8. Use of the 'damaged endothelium' model as a diagnostic tool in SCD. In Chapter 5, we examined platelet adhesion from SCD patient blood samples. However, we cannot know these patients' medical histories, nor their likelihood of medical complications due to SCD. It would be incredibly useful to work directly with clinicians in the future to determine if: 1. High levels of platelet adhesion to the damaged endothelium *in vitro* is predictive of VOC or future crises, or 2. High levels of platelet adhesion indicates whether a patient could benefit from increased or altered SCD treatments. If our *in vitro* flow model can accurately predict VOC or other complications, it would be an incredibly useful diagnostic tool for hematologists and other medical providers and ultimately, beneficial for SCD patients to receive proper care.
9. Determination of CO mechanism of action in SCD. In Chapter 5, we demonstrated that CORM pretreatment of SCD blood led to drastically reduced platelet adhesion for a subset of SCD patients. Based on untreated patients and those on hydroxyurea being more likely than chronically transfused patients to have an impact of CORMs on platelet adhesion, we hypothesized that CORMs are acting on stiffened RBCs. Specifically, we hypothesize that

CORMs are ‘softening’ rigid RBCs and are not directly acting on platelets. However, more work can be done to confirm this hypothesis; for example, the artificially stiffened RBC system can be utilized with CORMs used to treat only the stiffened RBCs to see if there is a downstream impact on platelet adhesion. Such experiments can elucidate the exact mechanism of action of CO treatment on platelet behavior for SCD patients.

Bibliography

1. Kim, S., Kai Ong, P., Yalcin, O., Intaglietta, M. & Johnson, P. C. The cell-free layer in microvascular blood flow. *Biorheology* **46**, 181–189 (2009).
2. Fogelson, A. L. & Neeves, K. B. Fluid Mechanics of Blood Clot Formation. *Annu. Rev. Fluid Mech.* **47**, 377–403 (2015).
3. Popel, A. S. & Johnson, P. C. Microcirculation and Hemorheology. *Annu. Rev. Fluid Mech.* **37**, 43–69 (2005).
4. Ley, K. & Tedder, T. F. Leukocyte Interactions with Vascular Endothelium New Insights into Selectin-Mediated Attachment and Rolling'. *J. Immunol.* **155**, 525–528 (1995).
5. Darbousset, R. *et al.* Tissue factor-positive neutrophils bind to injured endothelial wall and initiate thrombus formation. *Blood* **120**, 2133–43 (2012).
6. Cantat, I. & Misbah, C. Lift Force and Dynamical Unbinding of Adhering Vesicles under Shear Flow. *Phys. Rev. Lett.* **83**, 880–883 (1999).
7. Crowl, L. M. & Fogelson, A. L. Computational model of whole blood exhibiting lateral platelet motion induced by red blood cells. *Int. j. numer. method. biomed. eng.* **26**, 471–487 (2010).
8. Aarts, P. A. *et al.* Blood platelets are concentrated near the wall and red blood cells, in the center in flowing blood. *Arterioscler. An Off. J. Am. Hear. Assoc. Inc.* **8**, 819–824 (1988).
9. Uijttewaal, W. S., Nijhof, E. J., Bronkhorst, P. J., Den Hartog, E. & Heethaar, R. M. Near-wall excess of platelets induced by lateral migration of erythrocytes in flowing blood. *Am. J. Physiol.* **264**, H1239-44 (1993).
10. Vahidkhah, K., Diamond, S. L. & Bagchi, P. Hydrodynamic Interaction Between a Platelet and an Erythrocyte: Effect of Erythrocyte Deformability, Dynamics, and Wall Proximity. *J. Biomech. Eng.* **135**, 051002 (2013).
11. Kumar, A., Henríquez Rivera, R. G. & Graham, M. D. Flow-induced segregation in confined multicomponent suspensions: effects of particle size and rigidity. *J. Fluid Mech.* **738**, 423–462 (2014).
12. Schulze, H. & Shivdasani, R. A. Mechanisms of thrombopoiesis. *J. Thromb. Haemost.* **3**, 1717–1724 (2005).
13. Daly, M. E. Determinants of platelet count in humans. *Haematologica* **96**, 10 (2011).
14. Piel-Julian, M.-L. *et al.* Risk factors for bleeding, including platelet count threshold, in newly diagnosed immune thrombocytopenia adults. *J. Thromb. Haemost.* **16**, 1830–1842 (2018).
15. Patti, G. *et al.* Platelet Indices and Risk of Death and Cardiovascular Events: Results from a Large Population-Based Cohort Study. *Thromb. Haemost.* **119**, 1773–1784 (2019).
16. Christie, D. J., Kottke-Marchant, K. & Gorman, R. T. Hypersensitivity of platelets to adenosine diphosphate in patients with stable cardiovascular disease predicts major adverse events despite antiplatelet therapy. *Platelets* **19**, 104–110 (2008).
17. Davila, J. *et al.* A novel inflammatory role for platelets in sickle cell disease. *Platelets* **26**, 726–729 (2015).

18. Ruggeri, Z. M. & Mendolicchio, G. L. Adhesion mechanisms in platelet function. *Circulation Research* vol. 100 1673–1685 (2007).
19. Beumer, S. *et al.* Platelet Adhesion to Fibronectin in Flow: The Importance of von Willebrand Factor and Glycoprotein Ib. *Blood* **86**, 3452–3460 (1995).
20. Huizinga, E. G. *et al.* Structures of glycoprotein Ibα and its complex with von Willebrand factor A1 domain. *Science (80-.).* **297**, 1176–1179 (2002).
21. Chen, H., Locke, D., Liu, Y., Liu, C. & Kahn, M. L. The platelet receptor GPVI mediates both adhesion and signaling responses to collagen in a receptor density-dependent fashion. *J. Biol. Chem.* **277**, 3011–3019 (2002).
22. Shida, Y. *et al.* Analysis of the role of von Willebrand factor, platelet glycoprotein VI-, and α2β1-mediated collagen binding in thrombus formation. *Blood* **124**, 1799–1807 (2014).
23. CHEN, J. & LÓPEZ, J. A. Interactions of Platelets with Subendothelium and Endothelium. *Microcirculation* **12**, 235–246 (2005).
24. Turner, N. A., Nolasco, L., Ruggeri, Z. M. & Moake, J. L. Endothelial cell ADAMTS-13 and VWF: production, release, and VWF string cleavage. *Blood* **114**, 5102–5111 (2009).
25. Turner, N., Nolasco, L., Dong, J.-F. & Moake, J. ADAMTS-13 cleaves long von Willebrand factor multimeric strings anchored to endothelial cells in the absence of flow, platelets or conformation-altering chemicals. *J. Thromb. Haemost.* **7**, 229–232 (2009).
26. Sins, J. W. R. *et al.* Dynamics of von Willebrand factor reactivity in sickle cell disease during vaso-occlusive crisis and steady state. *J. Thromb. Haemost.* **15**, 1392–1402 (2017).
27. Carter, A. M., Catto, A. J., Mansfield, M. W., Bamford, J. M. & Grant, P. J. Predictive variables for mortality after acute ischemic stroke. *Stroke* **38**, 1873–80 (2007).
28. Furlan, M. *et al.* Deficient Activity of von Willebrand Factor-Cleaving Protease in Chronic Relapsing Thrombotic Thrombocytopenic Purpura. *Blood* **89**, 3097–3103 (1997).
29. Vilahur, G., Padro, T. & Badimon, L. Atherosclerosis and thrombosis: Insights from large animal models. *J. Biomed. Biotechnol.* **2011**, (2011).
30. Westrick, R. J., Winn, M. E. & Eitzman, D. T. Murine Models of Vascular Thrombosis. *Arterioscler. Thromb. Vasc. Biol.* **27**, (2007).
31. Palmer, O. R. *et al.* Update on the electrolytic IVC model for pre-clinical studies of venous thrombosis. *Res. Pract. Thromb. Haemost.* **2**, 266–273 (2018).
32. Diaz, J. A. *et al.* The electrolytic inferior vena cava model (EIM) to study thrombogenesis and thrombus resolution with continuous blood flow in the mouse. *Thromb. Haemost.* **109**, 1158–69 (2013).
33. Meng, H. *et al.* In Vivo Role of Neutrophil Extracellular Traps in Antiphospholipid Antibody-Mediated Venous Thrombosis. *Arthritis Rheumatol. (Hoboken, N.J.)* **69**, 655–667 (2017).
34. Yadav, V. *et al.* Ectonucleotidase tri(di)phosphohydrolase-1 (ENTPD-1) disrupts inflammasome/interleukin 1β-driven venous thrombosis. *J. Clin. Invest.* (2019) doi:10.1172/JCI124804.
35. Watson, B. D., Dietrich, W. D., Busto, R., Wachtel, M. S. & Ginsberg, M. D. Induction of reproducible brain infarction by photochemically initiated thrombosis. *Ann. Neurol.* **17**, 497–504 (1985).
36. Adili, R. & Holinstat, M. Formation and Resolution of Pial Microvascular Thrombosis in a Mouse Model of Thrombotic Thrombocytopenic Purpura. *Arterioscler. Thromb. Vasc. Biol.* **39**, 1817–1830 (2019).

37. Schmitt, A., Guichard, J., Massé, J. M., Debili, N. & Cramer, E. M. Of mice and men: Comparison of the ultrastructure of megakaryocytes and platelets. *Exp. Hematol.* **29**, 1295–1302 (2001).
38. Ware, J. Dysfunctional platelet membrane receptors: From humans to mice. *Thromb. Haemost.* **92**, 478–485 (2004).
39. Gupta, R. *et al.* Protease-Activated Receptor Antagonist for Reducing Cardiovascular Events – A Review on Vorapaxar. *Curr. Probl. Cardiol.* 101035 (2021) doi:10.1016/J.CPCARDIOL.2021.101035.
40. An, X., Schulz, V. P., Mohandas, N. & Gallagher, P. G. Human and murine erythropoiesis. *Curr. Opin. Hematol.* **22**, 206 (2015).
41. Mestas, J. & Hughes, C. C. W. Mouse and Human Immunology Of Mice and Not Men: Differences between Downloaded from. *J Immunol J. Immunol. Mirand Libr.* **172**, 2731–2738 (2004).
42. Cooley, B. C. Murine models of thrombosis. *Thromb. Res.* **129**, S62–S64 (2012).
43. Myers, D. D. Nonhuman primate models of thrombosis. *Thromb. Res.* **129**, S65–S69 (2012).
44. Pound, P., Ebrahim, S., Sandercock, P., Bracken, M. B. & Roberts, I. Where is the evidence that animal research benefits humans? *British Medical Journal* vol. 328 514–517 (2004).
45. Akhtar, A. The Flaws and Human Harms of Animal Experimentation. *Cambridge Q. Healthc. Ethics* **24**, 407–419 (2015).
46. Fenwick, N., Griffin, G. & Gauthier, C. The welfare of animals used in science: How the "Three Rs" ethic guides improvements. *Can. Vet. J.* **50**, 523 (2009).
47. Mangin, P. H. *et al.* In vitro flow-based assay: From simple toward more sophisticated models for mimicking hemostasis and thrombosis. *J. Thromb. Haemost.* **19**, 582–587 (2021).
48. Neeves, K. B. *et al.* Sources of Variability in Platelet Accumulation on Type 1 Fibrillar Collagen in Microfluidic Flow Assays. *PLoS One* **8**, 54680 (2013).
49. Bark, D. L., Para, A. N. & Ku, D. N. Correlation of thrombosis growth rate to pathological wall shear rate during platelet accumulation. *Biotechnol. Bioeng.* **109**, 2642–2650 (2012).
50. Chen, Z. *et al.* Device-induced platelet dysfunction in mechanically assisted circulation increases the risks of thrombosis and bleeding. *Artif. Organs* **43**, 745–755 (2019).
51. De Witt, S. M. *et al.* Identification of platelet function defects by multi-parameter assessment of thrombus formation. *Nat. Commun.* **5**, 1–13 (2014).
52. Gutierrez, E. *et al.* Microfluidic devices for studies of shear-dependent platelet adhesion. *Lab Chip* **8**, 1486–1495 (2008).
53. Barstad, R. M., Roald, H. E., Cui, Y., Turitto, V. T. & Sakariassen, K. S. A perfusion chamber developed to investigate thrombus formation and shear profiles in flowing native human blood at the apex of well-defined stenoses. *Arterioscler. Thromb. A J. Vasc. Biol.* **14**, 1984–1991 (1994).
54. Chen, H. *et al.* Hematocrit and flow rate regulate the adhesion of platelets to von Willebrand factor. *Biomicrofluidics* **7**, 64113 (2013).
55. Schoeman, R. M., Lehmann, M. & Neeves, K. B. Flow chamber and microfluidic approaches for measuring thrombus formation in genetic bleeding disorders. *Platelets* vol. 28 463–471 (2017).
56. Coenen, D. M., Mastenbroek, T. G. & Cosemans, J. M. E. M. Platelet interaction with

activated endothelium: Mechanistic insights from microfluidics. *Blood* vol. 130 2819–2828 (2017).
57. Zilberman-Rudenko, J. *et al.* Utility of microfluidic devices to study the platelet–endothelium interface. *Platelets* vol. 28 449–456 (2017).
58. Loessberg-Zahl, J., Beumer, J., Berg, A. van den, Eijkel, J. C. T. & Meer, A. D. van der. Patterning Biological Gels for 3D Cell Culture inside Microfluidic Devices by Local Surface Modification through Laminar Flow Patterning. *Micromachines 2020, Vol. 11, Page 1112* **11**, 1112 (2020).
59. Dijk, C. G. M. van *et al.* A new microfluidic model that allows monitoring of complex vascular structures and cell interactions in a 3D biological matrix. *Lab Chip* **20**, 1827–1844 (2020).
60. Engelmann, B. & Massberg, S. Thrombosis as an intravascular effector of innate immunity. *Nat. Rev. Immunol. 2012 131* **13**, 34–45 (2012).
61. Li, J., Kim, K., Barazia, A., Tseng, A. & Cho, J. Platelet-neutrophil interactions under thromboinflammatory conditions. *Cellular and Molecular Life Sciences* vol. 72 2627–2643 (2015).
62. von Brühl, M.-L. *et al.* Monocytes, neutrophils, and platelets cooperate to initiate and propagate venous thrombosis in mice in vivo. *J. Exp. Med.* **209**, 819–35 (2012).
63. Puhr-Westerheide, D. *et al.* Neutrophils promote venular thrombosis by shaping the rheological environment for platelet aggregation. *Sci. Rep.* **9**, 1–13 (2019).
64. Lisman, T. Platelet–neutrophil interactions as drivers of inflammatory and thrombotic disease. *Cell and Tissue Research* vol. 371 567–576 (2018).
65. Davì, G. & Patrono, C. Platelet Activation and Atherothrombosis. *N. Engl. J. Med.* **357**, 2482–2494 (2007).
66. del Zoppo, G. J. The role of platelets in ischemic stroke. *Neurology* **51**, S9–S14 (1998).
67. Huo, Y. & Ley, K. F. Role of Platelets in the Development of Atherosclerosis. *Trends Cardiovasc. Med.* **14**, 18–22 (2004).
68. McFadyen, J. D. & Kaplan, Z. S. Platelets are not just for clots. *Transfusion Medicine Reviews* vol. 29 110–119 (2015).
69. Ruggeri, Z. M. Platelets in atherothrombosis. *Nat. Med.* **8**, 1227–1234 (2002).
70. Yap, M. L. *et al.* Targeting Activated Platelets: A Unique and Potentially Universal Approach for Cancer Imaging. *Theranostics* **7**, 2565–2574 (2017).
71. Rossaint, J., Margraf, A. & Zarbock, A. Role of platelets in leukocyte recruitment and resolution of inflammation. *Frontiers in Immunology* vol. 9 2712 (2018).
72. Iba, T. & Levy, J. H. Inflammation and thrombosis: roles of neutrophils, platelets and endothelial cells and their interactions in thrombus formation during sepsis. *J. Thromb. Haemost.* (2017) doi:10.1111/jth.13911.
73. Vogel, S. & Thein, S. L. Platelets at the crossroads of thrombosis, inflammation and haemolysis. *Br. J. Haematol.* **180**, 761–767 (2018).
74. Zhang, D., Xu, C., Manwani, D. & Frenette, P. S. Neutrophils, platelets, and inflammatory pathways at the nexus of sickle cell disease pathophysiology. *Blood* **127**, 801–9 (2016).
75. Taus, F. *et al.* Platelets Promote Thromboinflammation in SARS-CoV-2 Pneumonia. *Arterioscler. Thromb. Vasc. Biol.* **40**, 2975 (2020).
76. Bombeli, T., Schwartz, B. R. & Harlan, J. M. Adhesion of Activated Platelets to Endothelial Cells: Evidence for a GPIIbIIIa-dependent Bridging Mechanism and Novel Roles for Endothelial Intercellular Adhesion Molecule 1 (ICAM-1), αvβ3 Integrin, and

GPIbα. *J. Exp. Med.* **187**, 329–339 (1998).
77. Thomas, M. R. & Storey, R. F. The role of platelets in inflammation. *Thromb. Haemost.* **114**, 449–458 (2015).
78. Schattner, M., Jenne, C. N., Negrotto, S. & Ho-Tin-Noe, B. Editorial: Platelets and Immune Responses During Thromboinflammation. *Front. Immunol.* **11**, 1079 (2020).
79. Swystun, L. L. & Liaw, P. C. The role of leukocytes in thrombosis. *Blood* vol. 128 753–762 (2016).
80. Ortel, T. L. *et al.* American Society of Hematology 2020 guidelines for management of venous thromboembolism: treatment of deep vein thrombosis and pulmonary embolism. *Blood Adv.* **4**, 4693–4738 (2020).
81. Jackson, S. P. Arterial thrombosis—insidious, unpredictable and deadly. *Nat. Med. 2011 1711* **17**, 1423–1436 (2011).
82. Barnes, P. J. How corticosteroids control inflammation: Quintiles Prize Lecture 2005. *Br. J. Pharmacol.* **148**, 245–254 (2006).
83. Tabas, I. & Glass, C. K. Anti-Inflammatory Therapy in Chronic Disease: Challenges and Opportunities. *Science (80-.).* **339**, 172 (2013).
84. Vane, J. R. & Botting, R. M. Anti-inflammatory drugs and their mechanism of action. *Inflamm. Res. 1998 472* **47**, 78–87 (1998).
85. Marques, M. B. Thrombotic Thrombocytopenic Purpura and Heparin-Induced Thrombocytopenia: Two Unique Causes of Life-Threatening Thrombocytopenia. *Clin. Lab. Med.* **29**, 321–338 (2009).
86. Wallentin, L. *et al.* Ticagrelor versus Clopidogrel in Patients with Acute Coronary Syndromes. *N. Engl. J. Med.* **361**, 1045–1057 (2009).
87. Bienvenu, J.-G. *et al.* Recombinant Soluble P-Selectin Glycoprotein Ligand-1-Ig Reduces Restenosis Through Inhibition of Platelet-Neutrophil Adhesion After Double Angioplasty in Swine. *Circulation* **103**, 1128–1134 (2001).
88. Phillips, J. W. *et al.* Single injection of P-selectin or P-selectin glycoprotein ligand-1 monoclonal antibody blocks neointima formation after arterial injury in apolipoprotein E-deficient mice. *Circulation* **107**, 2244–9 (2003).
89. Mertens, P. *et al.* Recombinant P-selectin glycoprotein ligand-immunoglobulin, a P-selectin antagonist, as an adjunct to thrombolysis in acute myocardial infarction. The P-Selectin Antagonist Limiting Myonecrosis (PSALM) trial. *Am. Heart J.* **152**, 125.e1-125.e8 (2006).
90. Tanguay, J.-F. *et al.* Efficacy of a novel P-selectin antagonist, rPSGL-Ig for reperfusion therapy in acute myocardial infarction: The RAPSODY trial. *J. Am. Coll. Cardiol.* **41**, 404–405 (2003).
91. Tardif, J. C. *et al.* Effects of the P-selectin antagonist inclacumab on myocardial damage after percutaneous coronary intervention for non-st-segment elevation myocardial infarction: Results of the SELECT-ACS trial. *J. Am. Coll. Cardiol.* **61**, 2048–2055 (2013).
92. Stähli, B. E. *et al.* Effects of P-selectin antagonist inclacumab in patients undergoing coronary artery bypass graft surgery: SELECT-CABG trial. *J. Am. Coll. Cardiol.* **67**, 344–346 (2016).
93. Diaz, J. A. *et al.* P-selectin inhibition therapeutically promotes thrombus resolution and prevents vein wall fibrosis better than enoxaparin and an inhibitor to von Willebrand factor. *Arterioscler. Thromb. Vasc. Biol.* **35**, 829–37 (2015).
94. Kato, G. J. *et al.* Sickle cell disease. *Nat. Rev. Dis. Prim.* **4**, 18010 (2018).

95. Piel, F. B., Steinberg, M. H. & Rees, D. C. Sickle Cell Disease. *N. Engl. J. Med.* **376**, 1561–1573 (2017).
96. Platt, O. S. *et al.* Mortality In Sickle Cell Disease -- Life Expectancy and Risk Factors for Early Death. *N. Engl. J. Med.* **330**, 1639–1644 (1994).
97. Vichinsky, E. P. *et al.* Causes and Outcomes of the Acute Chest Syndrome in Sickle Cell Disease. *N. Engl. J. Med.* **342**, 1855–1865 (2000).
98. Rahimi, Z. & Parsian, A. Sickle cell disease and venous thromboembolism. *Mediterr. J. Hematol. Infect. Dis.* **3**, e2011024 (2011).
99. Naik, R. P. *et al.* Venous thromboembolism in adults with sickle cell disease: a serious and under-recognized complication. *Am. J. Med.* **126**, 443–9 (2013).
100. Austin, H. *et al.* Sickle cell trait and the risk of venous thromboembolism among blacks. *Blood* **110**, 908–12 (2007).
101. Webb, J. & Kwiatkowski, J. L. Stroke in patients with sickle cell disease. *Expert Rev. Hematol.* **6**, 301–316 (2013).
102. Switzer, J. A., Hess, D. C., Nichols, F. T. & Adams, R. J. Pathophysiology and treatment of stroke in sickle-cell disease: present and future. *Lancet Neurol.* **5**, 501–512 (2006).
103. Talahma, M., Strbian, D. & Sundararajan, S. Sickle Cell Disease and Stroke. *Stroke* **45**, (2014).
104. Fitzhugh, C. *et al.* Cardiopulmonary complications leading to premature deaths in adult patients with sickle cell disease. *Am. J. Hematol.* **85**, 36–40 (2010).
105. Martin, C. R., Johnson, C. S., Cobb, C., Tatter, D. & Haywood, L. J. Myocardial infarction in sickle cell disease. *J. Natl. Med. Assoc.* **88**, 428–32 (1996).
106. Charache, S. *et al.* Effect of Hydroxyurea on the Frequency of Painful Crises in Sickle Cell Anemia. *N. Engl. J. Med.* **332**, 1317–1322 (1995).
107. Agrawal, R. K., Patel, R. K., shah, V., Nainiwal, L. & Trivedi, B. Hydroxyurea in Sickle Cell Disease: Drug Review. *Indian J. Hematol. Blood Transfus.* **30**, 91 (2014).
108. Thornburg, C. D. *et al.* Impact of hydroxyurea on clinical events in the BABY HUG trial. *Blood* **120**, 4304–4310 (2012).
109. Brawley, O. W. *et al.* National Institutes of Health Consensus Development Conference Statement: Hydroxyurea Treatment for Sickle Cell Disease. *Ann. Intern. Med.* **148**, 932 (2008).
110. Ribeil, J.-A. A Study Evaluating the Safety and Efficacy of the LentiGlobin BB305 Drug Product in Severe Sickle Cell Disease. *Clinical Trials* https://clinicaltrials.gov/ct2/show/study/NCT02140554#contacts (2018).
111. A Safety and Efficacy Study Evaluating CTX001 in Subjects With Severe Sickle Cell Disease. https://clinicaltrials.gov/ct2/show/NCT03745287?term=CRISPR&cond=Sickle+Cell+Disease&rank=2#contacts (2019).
112. Howard, J. Sickle cell disease: when and how to transfuse. *Hematology* **2016**, 625–631 (2016).
113. Chou, S. T. & Fasano, R. M. Management of Patients with Sickle Cell Disease Using Transfusion Therapy. *Hematol. Oncol. Clin. North Am.* **30**, 591–608 (2016).
114. Wun, T. *et al.* Platelet activation and platelet-erythrocyte aggregates in patients with sickle cell anemia. *J. Lab. Clin. Med.* **129**, 507–516 (1997).
115. Wun, T. *et al.* Platelet activation in patients with sickle cell disease. *Br. J. Haematol.* **100**, 741–749 (1998).

116. Papadimitriou, C. A., Travlou, A., Kalos, A., Douratsos, D. & Lalï, P. Study of Platelet Function in Patients with Sickle Cell Anemia during Steady State and Vaso-Occlusive Crisis. *Acta Haematol.* **89**, 180–183 (1993).
117. Proença-Ferreira, R. *et al.* Increased adhesive properties of platelets in sickle cell disease: roles for αIIbβ3-mediated ligand binding, diminished cAMP signalling and increased phosphodiesterase 3A activity. *Br. J. Haematol.* **149**, 280–288 (2010).
118. Proença-Ferreira, R. *et al.* Endothelial Activation by Platelets from Sickle Cell Anemia Patients. *PLoS One* **9**, e89012 (2014).
119. Rouzet, F. *et al.* Radiolabeled fucoidan as a p-selectin targeting agent for in vivo imaging of platelet-rich thrombus and endothelial activation. *J. Nucl. Med.* **52**, 1433–40 (2011).
120. Gunawan, S. T. *et al.* Multifunctional Thrombin-Activatable Polymer Capsules for Specifi c Targeting to Activated Platelets. 5153–5157 (2015) doi:10.1002/adma.201502243.
121. Pawlowski, C. L. *et al.* Platelet microparticle-inspired clot-responsive nanomedicine for targeted fibrinolysis. *Biomaterials* **128**, 94–108 (2017).
122. Hansen, C. E. *et al.* Platelet–Microcapsule Hybrids Leverage Contractile Force for Targeted Delivery of Hemostatic Agents. *ACS Nano* **11**, 5579–5589 (2017).
123. Anselmo, A. C. *et al.* Platelet-like Nanoparticles: Mimicking Shape, Flexibility, and Surface Biology of Platelets To Target Vascular Injuries. *ACS Nano* **8**, 11243–11253 (2014).
124. Brown, A. C. *et al.* Ultrasoft microgels displaying emergent platelet-like behaviours. *Nat. Mater.* **13**, 1108–1114 (2014).
125. Ravikumar, M., Modery, C. L., Wong, T. L. & Sen Gupta, A. Peptide-Decorated Liposomes Promote Arrest and Aggregation of Activated Platelets under Flow on Vascular Injury Relevant Protein Surfaces in Vitro. *Biomacromolecules* **13**, 1495–1502 (2012).
126. Girish, A. *et al.* Trauma-targeted delivery of tranexamic acid improves hemostasis and survival in rat liver hemorrhage model. *J. Thromb. Haemost.* **17**, 1632–1644 (2019).
127. Hickman, D. A. *et al.* Intravenous synthetic platelet (SynthoPlate) nanoconstructs reduce bleeding and improve 'golden hour' survival in a porcine model of traumatic arterial hemorrhage. *Sci. Rep.* **8**, 3118 (2018).
128. Chistiakov, D. A., Bobryshev, Y. V & Orekhov, A. N. Neutrophil's weapons in atherosclerosis. *Exp. Mol. Pathol.* **99**, 663–71 (2015).
129. Qi, H., Yang, S. & Zhang, L. Neutrophil Extracellular Traps and Endothelial Dysfunction in Atherosclerosis and Thrombosis. *Front. Immunol.* **8**, 928 (2017).
130. Sørensen, O. E. & Borregaard, N. Neutrophil extracellular traps — the dark side of neutrophils. *J. Clin. Invest.* **126**, 1612–1620 (2016).
131. Grommes, J. & Soehnlein, O. Contribution of Neutrophils to Acute Lung Injury. *Mol. Med.* **17**, 293–307 (2011).
132. Gollomp, K. *et al.* Neutrophil accumulation and NET release contribute to thrombosis in HIT. *JCI Insight* **3**, (2018).
133. Liu, M. *et al.* Influence of Dose on Neutrophil-Mediated Delivery of Nanoparticles for Tumor-Targeting Therapy Strategies. *AAPS PharmSciTech* **22**, 1–16 (2021).
134. Wang, S. *et al.* Sialic Acid Conjugate–Modified Liposomal Dexamethasone Palmitate Targeting Neutrophils for Rheumatoid Arthritis Therapy: Influence of Particle Size. *AAPS PharmSciTech* **22**, 1–18 (2021).
135. Lin, H. *et al.* Novel Combined Preparation and Investigation of Bergenin-Loaded

Albumin Nanoparticles for the Treatment of Acute Lung Injury: In Vitro and In Vivo Evaluations. *Inflammation* 1–17 (2021) doi:10.1007/S10753-021-01556-2/FIGURES/13.
136. Fromen, C. A. *et al.* Neutrophil–Particle Interactions in Blood Circulation Drive Particle Clearance and Alter Neutrophil Responses in Acute Inflammation. *ACS Nano* **11**, 10797–10807 (2017).
137. Brannon, E. R. *et al.* Polysalicylic Acid Polymer Microparticle Decoys Therapeutically Treat Acute Respiratory Distress Syndrome. *Adv. Healthc. Mater.* 2101534 (2021) doi:10.1002/ADHM.202101534.
138. Getts, D. R. *et al.* Therapeutic Inflammatory Monocyte Modulation Using Immune-Modifying Microparticles. *Sci. Transl. Med.* **6**, 219ra7 (2014).
139. Kelley, W. J., Onyskiw, P. J., Fromen, C. A. & Eniola-Adefeso, O. Model Particulate Drug Carriers Modulate Leukocyte Adhesion in Human Blood Flows. *ACS Biomater. Sci. Eng.* **5**, 6530–6540 (2019).
140. Schulz, C., Engelmann, B. & Massberg, S. Crossroads of coagulation and innate immunity: the case of deep vein thrombosis. *J. Thromb. Haemost.* **11**, 233–241 (2013).
141. Park, J. *et al.* Intravascular innate immune cells reprogrammed via intravenous nanoparticles to promote functional recovery after spinal cord injury. *Proc. Natl. Acad. Sci. U. S. A.* **116**, 14947–14954 (2019).
142. Haraldsen, G., Kvale, D., Lien, B., Farstad, I. N. & Brandtzaeg, P. Cytokine-Regulated Expression of E-Selectin, Intercellular Adhesion Molecule-1 (ICAM-1), and Vascular Cell Adhesion Molecule-1 (VCAM-1) in Human Intestinal Microvascular Endothelial Cells. *J. Immunol.* **156**, 2558–2565 (1996).
143. Charoenphol, P., Huang, R. B. & Eniola-Adefeso, O. Potential role of size and hemodynamics in the efficacy of vascular-targeted spherical drug carriers. *Biomaterials* **31**, 1392–1402 (2010).
144. Charoenphol, P. *et al.* Targeting therapeutics to the vascular wall in atherosclerosis–Carrier size matters. *Atherosclerosis* **217**, 364–370 (2011).
145. Fromen, C. A. *et al.* Evaluation of Receptor-Ligand Mechanisms of Dual-Targeted Particles to an Inflamed Endothelium. *Bioeng. Transl. Med.* **1**, 103–115 (2016).
146. Thompson, A. J., Mastria, E. M. & Eniola-Adefeso, O. The margination propensity of ellipsoidal micro/nanoparticles to the endothelium in human blood flow. *Biomaterials* **34**, 5863–71 (2013).
147. Safari, H., Adili, R., Holinstat, M. & Eniola-Adefeso, O. Modified two-step emulsion solvent evaporation technique for fabricating biodegradable rod-shaped particles in the submicron size range. *J. Colloid Interface Sci.* **518**, 174–183 (2018).
148. Thompson, A. J. & Eniola-Adefeso, O. Dense nanoparticles exhibit enhanced vascular wall targeting over neutrally buoyant nanoparticles in human blood flow. *Acta Biomater.* **21**, 99–108 (2015).
149. Fish, M. B. *et al.* Exploring deformable particles in vascular-targeted drug delivery: Softer is only sometimes better. *Biomaterials* **124**, 169–179 (2017).
150. Fish, M. B. *et al.* Deformable microparticles for shuttling nanoparticles to the vascular wall. *Sci. Adv.* **7**, eabe0143 (2021).
151. Kelley, W. J., Fromen, C. A., Lopez-Cazares, G. & Eniola-Adefeso, O. PEGylation of model drug carriers enhances phagocytosis by primary human neutrophils. *Acta Biomater.* **79**, 283–293 (2018).
152. Perry, J. L. *et al.* PEGylated PRINT Nanoparticles: The Impact of PEG Density on Protein

Binding, Macrophage Association, Biodistribution, and Pharmacokinetics. *Nano Lett.* **12**, 5304–5310 (2012).
153. Gutierrez, M. *et al.* Characterizing bulk rigidity of rigid red blood cell populations in sickle-cell disease patients. *Sci. Reports 2021 111* **11**, 1–10 (2021).
154. Huang, A. J. *et al.* Effects of human neutrophil chemotaxis across human endothelial cell monolayers on the permeability of these monolayers to ions and macromolecules. *J. Cell. Physiol.* **135**, 355–366 (1988).
155. Huang, R. B. & Eniola-Adefeso, O. Shear stress modulation of IL-1β-induced E-selectin expression in human endothelial cells. *PLoS One* **7**, e31874 (2012).
156. Walton, B. L. *et al.* Elevated hematocrit enhances platelet accumulation following vascular injury. *Blood* **129**, 2537–2546 (2017).
157. Sibbing, D. *et al.* Assessment of ADP-induced platelet aggregation with light transmission aggregometry and multiple electrode platelet aggregometry before and after clopidogrel treatment. *Thromb. Haemost.* **99**, 121–126 (2017).
158. Gurbel, P. A., Bliden, K. P., Etherington, A. & Tantry, U. S. Assessment of clopidogrel responsiveness: Measurements of maximum platelet aggregation, final platelet aggregation and their correlation with vasodilator-stimulated phosphoprotein in resistant patients. *Thromb. Res.* **121**, 107–115 (2007).
159. Lecka, J., Rana, M. S. & Sévigny, J. Inhibition of vascular ectonucleotidase activities by the pro-drugs ticlopidine and clopidogrel favours platelet aggregation. *Br. J. Pharmacol.* **161**, 1150–1160 (2010).
160. Lu, Y. *et al.* Inhibitory effect of caffeic acid on ADP-induced thrombus formation and platelet activation involves mitogen-activated protein kinases. *Sci. Reports 2015 51* **5**, 1–13 (2015).
161. Gutierrez, M., Ojeda, L. S. & Eniola-Adefeso, O. Vascular-targeted particle binding efficacy in the presence of rigid red blood cells: Implications for performance in diseased blood. *Biomicrofluidics* **12**, 042217 (2018).
162. Gutierrez, M., Fish, M. B., Golinski, A. W. & Eniola-Adefeso, O. Presence of Rigid Red Blood Cells in Blood Flow Interferes with the Vascular Wall Adhesion of Leukocytes. *Langmuir* **34**, 2363–2372 (2018).
163. Shamseddin, A. *et al.* Resveratrol-Linoleate protects from exacerbated endothelial permeability via a drastic inhibition of the MMP-9 activity. *Biosci. Rep.* **38**, (2018).
164. Rumbaut, R. E. *et al.* Endotoxin enhances microvascular thrombosis in mouse cremaster venules via a TLR4-dependent, neutrophil-independent mechanism. *Am J Physiol Hear. Circ Physiol* **290**, 1671–1679 (2006).
165. Cerwinka, W. H. *et al.* Superoxide mediates endotoxin-induced platelet-endothelial cell adhesion in intestinal venules. *Am. J. Physiol. - Hear. Circ. Physiol.* **284**, 535–541 (2003).
166. Reheman, A., Tasneem, S., Ni, H. & Hayward, C. P. M. Mice with deleted multimerin 1 and α-synuclein genes have impaired platelet adhesion and impaired thrombus formation that is corrected by multimerin 1. *Thromb. Res.* **125**, e177–e183 (2010).
167. Yau, J. W., Teoh, H. & Verma, S. Endothelial cell control of thrombosis. *BMC Cardiovasc. Disord.* **15**, 130 (2015).
168. Reiner, M. F. *et al.* Ticagrelor, but not clopidogrel, reduces arterial thrombosis via endothelial tissue factor suppression. *Cardiovasc. Res.* **113**, 61–69 (2017).
169. Lin, P.-Y. *et al.* The inhibition in tumor necrosis factor-α-induced attenuation in endothelial thrombomodulin expression by carvedilol is mediated by nuclear factor-κB

and reactive oxygen species. *J. Thromb. Thrombolysis* **29**, 52–59 (2010).
170. Xiang, Y. & Hwa, J. Regulation of VWF expression, and secretion in health and disease. *Current Opinion in Hematology* vol. 23 288–293 (2016).
171. Sonneveld, M. A. H. *et al.* Low ADAMTS-13 activity and the risk of coronary heart disease - a prospective cohort study: the Rotterdam Study. *J. Thromb. Haemost.* **14**, 2114–2120 (2016).
172. Sonneveld, M. A. H. *et al.* Low ADAMTS13 activity is associated with an increased risk of ischemic stroke. *Blood* **126**, 2739–2746 (2015).
173. Kopić, A. *et al.* Preclinical assessment of a new recombinant ADAMTS-13 drug product (BAX930) for the treatment of thrombotic thrombocytopenic purpura. *J. Thromb. Haemost.* **14**, 1410–1419 (2016).
174. Brouns, S. L. N., Provenzale, I., Geffen, J. P. van, Meijden, P. E. J. van der & Heemskerk, J. W. M. Localized endothelial-based control of platelet aggregation and coagulation under flow: A proof-of-principle vessel-on-a-chip study. *J. Thromb. Haemost.* **18**, 931–941 (2020).
175. Polanowska-Grabowska, R. *et al.* P-selectin-mediated platelet-neutrophil aggregate formation activates neutrophils in mouse and human sickle cell disease. *Arterioscler. Thromb. Vasc. Biol.* (2010) doi:10.1161/ATVBAHA.110.211615.
176. Joncour, A. Le *et al.* Neutrophil–Platelet and Monocyte–Platelet Aggregates in COVID-19 Patients. *Thromb. Haemost.* **120**, 1733–1735 (2020).
177. Cleator, J. H., Zhu, W. Q., Vaughan, D. E. & Hamm, H. E. Differential regulation of endothelial exocytosis of P-selectin and von Willebrand factor by protease-activated receptors and cAMP. *Blood* **107**, 2736–2744 (2006).
178. Panteleev, M. A. *et al.* Wall shear rates in human and mouse arteries: Standardization of hemodynamics for in vitro blood flow assays: Communication from the ISTH SSC subcommittee on biorheology. *J. Thromb. Haemost.* **19**, 588–595 (2021).
179. Jackson, S. P., Nesbitt, W. S. & Westein, E. Dynamics of platelet thrombus formation. *J. Thromb. Haemost.* **7**, 17–20 (2009).
180. Dong, J. *et al.* ADAMTS-13 rapidly cleaves newly secreted ultralarge von Willebrand factor multimers on the endothelial surface under flowing conditions. *Blood* **100**, 4033–4039 (2002).
181. Kawahara, J., Ishikawa, K., Uchimaru, T. & Takaya, H. Chemical Cross-Linking by Glutaraldehyde between Amino Groups: Its Mechanism and Effects. in *Polymer Modification* (eds. Swift, G., Carraher, C. E. & Bowman, C. N.) 119–131 (Springer, 1997). doi:10.1007/978-1-4899-1477-4_11.
182. Nylander, S. *et al.* Ticagrelor inhibits human platelet aggregation via adenosine in addition to P2Y12 antagonism. *J. Thromb. Haemost.* **11**, 1867–1876 (2013).
183. Kogan, T. P. *et al.* Novel synthetic inhibitors of selectin-mediated cell adhesion: Synthesis of 1,6-bis[3-(3-carboxymethylphenyl)-4-(2-α-D-mannopyranosyloxy)phenyl] hexane (TBC1269). *J. Med. Chem.* **41**, 1099–1111 (1998).
184. Hicks, A. E. R. *et al.* The anti-inflammatory effects of a selectin ligand mimetic, TBC-1269, are not a result of competitive inhibition of leukocyte rolling in vivo. *J. Leukoc. Biol.* **77**, 59–66 (2005).
185. Ramos-Kelly, J. R. *et al.* Multiple Selectin Blockade with a Small Molecule Inhibitor Downregulates Liver Chemokine Expression and Neutrophil Infiltration after Hemorrhagic Shock. *J. Trauma Inj. Infect. Crit. Care* **49**, 92–100 (2000).

186. Watz, H. *et al.* Inhaled pan-selectin antagonist Bimosiamose attenuates airway inflammation in COPD. *Pulm. Pharmacol. Ther.* **26**, 265–270 (2013).
187. Kirsten, A. *et al.* Efficacy of the pan-selectin antagonist Bimosiamose on ozone-induced airway inflammation in healthy subjects - A double blind, randomized, placebo-controlled, cross-over clinical trial. *Pulm. Pharmacol. Ther.* **24**, 555–558 (2011).
188. Takeuchi, Y. *et al.* Effects of histamine 2 receptor antagonists on endothelial-neutrophil adhesion and surface expression of endothelial adhesion molecules induced by high glucose levels. *J. Diabetes Complications* **21**, 50–55 (2007).
189. Pantziarka, P., Bouche, G., Meheus, L., Sukhatme, V. & Sukhatme, V. P. Repurposing drugs in oncology (ReDo)-cimetidine as an anti-cancer agent. *Ecancermedicalscience* **8**, (2014).
190. Kobayashi, K.-I., Matsumoto, S., Morishima, T., Kawabe, T. & Okamoto, T. Cimetidine Inhibits Cancer Cell Adhesion to Endothelial Cells and Prevents Metastasis by Blocking E-selectin Expression 1. *CANCER Res.* **60**, 3978–3984 (2000).
191. Finsterbusch, M., Schrottmaier, W. C., Kral-Pointner, J. B., Salzmann, M. & Assinger, A. Measuring and interpreting platelet-leukocyte aggregates. *Platelets* **29**, 677 (2018).
192. Mussbacher, M. *et al.* Cell type specific roles of NF-kB linking inflamation and thrombosis. *Front. Immunol.* **10**, (2019).
193. Shahid, M. *et al.* Histamine, Histamine Receptors, and their Role in Immunomodulation: An Updated Systematic Review. *Open Immunol. J.* **2**, 9–41 (2009).
194. Williams, M. R. *et al.* Gene expression of endothelial cells due to interleukin-1 beta stimulation and neutrophil transmigration. *Endothel. J. Endothel. Cell Res.* **15**, 73–84 (2008).
195. Dobesh, P. P. & Oestreich, J. H. Ticagrelor: Pharmacokinetics, Pharmacodynamics, Clinical Efficacy, and Safety. *Pharmacotherapy* **34**, 1077 (2014).
196. Nakamura, K. *et al.* Inhibitory effects of H2-receptor antagonists on platelet function in vitro. *Hum. Exp. Toxicol.* **18**, 487–492 (1999).
197. Gulcan, M., Varol, E., Etli, M., Aksoy, F. & Kayan, M. Mean Platelet Volume Is Increased in Patients With Deep Vein Thrombosis. *Clin. Appl. Thromb.* **18**, 427–430 (2012).
198. Montoro-García, S., Schindewolf, M., Stanford, S., Larsen, O. H. & Thiele, T. The role of platelets in venous thromboembolism. *Semin. Thromb. Hemost.* **42**, 242–251 (2016).
199. Silvain, J. *et al.* Composition of coronary thrombus in acute myocardial infarction. *J. Am. Coll. Cardiol.* **57**, 1359–1367 (2011).
200. Abu El-Makrem, M. A. *et al.* The role of platelets CD40 ligand (CD154) in acute coronary syndromes. *Thromb. Res.* **124**, 683–688 (2009).
201. Stavik, B. *et al.* EPAS1/HIF-2 alpha-mediated downregulation of tissue factor pathway inhibitor leads to a pro-thrombotic potential in endothelial cells. *Biochim. Biophys. Acta - Mol. Basis Dis.* **1862**, 670–678 (2016).
202. Marcus, A. J. *et al.* The endothelial cell ecto-ADPase responsible for inhibition of platelet function is CD39. *J. Clin. Invest.* **99**, 1351–1360 (1997).
203. McCormack, J. J., da Silva, M. L., Ferraro, F., Patella, F. & Cutler, D. F. Weibel-Palade bodies at a glance. *J. Cell Sci.* **130**, 3611–3617 (2017).
204. Kieffer, J. D. *et al.* Neutrophils, monocytes, and dendritic cells express the same specialized form of PSGL-1 as do skin-homing memory t cells: Cutaneous lymphocyte antigen. *Biochem. Biophys. Res. Commun.* **285**, 577–587 (2001).

205. Frenette, P. S. *et al.* P-selectin glycoprotein ligand 1 (PSGL-1) is expressed on platelets and can mediate platelet-endothelial interactions in vivo. *J. Exp. Med.* **191**, 1413–1422 (2000).
206. Butenas, S., Bouchard, B. A., Brummel-Ziedins, K. E., Parhami-Seren, B. & Mann, K. G. Tissue factor activity in whole blood. *Blood* **105**, 2764–2770 (2005).
207. Owens, A. P. & MacKman, N. Sources of tissue factor that contribute to thrombosis after rupture of an atherosclerotic plaque. *Thromb. Res.* **129**, S30–S33 (2012).
208. Fuchs, T. A. *et al.* Extracellular DNA traps promote thrombosis. *Proc. Natl. Acad. Sci. U. S. A.* **107**, 15880–15885 (2010).
209. Zhou, J. *et al.* Circulating platelet-neutrophil aggregates as risk factor for deep venous thrombosis. *Clin. Chem. Lab. Med.* **57**, 707–715 (2019).
210. Ott, I., Neumann, F.-J., Gawaz, M., Schmitt, M. & Scho¨mig, A. Increased Neutrophil-Platelet Adhesion in Patients With Unstable Angina. *Circulation* **94**, 1239–1246 (1996).
211. Hottz, E. D. *et al.* Platelet activation and platelet-monocyte aggregate formation trigger tissue factor expression in patients with severe COVID-19. *Blood* **136**, 1330 (2020).
212. Looney, M. R. *et al.* Platelet depletion and aspirin treatment protect mice in a two-event model of transfusion-related acute lung injury. *J. Clin. Invest.* **119**, 3450–3461 (2009).
213. Ortiz-Muñoz, G. *et al.* Aspirin-triggered 15-epi-lipoxin a4 regulates neutrophil-platelet aggregation and attenuates acute lung injury in mice. *Blood* **124**, 2625–2634 (2014).
214. Pan, Y. *et al.* Annexin V-Conjugated Mixed Micelles as a Potential Drug Delivery System for Targeted Thrombolysis. *Biomacromolecules* **18**, 865–876 (2017).
215. Namdee, K. *et al.* In vivo evaluation of vascular-targeted spheroidal microparticles for imaging and drug delivery application in atherosclerosis. *Atherosclerosis* **237**, 279–286 (2014).
216. Lam, F. W., Da, Q., Guillory, B. & Cruz, M. A. Recombinant Human Vimentin Binds to P-Selectin and Blocks Neutrophil Capture and Rolling on Platelets and Endothelium. *J. Immunol.* **200**, ji1700784 (2018).
217. Nelson, R. M., Dolich, S., Aruffo, A., Cecconi, O. & Bevilacqua, M. P. Higher-affinity oligosaccharide ligands for E-selectin. *J. Clin. Invest.* **91**, 1157 (1993).
218. Mosqueira, V. C. F. *et al.* Biodistribution of Long-Circulating PEG-Grafted Nanocapsules in Mice: Effects of PEG Chain Length and Density. *Pharm. Res. 2001 1810* **18**, 1411–1419 (2001).
219. Chen, J. *et al.* Neutrophils Enhance Cutaneous Vascular Dilation and Permeability to Aggravate Psoriasis by Releasing Matrix Metallopeptidase 9. *J. Invest. Dermatol.* **141**, 787–799 (2021).
220. Hoshyar, N., Gray, S., Han, H. & Bao, G. The effect of nanoparticle size on in vivo pharmacokinetics and cellular interaction. *Nanomedicine* **11**, 673 (2016).
221. Maeda, H., Wu, J., Sawa, T., Matsumura, Y. & Hori, K. Tumor vascular permeability and the EPR effect in macromolecular therapeutics: a review. *J. Control. Release* **65**, 271–284 (2000).
222. Cazareth, J., Guyon, A., Heurteaux, C., Chabry, J. & Petit-Paitel, A. Molecular and cellular neuroinflammatory status of mouse brain after systemic lipopolysaccharide challenge: importance of CCR2/CCL2 signaling. *J. Neuroinflammation* **11**, 132 (2014).
223. Wang, X., Qin, W., Song, M., Zhang, Y. & Sun, B. Exogenous carbon monoxide inhibits neutrophil infiltration in LPS-induced sepsis by interfering with FPR1 via p38 MAPK but not GRK2. *Oncotarget* **7**, 34250 (2016).

224. Johnson, J. L., Hong, H., Monfregola, J. & Catz, S. D. Increased Survival and Reduced Neutrophil Infiltration of the Liver in Rab27a- but Not Munc13-4-Deficient Mice in Lipopolysaccharide-Induced Systemic Inflammation. *Infect. Immun.* **79**, 3607 (2011).
225. Silva, J. F. *et al.* Acute Increase in O-GlcNAc Improves Survival in Mice With LPS-Induced Systemic Inflammatory Response Syndrome. *Front. Physiol.* **10**, 1614 (2020).
226. Proniewski, B., Kij, A., Sitek, B., Kelley, E. E. & Chlopicki, S. Multiorgan development of oxidative and nitrosative stress in LPS-induced endotoxemia in C57BL/6 mice: DHE-based in vivo approach. *Oxid. Med. Cell. Longev.* **2019**, (2019).
227. Lew, W. Y. W. *et al.* Recurrent Exposure to Subclinical Lipopolysaccharide Increases Mortality and Induces Cardiac Fibrosis in Mice. *PLoS One* **8**, e61057 (2013).
228. Keepers, T. R., Psotka, M. A., Gross, L. K. & Obrig, T. G. A Murine Model of HUS: Shiga Toxin with Lipopolysaccharide Mimics the Renal Damage and Physiologic Response of Human Disease. *J Am Soc Nephrol* **17**, 3404–3414 (2006).
229. Grosse, S. D. *et al.* Sickle Cell Disease in Africa: A Neglected Cause of Early Childhood Mortality. *Am. J. Prev. Med.* **41**, S398–S405 (2011).
230. Quinn, C. T. *et al.* Biochemical surrogate markers of hemolysis do not correlate with directly measured erythrocyte survival in sickle cell anemia. *Am. J. Hematol.* **91**, 1195–1201 (2016).
231. Eckstein, E. C., Bilsker, D. L., Waters, C. M., Kippenhan, J. S. & Tilles, A. W. Transport of Platelets in Flowing Blood. *Ann. N. Y. Acad. Sci.* **516**, 442–452 (1987).
232. Hebbel, R. P., Boogaerts, M. A. B., Eaton, J. W. & Steinberg, M. H. Erythrocyte Adherence to Endothelium in Sickle-Cell Anemia. *N. Engl. J. Med.* **302**, 992–995 (1980).
233. Rosse, W. F., Narla, M., Petz, L. D. & Steinberg, M. H. New Views of Sickle Cell Disease Pathophysiology and Treatment. *Hematol. Am. Soc. Hematol. Educ. Progr.* **2000**, 2–17 (2000).
234. Aarts, P., Heethaar, R. & Sixma, J. Red blood cell deformability influences platelets--vessel wall interaction in flowing blood. *Blood* **64**, (1984).
235. Dobbe, J. G. G. *et al.* Analyzing Red Blood Cell-Deformability Distributions. *Blood Cells, Mol. Dis.* **28**, 373–384 (2002).
236. Keiser, A. M., Booth, G. S. & Gehrie, E. A. With a simple calculation, the fraction of platelets remaining can be used to estimate the residual hemoglobin S percentage in sickle cell disease patients undergoing automated red blood cell exchange. *Transfus. Apher. Sci.* **57**, 250–252 (2018).
237. Du, E., Diez-Silva, M., Kato, G. J., Dao, M. & Suresh, S. Kinetics of sickle cell biorheology and implications for painful vasoocclusive crisis. *Proc. Natl. Acad. Sci.* **112**, 1422–1427 (2015).
238. Mehrabadi, M., Ku, D. N. & Aidun, C. K. A Continuum Model for Platelet Transport in Flowing Blood Based on Direct Numerical Simulations of Cellular Blood Flow. *Ann. Biomed. Eng.* **43**, 1410–1421 (2015).
239. Ryter, S. W. & Choi, A. M. K. Targeting heme oxygenase-1 and carbon monoxide for therapeutic modulation of inflammation. *Transl. Res.* **167**, 7–34 (2016).
240. Sirs, J. The use of carbon monoxide to prevent sickle-cell formation. *Lancet* **281**, 971–972 (1963).
241. Yallop, D. *et al.* The associations between air quality and the number of hospital admissions for acute pain and sickle-cell disease in an urban environment. *Br. J. Haematol.* **136**, 844–848 (2007).

242. Gomperts, E. *et al.* The role of carbon monoxide and heme oxygenase in the prevention of sickle cell disease vaso-occlusive crises. *American Journal of Hematology* vol. 92 569–582 (2017).
243. Beckman, J. D. *et al.* Inhaled carbon monoxide reduces leukocytosis in a murine model of sickle cell disease. *Am. J. Physiol. - Hear. Circ. Physiol.* **297**, (2009).
244. Belcher, J. D. *et al.* Oral carbon monoxide therapy in murine sickle cell disease: Beneficial effects on vasoocclusion, inflammation and anemia. *PLoS One* **13**, (2018).
245. Belcher, J. D. *et al.* MP4CO, a pegylated hemoglobin saturated with carbon monoxide, is a modulator of HO-1, inflammation, and vaso-occlusion in transgenic sickle mice. *Blood* **122**, 2757–2764 (2013).
246. Keipert, P. E. *et al.* Clinical evaluation of MP4CO: A phase 1b escalating-dose, safety and tolerability study in stable adult patients with sickle cell disease. in *Advances in Experimental Medicine and Biology* vol. 923 23–29 (Springer New York LLC, 2016).
247. Fayad-Kobeissi, S. *et al.* Vascular and angiogenic activities of CORM-401, an oxidant-sensitive CO-releasing molecule. *Biochem. Pharmacol.* **102**, 64–77 (2016).
248. Musameh, M. D., Fuller, B. J., Mann, B. E., Green, C. J. & Motterlini, R. Positive inotropic effects of carbon monoxide-releasing molecules (CO-RMs) in the isolated perfused rat heart. *Br. J. Pharmacol.* **149**, 1104–12 (2006).
249. Kim-Anh, N.-P. *et al.* Protective Effects of Carbon Monoxide Delivered By Corm-401 in Hyperhemolysis in Patients with Sickle Cell Disease. *Blood* **132**, 2367–2367 (2018).
250. Babu, D., Leclercq, G., Motterlini, R. & Lefebvre, R. A. Differential Effects of CORM-2 and CORM-401 in Murine Intestinal Epithelial MODE-K Cells under Oxidative Stress. *Front. Pharmacol.* **8**, 31 (2017).
251. Sakariassen, K. S., Orning, L. & Turitto, V. T. The impact of blood shear rate on arterial thrombus formation. *Futur. Sci. OA* **1**, fso.15.28 (2015).
252. Czaja, B. *et al.* The influence of red blood cell deformability on hematocrit profiles and platelet margination. *PLOS Comput. Biol.* **16**, e1007716 (2020).
253. Ballas, S. K. & Smith, E. D. *Red Blood Cell Changes During the Evolution of the Sickle Cell Painful Crisis*. *Blood* vol. 79 http://www.bloodjournal.org.proxy.lib.umich.edu/content/bloodjournal/79/8/2154.full.pdf (1992).
254. Barodka, V. M. *et al.* New insights provided by a comparison of impaired deformability with erythrocyte oxidative stress for sickle cell disease. *Blood Cells, Mol. Dis.* (2014) doi:10.1016/j.bcmd.2013.10.004.
255. Elliott, M. A. & Tefferi, A. Thrombosis and haemorrhage in polycythaemia vera and essential thrombocythaemia. *Br. J. Haematol.* **128**, 275–290 (2005).
256. Tomer, A., Harker, L. A., Kasey, S. & Eckman, J. R. Thrombogenesis in sickle cell disease. *J. Lab. Clin. Med.* **137**, 398–407 (2001).
257. Villagra, J. *et al.* Platelet activation in patients with sickle disease, hemolysis-associated pulmonary hypertension, and nitric oxide scavenging by cell-free hemoglobin. *Blood* **110**, 2166–2172 (2007).
258. Virani, S. S. *et al.* Heart disease and stroke statistics—2020 update: A report from the American Heart Association. *Circulation* **141**, E139–E596 (2020).
259. Mathers, C. D. & Loncar, D. Projections of Global Mortality and Burden of Disease from 2002 to 2030. *PLOS Med.* **3**, e442 (2006).
260. Wang, R. M. & Christman, K. L. Decellularized Myocardial Matrix Hydrogels: In Basic

Research and Preclinical Studies. *Adv. Drug Deliv. Rev.* **96**, 77 (2016).
261. Cleutjens, J. P. M. & Creemers, E. E. J. M. Integration of concepts: Cardiac extracellular matrix remodeling after myocardial infarction. *J. Card. Fail.* **8**, S344–S348 (2002).
262. Vanhoutte, D., Schellings, M., Pinto, Y. & Heymans, S. Relevance of matrix metalloproteinases and their inhibitors after myocardial infarction: A temporal and spatial window. *Cardiovasc. Res.* **69**, 604–613 (2006).
263. Kremastiotis, G., Handa, I., Jackson, C., George, S. & Johnson, J. Disparate effects of MMP and TIMP modulation on coronary atherosclerosis and associated myocardial fibrosis. *Sci. Rep.* **11**, 23081 (2021).
264. Hemalatha, T., Aarthy, M., Pandurangan, S., Kamini, N. R. & Ayyadurai, N. A deep dive into the darning effects of biomaterials in infarct myocardium: current advances and future perspectives. *Hear. Fail. Rev. 2021* **1**, 1–25 (2021).
265. van der Pol, A. & Bouten, C. V. C. A Brief History in Cardiac Regeneration, and How the Extra Cellular Matrix May Turn the Tide. *Front. Cardiovasc. Med.* **0**, 487 (2021).
266. Wang, Z. *et al.* Decellularized neonatal cardiac extracellular matrix prevents widespread ventricular remodeling in adult mammals after myocardial infarction. *Acta Biomater.* **87**, 140–151 (2019).
267. Bassat, E. *et al.* The extracellular matrix protein agrin promotes heart regeneration in mice. *Nat. 2017 5477662* **547**, 179–184 (2017).
268. Seif-Naraghi, S. B., Salvatore, M. A., Schup-Magoffin, P. J., Hu, D. P. & Christman, K. L. Design and characterization of an injectable pericardial matrix gel: A potentially autologous scaffold for cardiac tissue engineering. *Tissue Eng. - Part A* **16**, 2017–2027 (2010).
269. Ungerleider, J. L. *et al.* Extracellular Matrix Hydrogel Promotes Tissue Remodeling, Arteriogenesis, and Perfusion in a Rat Hindlimb Ischemia Model. *JACC Basic to Transl. Sci.* **1**, 32 (2016).
270. Wassenaar, J. W. *et al.* Evidence for Mechanisms Underlying the Functional Benefits of a Myocardial Matrix Hydrogel for Post-MI Treatment. *J. Am. Coll. Cardiol.* **67**, 1074 (2016).
271. Traverse, J. H. *et al.* First-in-Man Study of a Cardiac Extracellular Matrix Hydrogel in Early and Late Myocardial Infarction Patients. *JACC Basic to Transl. Sci.* **4**, 659–669 (2019).
272. Spang, M. T. *et al.* Healing Tissues From the Inside Out: Infusible Biomaterial for Targeting and Treating Inflammatory Tissues via Intravascular Administration. *bioRxiv* 4.10.028076 (2021) doi:10.1101/2020.04.10.028076.
273. Lidington, E. A., Moyes, D. L., McCormack, A. M. & Rose, M. L. A comparison of primary endothelial cells and endothelial cell lines for studies of immune interactions. *Transpl. Immunol.* **7**, 239–246 (1999).
274. Lehle, K., Straub, R. H., Morawietz, H. & Kunz-Schughart, L. A. Relevance of disease- and organ-specific endothelial cells for in vitro research. *Cell Biol. Int.* **34**, 1231–1238 (2010).
275. Chi, J.-T. *et al.* Endothelial cell diversity revealed by global expression profiling. *PNAS* **100**, 10623–10628 (2003).
276. Cines, D. B. *et al.* Endothelial Cells in Physiology and in the Pathophysiology of Vascular Disorders. *Blood* **91**, 3527–3561 (1998).
277. Wolberg, A. S. *et al.* Venous thrombosis. *Nat. Rev. Dis. Prim.* **1**, 15006 (2015).

278. Reitsma, P. H. & Rosendaal, F. R. Activation of innate immunity in patients with venous thrombosis: the Leiden Thrombophilia Study. *J. Thromb. Haemost.* **2**, 619–622 (2004).
279. Wakefield, T. W. *et al.* P-Selectin and TNF Inhibition Reduce Venous Thrombosis Inflammation. *J. Surg. Res.* **64**, 26–31 (1996).
280. Wajant, H., Pfizenmaier, K. & Scheurich, P. Tumor necrosis factor signaling. *Cell Death Differ.* **10**, 45–65 (2003).
281. Karsan, A. Tumor Necrosis Factor and Endothelial Cell Death. *Trends Cardiovasc. Med.* **8**, 19–24 (1998).
282. Chen, X. *et al.* Role of Reactive Oxygen Species in Tumor Necrosis Factor-alpha Induced Endothelial Dysfunction. *Curr. Hypertens. Rev.* **4**, 245 (2008).